DEPARTMENT OF PHYSICS
COLLEGE OF SCIENCES
OLD DOMINION UNIVERSITY
NORFOLK, VIRGINIA 23529

Technical Report No. PTR-90-2

THEORETICAL STUDIES OF SOLAR PUMPED LASERS

By

W.L. Harries, Principal Investigator

Final Report
For the period ending August 31, 1990

Prepared for the
National Aeronautics and Space Administration
Langley Research Center
Hampton, Virginia 23665-5225

Under
NASA Research Grant NSG-1568
Dr. Willard E. Meador Jr., Technical Monitor
SSD-High Energy Science Branch

Submitted by the
Old Dominion University Research Foundation
P.O. Box 6369
Norfolk, Virginia 23508-0369

May 1990

TABLE OF CONTENTS

TABLE OF CONTENTS (Continued)

TABLE OF CONTENTS (Concluded)

LIST OF TABLES

LIST OF FIGURES

LIST OF FIGURES (Concluded)

THEORETICAL STUDIES OF SOLAR PUMPED LASERS

By

W. L. Harries

1. INTRODUCTION

One concept for collecting solar energy is to use large solar collectors and then use lasers as energy converters whose output beams act as transmission lines to deliver the energy to a destination. The efficiency of the process would be improved if the conversion could be done directly using solar pumped lasers, and the purpose of this report is to study the possibility of making such lasers. The conversion from laser beam energy back to useful work is not discussed.

There are many applications for such lasers, and these are dealt with in Section 2. By including the applications first, the requirements for the lasers will be more evident. They are especially applicable to the Space program, and include cases where no other methods of delivering power seem possible. Using the lasers for conveying information and surveillance is also discussed.

Many difficulties confront the designer of an efficient system for power conversion. These involve the nature of the solar spectrum, the method of absorbing the energy, the transfer of power into laser beams, and finally, the far field patterns of the beams. The requirements of the lasers are discussed in Section 3.

Specific laser configurations are discussed in Section 4. The main thrust of this study is into gas laser systems, because for space applications, the laser could be large, and also the medium would be uniform and not subject to thermal stresses. Dye and solid lasers are treated briefly.

For gas lasers, a chart of the various possibilities will be shown in Section 4, and the various families of gas lasers divided according to the mechanisms of absorbing solar radiation and of lasing. Several specific models will be analyzed and evaluated according to the criteria of Section 3.

Overall conclusions for the program are summarized in Section 5, and the performances of the lasers related to the requirements of various applications.

2. APPLICATIONS OF SOLAR PUMPED LASERS

The main thrust of this study is to examine solar pumped lasers as energy converters to supply power. The possibility of providing communication and/or surveillance at much lower power levels is also discussed.

2.1 Solar Pumped Lasers as Power Converters

The use of very large solar collectors on orbiting space stations with lasers sending beams to earth to augment the electrical utilities does not seem feasible as the required power levels (many billions of MW) are far too high. There are also the problems of directing the beams into populated areas and of transmission through the atmosphere.

The use of solar pumped lasers for space applications however introduces exciting possibilities as more reasonable power levels are required ($\leq$ 100 KW), there are unobstructed paths for the beams and atmospheric absorption is eliminated in many instances. With planetary atmospheres, the laser frequency can be tailored to penetrate an atmosphere such as CO_2 on Mars, for instance.

For space applications, we may consider vehicle-to-vehicle power transfer whilst in flight, and also orbiting vehicle-to-ground power

transfer. In the first case, one vehicle in a mission of several vehicles would carry a large solar collector and use a laser to send power to the others which would not need to carry such large collectors, or could also be in the shadow of a planet.

The second possibility of an orbiting vehicle sending power to ground has the important application of providing power to rovers exploring a planetary surface. The use of beam power in this instance is one of the few methods possible for prolonged excursions. The NASA Office of Aeronautics and Space Technology, and the Office of Exploration sponsored a workshop at Langley to consider Beamed Space-Power[1] and our studies on a Martian Rover are summarized below.

2.2 Laser Powered Martian Rover

The power requirements considered for a Martian Rover were 4.5 KW for an unpressurized skeleton vehicle capable of a range of 10 Km and about 75KW for a vehicle visualized as a mobile habitat with full life support systems and unlimited range. The power was to be supplied from orbiting satellites with solar collectors a height h above the vehicle. Some calculations showing numbers are useful.

We assume the rover has a receiving dish of diameter D_r mounted on the vehicle. The transmitter must then be able to point at the receiver within an accuracy $\Delta\theta$

$$\Delta\theta \leq D_r/h \qquad (2\text{-}1)$$

The maximum attainable accuracy in practice is $\Delta\theta = 0.2''$ arc $= 10^{-6}$ radian. Thus, if $D_r = 2m$ (for the smaller vehicle) and $h = 2 \times 10^7 m$, (geosynchronous orbit for Mars) then $\Delta\theta = 10^{-7}$ rad, an impossible value, as the present limit of pointing accuracy is 10^{-6} rad. However, if h were reduced to $2 \times 10^6 m$, accurate pointing would be possible.

Accurate pointing is a necessary but not sufficient condition if the rover is in motion as then it must be tracked by the orbiting vehicle. As the rover is controlled from the ground, its motion can be regarded as random. The orbiting station S at height h above the rover, (Fig. 1) senses the position AB, and the sensing signal from AB takes a time $t = h/c$ to reach S where c is the velocity of light. The laser beam from S takes a similar time, so the total delay between being sensed and receiving the laser energy is $2h/c$. If the rover moves with velocity v on the ground surface, it moves a distance $2hv/c$ in this time, from AB to A'B'. We require $BB' \ll AB = D_r$ or $BB' = \alpha D_r$ where α is a precision factor (e.g. 0.1). Hence we require

$$2hv/c < \alpha D_r \qquad (2\text{-}2)$$

If $v = 10\text{Km/hr} = 2.8\ ms^{-1}$, $c = 3 \times 10^8 ms^{-1}$, $\alpha = 0.1$, $D_r = 2m$ then the condition is not satisfied at geosynchronous orbit, but is satisfied if $h = 2000$ Km.

Calculations showed that three orbiting satellites 2000 Km symmetrically above the Martian surface with a period of 3 hours 19 minutes and a velocity of 2821 ms^{-1} could cover 55% of the Martian surface with a view time of 56 mins 40s and dead time of 9 mins and 54s. A number greater than 3 would provide more than adequate coverage.

To beam the energy at the vehicle so that the majority is collected by the receiver dish, the sizes of both transmitting and receiving dishes must be greater than certain minimum values. If the diameter of the dishes are D_t (transmitting), D_r, respectively, and λ the wavelength of the signal then from the condition of diffraction limitation

$$D_t D_r \geq \frac{4}{\pi} \lambda h \qquad (2\text{-}3)$$

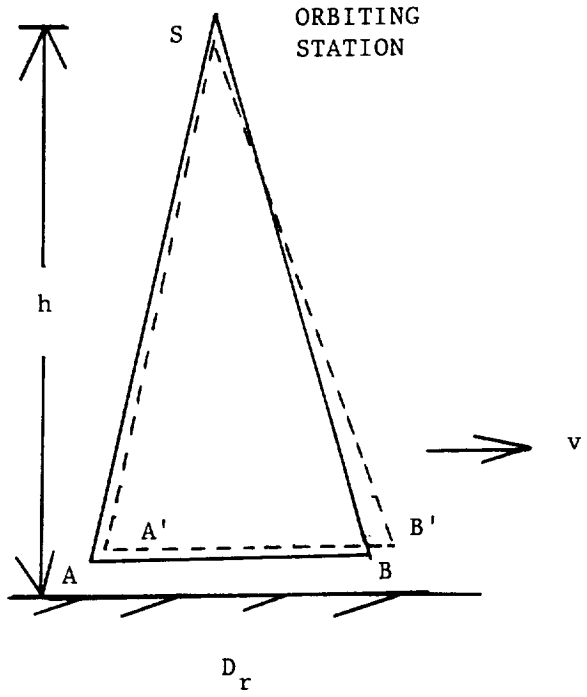

Figure 1. Tracking a moving vehicle, length AB, on the surface of Mars, from an orbiting station S, a height h above the surface.

where the factor $4/\pi$ assumes the best possible case with a Gaussian intensity profile. With a laser wavelength of $1\mu m$, $h = 2 \times 10^6$ m, then $D_t D_r \approx 2m^2$ and $D_t \approx 1$ m which are reasonable values. An important conclusion from Eq. 2-3 is that if instead of a laser beam, microwaves with $\lambda = 1$ cm were used, then $D_t D_r = 2 \times 10^4$; for $D_r = 2m$ then $D_t = 10Km$, impossibly large.

Thus, the orbiting lasers could supply essentially continuous power, and no storage requirements are necessary during the Martian nights. Powers of up to 75 KW are however not attainable at present, but the concept seems feasible and is probably the only way to power a rover.

The concept of laser beams powering a static ground station to which a rover would return to recharge its batteries is not viable as the solar collector dishes could be placed directly on the ground station. As the ground station could only collect solar energy at night, energy storage at both station and rover would be required.

2.3 Communication and Surveillance

Solar powered lasers could be used for line-of-sight communication and surveillance either in a space environment or left unattended in remote terrestrial locations. The requirements of high power are unnecessary here, hence lasers of low power such as have been investigated at Langley could be used. For operation on a continuous basis, even if the solar collector is in shadow part of the time, it is possible to use "black body pumped" lasers where a cavity is heated, and the heat energy stored to continue pumping the laser while the satellite is in the planet's shadow. For example, a geosynchronous satellite at $3{\cdot}6 \times 10^7$ m above the earth's surface is in the earth's shadow for about 1 hour and 10 minutes every 24 hours. Terrestrial solar pumped lasers could only operate during sunlight, unless they were black body lasers capable of storing heat over a period of over 10 hours.

3. GENERAL REQUIREMENTS FOR SOLAR PUMPED LASERS AS SOLAR ENERGY CONVERTERS

We consider the general requirements for solar pumped gas lasers acting as energy converters before we deal with specific systems.

The laser must be efficient in converting the solar energy into an output beam. The efficiency can be subdivided into a product of efficiencies according to the sequence of physical processes occurring.

The criteria for a solar pumped laser are as follows:

1. There must be broadband absorption;
2. Peak absorption should occur near the peak of the solar spectrum;
3. The absorbing medium (gas) must be at sufficient pressure to absorb most of the photons, otherwise a multipass arrangement must be used.
4. High quantum yield into a long-lived (metastable) state which serves as the upper laser level is necessary.
5. In general, quenching of the excited state should be small, but this condition is alleviated if
6. The lower level is rapidly depopulated to maintain inversion;
7. The upper and lower levels must be sufficiently separated to yield a reasonable quantum efficiency;
8. The process must be reversible; if not the components must be reconstituted by flow methods.
9. Operation at high temperature would be advantageous to reduce the weight of the radiator
10. The beam must diverge as little as possible.

Items 1 and 2 are included in a "solar utilization efficiency", item 3 is

included in an "absorption efficiency", items 4, 5 and 6 are included in a "kinetic efficiency", while item 7 is included in the "quantum efficiency". All of these terms are defined more fully in Appendix A, a paper in the AIAA J of Propulsion and Power.

In addition to efficiency another criterion for space applications is the output power per unit weight, as the lasers have to be lifted off a launch pad. Items 8 and 9 are of concern here. This also is considered in Appendix A where the effects of high temperature operation are outlined.

When the beam eventually leaves the laser, the far field pattern is of importance, and the divergence of the beam must be small. This aspect is item 10 above. The fraction of the output power that strikes a given target is termed the "collection efficiency". A study of far field patterns is given in Appendix B, Technical Report PTR-89-6. This study is different from any previous studies in that for large lasers it examines the effect of non-homogeneity of the medium, as would occur in a gas laser pumped from the outside. This study was not completed when the grant was terminated, but the preliminary results imply that lasers of large diameter and non-uniform media may suffer considerable divergence of their beams. The general criteria explained in Section 3 will next be applied in Section 4.

4. SPECIFIC LASER SYSTEMS

This study has concentrated almost entirely on gas lasers because for space applications, there are no stringent requirements on size (in contrast to weight) and also the medium would be uniform. In addition to gas lasers however, a limited study was made of dye lasers in liquid or vapor form which is included in section 4.3.

For gas lasers, investigations concentrated both on different lasing materials and also on different laser systems. The families of lasers investigated are shown in Figure 2. They are subdivided according to how the radiation is absorbed and utilized and then further subdivided according to specific mechanisms. The first subdivision is whether part of the solar spectrum is absorbed, (Section 4.1), or whether the whole solar spectrum is utilized (Section 4.2). Utilizing the whole spectrum may not be advantageous as we shall see.

4.1 Solar Lasers Which Utilize Only Part of the Solar Spectrum

Lasers of this type can be further subdivided according to whether the lasing medium is dissociated or not. If dissociation occurs then one of the species must be in an excited state, which forms the upper lasing level, and this is dealt with in Section 4.1.1. The non-dissociative types can be metal vapors such as Na_2, Cs_2 etc. where absorption of a photon results in the molecule being transformed into an electronically excited state-Section 4.1.2.

4.1.1 Dissociative Laser Media

We further subdivide dissociative lasers according to whether they possess a separate absorbing medium which forms an excited state, and that medium in turn then collides with and hands over energy to a second medium which acts as the lasant. The processes of absorption and lasing are thus separated, and each tailored to give the highest laser efficiency. Studies of this type are summarized in section 4.1.1.1 below. Following that section is a study of solar lasers that use the same material to both absorb the solar radiation and lase.

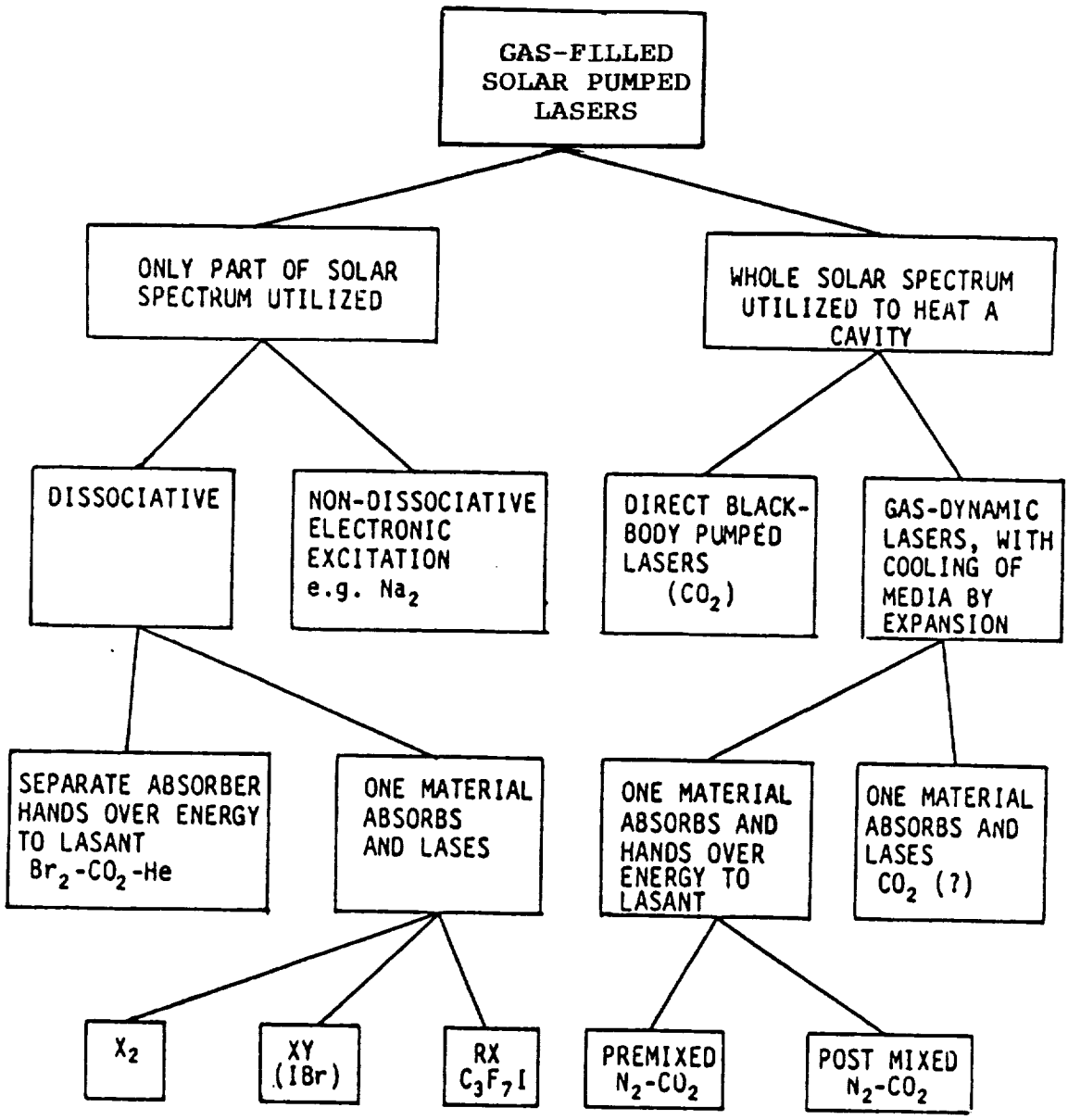

X = halogen, Y = different halogen atom
R = complex radical

Figure 2. Various families of solar pumped lasers.

4.1.1.1 Dissociative Lasers Which Use a Separate Absorber to Hand Over Energy to the Lasant

For this type of laser an investigation was made both of the physical processes involved and especially of what would be the best materials for lasing. The results are summarized in Appendix C, the paper "Solar-Pumped Electronic-to-Vibrational Energy Transfer Lasers" by W.L. Harries and J.W. Wilson, Space Solar Power Review 2, 367 (1981).

4.1.1.2 Solar Lasers Which Use One Material To Absorb and Lase

The results of the investigation in Section 4.1.1.1 implied that for all the materials considered, where a different material absorbed the radiation and another lased, that the efficiencies were below 5×10^{-3}. It was thought that the efficiency might be improved if the hand-over process was eliminated and a medium chosen which performed both the process of absorption and lasing. Reasons for the choice of material and the laser mechanisms were investigated and the results are summarized in Appendix D, the paper "Kinetic Modeling of an IBr Solar Pumped Laser" by W.L. Harries and W.E. Meador, Space Solar Power Review 4, 189 (1983).

4.1.1.3 Summary of Dissociative Lasers

The above studies indicate that as far as the materials investigated that for lasers with a separate absorbing medium the efficiencies were 5×10^{-3} or less. Where the same material (IBr) performed both absorption and lasing, the efficiencies could approach about 0.012.

Referring to Figure 2, the types X_2, and XY where X is a halogen and Y a different halogen atom have been covered above. Not covered is the type RX where R is a complex radial e.g. R = C_3F_7 or C_4F_q etc. and X is an Iodine atom. Considerable theoretical and experimental work was performed at Langley on this type of solar pumped laser, and the lasers operated

successfully driven by a solar simulator. Their absorption bands are included in Fig. 6 in Appendix C, but both theory and experiment at Langley were done by others and they are not included in this report.

Lasers of this type suffer the disadvantage that during lasing, the compounds break up into constituents and a flow system has to be introduced where the constituents have to be recombined to form the lasant. Also their absorption band occurs in a narrow band in the ultra violet (see Fig. 6 in Appendix C) and their solar efficiencies are low.

4.1.2 Non Dissociative Laser Media

Hitherto, the types of molecular lasers considered have been those where photodissociation occurred, but absorption of a photon can also yield an excited molecule in an upper electronic state (Fig.3). The transition occurs according to the Franck-Condon principle, and the molecule could return to the lower electronic level by emission of a stimulated photon.

A comprehensive article by Wellengehausen (IEEE J of Quantum Electronics, QE-15, 1108 (1979)) reported on the development of optically pumped cw dimer lasers[2] and listed a number of experiments where lasing had occurred in Na_2, Te_2, Br_2, Li_2, K_2, and S_2, as well as in the halogens I_2 and Br_2. The pumping in the experiments was done by lasers, either frequency doubled Neodymium (532.5 nm) or an argon ion laser (472.7 nm). These frequencies lie near the peak of the solar spectrum. The efficiencies quoted were up to 15%, but this has to be further reduced by a "solar efficiency" for solar pumping.

If the dimer were solar pumped (Fig. 4), the Franck-Condon transitions would result in vibrational levels much higher than the lasing level, shown here near the upper level minimum. If it were possible for the molecule to

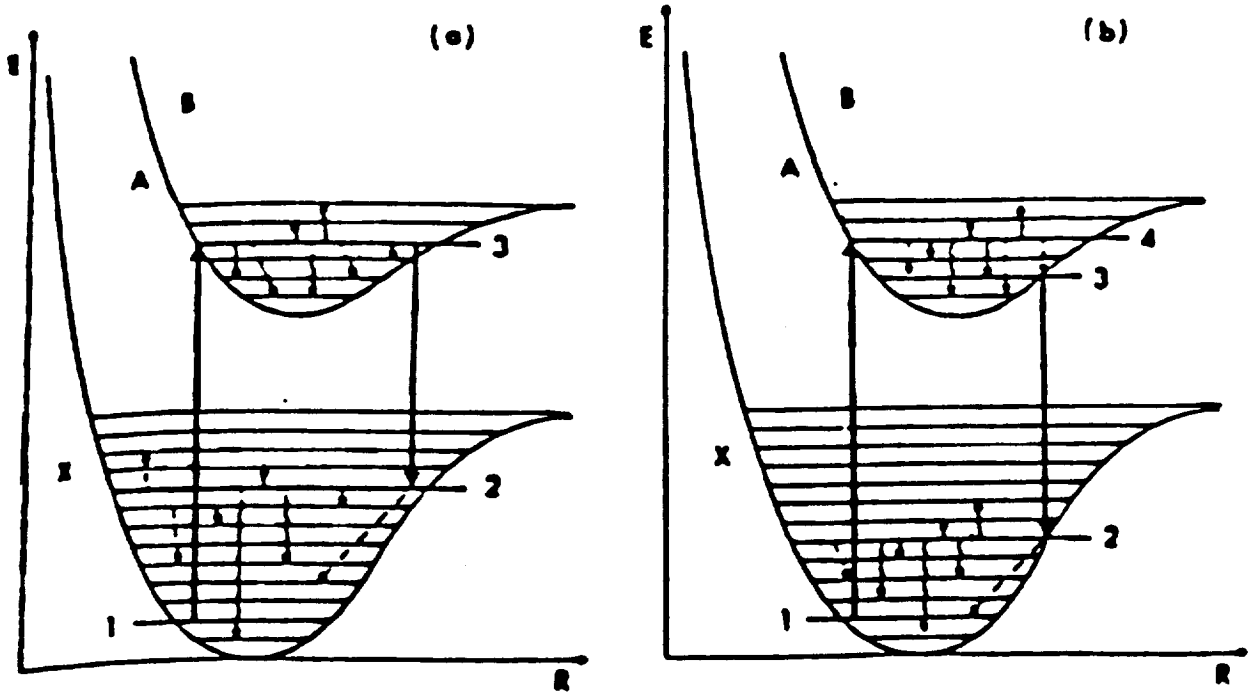

Figure 3. Laser cycles between bound electronic molecular states, (a) three-level cycle and (b) four-level cycle with radiative or nonradiative transitions between the levels 4 and 3.

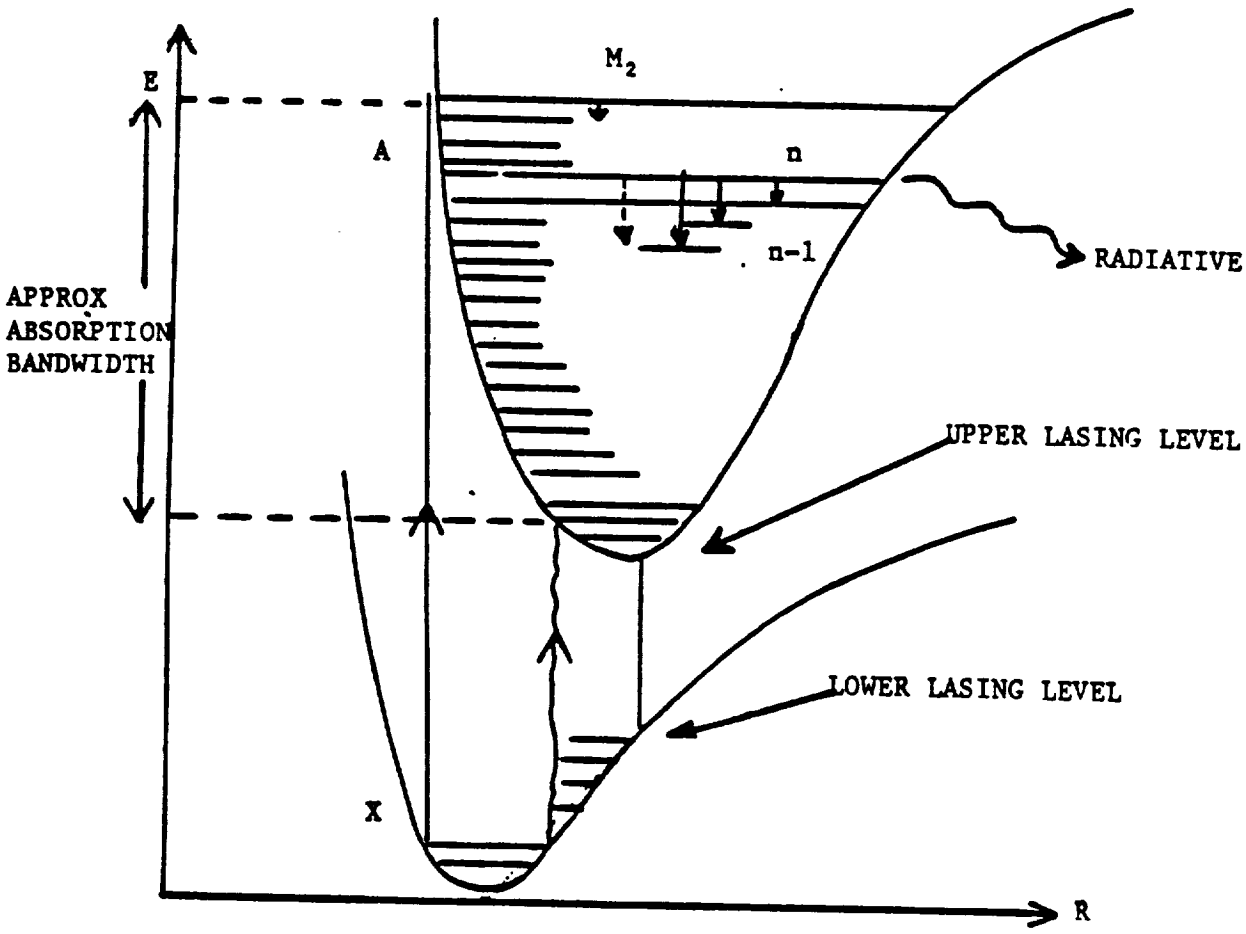

Figure 4. Energy level diagram for a solar pumped dimer molecule M_2. The vibrational levels only are shown. A molecule raised to the nth level of the upper electronic A state can either descend to the (n-1), (n-2) ..., levels by collisions, (continuous arrows) and radiation (dotted arrows) or else radiate a photon (wave arrow) and then drop to the lower electronic X state.

cascade down in energy without falling to ground level, then there would be a "funneling" to the upper laser level. The fraction that arrives at the upper laser level depends on the probability at each level of spontaneous emission with relaxation to the lower electronic level, and on the probability of descending to a lower vibrational-rotational level in the upper electronic state by collisions or radiation. For homonuclear diatomic molecules, radiative transitions between rotational vibrations of the same electronic state are not allowed.

If the "funneling" is efficient, then this type of laser would be very attractive. However, the wider the absorption band, the higher will be the initial vibrational level in the upper electronic state, and the less the probability of arriving at the upper lasing level without radiating. Also, the higher the initial vibrational level, the less will be the effective quantum efficiency. Hence, compromises will have to be made between solar kinetic and quantum efficiencies.

The possibility of lasing by solar pumping in metallic vapors such as those mentioned seemed hopeful from the point of view of efficiency. Also, the metal vapors would be at high temperatures, and high temperature lasers would need a smaller radiator, which would decrease the weight and hence improve the power to weight ratio. Lastly and very importantly was the possibility that these lasers might emit in the visible.

Considerable study was made of metal vapor lasers, but unfortunately as was pointed out by W.E. Meador, although experiments where lasers were used to pump Na_2 seemed to imply reasonable thresholds, the threshold levels for solar pumping were much too high for practical use. Normally for solar pumped lasers, the solar collector concentrates the radiation. The upper limit of concentration is believed to be around 20,000-- a

limitation of the optics based on the fact that the sun is not a point but distributed source. Accordingly, the investigation of lasing by metal vapors was deemphasized around 1987, but as several aspects of metal vapors as lasing media had been completed and as they might be useful for future studies of optical pumping, they are included below.

The problem of self-absorption of stimulated emission is a general one and the case of sodium is treated in Section 4.1.2.1. Another important question is the ratio of dimers to monomers in metallic vapors which depends on temperature. Although curves existed in the literature, we were unable to find a reasonable mechanism or physical picture and a simple treatment and formulae are given in Section 4.1.2.2. The problem of metastability of a dimer molecule is also a general one in lasers and is treated in Section 4.1.2.3

At the same time as these studies were performed, an experimental program under Dr. N. Jalufka of NASA/Langley was undertaken to study absorption and emission in Na_2 vapor. A new electronic transfer process was suggested by Jalufka, and the experiments and theory were written up as a paper entitled "Electronic Energy Transfer in Molecular Sodium" by N.W. Jalufka and W.L. Harries and submitted to the Journal of Molecular Spectroscopy. This is included in Appendix E. Calculations on a possible sodium laser are shown in Section 4.1.2.4, A and on Lithium in Section 4.1.2.4, B. Although it is felt that these metallic vapors may not be useful for solar pumped lasing, these calculations might be useful in other laser applications.

4.1.2.1 Stimulated Emission and Self Absorption in Sodium Vapor

A. Introduction

In any lasing medium, the emission wavelength should be chosen where there is little self absorption. As emission and absorption spectra for metallic vapors did not seem available, therefore, estimates were made of these cross sections for sodium vapor as functions of wavelength. Although absolute values were not obtained, information on where the emission wavelength should occur became evident.

In Section 4.1.2.1B, the method of obtaining quantities proportional to the cross sections versus wavelength is outlined. A further comparison based on alternative expressions for the absorption and emission cross sections over a limited wavelength range is made in Section 4.1.2.1C which supports the evidence of Section 4.1.2.1B.

B. Absorption and Emission Probabilities for Na_2 Vapor

The probabilities can be estimated if the Franck-Condon factors F(v", v') are known for transitions from the various vibrational levels v" in the ground state $X^1 \Sigma_g^+$ of Na_2, to vibrational levels v' in an electronically excited state. An excited state which would correspond to absorption in the visible is the $B^1\Pi_u$ and fortunately, a very complete table of Franck-Condon factors was given by Kusch and Hessel.[3] The amount of absorption from any level v" would depend on the relative population of the level to the other levels in the same electronic state. The levels would be filled according to Boltzmann statistics. Similarly, the emission would depend on the relative population of the upper vibrational levels.

For the ground electronic state the energy of the level v" in cm-1 was

$$E(v") = W_e(v" + \frac{1}{2}) - W_e\chi_e(v" + \frac{1}{2})^2 \qquad (4\text{-}1)$$

where $W_e = 159.1\ cm^{-1}$, and $W_e\chi_e = 0.7254\ cm^{-1}$ and the lowest energy $E_0 = E(v" = 0)$.[4]

The probability of filling level v" was

$$P(v") = \exp \frac{E(v")-E_0}{kT} \qquad (4\text{-}2)$$

when k is Boltzmann's constant and T the temperature in degrees Kelvin. The fraction of molecules in this state was

$$f(v") = \frac{P(v")}{\sum_{v"=0}^{n} P(v")} \qquad (4\text{-}3)$$

where n was taken as 45.

The minimum of the potential curve for the $B^1\Pi_u$ state was at 20,319 cm^{-1}, and the energy of the v' state was

$$E(v') = w_e' \left(v' + \frac{1}{2}\right) - w_e\chi_e' \left(v' + \frac{1}{2}\right)^2 + 20{,}319 \qquad (4\text{-}4)$$

where $w_e' = 124.9\ cm^{-1}$, and $w_e\chi_e' = 0.6999$[4], and the lowest vibrational energy level $E_0' = E(v' = 0)$. The fraction of molecules filling level v', namely f(v') was calculated as in equations (2) and (3), except n was now taken as 28. The number n for both ground and excited electronic states was determined by the availability of Franck-Condon factors. Both numbers are sufficiently large so that inclusion of any higher levels would not change the results appreciably.

A quantity proportional to the absorption cross section, which is a function of wavelength λ is[5]

$$Q(\lambda) = F(v", v')\ f(v")\nu \qquad (4\text{-}5)$$

where F(v",v') is the Franck-Condon factor for the transition v"→v', ν is the frequency of the absorbing photon determined by E(v') - E(v"). Plots of $Q(\lambda)$ vs. λ for transitions from level v" to v' corresponding to

$0 \leq v'' \leq 45$, or $0 \leq v' \leq 28$ are shown in Figure 5. The overall outline resembles a Gaussian absorption curve.

The values of $Q(\lambda)$ were then averaged over an interval of 5 nm to give smoother curves and are shown in Figure 6 for temperatures of 500, 650 and 1000°C. The curves now resemble Gaussian absorption curves and increasing the temperature decreases the peak value and widens the wings, as it should.

An estimation of a quantity proportional to a stimulated emission cross section can be made in a similar manner. The probability of filling a vibrational level in the upper electronic state was again assumed to occur according to Boltzmann statistics. This assumption, however, may lead to error because the levels in the upper state are filled from the ground state, and their population densities are dependent on the rate of arrival from the ground state. If they remain in the upper state for many collisions, a Boltzmann distribution should result, but if they are quickly quenched such a distribution is unlikely.

Assuming the fraction in level v' is $f(v')$ as previously calculated, then a quantity $R(\lambda)$ proportional to the stimulated emission cross section is given by[6]

$$R(\lambda) = F(v'', v')\, f(v')\, \nu^2 \qquad (4\text{-}6)$$

Plots of $Q(\lambda)$, $R(\lambda)$ vs. λ are shown in Figure 7. The values have been smoothed from those of Figure 5 by averaging over a 5 nm bandwidth. It should be noted that for both quantities, the ordinate is arbitrary, and that they are only proportional to the absorption and stimulated emission cross sections. Hence, if Figure 7 is regarded as a plot of the cross sections then they are not normalized with respect to each other. The temperature values are 500°C and 1000°C.

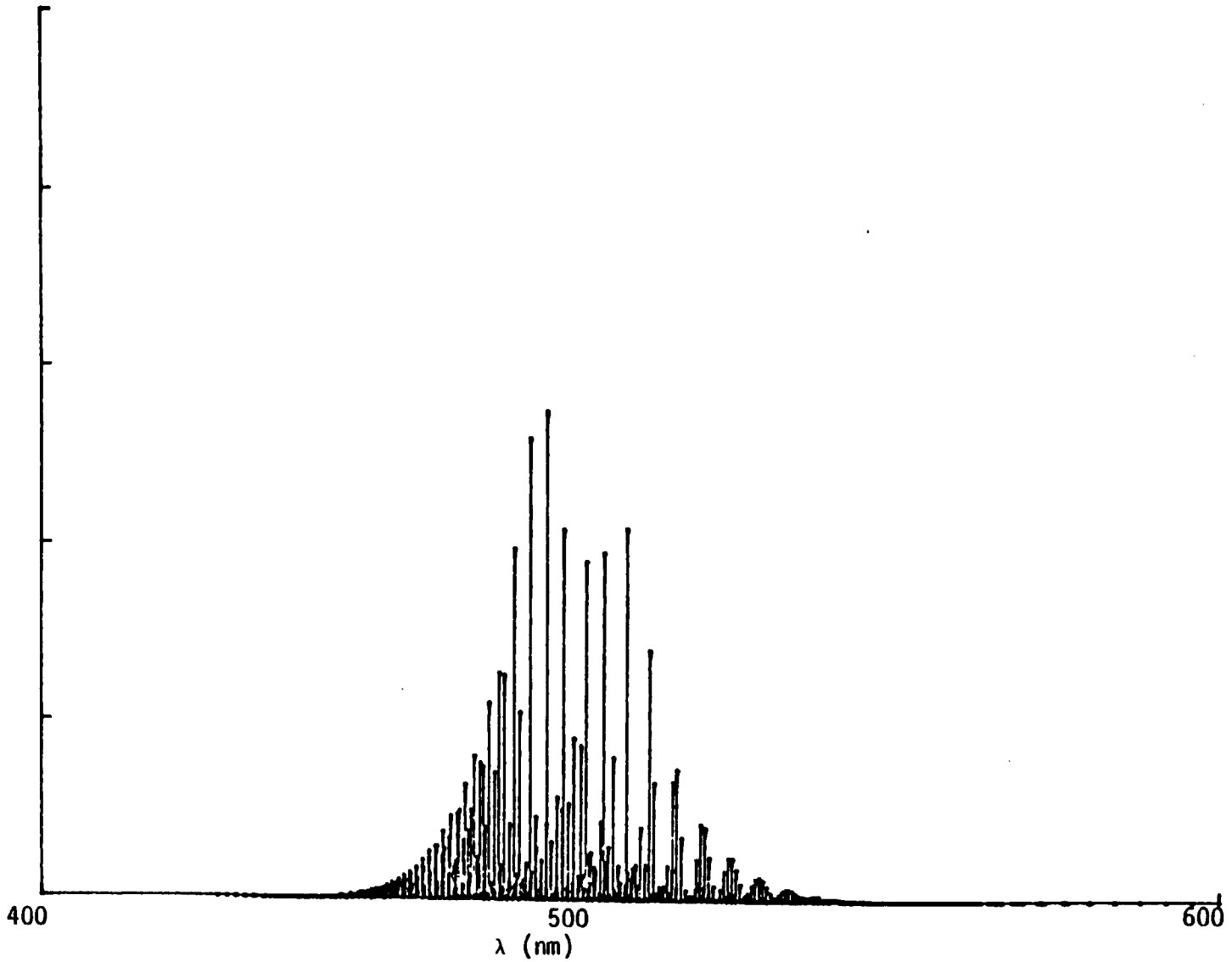

Fig. 5. Plot of $Q(\lambda)$ vs λ for Na_2 at 650°C. The ordinate is arbitrary.

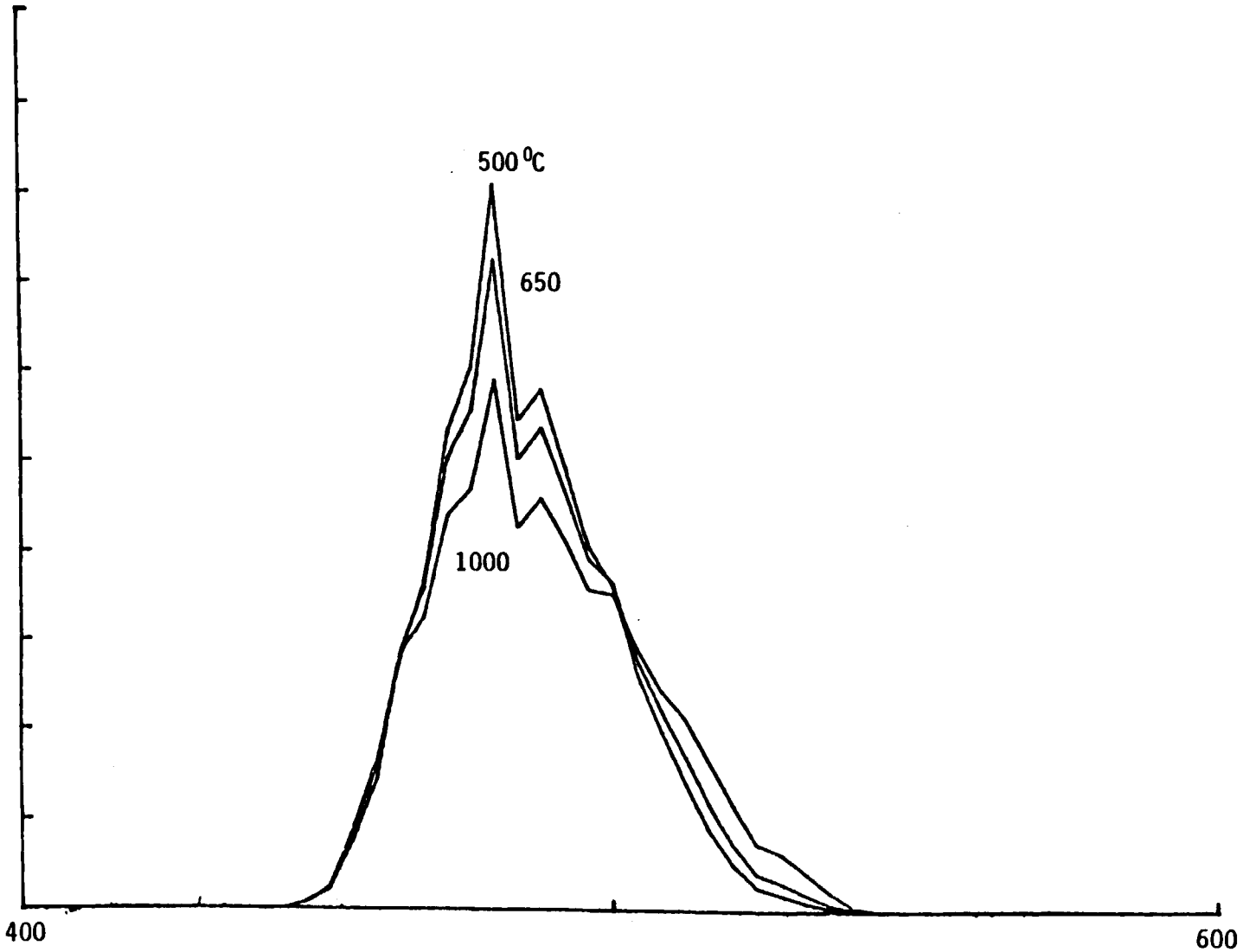

Fig. 6. Plots of $Q(\lambda)$ vs λ for different temperatures where the values have been averaged over 5 nm intervals.

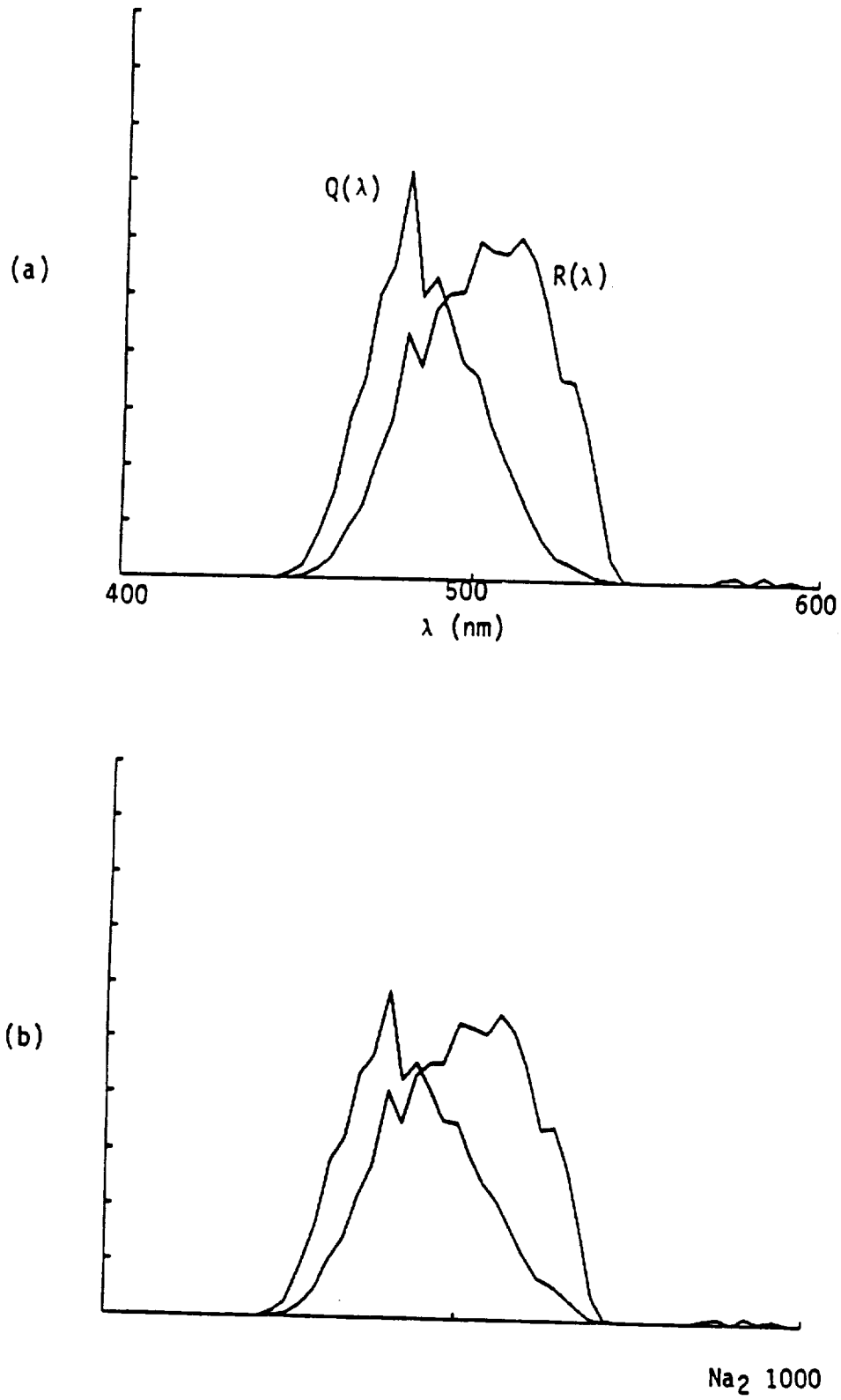

Fig. 7. Comparison of the quantities $Q(\lambda)$ and $R(\lambda)$ as functions of λ. The quantities are not normalized to each other, (a) T = 500°C, (b) T = 1000°C. The bandwidths are assumed to be 5 nm.

It is evident that the R(λ) curve is shifted to the right of the Q(λ) curve, suggesting a region between 500 and 540 nm where stimulated emission would dominate over self absorption.

C. Alternative Method of Comparing Emission and Absorption Cross Sections

The absorption cross section for a molecule is given by[6]

$$\sigma_a = \frac{A_{13}}{8\pi c^3} \lambda_a^2 \qquad (4\text{-}7)$$

where A_{13} is the Einstein coefficient for the transaction $1 \rightarrow 3$, λ_a is the absorption wavelength, and c the velocity of light. The emission cross section is given by

$$\sigma_e = \frac{\lambda_e^4 A_{32}}{4\pi^2 c \, \Delta\lambda_e} \qquad (4\text{-}8)$$

where λ_e is the emitted wavelength, A_{32} the Einstein coefficient for the transition from level 3, the upper lasing level to level 2 the lower lasing level $\Delta\lambda_e$ here is the emission bandwidth. If we consider the possibility of absorbing the wavelength λ_e, then $\lambda_a = \lambda_e$ and the ratio $\frac{\sigma_e}{\sigma_a}$ is then

$$\frac{\sigma_e}{\sigma_a} = \frac{2c^2}{\pi} \frac{A_{32}}{A_{13}} \frac{\lambda_e^2}{\Delta\lambda_e} \qquad (4\text{-}9)$$

and increases with λ_e^2. The expression may hold in the region between 5 and 5.4 nm in Figure 7, but clearly does not hold elsewhere.

Assuming λ_e = 525 nm, $A_{13} = A_{32} = 1.9 \times 10^7$ s-1 and that $\Delta\lambda_e$ is determined by Doppler broadening, ($\Delta\nu$ = 3 Ghz, $\Delta\lambda_e = 9.2 \times 10^{-13}$m)[7] then $\sigma_a = 6.9 \times 10^{-14}$ cm^2, $\sigma_e = 1.3 \times 10^{-12}$ cm^2 and the ratio $\frac{\sigma_e}{\sigma_a} = 19$.

D. Conclusions

The above independent check of the values of σ_e and σ_a in the wavelength range 5 to 5.4 nm showed $\frac{\sigma_e}{\sigma_a} = 19$. The plots of $Q(\lambda)$ and $R(\lambda)$ are not normalized, but at 5.25 nm show the ratio $\frac{R(\lambda)}{Q(\lambda)}$ to be about 3, suggesting the $R(\lambda)$ curve should be about six times higher. The form of the curves show that the only region where lasing should be attempted in Na_2 is between 5.2 and 5.4 nm. This conclusion is consistent with the fact that lasing at 5.25 nm has been reported by Wellegehausen.[6]

4.1.2.2 Densities of Dimers and Monomers in Metallic Vapors

A. Summary

The dimer/monomer ratio is derived for metallic vapors as a function of temperature. The basic physical mechanisms are dissociation caused by collisions with energetic atoms, and three body recombination in the gas phase, and the creation of a saturated vapor at the gas-liquid interface. Increasing the temperature increases the collision and recombination rates so the dimer/monomer ratio rises. The effect of Na_2 acting as a third body in the recombination process is included for the first time.

B. Introduction

The possibility of using metallic vapors in lasers for solar energy conversion is appealing as they could operate at high temperatures. The lasing medium would be the dimers, which in many instances consist of only a small fraction of the gas particles. Plots of this fraction as a function of temperature were given by Lapp and Harris,[8] from results of Stull and Sinke[9] but without explanation. The purpose of this paper is to understand the processes which are occurring and to duplicate these

results. The effect of the dimers acting as third bodies are included for the first time.

C. Physical Processes Occurring in Metallic Vapors

The vapor consists of a mixture of monomers and dimers boiled from the liquid phase, with a metallic wick connecting the regions of high and low temperatures. In the vapor phase, it is assumed that the reactions of dissociation and recombination can occur as shown in Table I.

Table I. Reactions Occurring in the Vapor Phase

Type of reaction

Dissociation	a	$Na_2 + Na' \xrightarrow{-k_f} Na + Na + Na$
Three body recombination	b	$Na + Na + Na \xrightarrow{k_r} Na_2 + Na$
	c	$Na + Na + Na_2 \xrightarrow{k_s} Na_2 + Na_2$

It is assumed that dissociation of Na_2 occurs according to reaction a in Table I where k_f is the rate coefficient, and Na' is an atom with kinetic energy exceeding D_o, the dissociation energy of Na_2, and hence in the tail of a Maxwellian distribution:

$$Na'/Na = \exp(-D_o/kT) \tag{4.10}$$

Recombination in the gas occurs by three body collisions, and it will be assumed first that the predominating third body is Na, an assumption that works well at low temperatures as will be seen later. Hence, reaction b of Table I dominates. The rate equation for Na_2 is then

$$\frac{d(Na_2)}{dt} = -k_f\, Na_2\, Na' + k_r\, (Na)^3 \tag{4.11}$$

In the steady state, equations (4-10) and (4-11) yield

$$\frac{Na_2}{(Na)^2} = \frac{k_r}{k_f} \exp\ (D_o/kT) = K \qquad (4.12)$$

where K is a constant for a given temperature.

Fortunately, reference (8) gave values of the partial pressures of dimers and monomers at a fixed temperature for several metals and if D_o is known, then the quantity k_r/k_f can be calculated. Equation (4-12) can then be used to calculate $Na_2/(Na)^2$ for any temperature.

The saturated vapor pressures of metals are well known and usually given in the form[10]

$$\log_{10} p = -\frac{0.05223}{T} a + b \qquad (4.13)$$

where p is in torr, T in degrees K and a and b are characteristic of the metal. The expression is valid from 180°C to 883°C.

The vapor pressure is also

$$p = (Na_2 + Na)\ kT \qquad (4.14)$$

and on rearranging equations (4-13) and (4-14)

$$Na_2 + Na = \frac{1}{kT} C \exp(-Q/kT) \qquad (4.15)$$

where C and Q are obtained from equation (4-13). Equations (4-12) and (4-15) then give solutions to Na, Na_2, and Na_2/Na.

Data for four metals are given in Table II, and plots of Na_2/Na are shown in Figure 8. The plots showed excellent agreement with the curves of Stull and Sinke.[9] For all the vapors, the dimer-monomer ratio increases with temperature. The reason is that at higher temperatures the densities of the particles increase and hence, the recombination rate which is dependent on three body collisions increases faster than the dissociative rate.

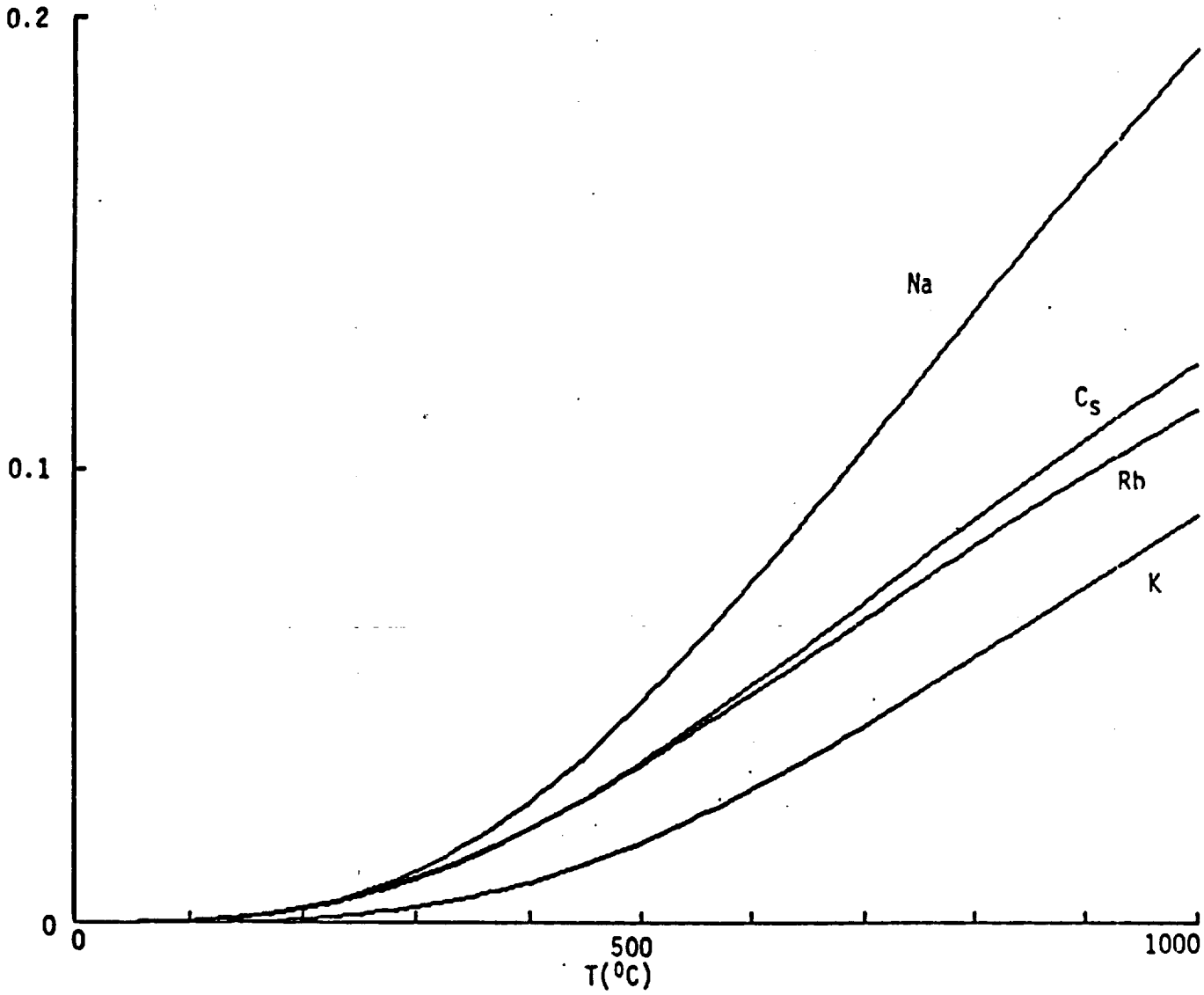

Fig. 8. Plots of dimer/monomer ratio vs T for different metal vapors.

Table II. Data for Metals

Vapor pressure constants[3]			Partial Pressures at 700K (torr)[1,2]		D_o(eV)
	a	b	Monomer	Dimer	
Na_2	103300	7.553	0.69	2.2×10^{-2}	0.730
Rb	76000	6.976	19.40	0.454	0.490
Cs	73400	6.949	27.60	0.625	0.450
K	84900	7.183	7.24	8.2×10^{-2}	0.510

Three body collision where Na_2 is the third body have been neglected above. Also dissociative collisions from Na_2 molecules in the tail of the distribution. The error introduced is small within the temperature range of Figure 8, as at most they constitute less than 8% of the total particles.

D. Effect of Na_2 as a Third Body

The Na_2 molecules acting as third bodies contribute an additional recombination reaction (c) to reaction (b) in Table I. A rate coefficient k_s is introduced, different from k_r, but unfortunately, the values of k_r, k_s are not known. The rate equation for Na_2 now becomes

$$\frac{d(Na_2)}{dt} = - k_f Na_2 Na' + k_r Na^3 + k_s Na^2 Na_2 \qquad (4\text{-}16)$$

and in the steady state, using equation (4-10), we obtain

$$\frac{Na_2}{Na^2 + \frac{k_s}{k_r} NaNa_2} = \frac{k_r}{k_f} \exp (D_o/KT) \qquad (4\text{-}17)$$

Equations (4-17) and (4-15) then given solutions of Na, Na_2 and Na_2/Na.

Plots of Na_2/Na vs. temperature are shown in Figure 9 for the case of sodium where the effect of the dimers as third bodies is shown in terms of a parameter α defined as $\alpha = k_s/k_r$. Thus, when $\alpha = 0$ we revert to the case of Na_2 in Figure 8. The temperature scale is shown to be 1000°C although the range of validity of Equation (4-13) which leads to Equation (4-15) is only up to 883°C. As the ratio k_s/k_r is not known, the behavior of k_s can only be illustrated by the parameters $\alpha = k_s/k_r$.

E. Conclusions

The dimer/monomer ratio calculated as a function of temperature for four different metal vapors showed excellent agreement with the curves of Stull and Sinke,[9] indicating that dissociation, three body recombination, and the creation of a saturated vapor were the basic processes occurring. Inclusion of the dimers at third bodies, in recombination collisions, increased the dimer/monomer ratio slightly at higher temperatures.

4.1.2.3 Metastability of N_2, Na_2, and CO

N_2 and CO when vibrationally excited are long lived and metastable, whereas the vibrational levels in Na_2 are short lived. An investigation showed that polarizability was not the cause of the short lifetimes--the Na_2 had the smallest polarizability. A comparison of the vibrational frequencies, ω_e, showed that the metastable N_2 and CO had much greater values by a factor of over 10, to the Na_2; the reduced masses, μ, were of the same order for all three. The spring constants of the molecules, proportioned to $\omega_e^2\mu$ were about 100 times greater for N_2 and CO than for Na_2.

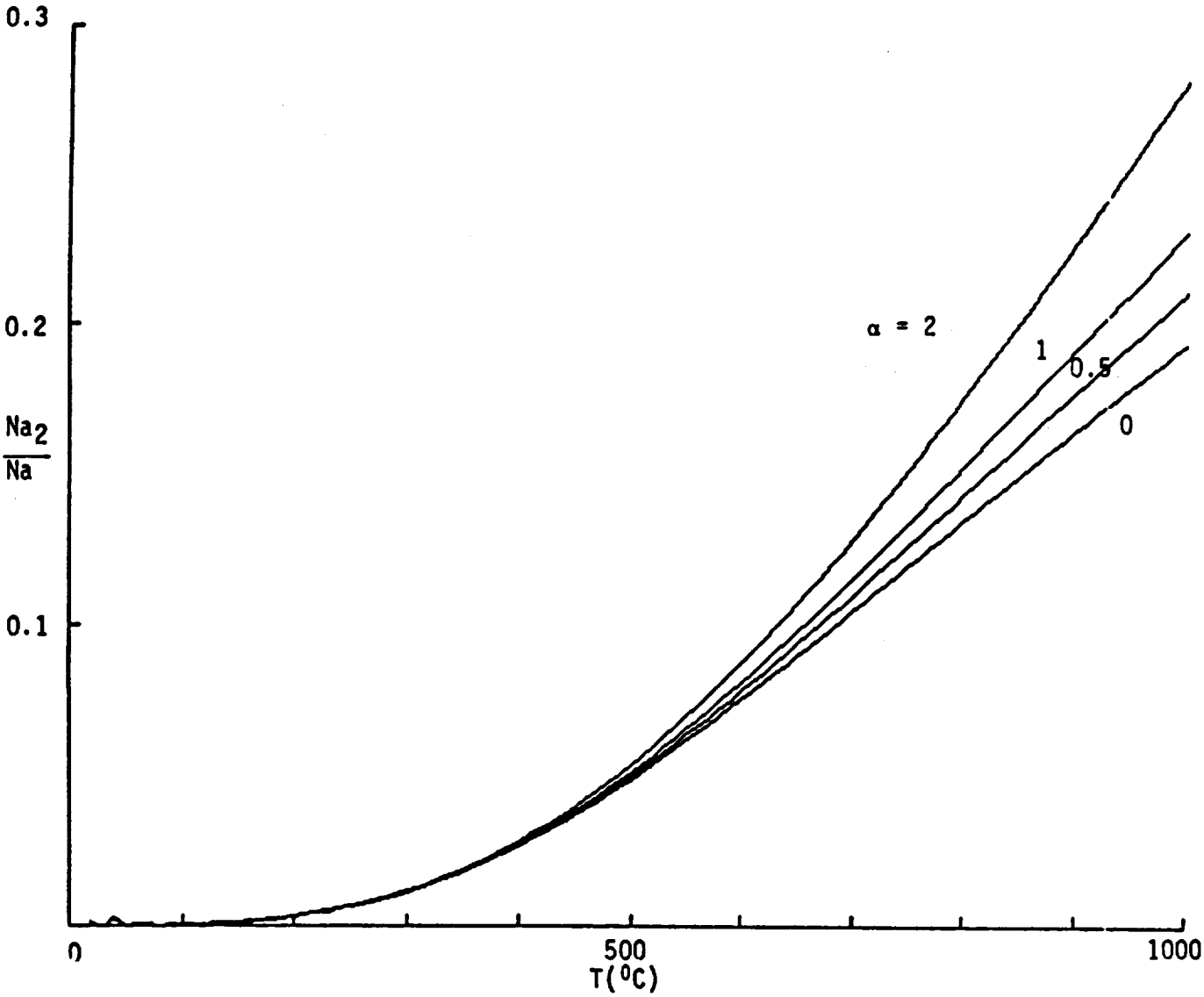

Fig. 9. Effect of Na_2 as a third body on the dimer/monomer ratio vs temperature. The quantity α is equal to k_s/k_r where k_s is the rate coefficient for three body recombination where Na_2 is the third body, k_r where Na is the third body. The case $\alpha = 0$ corresponds to the curve for sodium in figure 2.1. The curves were valid only up to 883°C.

The spring constant determines the shape of the potential energy curves for the molecules; these are very flat with closely spaced vibrational energy levels for Na_2. In contrast they are very steep sided with widely spaced vibrational energy levels for N_2 and CO. In the case of Na_2, the vibrational levels have a spacing of the same order as the thermal energy of the molecules, ~0.02 eV and thermal collisions can deactivate the Na_2. With N_2 and CO, the spacing is of order 0.3 eV--much greater and consistent with the long lived behavior.

The short time of transfer from one vibrational level to the other in Na_2 may be advantageous as the energy from levels which are several quantum numbers above the upper laser level could be transferred to it. The population of the lower laser level would also in turn be quickly depleted by thermal collisions.

4.1.2.4 Specific Metallic Vapor Laser Systems

A. The Na_2 Metallic Vapor Laser

A.1 Photon Absorption

The Einstein coefficient for transitions from the lower level 1 to the upper level 3 (Figure 10) of the Na_2 laser is $A_{13} = 107$ s-1.[11] The absorption cross section is large, $\sigma_a = A_{13}/8\pi c\nu^2_{13} = 3\times10^{-14}$ cm^2 for absorption around 500 nm. The absorption length L then turns out to be $10^{-3}/p$ (cm) where p is the pressure of Na_2 vapor in torr. For reasonable active lengths, low pressures are necessary. The estimate of L is consistent with lasing in supersonic beams of Na_2 with an active length of order 1 mm. However, the fraction of the vapor which is in the form of Na_2 is about 0.04 by number, with the remainder in the form of Na at around 700K where the laser operated.[12]

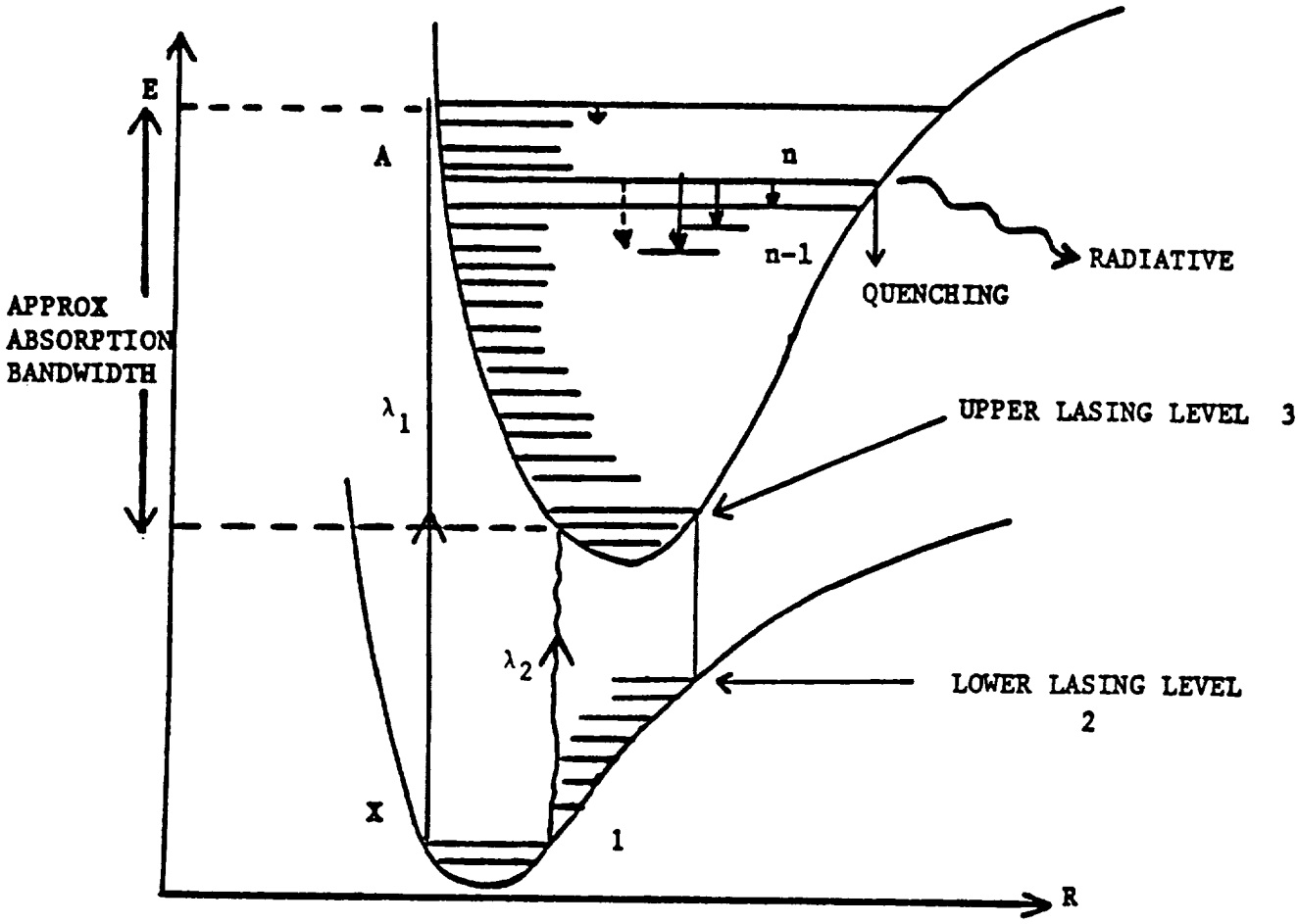

Figure 10. Energy level diagram for a solar pumped dimer molecule M_2. The vibrational levels only are shown. A molecule raised to level v' of the upper electronic A state can descend to the (v'-1), (v'-2)..., levels by collisions (continuous arrows) (and radiation-dotted arrows for heteronuclear molecules) and remain in the upper electronic state. Otherwise, it may radiate a photon (wave arrow) or be quenched and then drop to the lower electronic X state.

A.2 Choice of the Lasing Levels

The lower laser level 2 (Figure 10) must have a population of less than half that of the ground level 1 so that it can be adequately depleted.[12] The reason is that the maximum population density achievable in level 3 with a strong pump source is $\bar{n}_3 = \bar{n}_1$. This means that (neglecting statistical weights) the density of level 1 at temperature T is divided into 2 between levels 3 and 1: $\bar{n}_3 = \bar{n}_1 = n_1(T)/2$ where $n_1(T)$ is the normal Boltzmann population. Population inversion is therefore possible only if $n_1(T)/2 > n_2(T)$.[11] At 800 K, the lowest value of the quantum number v" for level 2 is v" = 3. Lasing to the v" = 3 level would originate near the v' = 0 level in the upper electronic state. The low value of v' is helpful in utilizing most of the populations of states with higher v', provided they can relax downward. Level 2 must be depleted by collisions thus requiring a buffer gas such as Argon.

The closeness of the vibrational energy levels in both ground and electronically excited states raises the question of whether there could be lasing from more than one upper level to a corresponding lower level. The two transitions would have to be equal in frequency within the emission bandwidth of 3 GHz, but this is unlikely because the spacing of the vibrational levels is around 6×10^{12} Hz or 2000 times greater.

A.3 Requirement for Collisional Relaxation in the Upper Electronic State

The collisional relaxation rate for levels near the upper laser level must exceed the spontaneous emission rate (neglecting quenching for the moment), other wise the density of molecules in the upper level will not increase before threshold. If Argon collisions dominate, the requirement is:

$$(Na_2)\ (Ar)\sigma_3 v_3 > (Na_2)\gamma^\circ_3 \qquad (4\text{-}18)$$

where the quantities in parenthesis are densities, σ_3 the cross section, v_3 the relative velocity and γ_3° the spontaneous emission rate. With σ_3 = 5×10^{-15} cm^2, $v_3 = 7 \times 10^4$ cm^{-1} and $\gamma_3^\circ = 1.4 \times 10^8$ s_1^{-1} (Appendix D) the inequality is satisfied for Argon pressures greater than 11 torr.

A.4 Requirement for Stimulated Emission to Exceed Collisional Relaxation

Lasing requires the stimulated emission rate to exceed the collisional relaxation rate out of v_u' of the upper state. The stimulated emission depends on the inverted population density and emission cross sections. Assuming the upper level to be $B^1\Pi_u$, with an angular momentum quantum number of 1, and the lower level to be $X^1\Sigma_g^+$ with no angular momentum, then the multiplicities for the upper and lower levels are $g_u = 2$ and $g_e = 1$. The inverted populated density is:

$$\Delta n = (Na_2, v_u') - 2(Na_2, v_\ell'') \qquad (4\text{-}19)$$

where the quantities in parentheses are the densities in the upper and lower laser levels, respectively. It follows that (Na_2, v_u') must exceed 2 (Na_2, v_ℓ'') for lasing. The emission cross section $\sigma_e = \lambda_e^4 A_{32}/4\pi^2 c\Delta\lambda_e cm^2$ is evaluated at 1.3 x 10-12 cm^2.[11] Here λ_e is the emission wavelength 525 nm, $A_{32} = 1.9 \times 10^7$ s^{-1} and the emission bandwidth $\Delta\nu = 10^9$ Hz (corresponding to Doppler broadening at 800K). The above value for σ_e agrees roughly with the quoted value 3×10^{-12} cm^2.[11] The requirement that stimulated emission exceeds depletion by collisions of the upper level is:

$$nc\ \sigma_e\ \Delta N > (Na_2, v_u')\ (Ar)\ \sigma_3\ v_3 \qquad (4\text{-}20)$$

where n is the photon density during lasing. For pressures corresponding to 0.04 torr of Na_2 and 0.96 torr of Na and 60 torr of Argon, this is equivalent to requiring $n\Delta n/(Na_2, v_u') > 2 \times 10^{10}(cm^{-3})$ which should be

easily satisfied if $n\Delta n \geq 10^{12}$ and less than 10 percent of the Na_2 atoms were in the upper laser level.

A.5 Requirement for Collisional Relaxation in the Lower Laser Level

For CW operation the total relaxation rate for the lower laser level must be greater than the spontaneous transition rate for a specific transition 3→2 or (Na_2, v_l'') (Ar) $\sigma_3 v_3 > (Na_2, v_u')\ A_{32}$. With the above numbers and $A_{32} = 1.9 \times 10^7 s_1^{-1}$, the condition is equal to $(Na_2, v_u') / (Na_2, v_l'') < 40$, which is easily realized.

A.6 Probability of Filling the Upper Laser Level

The energy level diagram of Na_2 (Figure 11)[13] shows numerous vibrational levels (of quantum numbers v' and v" in the upper and lower electronic states) spaced closely together. At 800 K, there is a one percent probability of filling the v" = 10 vibrational state, and an absorption transition then populates an upper vibrational level with v' about 30. The energy must be transferred to the upper laser level without being dissipated from the molecule. A rough estimate of the probability of arriving at the upper lasing level v_u' from a higher vibrational level v' will now be made.

The molecule can drop from a higher to a lower vibrational level by collisions. A model by Landau and Teller[14] enables an estimate to be made of the number of collisions required for a transfer of vibrational into translational energy and the number is of order 1 for Na_2 ($^{4.1.2.4}$ C). The vibrational levels in the upper electronic state are about 120 cm^{-1} apart corresponding to 170 K. If the gas temperature is 800 K, assuming the energy exchanged is equal to half the kinetic energy, then the jump in vibrational levels corresponds to $\Delta v' = \pm 2$, and the transition can be

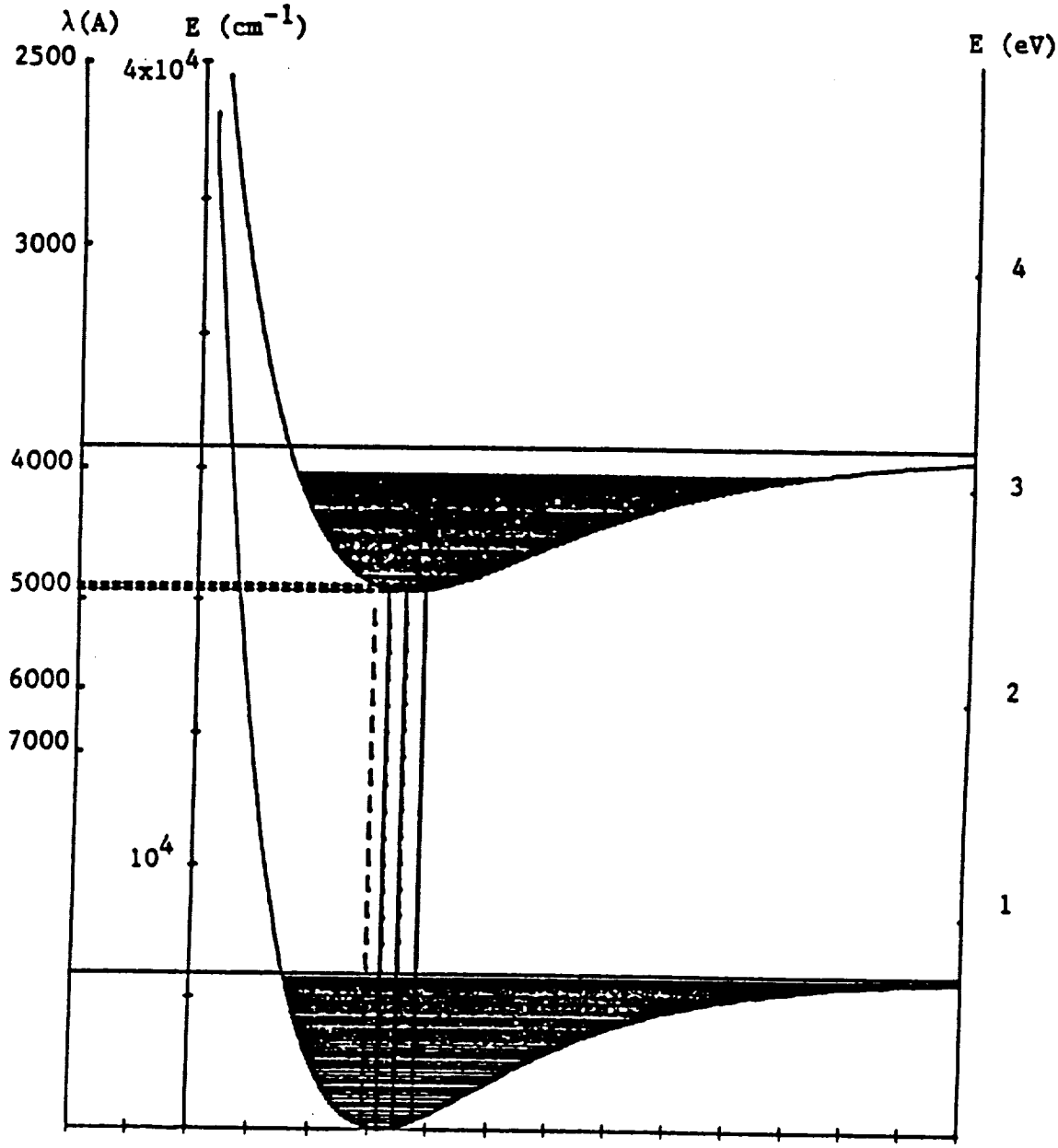

Figure 11. Energy diagram for Na_2 showing the lower level $(X)^1\Sigma_g^+$ and the upper level $B^1\Pi_u$. There are 109 vibrational levels in the lower electronic state; only 45 are shown. There are 88 levels in the upper state; 50 are shown. The vertical dotted lines correspond to Franck Condon transitions upward from the v" = 0 level. The solid lines correspond to downward transitions from the v' = 0 level in the $B^1\Pi_u$ state which end in the v" = 3 level.

either upwards or downwards. Such collisions can be due either to Na_2 molecules or Argon atoms ($\sigma_3 = 5 \times 10^{-15}$).[11] Collisions of this kind leave the molecule still in a vibrational level in the upper electronic state.

The rate equation for relaxing from level v' to level (v' ± Δv') is:

$$\frac{d}{dt_r} (Na_2,v') = (Na_2,v') \ (Na_2)\ \sigma_1 v_1 + (Na_2,v')\ (Ar)\sigma_3 v_3 \qquad (4\text{-}21)$$

where (Na_2,v') is the density of Na_2 molecules of vibrational quantum level v', and $\sigma_1 = 10^{-14}$ cm^2 and $\sigma_3 = 5 \times 10^{-15}$ cm^2 are the cross sections for collisions with Na_2 molecules of relative speed v_1 and Argon of relative speed v_3. All collisions with Na are assumed to result in quenching,[11] (see below).

The processes which cause the molecule to relax from the upper to the lower electronic state (apart from stimulated emission) are spontaneous emission of a photon (rate coefficient $\gamma_3^\circ = 1.4 \times 10^8 s^{-1}$)[11] and quenching. Hence, the rate of spontaneous emission from the upper electronic state to the ground state is:

$$\frac{d}{dt_s} (Na_2,v') = (Na_2,v')\ \gamma_3^\circ \qquad (4\text{-}22)$$

Quenching can be due to Na_2 or Na. The quenching cross section for Na_2, σ_4 is probably around 10^{-14} cm^2, but the fraction of Na_2 is small. The quenching cross section of Argon is assumed to be negligible as it has no degrees of freedom. The cross section for Na is large ($\sigma_5 = 6 \times 10^{-14}$ cm^2).[11] The reason is that the Na forms complexes with Na_2 which have internal degrees of freedom and can absorb the energy drop of 2×10^4 cm-1, before splitting up into an Na_2 molecule in the lower electronic level possessing vibrational and rotational energy and an Na atom, both with high kinetic energy.

$$(Na_2,v') + Na \rightarrow Na_3^* \rightarrow Na_2 + Na + \Delta E$$

The quenching rate from vibrational quantum level v' is:

$$\frac{d}{dt_Q}(Na_2,v') = (Na_2,v')\,(Na_2)\sigma_4 v_1 + (Na_2,v')(Na)\sigma_5 v_2 \qquad (4\text{-}23)$$

and v_2 is the relative speed of Na.

The probability that a collision will leave the molecule in the upper electronic state is then:

$$f = \frac{d}{dt_r}(Na_2,v') \cdot \left\{ \frac{d}{dt_r}(Na_2,v') + \frac{d}{dt_s}(Na_2,v') + \frac{d}{dt_Q}(Na_2,v') \right\}^{-1} \qquad (4\text{-}24)$$

The Na_2 laser experiments were performed at a total pressure of Na + Na_2 of about one torr with Argon pressures of many tens of torr. A plot of f vs. Argon pressure for these conditions for different percentages by number of Na_2 (from 2 to 20 percent) (Figure 12) shows that f increases with Argon pressure but is not very sensitive to the Na_2 fraction (and therefore also to σ_1 and σ_4).

The experiments with laser pumped Na_2 vapor showed that the power output dropped to zero at about 70 torr of Argon, and the reason quoted was the increase of the relaxation rate of the upper laser level due to Argon collisions.[11] It is possible this effect would not occur in a solar pumped laser, because the relaxation process would supply the upper laser level from levels above v'_u, as well as deplete it. Should pressures above 70 torr be unworkable then $f \leq 0.7$ (Figure 11). On the other hand, if it were possible to use 300 torr of Argon then $f \simeq 0.9$. The quenching by Argon is assumed small.[12]

There are 88 vibrational levels in the $B^1\Pi_u$ state, and levels up to about n = 30 will be occupied. The probability of arriving at $v'_u = 0$ from a higher v' is next roughly estimated. The spacing of the vibrational levels is assumed constant at ω_e cm^{-1}. The collisions that transfer

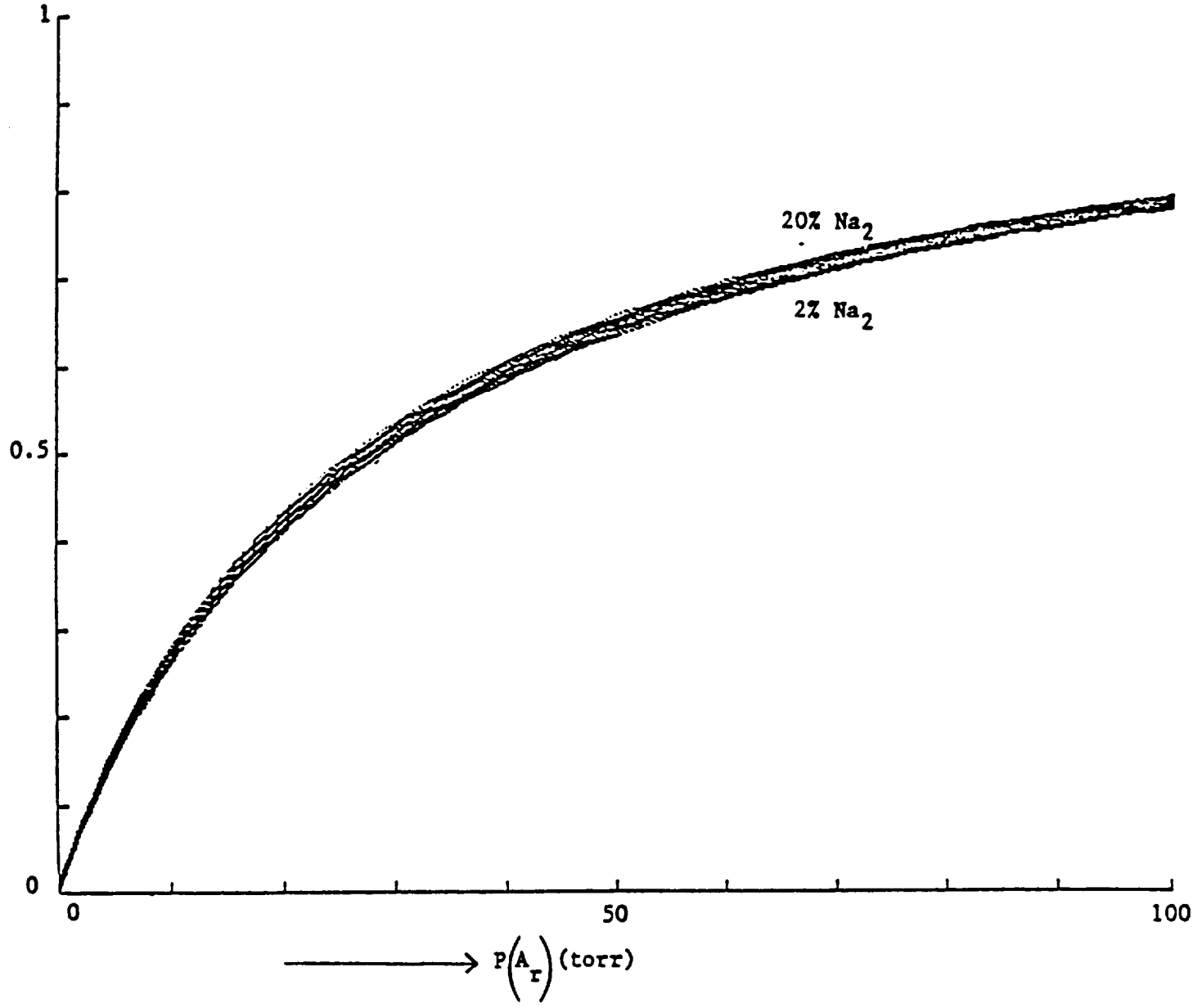

Figure 12. Plot of f, the fraction of molecules that stay in the upper level per collision vs Argon pressure for different fractions of Na2 in a total pressure Na + Na2 of one torr.

vibrational to translational energy can raise or lower the molecule from vibrational level v' to $v' \pm \Delta v$. The molecule as it changes its vibrational levels through collisions, performs a one dimensional random walk in energy space with a step length $\Delta v' \omega_e$ (cm^{-1}) and has to travel a distance $(v'_u - v'_e)\omega_e$ to arrive at the upper lasing level v'_u. The "diffusion coefficient is $(\Delta v' \omega_e)^2 \nu_c$ where ν_c is the collision frequency. The diffusion equation $(v' - v'_u)^2 \omega_e^2 = (\Delta n \omega_e)^2 \nu_c t$, gives the number of collisions $N = \nu_c t$ as:

$$N = (v' - v'_u)^2 / (\Delta v')^2 \qquad (4\text{-}25)$$

The equation is approximate as it assumes a constant step length, but is sufficient for illustration.

If a fraction f of the molecules stays in the upper electronic state at each collision, then in N collisions, the fraction remaining is on the average:

$$F = f^N \qquad (4\text{-}26)$$

e.g., if for Na_2 $f = 0.7$, $\Delta v' = 2$, $v' - v'_u = 10$, then $F = 1.3 \times 10^{-4}$. But if $f = 0.9$, then $F = 0.39$.

Assuming all the vibrational levels above v'_u are filled with equal probability (not too inaccurate an assumption because only levels near v'_u contribute), then the contribution to the level v'_u from all levels is

$$S = \sum_{v'=v'_u+1}^{\infty} f^{[(v' - v'_u)/Dv']^2} \qquad (4\text{-}27)$$

The summation converges rapidly with increasing v' especially if f is small. For example, if $f = 0.7$, $\Delta v' = 2$ then $S = 2.47$, but if $f = 0.9$ then $S = 4.96$. This is equivalent to saying that the first 2 (for $f = 0.7$) and 5 (for $f = 0.9$) levels, respectively, are the only ones that contribute to the upper lasing level.

If levels above n = 5 are essentially unusable for lasing, then Figure 11 shows the absorption bandwidth would correspond to 15 nm, the region between 476.6 to 490.6 nm. The solar efficiency ν_s for this narrow region is less than two percent.

A.7 Overall Efficiency of Na_2 Vapor Laser

The absorption efficiency η_A can be made to approach unity with very low Na_2 pressure if a path length of 1 cm is used. A rough estimate of the fraction of molecules of vibrational levels $v' \leq 5$ that arrive at the $v'_u = 0$ level can be made using Equation 4-27 which gives a value of about 0.5 if $f = 0.7$. We may call this a kinetic efficiency η_K. The quantum efficiency η_Q here approaches unity. Thus the overall efficiency $\eta = \eta_s\eta_A\eta_K\eta_Q$ is about 1 percent. If it is possible to increase the Argon pressure sufficiently to raise f to 0.9, then the overall solar efficiency would approach 2 percent.

B. The Li_2 Metallic Vapor Laser

The temperature required to operate the Li_2 laser was reported at 1000 K[11]--easily attainable with large solar collectors. The laser was also reported as having the lowest threshold power. The criteria of Section 3 should be satisfied for Li_2 as well as Na_2, as the coefficients are probably not very different.

B.1 Probability of Filling the Upper Laser Level

The critical item in the efficiency calculation is the probability $F = f^N$ (Eq. 4-26). The energy level diagram for the $X^1\Sigma_g^+$ and the $B^1\Pi_u$ states of Li_2 [13] shows the spacing of the vibrational levels is greater than Na_2. At 1000 K there would be one percent of the atoms in the $v'' = 7$ level and transitions up to about $v' = 30$ are possible.

The spacing of the vibrational levels in the upper state is about 250 cm^{-1} = 360 K or approximately half the gas temperature, and hence $\Delta v'$ here is about 1. Hence, $N = (v' - v'_u)^2$. The cross section for relaxation from vibrational level v' by collision is the same order of magnitude for Li_2 as for Na_2 (Section 4.1.2.4 C below). The rates and cross sections for Li_2 are not known, but should not be greatly different from Na_2.

B.2 Efficiency of the Li_2 Vapor Laser

At 1000 K vibrational level v" = 7 will have one percent probability of being occupied and the absorption bandwidth is from 400 to 490 nm. The cross sections and rate coefficients for Li_2 are not known, but it is likely that the overall efficiency would be of the same order as that of Na_2.

C. Probability of Vibrational to Translational Energy Transfer

The number of collisions Z required to deexcite a vibrational level n to a vibrational level $n \pm \Delta n$ is given by[14]

$$Z = Z_o \, Z_{osc} \, Z_{tr} \tag{4-28}$$

where Z_o is a geometrical factor of order 3, Z_{osc} is dependent on the vibration of the molecule and Z_{tr} or the translational energy of the impacting particle. Then for a molecule B C Struck by an atom A:

$$Z_{osc} = \frac{2M_B M_C}{M_B^2 + M_C^2} \cdot \frac{M_A + M_B + M_C}{M_A} \frac{1}{2\pi^2} \frac{\theta'}{\theta} \tag{4-29}$$

where the M's are the respective masses. The quantities θ and θ' are characteristic temperatures defined by

$$k\,\theta = h\nu = hc\,\omega_e \tag{4-30}$$

where k, h, c have their usual meaning and ω_e corresponds to the vibrational energy in cm^{-1}.

The temperature θ' is defined by

$$k\,\theta' = 16\,\pi^4\,\tilde{M}\,\nu^2\,L^2 \qquad (4\text{-}31)$$

where $\tilde{M}$ is the reduced mass, $\nu = \omega_e c$ the vibrational frequency, and L an interaction distance usually taken as 0.2 to 0.3A.

The quantity Z_{tr} is defined

$$Z_{tr} = \pi^2 \left(\frac{\theta}{\theta'}\right)^2 \sqrt{\frac{3}{2\pi}} \left(\frac{T}{\theta'}\right)^{1/6} \exp\left[\frac{3}{2}\left(\frac{\theta'}{T}\right)^{1/3} - \frac{\theta}{2T}\right] \qquad (4\text{-}32)$$

and T is the gas temperature in degrees Kelvin.

For the $B^1\Pi_u$ state of Na_2 with $\omega_e = 117.3$, L = 0.2A, then $\theta = 168.3$K, $\theta' = 2.316 \times 10^4$ K.

For T = 800 K, then $Z_{osc} \sim 7$, $Z_{tr} = 3.5 \times 10^{-2}$ which gives Z = 0.7 or on average all collisions with Argon deexcited the Na_2.

For the $B^1\pi_u$ state of Li_2 with $\omega_e = 255.5$, L = 0.2A then $\theta = 367.9$K and $\theta' = 1.552 \times 10^4$ K. Again taking Argon and T = 1000 K, then $Z_{osc} = 2.9$, and $Z_{tr} = 8.5 \times 10^2$. Hence, $Z \approx 0.7$ and approximately every collision deexcites the Li_2.

4.1.2.5 Summary of Non-Dissociative Lasers

A class of non-dissociative metallic vapor dimer lasers was investigated as potential solar energy converters. The high temperatures required for vaporization cause vibrational levels up to about v" = 10 to be occupied in the lower electronic state of Na_2. This allows broad band absorption essential for high efficiency and yields a wide range of levels (up to v' = 30) to be occupied in the upper electronic state. The upper laser level is at or near $v'_u = 0$, and the probability of the molecule relaxing to v'_u from higher v' is small because it has to do so in a number of collisions, for each of which there is the possibility of being quenched to the lower electronic state. Inclusion of Argon is essential to increase

the collisional relaxation rate to overcome quenching. In laser-pumped experiments, the upper limit of Argon pressure in Na_2 was about 70 torr, in which case the ratio of relaxation to total (including quenching) collisions would be 0.7. This means that for Na_2, essentially all levels above $v' = 5$ would contribute little to the lasing power, and that portion of the solar spectrum which caused transitions to $v' > 5$ was essentially unused. For levels with $v' \leq 5$ approximately half the collisions resulted in relaxation to level v'_u. Even so, the overall solar efficiency was 1 percent, a number which compares favorably with 1.2 percent for an IBr solar pumped laser.[12] If Argon pressures greater than 70 torr are possible, the efficiency would be increased. The numbers for Li_2 are not known, but it is probably its efficiency would not be greatly different. In addition to low efficiency, calculations by W.E. Meador of NASA/Langley have suggested that the threshold pumping levels would be much too high for practical use.

4.2 Lasers Which Absorb All the Solar Spectrum: Indirect or Blackbody Lasers

Indirect solar pumped lasers are often called blackbody lasers. The concept is that the total sun solar spectrum will be captured and changed into heat. A high temperature cavity will be created and thermal radiation from the blackbody cavity will be used as the pumping radiation for the lasers. Whatever bandwidth is absorbed by the lasing medium, the "hole" left in the spectrum, is then continually replenished by the blackbody radiation in the cavity. Thus, heat energy at wavelengths other than the absorbing wavelength is transferred into this part of the spectrum, and the whole spectrum is utilized.

Blackbody lasers have several advantages. First, in space, with appropriate thermal energy storage, they can operate in the earth's shadow

throughout an entire orbit. Second, they do not depend on the spectrum of the incident light, but only on the total quantity of energy which is degraded into thermal energy. Thus, chemical, electrical or nuclear energy can be used. Third, because the whole solar spectrum is utilized, the size of the collector-concentrator is reduced.

There are two types of blackbody lasers, the cavity type and the gas transfer type. In a cavity laser, the laser is enclosed within the blackbody cavity. Thus the lasant is subjected directly to the thermal radiation pumping. In the transfer laser, two gases are involved. The first of these, the transfer gas, flows through the blackbody cavity and becomes vibrationally excited by the blackbody radiation. Then the transfer gas is mixed with the lasant. Energy transfer occurs and the lasant emits radiation in the laser cavity. In 1982, the first in-cavity blackbody CO_2 laser was achieved by Professor Walter Christiansen at the University of Washington. In 1984, he achieved blackbody lasing with N_2O as the lasant. Also, in 1984, a model for comparison with the experiment was developed at the University of Washington to explain the results of some of the recent experimental work.(16) The author also developed a theoretical model for the in-cavity CO_2 laser in 1984.

In 1982, Langley developed its own transfer laser program starting with N_2 into CO_2. In 1985, the emphasis was shifted to other transfer-gas/lasant combinations particularly CO/CO_2 and CO/N_2O. Also in 1985, mathematical models of the CO/CO_2 and N_2/CO_2 lasers were initiated by the author at Langley, but the results were inconclusive as both the values and the variation of the rate coefficients with temperature were not well known. The portion of Figure 2 on page 10 starting with gas dynamic lasers was therefore studied only in a very preliminary fashion and no concrete

results were obtained. The work on both types of blackbody lasers was dropped in 1988 when the author pointed out that there was a serious limitation to all blackbody lasers. The limitations arose because the energy density in a cavity, determined by Planck's radiation formula, is limited. To get sufficient energy flow for high power would require the surface area of the lasing medium to be too large for practical use in high power lasers of outputs of order 100 KW to 1 MW. However the theoretical work carried out on direct blackbody pumped lasers could be useful in future investigations, especially of lower power lasers.

In Section 4.2.1, some general considerations for designing cavity blackbody lasers are outlined, and a calculation is made of the dimensions of the surface area of the laser medium for a 1MW laser. One factor in estimates of the power absorbed from blackbody radiation is that for certain geometries, e.g., slab or cylinder, illuminated from the outside the oblique rays travel along much greater path lengths than those normal to the surface. A method of calculating the effect was published in Optics Communications[17] and is shown as Appendix F. An actual CO_2 cavity laser is studied theoretically in Appendix G. Both steady and non-steady state outputs are illustrated and rough estimates of efficiency are given. The limitation on blackbody lasers due to the energy density and power flow is discussed in Section 4.2.2. Section 4.2.2, F gives overall conclusions for cavity blackbody lasers.

4.2.1 General Considerations for Designing Cavity Blackbody Lasers**

A. Introduction

The purpose of this study is to review briefly the physical processes which occur in a blackbody cavity laser and show how the characteristics of the lasing medium affect the efficiency when used as a solar energy converter. The characteristics of an "ideal" lasant will then be described. The blackbody concept[18] has been outlined by Dr. Walter Christiansen in the previous talk.

B. Overall Considerations of Lasing Media

In general, high laser efficiency requires a lasing medium of the molecular rather than atomic variety. The reason is that the laser efficiency depends on the "quantum efficiency" η_Q:

$$\eta_Q = (E_u - E_l)/E_u \tag{4-33}$$

where E_u and E_l are the energies of the upper and lower laser levels, respectively, Each absorbed photon gives up energy E_u, while the emitted photon possesses energy $E_u - E_l$, and to recover the absorbed energy η_Q should be high. Figure 13 compares atomic with molecular systems. For the atomic system shown $\eta_Q = 1/6$. Also shown is a range of energies for molecular dissociation leading to an excited atom X* which causing lasing. If 5eV were needed for dissociation, then as the energy of X* is usually 0.1 - 1eV, then $\eta_Q \leq 0.2$. Molecular levels are a few tenths of an eV above ground, but although both E_u and E_l are now quite low, η_Q is much higher, typically around 0.5 as shown. For CO_2, which we shall take as an example for the rest of this talk, $\eta_Q = 0.43$.

**Talk given in the Workshop on Lasant Materials for Black-body Pumped Lasers at NASA Langley, September 1985.

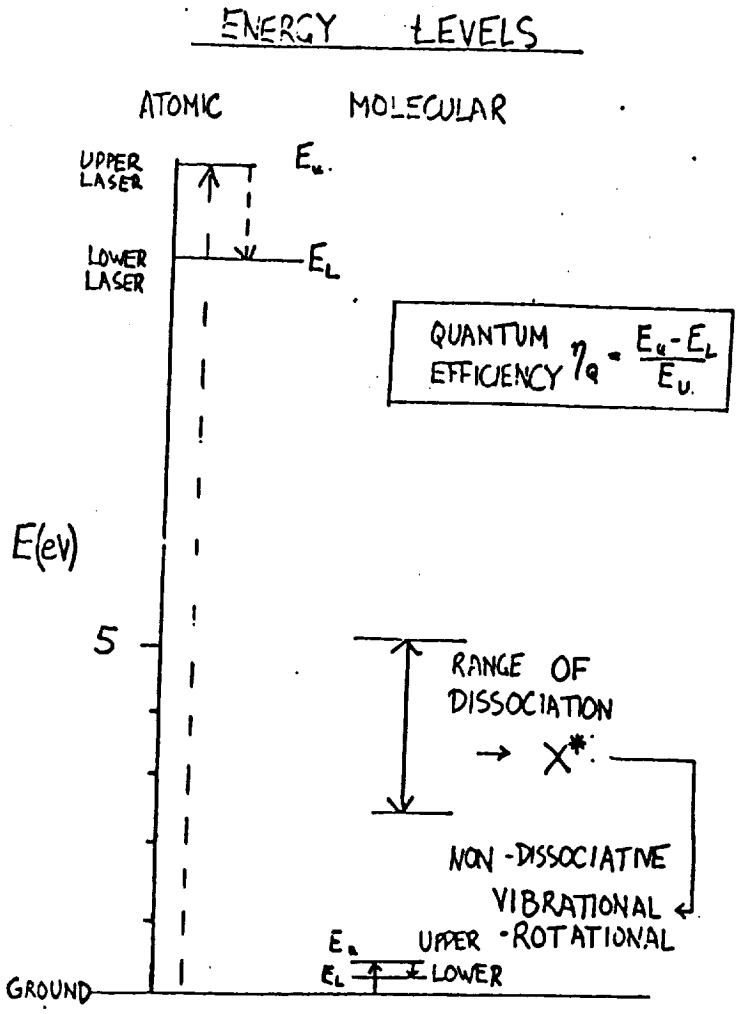
ENERGY LEVELS
ATOMIC
MOLECULAR
UPPER LASER
E_u
LOWER LASER
E_L
QUANTUM EFFICIENCY $\eta_Q = \frac{E_u - E_L}{E_u}$
E(eV)
5
RANGE OF DISSOCIATION
$\rightarrow X^*$
NON-DISSOCIATIVE
VIBRATIONAL
ROTATIONAL
E_u UPPER
E_L LOWER
GROUND

Figure 13

C. The Blackbody Cavity

The intensity of radiation in a blackbody cavity is given by Planck's radiation law and the radiation flux, $E(\lambda, T_b)$ per unit wavelength vs. λ for different cavity temperatures T_b are given in Figure 14. Also shown are the location of the absorption line for CO_2 at 4.256 μm, and a possible dissociation wavelength at 0.5 μm (2eV for Br_2). The peak wavelength λ_m and blackbody temperature T_b are connected by Wien's displacement law: $\lambda_m T_b = 0.29$ (cm K). An ideal lasant should absorb at a wavelength λ_a which approaches λ_m so that the increased radiation intensity would give higher laser output and also E_u and η_Q would be higher.

The blackbody cavity would re-radiate out through the orifice where the Sun's radiation entered (Prevost's theory of exchanges), leading to a cavity efficiency η_c:[18, 19]

$$\eta_c = 1\text{-}4(T_b/5785)^4 \qquad (4\text{-}34)$$

where 5785 is the Sun's temperature. A plot of η_c vs. T_b (Fig. 15) indicates that T_b should not be much greater than 2000 K, a value also predicated from material considerations.

D. The "Source Term" for the Upper Laser Level

The source term is the rate of pumping the upper laser level. It depends on the energy flux in the cavity, $E(\lambda_a, T_b)d\lambda_a$ (W-cm^{-2}) where λ_a is the absorption wavelength and $d\lambda_a$ the absorption bandwidth. This energy flux enters the laser medium and the fraction F per unit volume absorbed between a depth X_1 and X_2 below the surface is

$$F = \{\exp(-(CO_2)\ \sigma_a\ X_1) - \exp(-(CO_2)\ \sigma_a X_2)\}/(X_2 - X_1) \qquad (4\text{-}35)$$

where (CO_2) is the density of the absorbing medium, and σ_a its absorption cross section:

$$\sigma_a = \lambda_a^4\ A_{Gu}/4\pi^2 c\ d\lambda_a \qquad (4\text{-}36)$$

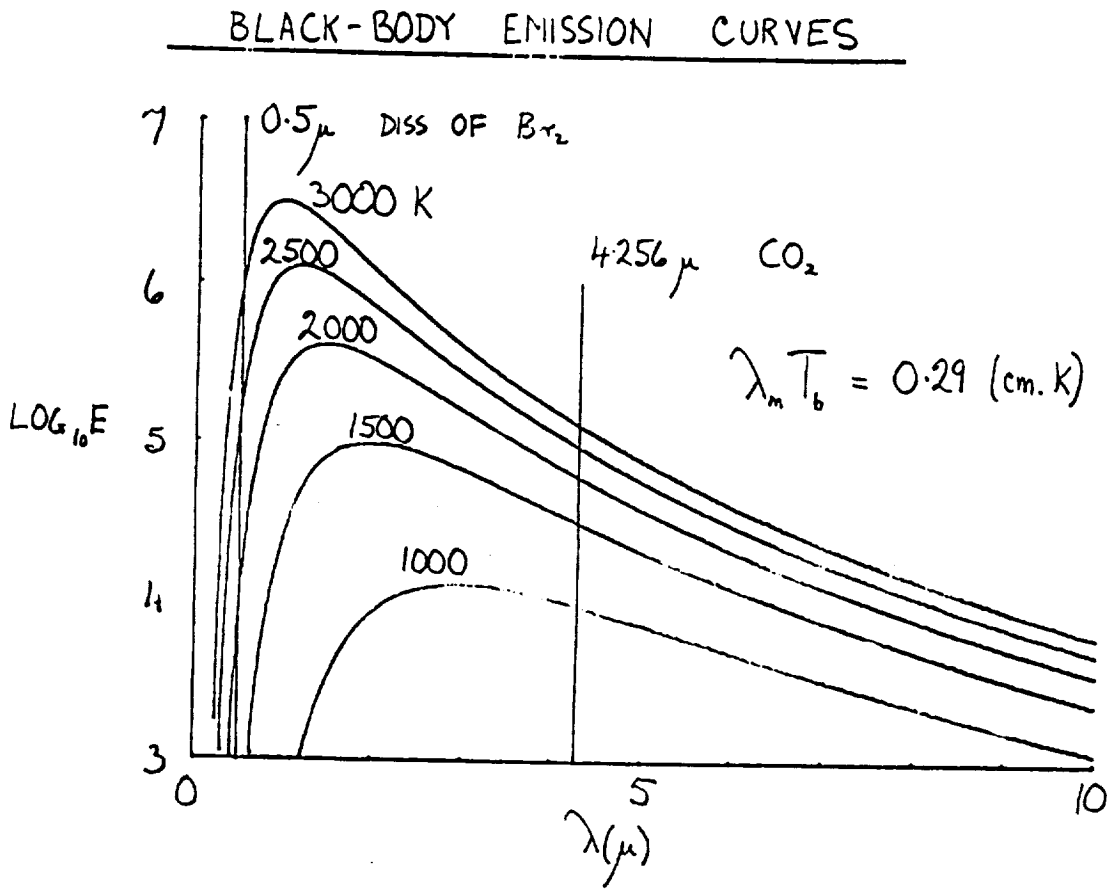
BLACK-BODY EMISSION CURVES
0.5μ DISS OF Br2
3000 K
2500
2000
1500
1000
4.256μ CO2
λm Tb = 0.29 (cm. K)
LOG10E
7
6
5
4
3
0
5
10
λ(μ)

Figure 14.

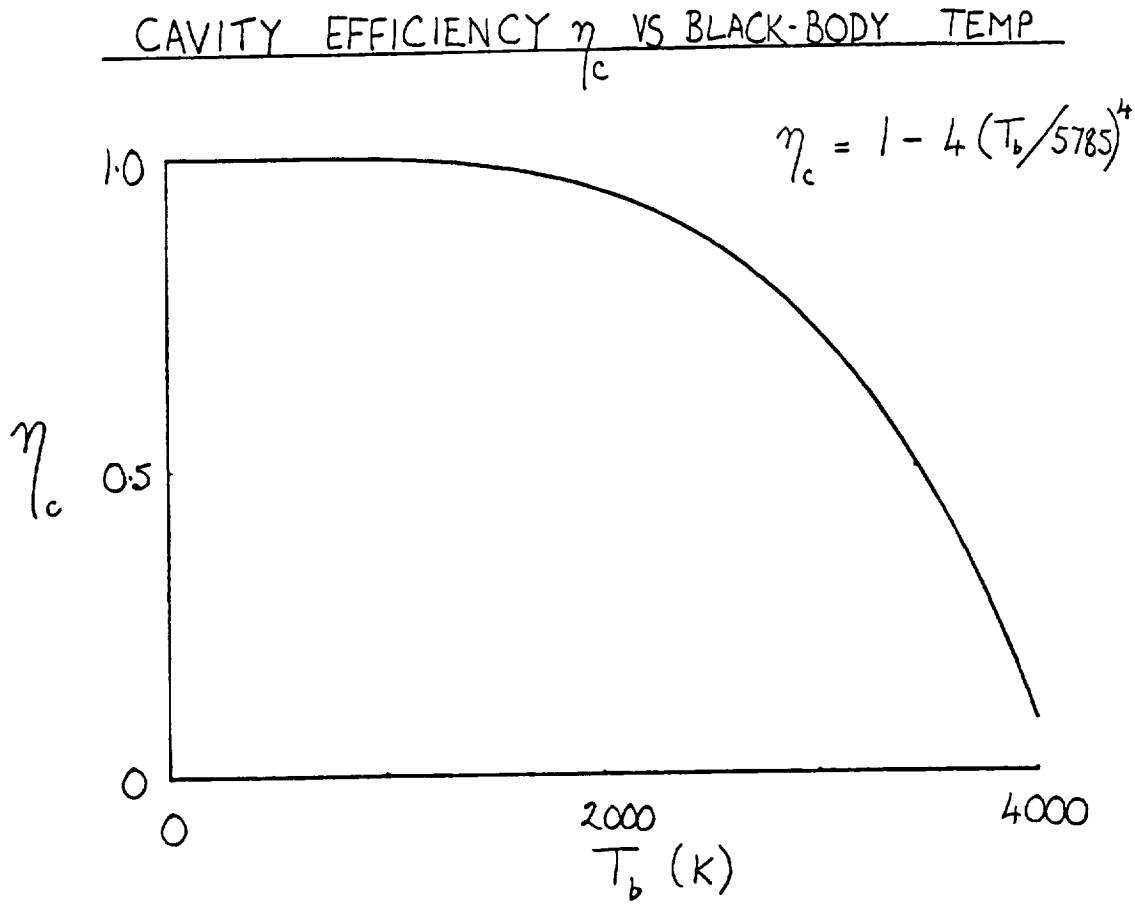
CAVITY EFFICIENCY η_c VS BLACK-BODY TEMP
$\eta_c = 1 - 4(T_b/5785)^4$
1·0
0·5
0
η_c
0
2000
4000
T_b (K)

Figure 15

where A_{Gu} is the Einstein coefficient for the transition ground to upper level, and c is the velocity of light.

The number of CO_2 molecules in the upper laser level (the asymmetric stretching mode, $CO_2(001)$) produced per cc per sec is

$$S = E(\lambda_a, T_b)\, d\lambda_a\, F\, \lambda_a/hc \qquad (4\text{-}37)$$

where h is Planck's constant and dividing by hc/λ_a converts the energy flux absorbed into frequency of events producing the upper laser level per cc.

The characteristics of the lasing material determining S are λ_a, $d\lambda_a$ and A_{Gu}, but S also depends on the density of the absorbing medium. The absorbing wavelength λ_a should be chosen to approach λ_m (Fig. 14). The value of σ_a is not too important, as S depends on $(CO_2)\ \sigma_a$--and a low σ_a can always be compensated for by increased CO_2 pressure (similarity law). Too high a value of the product $(CO_2)\ \sigma_a$ results in all the radiation being absorbed at the outer edges of the lasing medium near the walls, and X_1, X_2 and pressure should be chosen to maximize S. The absorption bandwidth $d\lambda_a$ should be high to increase $E(\lambda_a)d\lambda_a$, but high $d\lambda_a$ results in a lower σ_a.

The bandwidth $d\lambda_a$ for CO_2 absorbing at 4.256 μm is actually the sum of the bandwidths of about 30 closely spaced rotational levels near the asymmetric stretching mode vibrational level (Fig. 16). Each rotational level has a Doppler bandwidth $d\lambda_D$:

$$\frac{d\lambda_D}{\lambda_a} = 7.2 \times 10^{-7} \left(\frac{T_G}{M} \right)^{1/2} \qquad (4\text{-}37)$$

where T_G is the CO_2 gas temperature ($\approx$360 K) and M the molecular weight of 44. The Doppler widths could be increased with an ideal lasant of low M operating at high gas temperature. Increasing the bandwidths by pressure broadening might not be feasible if increased collisions depopulated the upper level.

ABSORPTION CROSS - SECTION

$$\sigma_a = \frac{\lambda_a^4 A_{GL}}{4\pi^2 c \, \Delta\lambda_a}$$

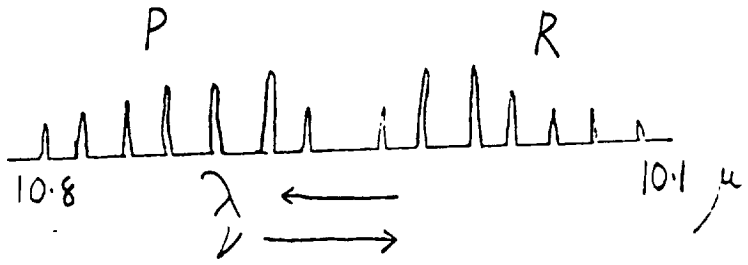

CO_2 HAS ABOUT 40 LINES EACH

WITH A DOPPLER WIDTH.

$$\frac{\Delta\nu_D}{\nu} = \frac{\Delta\lambda_D}{\lambda} = 7.2 \times 10^{-7} \left(\frac{T}{M}\right)^{\frac{1}{2}} \longleftarrow$$

SPACING OF ROTATIONAL LEVELS

$$\Delta\nu_R = \frac{\hbar}{2\pi I} \longleftarrow$$

I IS MOMENT OF INERTIA

Figure 16.

The spread of rotational lines from 10.1 to 10.8 μm in Figure 16 increases with gas temperature. The effective $d\lambda_a$ would increase if there were more lines, or the spacing of the rotational levels could be decreased. The spacing in frequency is

$$\Delta\nu = h/4\pi^2 I \qquad (4\text{-}38)$$

where h is Planck's constant and I the moment of inertia of the molecule. The ideal lasant should also have a low moment of inertia.

E. Kinetics of the CO_2 Blackbody Cavity Laser

The lasant must not be at high temperature or the lower level will be filled as will be shown shortly, and as helium has excellent heat conductivity, it is usually introduced. A buffer gas such as Argon may also be introduced, which if possible should enhance losses from the lower laser level without affecting the upper level. The ideal lasant may therefore be a mixture of gases, making the choice still more complex. In addition to making the source term S as high as possible, an ideal lasant should have a high density of upper level states N_u, and a low density of lower level states N_l, to give as high an inversion population $(N_u - N_l)$ as possible. (Fig. 17) A specific example of the processes determining N_u and N_l in a CO_2-He-Ar mixture is illustrated in Figure 18.

The ideal lasant should have low cross sections for collisions that deexcite N_u, i.e. low rate coefficients k_1, k_2, k_3, and a low Einstein coefficient A_{Gu}, from the upper level to ground. A low value of A_{Gu} means a metastable upper state. Even more important, the filling of the lower level (Figs. 17, 18) from the upper state should be small, as this has a bigger effect on $N_u - N_l$. (Fig. 18--k_7, k_9, k_{12}, k_{13} should be small.) However, collisions which remove the lower level (k_{10}, k_{11}) are helpful. Losses of all levels to the tube wall occur by gaseous diffusion, which is important at low gas pressures (few torr total pressure).

PHYSICAL PROCESSES IN BLACK-BODY CAVITY LASER

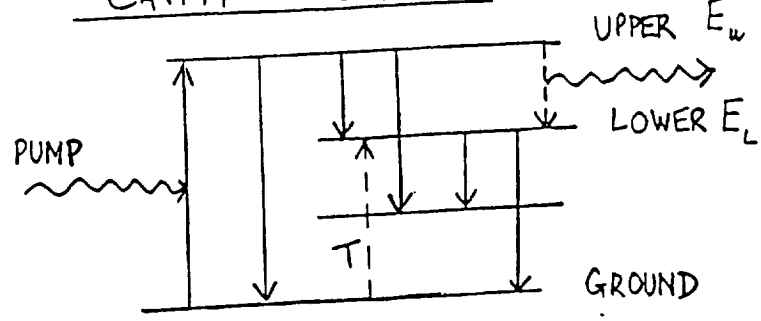

1. ABSORPTION AND PUMPING. ↑
2. LOSS FROM UPPER LEVEL BY COLLISIONS SPONTANEOUS EMISSION & DIFFUSION. ↓
3. FILLING LOWER LEVEL FROM UPPER. ↓
4. FILLING LOWER LEVEL BY TEMPERATURE EFFECTS ↓
5. REMOVE LOWER LEVEL RAPIDLY ↑

∴ NEED NEED LASANT WITH HIGH ABSORPTION, COOLANT (He), AND PROB-ABLY A THIRD MATERIAL TO ENHANCE 5 WITHOUT INCREASING 2 & 3

Figure 17

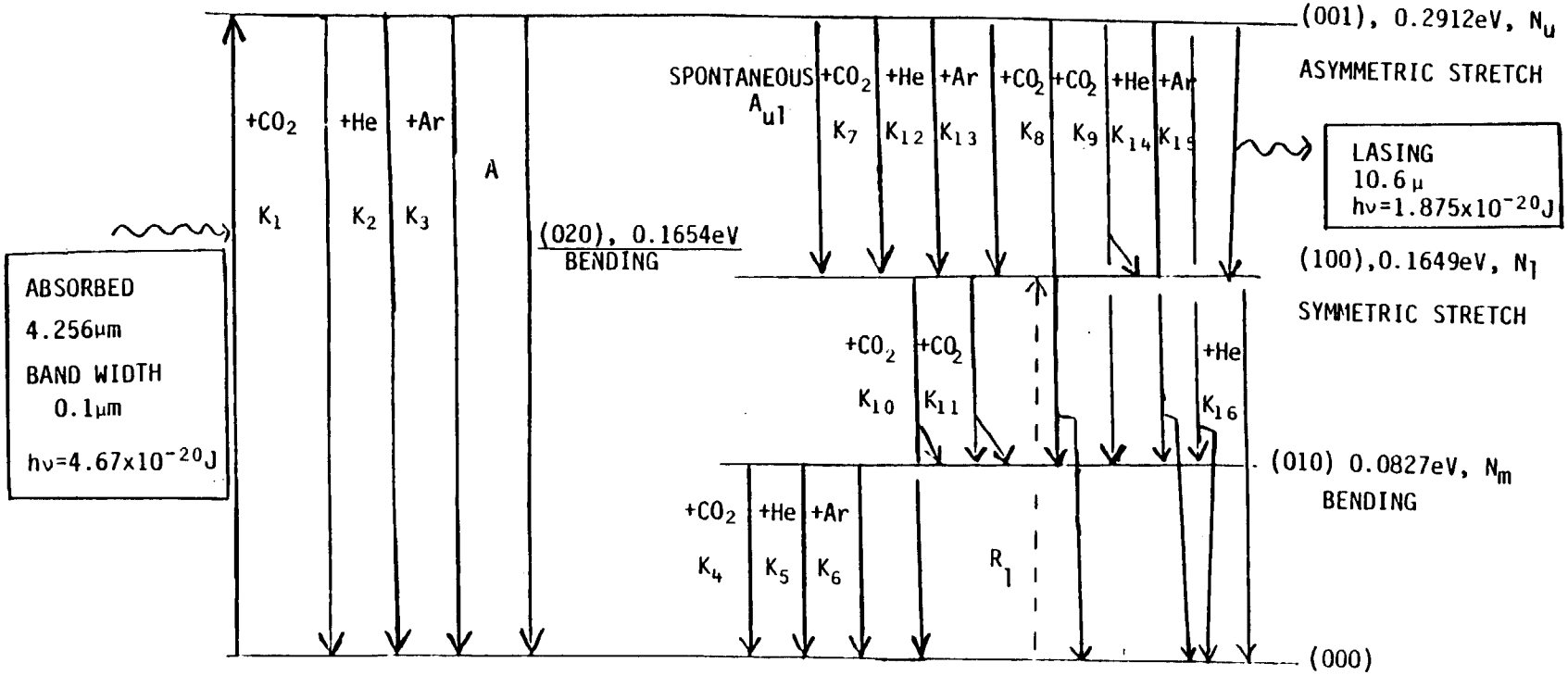

Figure 18. Flow Diagram for CO_2 Black Body Laser

F. Temperature Criterion

Experimentally, it was found that if the CO_2 lasant became hot, lasing was inhibited.[18] Most of the energy absorbed is deposited as heat in the lasant and must be removed by diffusion to the walls. In gaseous mixtures, the coefficient of heat conduction is independent of the total pressure, but depends on the gas ratios, with helium the best heat conductor. Assuming planar geometry the temperature of the lasant in the center of the laser can be calculated, and for CO_2-He-Ar mixtures, values around 360-400 K were obtained.

Increasing the gas temperature T_G fills the lower laser level by Boltzmann statistics, and E_1 is only 0.165 eV above ground for CO_2. In the steady state the fraction of CO_2 molecules with energies this high is $\exp(-E_1/kT_G) = \exp(-1972/T_G)$ or 0.5 percent at T_G = 360 K. Collisions with molecules whose energy is above E_1 can result in the symmetric stretching mode oscillation--the $CO_2(100)$ lower lasing level. Only one in several thousand collisions accomplishes this, but nevertheless at elevated gas temperatures, the density of the lower laser level N_1 state can exceed that of the upper laser level N_u, and lasing will cease. The lasant must therefore be cooled and the cooling requirement is yet another reason why an important characteristic of an ideal lasant would be to have E_1 as high as possible above ground.

G. Characteristics of an Ideal Lasant

The lasing medium X is usually mixed with a cooling agent Y, (usually He) and a buffer gas Z which preferable deexcites the lower level. All three components interact in the kinetics of the laser. The ideal lasant should satisfy the following criteria: (1) Number of atoms in the molecule: the lasing medium should have at least three atoms so that there are

several energy levels to provide an upper level, and a lower level which cannot be the ground level. (2) Absorption cross section σ_a: it should have an absorption cross section $\sigma_a > 0$ at an appropriate absorption wavelength, λ_a. The cross section need not be large as increasing the pressure can compensate for small σ_a. (3) Absorption bandwidth $d\lambda_a$: this should be as large as possible (although $\sigma_a \propto (d\lambda_a)^{-1}$--see 2 above), as a greater portion of the blackbody spectrum is now utilized. An ideal lasant would have large $d\lambda_a$ if it had a small molecular weight M, and a large moment of inertia I. (4) The laser energy levels E_u, E_l: E_u should be high so λ_a is small, and approaching the peak of the blackbody curves, where the radiation density per unit wavelength is higher and raising $\eta_Q = (E_u-E_l)/E_u$. The lower laser level, E_l, should be high so that the level is not filled by temperature effects. However, both E_u and E_l must give a reasonable η_Q. (5) Pumping the upper laser level: absorption in the lasant X at a density (X) cm^{-3}, depends on the correct ((X) σ_a d), where d is the average depth (between x_1 and x_2) and d should be small, to enable adequate heat conduction to the walls. (6) Losses from the upper laser level: the ideal lasant X should have low losses from its upper level X_u, meaning collisions of the type X_u + X,Y,Z should not deexcite (see Fig. 18). Spontaneous emission from X_u should also be small, or Einstein coefficient A_{uG} should be small, i.e., a metastable upper level is desirable. (7) Stimulated emission cross section σ_e: should be large for low threshold, high gain, and high power:

$$\sigma_e = \lambda_e^4 A_{uL}/4\pi^2 c d\lambda_e \qquad (4\text{-}39)$$

Here λ_e, the lasing wavelength is fixed by E_u-E_l, A_{uL} the Einstein coefficient for spontaneous emission should be large and $d\lambda_e$ the emission bandwidth should be small. (8) Filling the lower laser level: the rate

should be small. The two main contributions are collisions from the upper level, requiring rate coefficients such as k_7, k_{12}, k_{13} (Fig. 18) to be small, and filling by temperature effects should be small meaning E_1 should be high, and the gas temperature T_G low. (9) Losses from the lower laser level: should be large so that the density of the lower level states (X_L) is small and (Xu) - (X_L) >> 0. Hence collisions of the type X_L + X, Y, Z should have large deexcitation cross sections (large rate coefficients K_4, K_5, K_6 in Fig. 18). It is also helpful to have other vibrational modes at energies in near resonance with E1, which provide pathways to deplete the lower laser level, e.g., for CO_2, we have (100)→(020)→(010)→(000).

H. Scaling of a Blackbody Cavity CO_2 Laser to 1 MW

In scaling a CO_2 blackbody cavity laser to 1 MW there is a serious limitation due to Planck's Radiation Law, which leads to excessively large surface areas for the laser. If a flat "box-type" laser is assumed, the surface areas of the solar collector, and heat radiator are considerably smaller.

H.1 Power Density in a Blackbody Cavity

The CO_2 laser absorbs at a wavelength λ_a = 4.256 μm, with a bandwidth $d\lambda_a = 4 \times 10^{-4}\mu m$. Planck's radiation formula then gives the power entering unit area of the laser surface as

$$E(\lambda_a)d\lambda_a = \frac{1.07 \times 10^{-2}}{\exp(3381/T_b) - 1} \ (W\text{-}cm^{-2}) \qquad (4\text{-}40)$$

where T_b is the cavity temperature. For T_b = 1500K, and 3000K, respectively, $E(\lambda_a)d\lambda_a$ = 1.26 and 5.14 mW per square cm, values which are very small. Large power outputs therefore require a large laser surface A_L. There is no concentrating of input flux inside the blackbody cavity, as with parabolic collectors.

We define a device efficiency η as P_{out}/P_{in} where P_{in} is the absorbed power to produce $CO_2(001)$ the upper laser level, and P_{out} is the output power assumed to be 1 MW.

H.2 Calculation of the Dimensions of a 1 MW Laser

The model is shown in Figure 19. A parabolic collector of area A_c collects the sun's radiation of 1.4 KWm^{-2} and the total power P_c is directed into the cavity, which has negligible losses. All of P_c is assumed to be input power P_{in} to the laser of surface area A_L. Although the cavity is at temperature T_b, the temperature of the gas T_G is assumed much lower - 400K. A cooling system removes heat to a radiator of area A_r, at temperature T_r which emits power P_r by Stefan's Law: $P_r = A_r \varepsilon \sigma T_r^4$ where ε the emissivity is assumed unity, σ is Stefan's constant, and $T_r = T_G$. As η is usually much less than 1, $P_r \approx P_{in}$. With these assumptions the areas of the collector A_c and radiator surface A_r can be calculated as shown in Fig. 20.

In this simplified treatment A_c, A_L, A_r are proportional to P_{out}/η, only A_L depends on Planck's formula. Assuming cavity temperatures T_b = 1500K and 3000K, and efficiencies of 1% and 10%, the values of the areas are given in Figure 21. Also given is a representative linear dimension L where L^2 = area, to give a feeling for the size of these components. The radiator may to some extent be folded, while the laser area, A_L, can be shared by the two sides of the laser. However, a folded geometry for A_L would be difficult because the surface has to be cooled as shown. Even in the extreme limit with T_b = 3000K and η = 1, A_L is still 20000 m^2 if P_{out} = 1 MW.

SCALING OF 1MW CO_2 BLACK-BODY CAVITY LASER

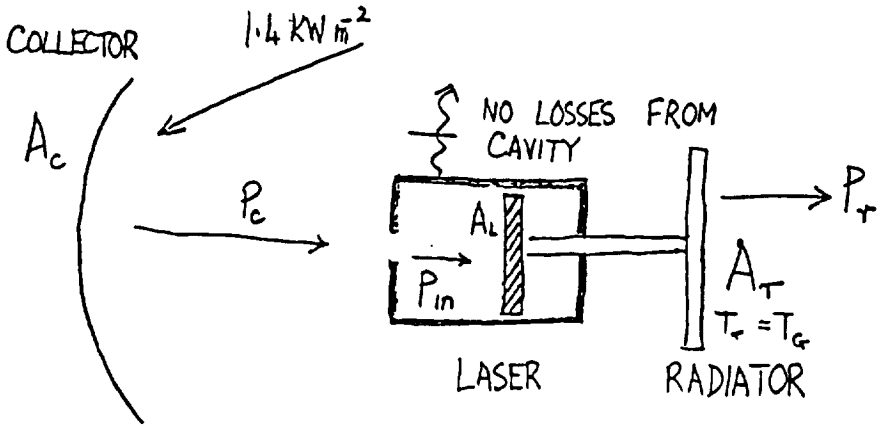

ASSUME: $P_c = A_c \times 1400$ (W)

NO LOSSES FROM OUTSIDE CAVITY

$$P_{in} \simeq P_c$$

$$P_{out} = (1-\eta) P_{in}$$

$$P_r = (1-\eta) P_{in} \simeq P_{in}; \quad \eta \ll 1.$$

$$P_r = A_r \varepsilon \sigma T_G^4; \quad \varepsilon = 1$$

$$T_G = 400 \text{ K}.$$

Figure 19.

SURFACE AREA OF COLLECTOR, A_c

ASSUME ALL POWER COLLECTED → $E(\lambda_a)\, d\lambda_a$, – NO LOSSES FROM CAVITY.

$$A_c\,(m^2) \times 1400\,(W\,m^{-2}) \times \eta = P_{out}(W)$$

$$A_c(m^2) = P_{out}(W) \,/\, 1400\,\eta$$

SURFACE AREA OF LASER, A_L

$$P_{in}(W) = E(\lambda_a)\, d\lambda_a (W cm^{-2}) A_L\,(m^2) \times 10^4$$

$$P_{out}(W) = \eta\, P_{in}(W)$$

$$A_L(m^2) = P_{out} \,/\, 10^4 \eta\, E(\lambda_a)\, d\lambda_a$$

SURFACE AREA OF RADIATOR, A_r

ASSUME $P_r \approx P_{in} = P_{out}/\eta$

$$P_r = A_r\, \varepsilon\, \sigma\, T_r^4$$

ε = EMISSIVITY = 1, σ = STEFAN = $5.67 \times 10^{-8}\ W m^{-2} T^{-4}$

$$A_r\,(m^2) = \frac{P_{out}}{\eta\, \varepsilon\, \sigma\, T_r^4}$$

Figure 20.

1 MW CO_2 BLACK-BODY LASER: AREAS & LENGTH OF SIDE (IF SQUARE) OF COLLECTOR LASER & HEAT RADIATOR

$T_r = 400\,K$

η	T_b (K)	COLLECTOR		LASER		RADIATOR	
		A_c (m^2)	L_c (m)	A_L (m^2)	L_L (m)	A_r (m^2)	L_r (m)
0.1	3000 1500	7×10^3	84	1.94×10^5 7.94×10^5	441 890	7×10^3	83
0.01	3000 1500	7×10^4	265	1.94×10^6 7.94×10^6	1,390 2,818	7×10^4	263

IF $\eta \to 1$, $T_b = 3000\,K$

$A_L = 1.94\times10^4\,m$, $L_L = 140\,m$

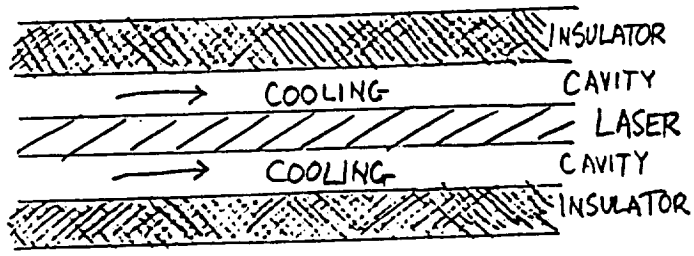

Figure 21.

I. Conclusions

The characteristics of an ideal blackbody cavity lasant have been outlined. The choice of an ideal lasant is a complex process depending on a large number of factors, including the choice of a cooling medium and a buffer gas.

Planck's radiation law limits the power input per unit area into a CO_2 blackbody cavity laser making the surface area for high powered lasers excessively large. It is suggested that an alternative application might be small 1 W lasers for communication and surveillance, because it would be easy to maintain the cavity temperatures in synchronous orbits where 72 minutes each day are spent in the earth's shadow.

4.2.2 A Limitation in Scaling up a Blackbody Laser

A. Summary

A blackbody pumped CO_2+ buffer gas laser is assumed cylindrical of length L and radius r. The pumping rate is determined by the rate of arrival of radiation in a bandwidth 0.1μ at the laser surface according to Planck's radiation formula. The power input per unit volume however is proportional to $1/r$. A maximum value of r is determined from experimental results for threshold at 1500 K. Increased power can only be achieved by increasing L which becomes impossibly large. The limitation can be circumvented by a box type laser.

B. Introduction

The purpose of this section is to illustrate a limitation on the pump power input into a blackbody laser if the geometry is cylindrical. The input energy flux is limited by Planck's radiation formula, and there is no

means of concentrating it, as would be done by parabolic solar reflectors. The pump power per unit volume is estimated from the experimental results of Insuik et al.[16, 20] To attain a given power input per unit volume, it will be shown that there is an upper limit to the radius. Hence in scaling up to large power output, a cylindrical laser turns out to be impossibly long. A method of overcoming the limitation using a box laser geometry is given.

C. Absorption of Blackbody Radiation

Experiments have shown that for a CO_2 blackbody laser, with a buffer gas, absorption occurs at 4.256 μ with a bandwidth of 0.1μ.[18] The lasing medium in the form of a cylinder of radius r and length L receives energy from the blackbody cavity at a rate per unit surface area given by Planck's radiation formula.

$$E(\lambda)\, d\lambda = \frac{3.74 \times 10^{-12}\, d\lambda}{\lambda^5 (\exp \frac{1.439}{\lambda T} - 1)} \text{ watts cm}^{-2} \qquad (4\text{-}41)$$

where λ is the wavelength, $d\lambda$ the absorption bandwidth both in cm and T the temperature in degrees Kelvin. For the above wavelength and bandwidth:

$$E(\lambda)\, d\lambda = \frac{2.68}{\exp\left(\frac{3381}{T}\right) - 1} \text{ watts cm}^{-2} \qquad (4\text{-}42)$$

a function of temperature only.

The power entering the laser medium is then $E(\lambda) \cdot 2\pi r L d\lambda$, but to obtain the power P entering unit volume on the average we must divide by $\pi r^2 L$, or

$$P = 2E(\lambda)d\lambda/r \qquad (4\text{-}43)$$

Hence, increasing r, decreases P, and there is a limitation on r, which has a maximum value given by equation (4-43) when P is just

sufficient for threshold. To scale up for high power output, (for a given efficiency) the only remaining alternative is to increase L.

Some illustrative values of $E(\lambda)d\lambda$ and P are shown in Table III, where r is assumed to be 1 cm.

Table III. Values of $E(\lambda)d\lambda$, the power per square cm and P, the power per cc vs.temperature

Blackbody temp K	$E(\lambda)d\lambda$ watts cm^{-2}	P watts cm^{-3}
1000	0.094	0.188
1100	0.130	0.260
1200	0.170	0.340
1500	0.314	0.628
2000	0.606	1.212
3000	1.285	2.569

D. Estimate of Threshold Input Power

An approximate estimate of the pump power per cc to attain threshold can be obtained from the experimental results of Insuik et al.[20] Their experiment was done in a sapphire tube of internal diameter 8 mm, outside diameter of 9.5 mm, with 50 cm of its length in a hot zone. The medium was CO_2 with He and Ar as buffer gases. Lasing occurred with the blackbody temperatures ranging from about 1100 to 1500 K.

By varying the pressure, it was found that a drop off in power occurred around 7 torr total pressure when there was 21% CO_2, suggesting that the pressure and path length were just great enough to absorb all the input radiation. Assuming the absorption length L' to be of order 0.8 cm, this leads to an absorption cross section $\approx 3 \times 10^{-17}$ cm^2 and a relation between the path length and CO_2 pressure:

$$L' \, p \approx 1 \text{ (cm torr)} \qquad (4\text{-}44)$$

where $L = 2r$ is in cm, and p in torr for maximum output. Neither the pressure of CO_2 nor r can be increased indefinitely in scaling to higher

power, otherwise the radiation will not penetrate to the center of the tube. If Lp is too small, the radiation will not be absorbed.

A very rough estimate of the pump power per cm^3 for threshold can be made. A number of experiments[20] showed that maximum output power occurred over a narrow range of total pressures P_t; $2.5 < P_t < 12.5$, and CO_2 pressure p; $0.5 < p < 2.5$ torr. A laser power output vs. temperature curve for $P_t = 7$ torr, $p = 1$ torr showed that threshold occurred around 1100° and the power output rose linearly to a value of 4 mW at 1500 K. Assuming 1100 K to be the threshold temperature for $r = 0.4$ cm, then equation (4-43) gives the minimum power per cm^3 for threshold to be $P_{min} = 0.65$ watts cm^{-3}.

Now P_{min} may not be a constant value if r is varied; increasing r decreases wall losses. Assuming it is correct in order of magnitude, then the maximum value of r is obtained from equation (4-43)

$$r_{max} = 2E(\lambda)d\lambda/P_{min} \qquad (4\text{-}45)$$

with $P_{min} = 0.65$ watts cm^{-3}, e.q. at T = 1100° $r_{max} = 0.4$ cm, and at 1500°C $r_{max} = 1$ cm.

E. Power Output and Laser Dimensions

If the overall efficiency of the laser is η, then the power output P_o is

$$P_o = \eta\ 2\pi rL\ E(\lambda)d\lambda \qquad (4\text{-}46)$$

and increases with rL for a given cavity temperature T. To increase P_o, r should approach r_{max}, determined for given T from Equation (4-46). Then given η, L can be calculated; e.g. for $P_o = 10$KW, T = 1500 K, $\eta = 0.1$, $r_{max} = 1$ cm, then L = 500 m for a laser tube of 1 cm radius. The length L is impossibly large.

The difficulty can be overcome by a box laser arrangement (Fig. 22) when the medium is in the form of a flat plate. The output power is now

$$P_o = 2\ \eta\ xy\ E(\lambda)d\lambda \qquad (4\text{-}47)$$

the factor 2 arising as it is pumped from two sides. Using the same numbers as above, then $xy = 16\ m^2$, or $x = y = 4m$, much more reasonable values.

F. Conclusions

In scaling up a blackbody cavity laser to high powers, there is an inherent limitation because the energy flow into the laser medium is limited by the Planck radiation formula. Concentrating it by parabolic reflectors does not seem possible. In addition, the power input per unit volume varies inversely as the radius if the medium is cylindrical, and the value of the radius is limited by a threshold condition. For high power, the length L must therefore be increased to a value impossibly large.

The limitation can be overcome by using a box laser arrangement, which essentially offers a greater area for pumping in a much more compact arrangement.

4.3 Dye Lasers as Solar Energy Converters

In 1982, a preliminary survey of Dye Lasers for solar power conversion was made. The reason for the survey was that the efficiencies of the systems considered hitherto were found to be very low. In brief, the previous investigations had first considered different absorbing (Br_2) and lasing media (CO_2, HF, HCN, H_2O) and the overall efficiency for all combinations was less than 0.5%.(21, Appendix C) Investigation of an IBr laser which uses the same medium for absorption and lasing and where the "transfer efficiency" was largely eliminated showed the final efficiency 1.2% or less.(15, Appendix D)

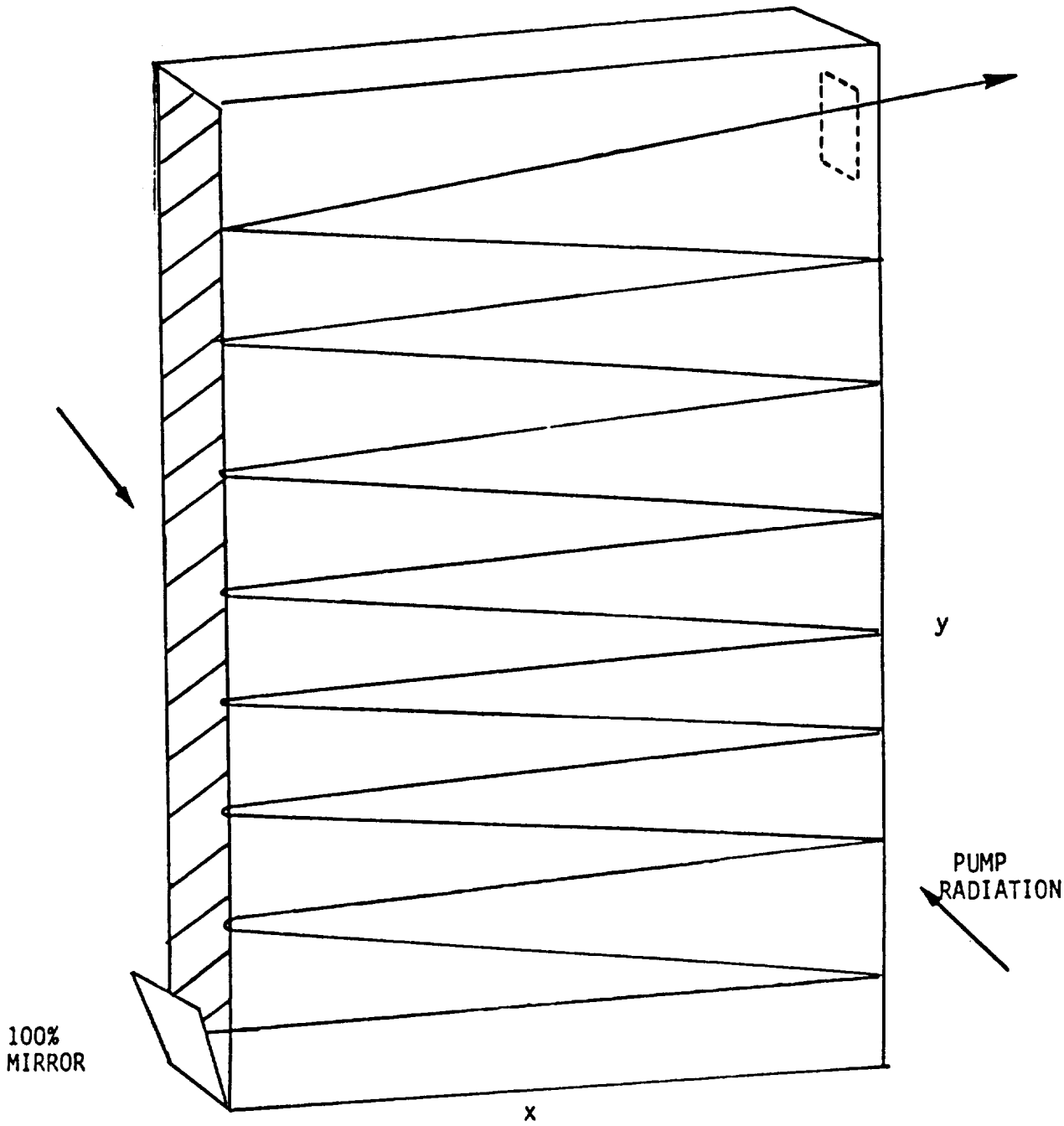

Fig. 22. Box laser arrangement.

The new types considered were (1) liquid dye lasers and (2) vapor dye lasers.

4.3.1 Liquid Dye Lasers as Solar Energy Converters

An experimental investigation of liquid dye lasers was carried out by M.D. Williams of the National Aeronautics and Space Administration in 1982.

In general, such lasers have high gain and operate at room temperature under giant pulse pumping. For solar pumping in the steady state a number of difficulties arise.

Lasing in organic dyes differs from one material to the other, but in general, the molecules possess a pair of electrons which possess a certain freedom of motion within the molecule. The motion of this electron pair determines the electronic configuration of the molecule. The lowest electronic configuration S_0 is a singlet state (spins opposite). There are excited singlet (S_1, S_2,...) and triplet (T_1, T_2,...) states. Transitions between singlet states are "allowed" by the spectroscopic selection rules. They give rise to intense absorption and emission spectra. Transitions between different triplet states are also allowed, but singlet-triplet transitions, known as inter-system crossings, are forbidden.

The presence of molecules in one of the metastable triplet levels may be detrimental for laser action in several ways. First, the molecules stored in a triplet level are eliminated from participating in the laser cycle. Second, when some of the lowest triplet levels are populated, the material may become absorbent for the laser radiation because of triplet-triplet transitions that overlap the laser line.

It is possible to quench the triplet states, for example, by saturating the solution with oxygen, and pulses of 500 μs duration have been achieved by Schmidt[22] in air saturated rhodamine 6G solution. Commerical

cw dye lasers are now available, but they have to be pumped by ultraviolet lasers. An excellent compendium on cw Dye Lasers is given by Snavely[23] and Schafer[24].

Another problem is the inducement of optical inhomogeneities (differences in reproactive index) caused by the heating and non-uniform excitation of the solution.

In conclusion, the quenching of triplet states, the presence of optical inhomogenieties, and the problem of cooling the liquid at high power levels to prevent boiling would raise severe problems for cw solar pumped liquid dye lasers.

4.3.2 Vapor Phase Dye Lasers

The use of vapors is advantageous for solar pumping because of structural simplicity and uniformity of medium. Recently, a paper by Basov et al.[25] reported experiments with vapor phase dye lasers. The results enable some tentative conclusions to be drawn on whether they would be feasible for solar pumping.

The pumping was performed with the third harmonic of a neodymium laser at 355 nm. This wavelength lies on the low wavelength side of the solar spectrum peak which is at 500 nm, and the number of photons per unit wavelength is about half that at the peak. The absorption bandwidths of dyes in liquids are typically of order 100 nm, and if this is also true in the vapor phase, then the fraction of photons in the solar spectrum absorbed--the solar efficiency--would be somewhere in the region of 3%.

Values of efficiencies of the vapor lasers were quoted, but these numbers did not include a "solar efficiency." The highest "efficiency" for a vapor phase laser was for the material POPOP, which is

p-bis [2-(5-phenyloxalyl)] benzene and was 23%. Inclusion of the solar efficiency shown gives an overall efficiency of the order of 1%. An efficiency of over twice the above value was quoted for POPOP in liquid ether solution, a liquid dye laser. It would be unlikely that temperatures sufficiently low to keep the ether in the liquid state would be possible in a solar laser.

As steady state working would be desirable for solar lasing, the threshold pumping intensity is important. The lowest value quoted was 20 kW cm^{-2} which would correspond to the sun's radiation being concentrated 1.4×10^5 times. However, the length L of the active region of the laser was only 2.4 cm. If it is true, as in the IBr laser, that the product CL, where C is the concentration factor, is roughly constant, then C would be about 3×10^3 for L = 1m.

In conclusion, the threshold pumping intensity for such a vapor laser would be within reasonable bounds, and its overall efficiency would be comparable to IBr. It is noted that the experiments were performed with ether as the buffer gas at 36 atmospheres.

4.3.3 Conclusions on Dye Lasers as Solar Energy Converters

It was concluded that liquid dye lasers would probably not be feasible. Vapor phase dye lasers offer some possibility although their overall efficiency would not be much greater than IBr at around 1%.

5. OVERALL CONCLUSIONS

Solar pumped lasers used as energy converters have many important applications for NASA's space program. They can be used to beam power from one space vehicle in a mission to other more maneuverable vehicles, or else

from orbiting vehicles to rovers on the surface of planets. Low powered solar pumped lasers (in space or terrestrial) can also be used for communication and surveillance without the need for auxiliary power sources. An important criterion from the space program's point of view is high output power/weight (Section 3, Appendix A). The main weight would be that of the heat radiator, and its size would be reduced if the overall efficiency of the laser would be maximized, and also if the laser could run at high temperature. Studies of the far field patterns indicate so far that if the power outputs are high, then the area of cross section of the lasers will be large, giving rise to modes at right angles to the axis with resulting spread of the beams. This aspect needs further study.

The mechanisms of the lasers and the various families of solar pumped lasers are shown in Fig. 2 (p. 10). The class of lasers utilizing only a band of the solar spectrum were studied in detail. The dissociative types were divided into two, namely where one material absorbs and hands over energy to another which lases and second where the same material absorbs and lases. A detailed study of the first type in the form of Br_2-CO_2-He (absorber, lasant, coolant) Br_2-H_2O-He, Br_2-HCN-He, and I_2-HF-He showed that in all cases, even assuming complete absorption, the overall efficiencies were below 5×10^{-3}. (Appendix C) For the second type--IBr--the estimated efficiency was 1.2%. (Appendix D)

In the case of the non-dissociative lasers, the studies first concentrated on some physical aspects. First, it was shown that stimulated emission in Na_2 occurred at somewhat different wavelengths to regions of self absorption, a necessary condition for lasing (Section 4.1.2.1). Second, a simple theory was obtained to estimate the ratio of dimers to monomers in metallic vapors as a function of temperature (Section 4.1.2.2).

Third, the question of metastability in N_2 and CO while the vibrational levels in Na_2 are short lived was explained by estimating the spring constants of the molecules and relating these to the spacing of the levels. For Na_2, the spacing is of order the thermal energy, for N_2 and CO_2 the spacing is 15 times greater-hence thermal collisions can deactivate the higher vibrational levels in Na_2, but not N_2 and CO_2. Fourth, a new hypothesis on the electronic energy transfer in Na_2 based on a suggestion by N. Jalufka was proposed.(Appendix E) It is based on the blackbody radiation in the oven at 750°C causing stimulated emission between the electronic bands $B^1\Pi_u$ and $2^1\Sigma_g^+$. The results have been submitted to the Journal of Molecular Spectroscopy.

Specific metallic vapor phase laser systems in the case of Na_2 and Li_2 were studied and the overall solar efficiencies were estimated at around 1%. However it was pointed out by W.E. Meador that the threshold potentials for these materials as solar pumped lasers would be far too high for practical use and it seems unlikely that they would be useful.

The blackbody lasers have the advantage of thermal storage and can operate in the earth's shadow. The size of the collector is reduced as the whole solar spectrum is absorbed. A physical problem addressed was the effect of isotropy of the radiation for certain geometries of absorber and a paper was published in Optics Communications[17] (Appendix F). A theoretical study of a solar pumped blackbody CO_2 laser outlined the physical mechanisms and estimates were made of output power as blackbody and gas temperature. The results depended critically on the values of the rate coefficients which were not well known, and the agreement with the experimental results of Insuik and Christiansen (IEEE J. Quantum Electronics QE-20 622, (1984)) was poor. However, the author pointed out

that there was a limitation in scaling up blackbody lasers because the energy density in the cavity was limited by Planck's radiation formula, and for high powers, the area of the absorbing surface of the lasant would have to be impossibly large for space applications.

A brief period was spent studying liquid and vapor phase dye lasers, and it was concluded that they would not be feasible.

The overall picture obtained is that it is possible to obtain lasing by solar pumping, and indeed, experiments on IBr, on the perfluoroalkyl halides and on black-body lasers have borne this out. So far, for energy conversion, the conversion efficiencies which in turn effect the output power to weight ratio, seem too low for immediate application and further study is needed. The question of far field patterns which was put in abeyance also needs further study.

6. ACKNOWLEDGEMENTS

The author gratefully acknowledges useful discussions with Drs. W.E. Meador, J.W. Wilson, N.W. Jalufka, J.H. Lee, and Mr. W.D. Williams of NASA. He also wishes to express his appreciation to Dr. E. Conway for the facilities provided at the NASA/Langley Research Center.

7. REFERENCES

1. Harries, W.L., Meador, W.E., Miner, G.A., Schuster, C.L., Walker, G.H., and Williams, M.D., "Laser Powered Martion Rover," Proceedings of the Second Beamed Power Workshop at NASA/Langley Research Center, Hampton, Virginia, February 28 - March 2, 1989, NASA Conference Publication 3034.

2. Wellegehausen, B., IEEE J Of Quantum Electronics, QE-15, 1108 (1979).

3. Kusch, P. and Hessel, M.M., J. Chem. Physics 68(6), 2591 (1978).

4. Huber, K.P. and Herzberg, G., "Molecular Spectra and Molecular Structure-Constants of Diatomic Molecules," Van Nostrand, 1978.

5. Herzberg, G., "Spectra of Diatomic Molecules," Van Nostrand, 2nd Edition, 1950, p. 383.

6. Ibid, p. 20.

7. Wellegehausen, B., IEEE J. Quantum Electronics QE-15, No. 8 (1979).

8. Lapp, M. and Harris, L.P., J. Quant. Spectroscopy Radiat. Transfer 6, 169 (1966).

9. Stull, D.R. and Sinke, G.C., "Thermodynamic Properties of the Elements," Adv. Chem Series. No. 18 (1956).

10. Handbook of Chemistry, 9th ed. edited by N.A. Lange, p. 1424 etc., Handbook Publishers Inc., 1956.

11. Wellegehausen, B. IEE J of Quantum Electronics QE-15, 1108, (1979).

12. Jones, P.L., U. Gaubatz, U. Hefter, K. Bergmann and B. Wellegehausen. Applied Phys. Lett 42 222 (1983).

13. The data for the Morse Curves and the energy levels are taken from G. Herzberg, "Molecular Spectra and Molecular Structure I: Spectra of Diatomic Molecules," Van Nostrand, New York, 1950.

14. Herzfeld, K.F. and T.A. Litovitz. "Absorption and Dispersion of Ultrasonic Waves," Academic Press (1959) p. 262.

15. Harries, W.L. and W.E. Meador. "Kinetic Modeling of an IBr Solar Pumped Laser," Space Solar Power Review 4, 189 (1983).

16. R.J. Insuik and W.H. Christiansen, IEEE J. Quantum Electronics QE-20, 682 (1984).

17. Harries, W.L., "Absorption of Isotropic Radiation," Optics Communications 63, 361 (1987).

18. Christiansen, W.A., "A New Concept for Solar Pumped Lasers," pp. 346-356 in "Radiation Energy Conversion in Space, vol. 61 of Progress in Astronautics & Aeronautics, 1979, K.H. Billman, editor.

19. Taussig, R, Bruzzone, C., Nelson, L., Quimby, D., and Christiansen, W., AIAA Terrestrial Energy Conference, June 4-6, 1979, Orlando, Florida.

20. Insuik, R.J., Christiansen, W.H., Private communication.

21. Harries, W.L. and Wilson, J.W. Space Solar Power Review 2, 367, 1981.

22. Schmidt, W. Laser 2, 47, 1970.

23. Snavely, B.B. Topics in Applied Physics. Dye Lasers, 2nd edition, edited by Schafer, F.P., Ch. 2, p. 120. Springer Verlag, N.Y.

24. Schafer, F.P. Ref. 3, p.265.

25. Basov, N.G., Logunov, O.A., Startsev, A.V., Stoilov, Yu, Yu, and Zuev, V.S. J. of Molecular Structure 79, 119, 1982.

APPENDIX A

Criteria for the Evaluation of Laser Solar Energy Converter Systems

W. L. Harries

Reprinted from

Journal of Propulsion and Power

Volume 1, Number 5, September-October 1985, Page 411

AMERICAN INSTITUTE OF AERONAUTICS AND ASTRONAUTICS • 1633 BROADWAY • NEW YORK, N.Y. 10019

Criteria for the Evaluation of Laser Solar Energy Converter Systems

W.L. Harries*
Old Dominion University, Norfolk, Virginia

I. Introduction

ONE concept for collecting solar energy is to use large solar collectors on orbiting space stations, which then transmit the energy as laser beams. Direct conversion by solar pumped gas lasers has already been considered and the power conversion efficiency disscussed.[1-3] However, a figure of merit, of more importance for space missions, is the output power per unit weight ratio.

An idealized energy conversion system is shown in Fig. 1. The solar radiance is collected in a parabolic reflector and, for a required output power, its area is determined by the laser efficiency. The power not converted into the laser beam must be dissipated by a heat radiator emitting by Stefan's Law which, as the converter efficiency is usually low, will contribute the major part of the total weight of the system.

The overall efficiency of the laser can be decomposed into the product of several efficiencies, which affect the collector and radiator in different ways. The efficiencies are described in Sec. II and the energy flow is discussed in Sec. III. The dependencies of weight on area are then assumed, which determine the weight for a given output power. Some comparisons will be shown of different laser systems.

II. Efficiency of Solar Pumped Lasers

The overall efficiency of solar pumped lasers can be subdivided into the product of four efficiencies.[1] First, it aborption occurs over a bandwidth λ_1 to λ_2, the fraction of the solar spectrum used, or "solar utilization efficiency," is η_S,

$$\eta_S = \int_{\lambda_1}^{\lambda_2} \Phi(\lambda)d\lambda / \int_0^{\infty} \Phi(\lambda)d\lambda$$

where $\Phi(\lambda)$ is the solar radiance in photons per square meter between λ and $\lambda + d\lambda$.

The absorption efficiency η_A is that fraction of photons within the absorption bandwidth absorbed by the gas: $\eta_A = 1 - \exp(-\sigma_a(N)d)$, where σ_a is the absorption cross section, (N) the density of absorbers, and d the thickness of gas.

Of the photons absorbed, only a fraction, η_K, end up producing a lasing transition. The kinetic efficiency η_K is determined by the detailed kinetics of the laser and, for example, it takes accounts of losses in the upper laser level due to quenching, etc.[2,3] Finally, the quantum efficiency η_Q is the ratio of the energy of the emitted photon to the average energy of the absorbed photons.

The device efficiency would then be $\eta_D = \eta_A\eta_K\eta_Q$, and the overall solar efficiency $\eta = \eta_S\eta_A\eta_K\eta_Q$, which is usually an order of magnitude less than η_D.

Received Nov. 20, 1984; Technical Note received April 22, 1985.

*Professor, Department of Physics.

III. Energy Flow in Solar Pumped Lasers

The energy flow for the idealized model in Fig. 1 is shown in Fig. 2. The solar power falling on the collector of area A_c is P_i. The mirror of reflectivity r concentrates the flux, and a fraction rP_i reaches the first transparent wall containing the lasing medium. However, a fraction $(1-r)P_i$ has been absorbed by the mirror and has to be radiated. The first container wall is assumed to have a transmittance τ_1, so the power arriving at the lasing medium is $\tau_1 rP_i$, and the power absorbed by the wall is $(1-\tau_1)rP_i$, which also has to be radiated.

The power arriving at the laser medium is distributed in wavelength over the solar spectrum; only a fraction, η_S, can be utilized, and of that only η_A is absorbed. The power absorbed P_A is $\eta_S\eta_A\tau_1 rP_i$ and the output power P_O is $\eta_K\eta_Q P_A$, while the part lost due to the lasing process, $(1-\eta_K\eta_Q)P_A$, has to be radiated. The power not absorbed by the lasing medium is $(1-\eta_S\eta_A)\tau_1 rP_i$ and reaches the second wall of transmittance τ_2. Then $\tau_2(1-\eta_S\eta_A)\tau_1 rP_i$ is transmitted through it, but an amount $(1-\tau_2)(1-\eta_S\eta_A)\tau_1 rP_i$ absorbed in the wall has to be radiated.

The total power that has to be radiated is P_r

$$P_r = P_i[(1-r) + r(1-\tau_1) + r\tau_1\eta_S\eta_A(1-\eta_K\eta_Q) + r\tau_1(1-\eta_S\eta_A)(1-\tau_2)] \quad (1)$$

As the output power P_O and input power P_i are related by $P_O = r\tau_1\eta P_i$, the relation between the radiated and output power is

$$P_r = KP_O/\eta \quad (2)$$

where

$$K = (1/r\tau_1)[(1-r) + r(1-\tau_1) + r\tau_1\eta_S\eta_A(1-\eta_K\eta_Q) + r\tau_1(1-\tau_2)(1-\eta_S\eta_A)] \quad (3)$$

IV. Output Power to Weight Ratio

The solar irradiance I_0 is 1.4 KWm^{-2}, and if the output power is $P_O(kW)$, then the area of the collector $A_c(m^2)$ is

$$A_c = P_O/(I_0\eta r\tau_1) \quad (4)$$

The radiator emits by Stefan's Law and its area is

$$A_r = P_r/\sigma\epsilon T^4 \quad (5)$$

where σ is Stefan's constant, ϵ the emissivity, and T, the temperature of the emitting surface. It is assumed that efficient conduction by heat pipes causes T to approach the work-

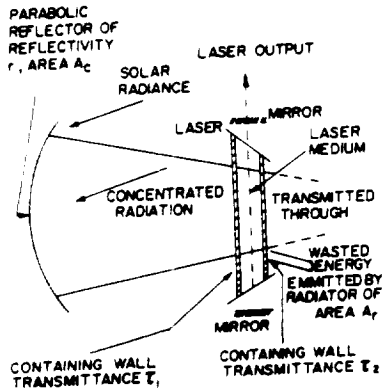

Fig. 1 Idealized arrangement for a solar pumped laser.

Table 1 Comparison of various lasing materials in solar pumped lasers

Material	η_S	η_A	η_K	η_Q	η	T,K	P_O/W	
							$\beta/\alpha = 1$	$\beta/\alpha = 10$
IBr	0.12	1	0.57	0.18	1.2×10^{-2}	423	1.2×10^{-2}	4.4×10^{-3}
C_3F_7I	10^{-2}	1	1	0.22	2.2×10^{-3}	873	2.69×10^{-3}	2.48×10^{-3}

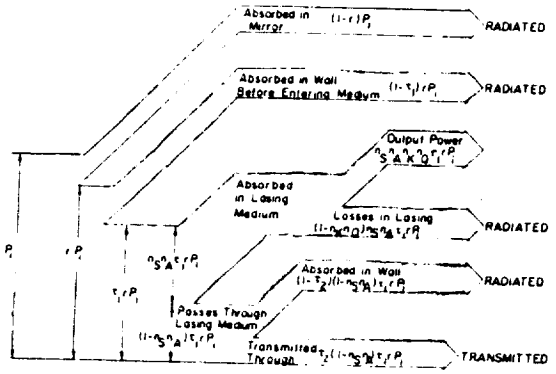

Fig. 2 Energy flow chart for a solar pumped laser.

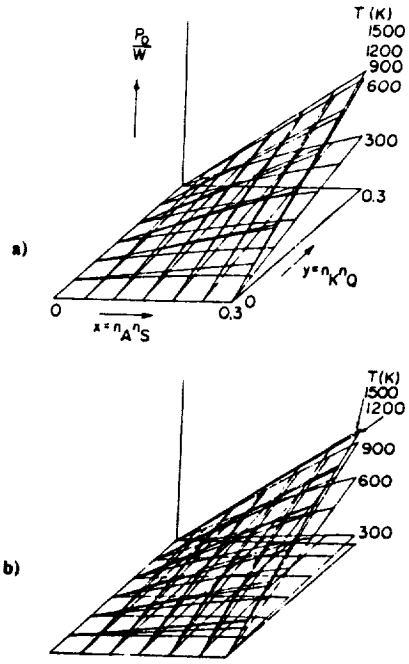

Fig. 3 Plot of P_O/W on an x,y plane for different temperatures showing effect of varying β/α. Both x and y are dimensionless, while α and β are in units of kg/m^{-2}. Values assumed are $r = 0.98$, $\tau_1 = \tau_2 = 0.9$. a) $\beta/\alpha = 1$; b) $\beta/\alpha = 10$, an extreme case.

ing temperature of the laser and that A_r is just sufficient to radiate the power required.

Assumptions must now be made about the dependence of the weights of the collector W_c and radiator W_r on their respective areas A_c and A_r; here, both are assumed proportional to their areas, $W_c = \alpha A_c$, $W_r = \beta A_r$, where α and β (Kgm^{-2}) are constants of proportionality. (The latter assumption may only be approximate as, for example, heat pipes may be needed to conduct to the radiator.)

The total weight W of the laser, collector, and radiator is $W = W_r + W_c + W_L$, where W_L is the weight of the laser. It is not unreasonable to assume $W_L \ll W_c$, W_r and, if so, the output power to weight ration P_O/W is

$$P_O/W = \eta/[(\alpha/1.4r\tau_1) + (\beta K/\sigma\epsilon T^4)]; \quad W_L \ll W \qquad (6)$$

Assuming that α and β, which are determined by structure design, are constants for all lasers, then Eq. (6) enables a comparison to be made for different lasing materials, provided the various efficiencies at the working temperatures are known. For fixed α, we may also make comparisons in terms of β/α. The dependence on the efficiencies is $P_O/W = f(x,y)$, where $x = \eta_S\eta_A$ and $y = \eta_K\eta_Q$. A plot of P_O/W on an xy plane is shown in Fig. 3, for $r = 0.98$, $\tau_1 = \tau_2 = 0.9$. (The value 0.9 is achievable if the walls are either KCs or CsI.[4]) The values of β/α are taken as 1 and 10, the latter being an extreme case for illustrative purposes. The range of x and y is only 0-0.3, corresponding to actual efficiencies in practice; $\epsilon = 0.9$, and $300 \le T \le 1500$ K.

For both cases P_O/W is either constant or increases monotonically with both x and y. The effect of β/α is large at low temperatures, (comparing Fig. 3a and 3b) and here $P_O/W \propto 1/\beta$. At high temperatures, the T^4 dependence quickly makes the area required for the radiator small, and P_O/W is independent of both T and β/α, provided T is high.

A comparison of IBr and C_3F_7I lasers is shown in Table 1. It is assumed that the gas pressure and depth are sufficiently high, $\eta_A = 1$. The kinetic efficiency of C_3F_7I is assumed as 1. The value of P_O/W, is calculated from Eq. (6), assuming $r = 0.98$, $\tau_1 = \tau_2 = 0.9$, $\alpha = 1$. The temperatures are approximate working temperatures. Table 1 shows that the IBr laser has a power/weight ratio several times higher than the C_3F_7I laser for $\beta/\alpha = 1$ and 10.

V. Conclusion

Assuming that a laser solar energy converter has a radiation collector and heat emitter whose weights are proportional to their areas, and that the weight of the laser is negligible in comparison, the output power per unit weight can be expressed in terms of the efficiencies and working temperatures of the system. This ratio seems to be several times higher for an IBr than a C_3F_7I laser because η_S is greater for the former, although the working temperature is lower. However, future converters should operate both at high efficiencies and at high temperatures.

Acknowledgments

The work was supported by Grant NSG-1568 from NASA Langley Research Center, Hampton, Virginia. The author acknowledges many useful discussions with Dr. J.H. Lee of NASA Langley, who first pointed out the significance of the power-to-weight ratio.

References

[1] Harries, W.L. and Wilson, J.W., "Solar-Pumped Electronic-to-Vibrational Energy Transfer Lasers," *Space Solar Power Review*, Vol. 2, April 1981, p. 367.

[2] Harries, W.L. and Meador, W.E., "Kinetic Modeling of an IBr Solar Pumped Laser," *Space Solar Power Review*, Vol. 4, No. 3, Sept. 1983, p. 189.

[3] Lee, J.H. and Weaver, W.R., "A Solar Simulator-Pumped Atomic Iodine Laser," *Applied Physics Letter*, Vol. 39, July 1981, p. 137.

[4]Taussing, R., Bruzzone, C., Nelson, L., Quimby, D., and Christiansen, W., *Proceedings, of the AIAA Terrestrial Energy Systems Conference*, Orlando, FL, June 4-6, 1979, pp. 1-17.

APPENDIX B

FAR FIELD PATTERNS OF HIGH-POWERED LASERS

By

Wynford L. Harries*

I. INTRODUCTION

The overall purpose of this investigation is to study the feasibility of using lasers as solar energy converters, with special emphasis on their role in space missions. Examples would be sending power from one space vehicle to others, or from an orbiting vehicle to vehicles on the ground[1]. The criteria for lasers as solar-energy converters have been given already[2], and high efficiency, and high output power per unit weight are important. Apart from the above criteria of efficiency, power/weight, and low threshold, another problem for high power lasers is the far field pattern, especially where the geometry of the lasing medium is large. Emphasis in Langley Research Center at the moment is on iodine lasers, and on solid state lasers such as coupled-diode arrays[3,4]. The theoretical studies of diode arrays have concluded that reasonable far field patterns are feasible - 80% collection efficiency into a 3m diameter dish placed 5×10^4 Km away.

In the period 16 January to 15 June 1989, a preliminary study has been made of obtaining far field patterns for a continuous lasing medium in the form of a right circular cylinder pumped radially. Thus the method of pumping from the outside is entirely different to the diode array. For either a master oscillator-power amplifier (MOPA) system, or an oscillator, we consider the last pass through the medium. The effect of amplification is included, and most important is the effect of amplification which varies with

radius. The medium could be solid, liquid or gas. The entering wavefront amplitudes are assumed planar or Gaussian with constant phase, tailored for best mode pattern. Although the discussion assumes a steady state CW laser, the concepts here can in general be applied to steady or pulsed lasers.

In sections II and III, the minimum size of the laser is discussed for a given output power, and the difficulties arising from large size. The advantages of a master oscillator-power amplifier are given in section IV, and section V describes further difficulties with large amplifiers. Section VI describes the method of analysis, which is based on the method of Fox and Li[5] for plane parallel resonators. The differences in our treatment are emphasized and preliminary results are shown. Sections VII and VIII give conclusions and future work required.

II. MINIMUM CROSS-SECTION FOR A HIGH POWERED LASER/AMPLIFIER

The power P from a laser of cross-section A is given by[6]

$$P = \frac{1}{2} \; n \; h\nu c \; T \; A \qquad (1)$$

where n is the density of the lasing photons, h is Planck's constant, c the velocity of light and T the transmission factor of the output mirror. High values of P require A to be large for a given n, e.g. if $n \approx 10^{12}$ as in a gas laser with $h\nu = 0.44$eV and $T = 0.05$ a power of 1 MW would require $A \sim 0.7 m^2$ with a radius ~ 0.5m. On the other hand, if a one pass amplifier were used with $T = 1$, then for the same n, A would be reduced 20 times and the radius would now be about 0.11 m.

Again the intensity I of the lasing photons ($I = n\, h\nu c$) must be less than the saturation intensity $I_s = h\nu/2\sigma\tau$ where σ is the stimulated emission cross-section, and τ the spontaneous lifetime for the lasing medium[7].

The power output

$$P = AI < AI_s = \frac{A\ h\nu}{2\sigma\tau} \qquad (2)$$

Again we require A to be large, for large power.

(Equations 1 and 2 are almost equivalent as $\frac{1}{\sigma\tau} = c\ \Delta N$ where ΔN is the population difference and $\Delta N \approx n$ near saturation.)

III. MODES ARISING WITH LARGE RADII

We consider a laser in form of a cylinder of length L and radius r. The larger these values, the greater the number of modes possible because the frequency spacing between two consecutive modes, either along the axis or perpendicular to it would be[8]

$$\nu_{n+1} - \nu_n = \frac{c}{2L'} \qquad (3)$$

where L' can be either L axially, or 2r in the plane of cross section. (For solid and liquid lasers the refractive index must be included.) These modes will have wave numbers k_{nL} axially, k_{mr} radially, and hence, the waves can add to give a resultant wave number $k_{n,m}$ given by[8]

$$k_{nm}^2 = k_{nL}^2 + k_{mr}^2 \qquad (4)$$

Thus the number of modes can be large, and picking one mode only, difficult. This difficulty can be overcome by using a master oscillator-power amplifier system.

IV. ADVANTAGES OF A MASTER-OSCILLATOR POWER AMPLIFIER SYSTEM

The use of a laser amplifier-oscillator combination offers an advantage over a stronger laser-oscillator that is the same as in conventional electronics. It is possible to design and control the low-power oscillator more

precisely than an oscillator of large power-generating capability. A low-level laser oscillator may be built with confinement of excitation to relatively few modes. The amplifier that follows the oscillator need not be highly selective, but it must provide amplification in the frequency range containing the oscillator output.

The gain of a laser amplifier is limited because a very long amplifier or one very highly excited, may turn itself into a pulse generator. Therefore, when a laser system with a very large gain is required, it must be built using several amplifiers in series, and the passage of radiation in the reverse direction must be inhibited by isolators.

Without the isolators, if the gain of one stage were G and the reflectivity of the window of the next stage γ, then instability would occur if $G\gamma > 1$. A series of amplifiers would require isolator stages and beam expanders.

Also the problems of threshold and amplification of high power are relegated to separate units. It can be advantageous to use unstable mirror systems which reverse the radiation back through the same amplifier, but here our discussion centers on an axisymmetrical cylindrical one pass amplifier, the last stage of the series. It is assumed that a plane or Gaussian wavefront enters this amplifier and that adequate phase conjugation has been attained prior to this final amplifier[9,10]. The sides are considered transparent to enable penetration of the pumping radiation.

V. MODE PATTERNS WITH AMPLIFIERS OF LARGE RADIUS

5.1 Oblique Rays

If there were no amplification in a medium in the form of a cylinder (Fig. 1), then a beam of light entering on the left would be expected to

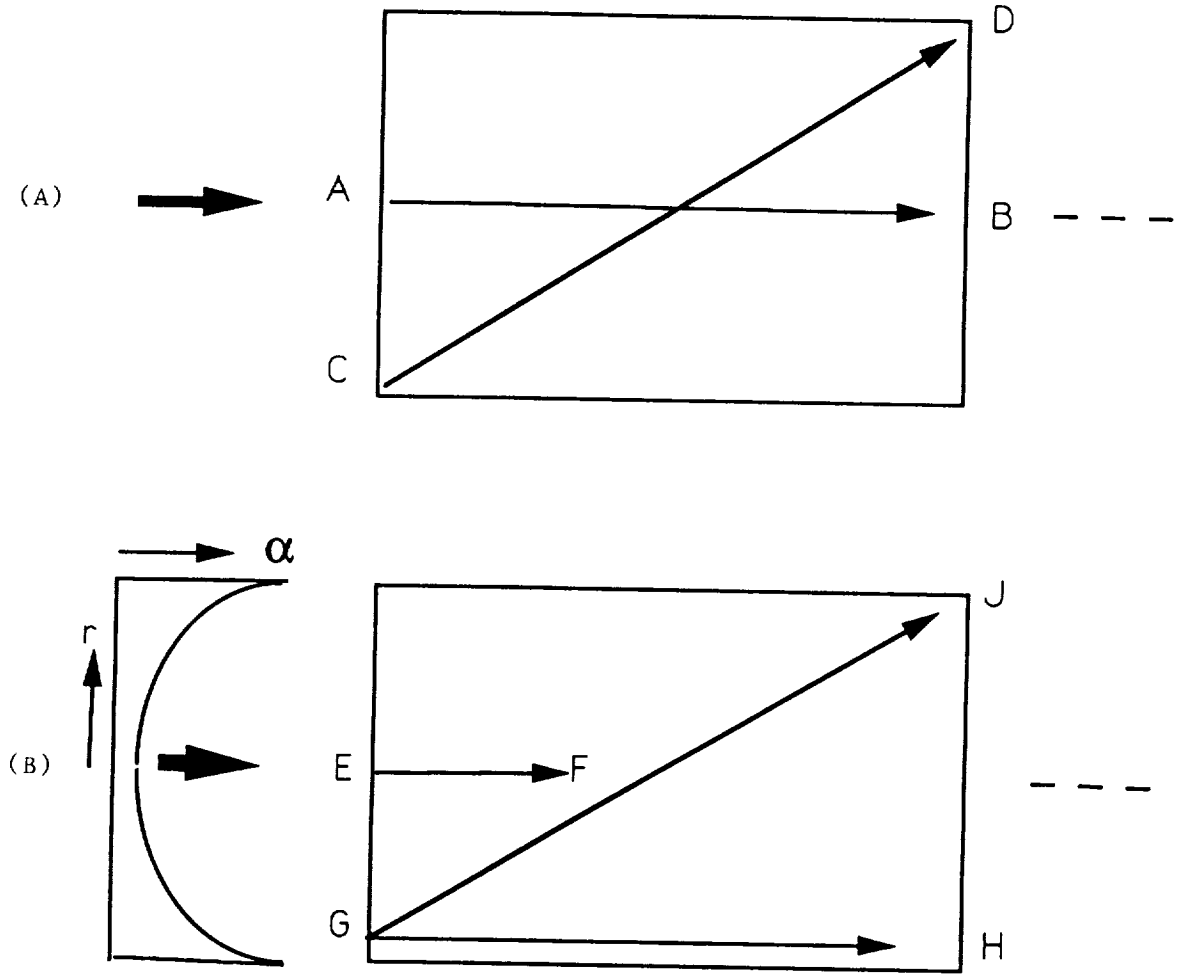

Figure 1. Medium in the form of a cylinder with wavefront entering from left. (A) Amplification α constant, ray CD gets amplified more than AB as longer path length; (B) α varies with radius; ray EF gets amplified less than GH, while GJ travles over regions of varying α.

continue to travel as a straight beam if $r \gg \lambda$ (Ray Optics). The beam profile could be found by Huygen's Principle, where each point at entry is assumed to emit a spherical wavefront and the wavefronts interfere. With amplification however, there may be changes to the beam pattern.

First, with constant gain α, if r/L is appreciable, ray CD will be amplified (Fig. 1a) more than ray AB, as CD passes through a greater length of medium. Obliqueness is neglected in the usual axial approximation.

If α varied with radius, and were greatest near the outside for example, then (Fig. 1b) the amplitude of ray EF would be less than GH, while ray GJ could be intermediate. The value of α would depend on a number of factors, one of which is how the pumping frequency is absorbed.

5.2 Absorption of Pumping Frequency

The absorption efficiency η_A is the fraction of the pumping radiation in the absorbed bandwidth that is deposited in the medium and should be high.[2] For one pass of pumping radiation, we require that the absorption length λ_a be $\ll 2r$, but if so the profile of the intensity of the pumping radiation could be much higher at the outer surface of the cylinder than on axis radiation. The gain $\alpha = \sigma_s (N_u - N_l)$, where σ_s is the stimulated emission cross-section, depends on N_u and N_l, the densities of the upper and lower laser levels. Now the rate of production of N_u depends on the pump intensity, the rates of stimulated emission (proportional to the laser photon density), spontaneous emission, the quenching rate and the rate of diffusion of upper level states in the medium. If the pump intensity were small on axis, then N_u and α could be small there also.

5.3 Multipass Pumping

A reduction in the variation of N_u with radius would be achieved by sending the pumping radiation through the medium several times by reflection,

with the absorption small (low pressure gas) during each pass (Fig. 2). However for a number of passes, the beam at each reflection has to pass through the outside surface twice, where some loss occurs, and be reflected with reflection losses. If the fraction remaining after each reflection is R and there are n passes, the absorption efficiency or fraction of radiation deposited in the gas is

$$\eta_a = (1 - \exp(-\gamma d)) \sum_{n=1}^{\infty} R^{(n-1)} \exp(-\gamma d(n-1)) \qquad (5)$$

where γ is the absorption coefficient to create the upper level ($\gamma = N\sigma_a$, N is the density of absorbers in the medium, σ_a the cross-section for absorption), and d is one path length through the medium; $d \simeq 2r$. A plot of η_a versus number of passes n for different R is shown in (Fig. 3) for $\gamma d = 0.01$ (i.e. absorption length 100 d). It can be seen even for R = 99% that only half the energy is deposited in the gas, however many passes. To increase η_a then γd must approach unity - in which case then the pumping radiation will be mostly absorbed just within the outside surface of the cylinder.

5.4 Saturation

The gain $\alpha(r)$ will also be reduced on axis if a wavefront with a Gaussian amplitude profile, with its maximum on axis is transmitted through the medium, and conditions are near saturation on axis. Then neglecting other factors, α will be reduced to $\alpha_u/2$ on axis, where α_u is the unsaturated gain.[8] Evidently, the effect of gain varying with radius must be investigated.

VI. METHOD OF ANALYSIS

To find the field patterns of a cylindrical laser, the method of Fox and Li was applied.[5] Their original work investigated a plane-parallel resonator

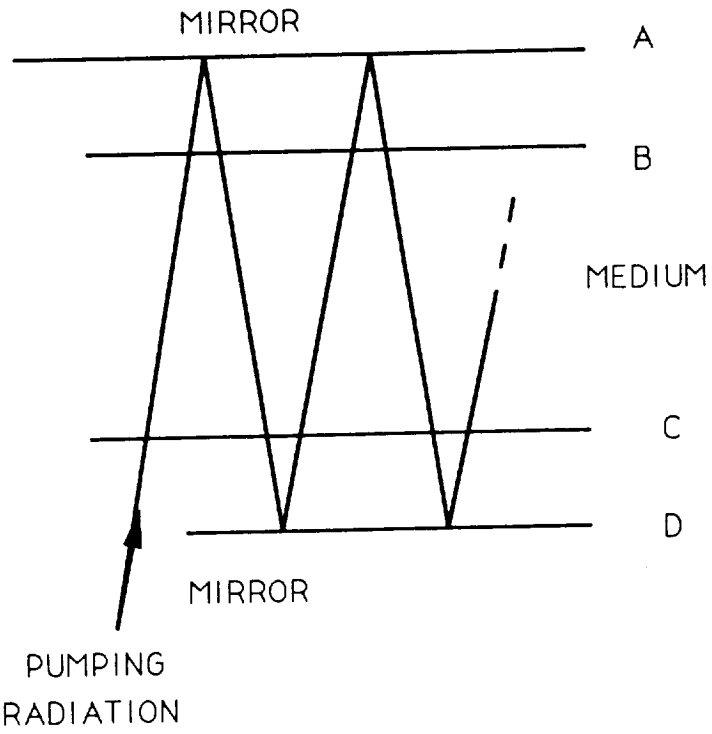

Figure 2. Miltipass absorption where pumping radiation is reflected through medium several times. Mirror losses occur at A and D, surface losses at B and C such as absorption in a containing vessel wall if the medium is a gas.

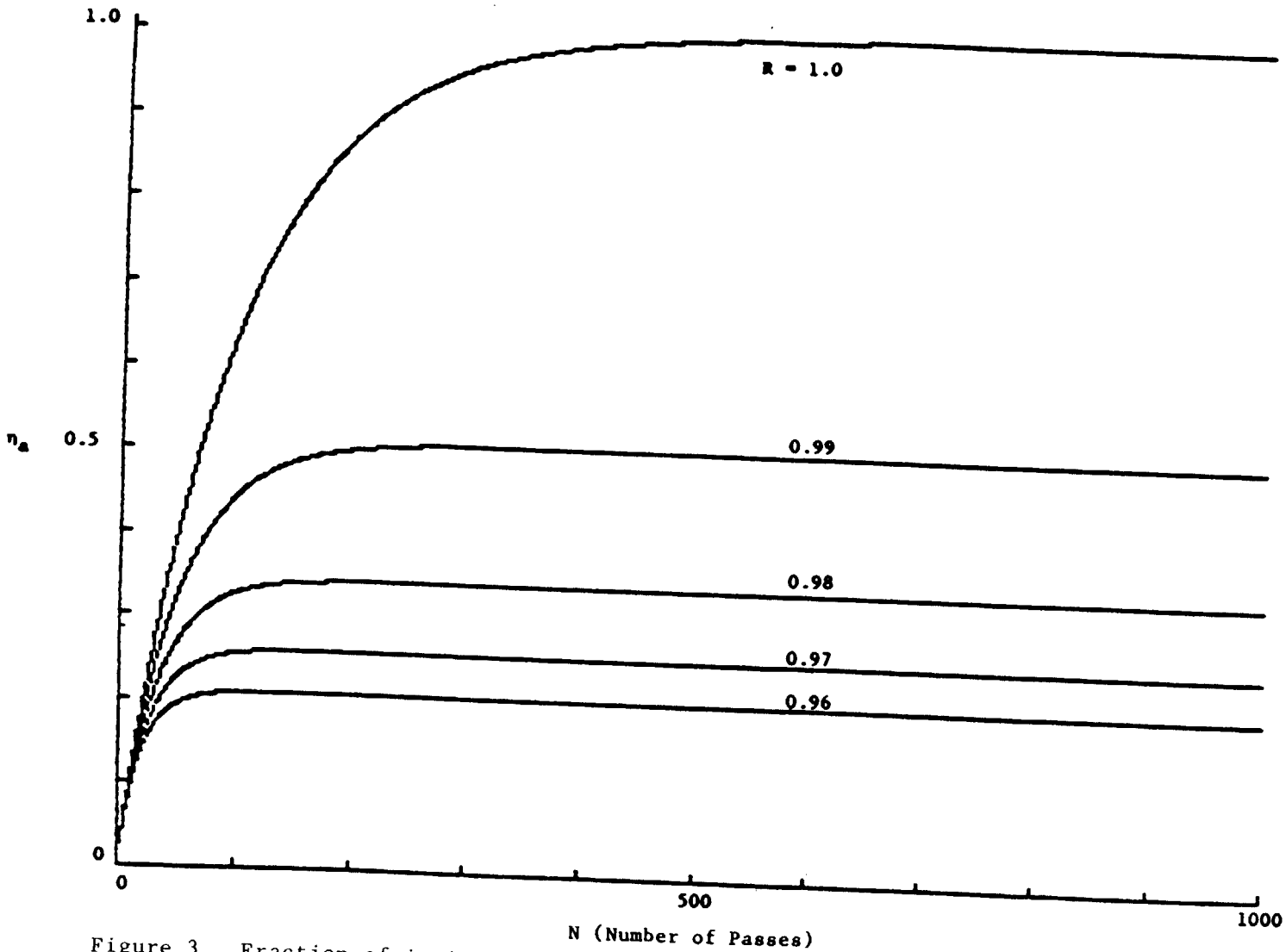

Figure 3. Fraction of incident radiation absorbed versus number of passes for various values of R which includes reflection and wall losses. The absorption length is 100 times the single path length ($\gamma d = 0.01$)

with the radiation reflected many times, and showed how modes would arise. Here we consider one pass only through an amplifier where the initial amplitude is either planar or a Gaussian, produced by the previous amplifier. Thereafter, it proceeds onwards without amplification to form a far field pattern. The treatment in this report so far is for transmission through the amplifier medium only. The present method differs from the original in several ways. Here the exact Kirchoff integral is used, and not the paraxial treatment, as large radii would ensure offaxis rays. Amplification in the medium is also included.

The electric field distribution is assumed known at plane 1 (Fig. 4) and is represented by a quantity $U_1(x_1,y_1)$ where U_1 consists of two parts U_{r1} and U_{i1}, real and imaginary. The quantity $\sqrt{U_{r1}^2 + U_{i1}^2}$ is then the amplitude, and the phase is $\tan^{-1}(U_{i1}/U_{r1})$. The amplitude squared is proportional to the energy density, and when integrated over the surface is proportional to the total power. To obtain the distribution on plane 2, the Kirchoff integral is used.[5]

$$U_2(x_2,y_2) = \frac{-i}{2\lambda} \int\int \frac{U_1(x_1,y_1)\exp(ikr)\ (1+\cos\theta)dx_1dy_1}{R} \qquad (6)$$

where R is the distance between P_1 and P_2, θ is the angle P_1P_2 makes with the normal to the surface at P_1, λ is the wavelength of the radiation; k the wave number and dx_1dy_1 is the element of surface around P_1. By writing $U_1 = U_{r1} + iU_{i1}$, the quantities $U_{r2}(x_2,y_2)$, $U_{i2}(x_2,y_2)$ are obtained for each point P_2 in plane 2. The integral is evaluated over all surface 1 for each point P_2 in plane 2. It is claimed the integral cannot be performed analytically and integration was performed element by element, by computer.

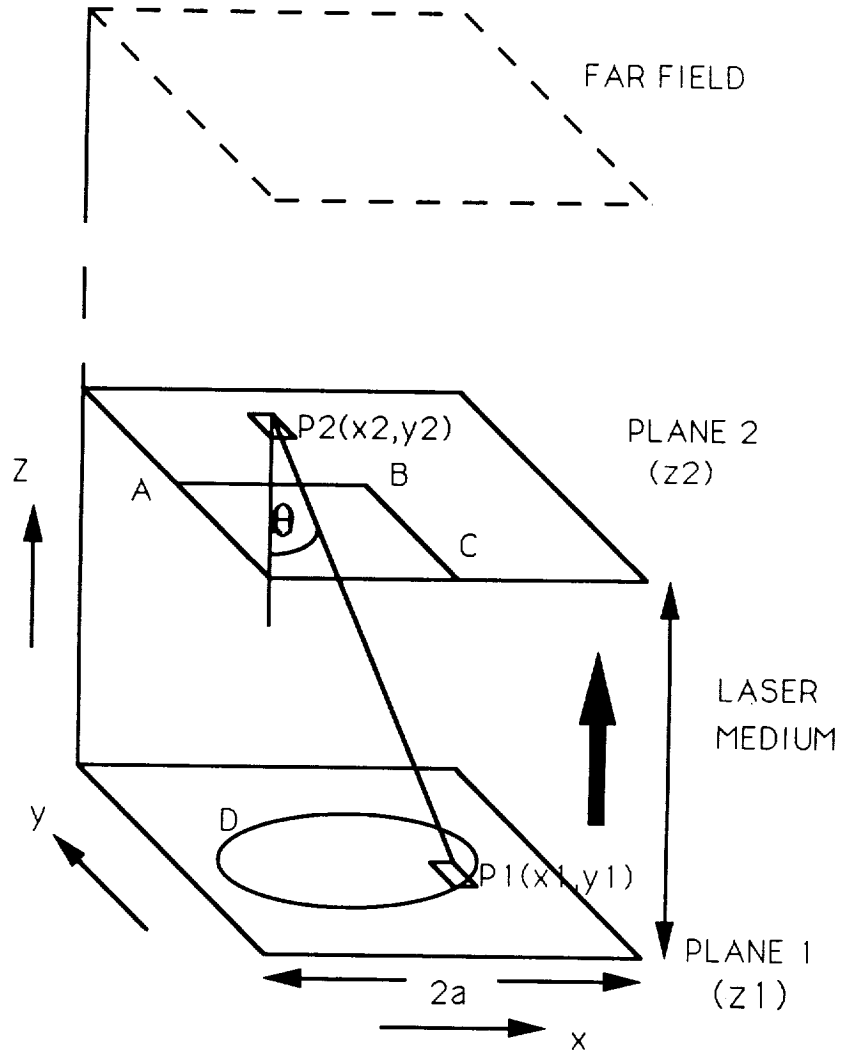

Figure 4. Method of solving the Kirchoff Integral.

If the values for each point in plane 2 are stored, a reiteration process can then find the pattern for plane 3 etc., as was done by Fox and Li.[5] So far, amplification has not been introduced.

6.1 Criterion of Step Length

A critical factor in the calculation is the step length dx_1, dy_1 and the number of steps $n=2a/dx_1$ in one dimension. The number of steps required depends on the Fresnel number

$$N_F = \frac{a^2}{L\lambda} \tag{7}$$

where (Fig. 4) L is Z_2-Z_1, and λ is the wavelength. The Fresnel number is the number of diffraction fringes in a width 2a a distance L away. To get accuracy at plane 2 there should be about 10 points per fringe, and therefore a criterion for n is

$$n \geq 10\ N_F \tag{8}$$

Initial runs were made with 20 x 20 steps and therefore should be accurate for $N_F \lesssim 2$. Higher values of N_F caused instabilities in the program[11] evidenced by very large fluctuations of U_{r2}, U_{i2} and indicating values of power in plane 2 greater than plane 1, which is inadmissible.

For $\lambda \approx 10^{-6}$m a value of $N_F = 2$ indicates a laser that is too long and too narrow, e.g. if a = 0.1 m then L = 5000 m. More reasonable numbers: a = 0.1 m, L = 1 m give $N_F = 10^4$ and then $n \geq 10^5$. With n^2 increments in plane 1 feeding into n^2 increments in plane 2, the total number of additions would be n^4, impossibly large, and the programs too long.

Two methods were used to reduce computer time, and were tried with 20 x 20 and 200 x 200 runs. The first consisted in storing values only for the square ABC (Fig. 4), and then using these values to fill in the mirror images

of the rest of plane 2, as axisymmetry could be assumed. However this only cut down the time to 1/4. A better and faster method could be used for cylinders where it was assuming $U_r, U_i = 0$ outside the dotted circle D in plane 1. Then values were filled in only for the 10 elements in the radius AB of plane 2. The program then filled in all the units of plane 2 by giving them values equal to those units in AB which were the same radius from the center B. The number of additions was now $n^3/2$, and the program lengths were more reasonable.

6.2 Initial Results with 20 x 20 Arrays

The first task was to see if runs with only 20 x 20 in 200 x 200 steps gave correct results and to recover the results of Fox and Li. Initial runs confirmed that a planar amplitude distribution in plane 1 produced Gaussian-like distributions with subsequent passes as expected.[5] Results were obtained for TM00 modes where the initial amplitude was constant over plane 1 (Fig. 5a-1) or was finite only inside circle D of Fig. 4 (Fig. 5a-3). Results for a TM01 mode were obtained when the sign of U was changed halfway across plane D1 (Fig. 5b). Only the results of the first pass are included in Fig. 5 although up to five passes were recorded. For small values of N_F the program runs correctly.

6.3 Collection Efficiency

The plots of intensity vs position can give a measure of collecting efficiency or the fraction of energy emitted at plane 1 which is received by plane 2. The energy emitted at plane 1 is $E_1 = \int^{A_1} I_1(x_1,y_1)dx_1,dy_1$, over the area A_1, calculated by summation over the elements dx_1dy_1 and that received at plane 2 is likewise $E_2 = \int^{A_2} I_2(x_2,y_2)dx_2,dy_2$. If gain G

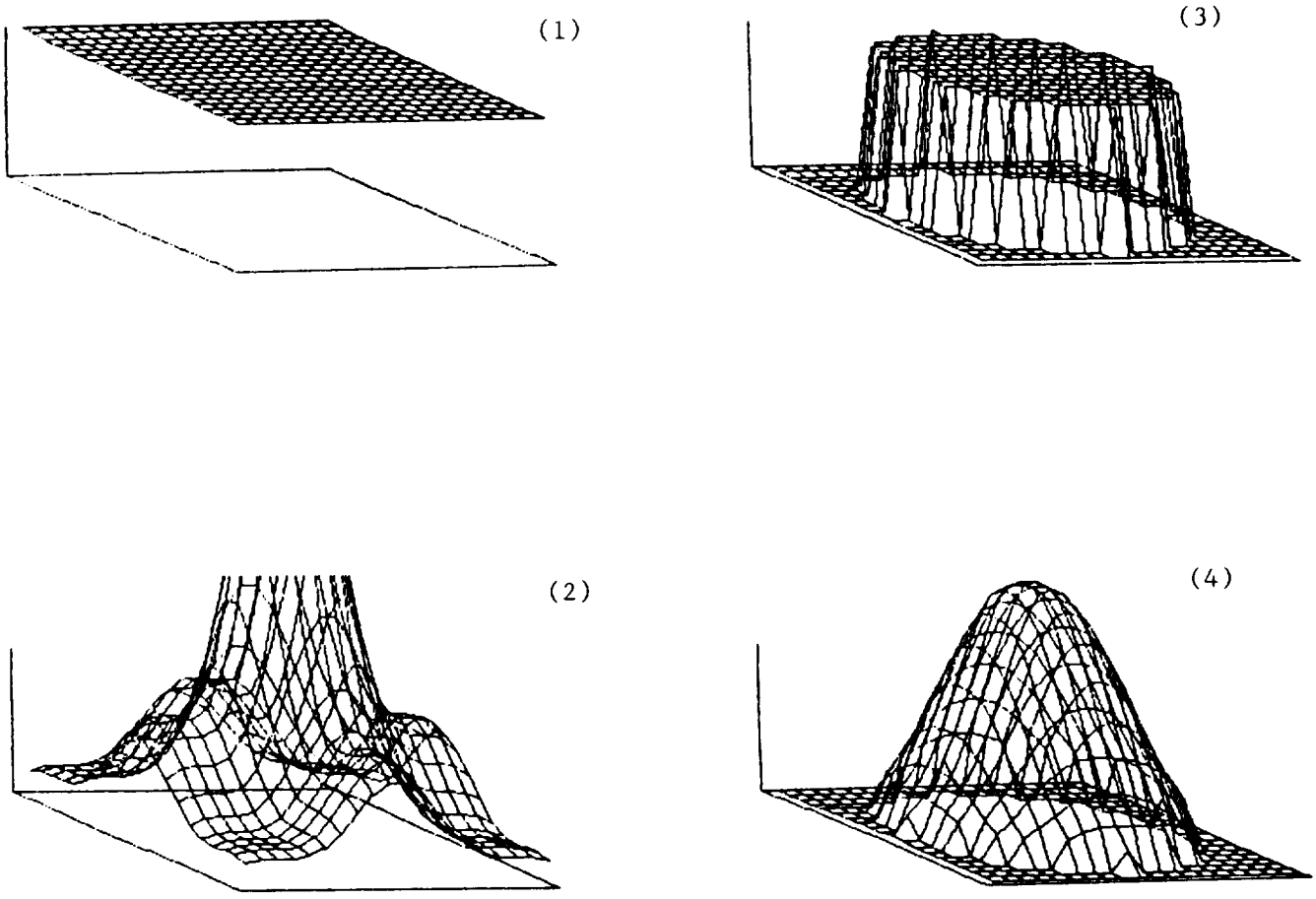

Figure 5(a). Results after one pass for different cross-sections.
(1) Initial intensity
(2) Intensity after one pass
(3) Initial intensity, circular cross-section
(4) After one pass
No amplification. N_F = 0.465. Mode is TM00.

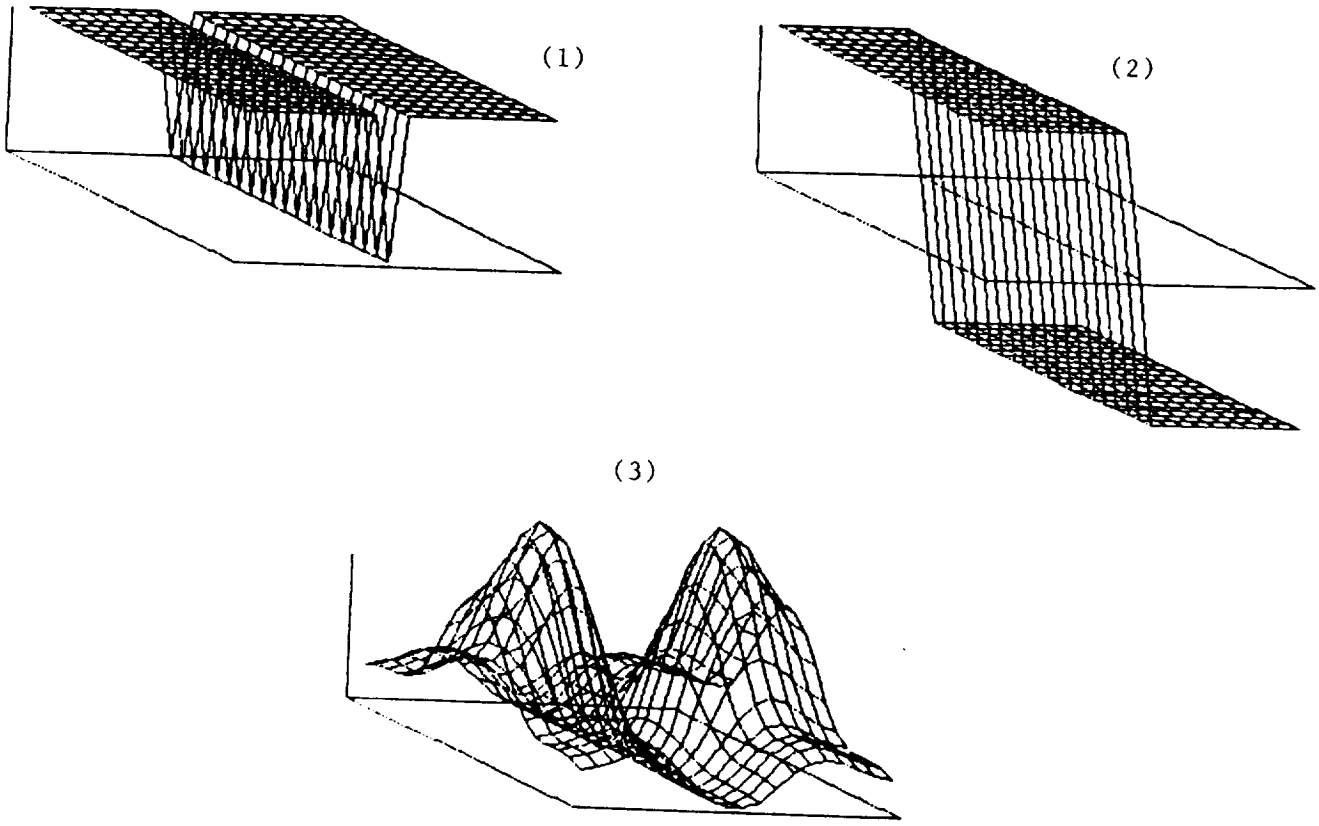

Figure 5(b). Results after one pass for a TM01 Mode.
(1) Intensity was assumed constant over initial plane
(2) U_r was assumed to have opposite phase over right side of plane
(3) Intensity after one pass

occurs in the medium, then a measure of the "collecting efficiency" over an area A_2 would be E_2/GE_1. This quantity will be used in section 6.4.

6.4 Spherical Mirrors and Focussing

Analytical methods are possible for plotting the mode patterns of confocal unstable resonators using Hemite-Gaussian functions[11], and computer runs gave good results. However the inclusion of gain, and gain varying with radius resulted in functions which were not tractable (incomplete Bessel functions), and this analytic method was not pursued further.

The effect of spherical mirrors or lenses can be included into the computer program by assuming that the rays emanating from plane 1 (Fig. 4) do not originate in the (x,y) plane of plane 1 (Huygen's principle) but from the surface of a sphere or paraboloid resting above and tangentive to it (Fig. 6). If O is the origin, then at (x_1,y_1), distance r from the origin, $(r = \sqrt{x_1^2 + y_1^2})$ the ray from B is assumed to start not at $z_1 = 0$, but $z_1 = \Delta z$. Assume a plane wave approaches along front BD. Then for the wave to focus at C, the path lengths BC and DO + OC must be equal. Now OC = f the focal length and therefore

$$z_1 = \Delta z \simeq \frac{r^2}{4f} \tag{9}$$

and equation (9) applies to paraboloidal mirrors.

The program ran successfully for $N_F \leq 4$ (few fringes mean large spread) for various values of f, and focussing was evident; the effect creased as N_F increased from 0.5 to 4. The method may be applied later for higher N_F, where the rays would be more beam-like (ray optics).

6.5 Variation of Gain with Radius

An estimate of the gain α as a function of radius based on laser

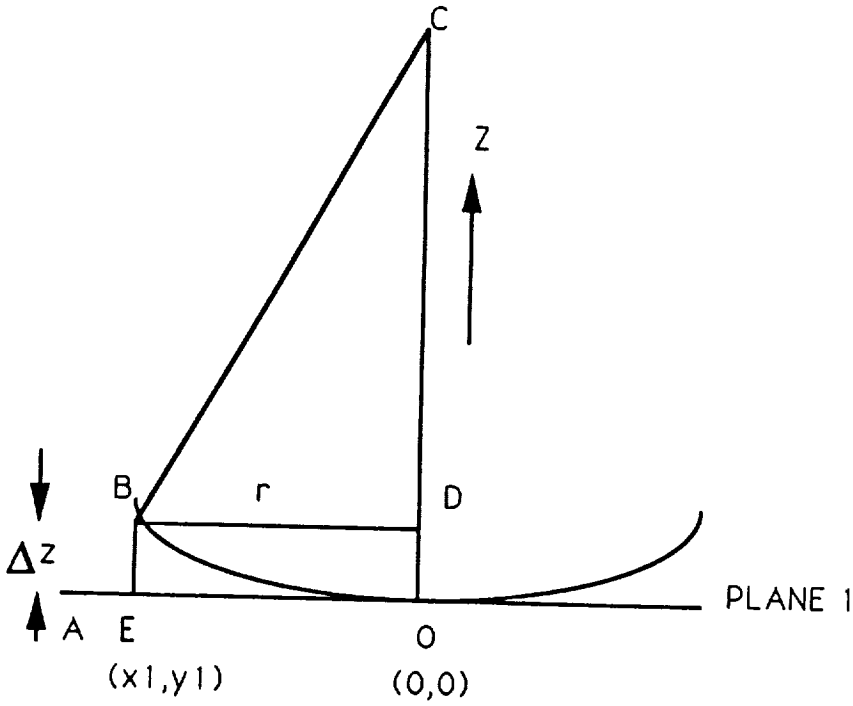

Figure 6. Method of treating a lens or curved surface of wavefront. Rays from D at radius r are assumed to start from B, where BE = Δz.

parameters has not yet been carried out. To simulate such variations we assume α is a parabolic function of r.

The total gain of the laser over a distance L, is G= exp(αL), where α is the gain per unit length. This is the gain in intensity I, which is proportional to $U_r^2 + U_i^2$. We assume that to attain G in intensity that U_r and U_i were both amplified equally by $\sqrt{G}$. We now define a gain α' per unit length, which is such that exp (α'L) = $\sqrt{G}$ and use α' to operate on U_r, U_i. It follows $\alpha' = \alpha/2$, and variations in α and α' with radius are connected linearly. We assume that $\alpha'(r)$ can be a symmetrical parabola about the axis:

$$\alpha'(r) = \alpha'_o \ (1 + \beta r^2) \tag{10}$$

where β is a constant. The sign of β determines whether the gain is a maximum ($\beta < 0$) or minimum ($\beta > 0$) on axis. A maximum on axis might result if the effect of focussing the pumping radiation on axis outweighed other considerations. Here we shall consider α' has a minimum value on axis consistent with the arguments of section 5.2 and 5.4.

Consider a maximum gain G_{max} at the edge of a cylinder and a minimum gain G_{min} at r = 0. The corresponding values of α' are

$$a'_{max} = \ln \left(\sqrt{\frac{G_{max}}{L}} \right) \quad ; \quad a'_{min} = \ln \left(\sqrt{\frac{G_{min}}{L}} \right) \tag{11}$$

By equation 10 also,

$$a'_{max} = a'_{min} \ (1 + \beta r^2_{max})$$

and β can be evaluated

$$\beta = \left(\frac{\ln \sqrt{G_{max}}}{\ln \sqrt{G_{min}}} - 1 \right) / r^2_{max} \tag{13}$$

It is convenient to use G_{max} and G_{min} when inserting numerical values.

Next consider a cylindrical laser with gain a function of radius (Fig. 7) and axis at $(x_1,y_1) = (0,0)$. We calculate the total gain

$G = \int_1^2 \alpha(r) \cdot dl$ from point (x_1, y_1, z_1) to (x_2, y_2, z_2). For any point at height z the x,y coordinates are

$$x = \left(\frac{x_2 - x_1}{z_2} \right) z + x_1 \tag{14}$$

$$y = \left(\frac{y_2 - y_1}{z_2} \right) z + y_1 \tag{15}$$

At height z, between z and z + dz the gain α' is

$$\alpha'(z) = \alpha'_o \left(1 + \beta (x^2 + y^2) \right) \tag{16}$$

and amplitude U_r (or U_i) is increased by dU_r in traversing path dl (Fig. 7).

$$dU_r = U_r \alpha'(z) dl \tag{17}$$

But dl/dz = constant and therefore

$$dU_r = \frac{dl}{dz} U_r \alpha'(z) dz \tag{18}$$

Expressing x and y in (Eq. 16) in terms of z, (Eq. 18) can be integrated, and leads to an effective α' over the path AB:

$$\alpha'_{eff} = \alpha'_o \sqrt{(x_2 - x_1)^2 + (y_2 - y_1)^2 + (z_2 - z_1)^2}$$

$$\left[1 + \frac{\beta}{3} (x_2^2 + x_2x_1 + x_1^2 + y_2^2 + y_2y_1 + y_1^2) \right] \tag{19}$$

The total gain g_{AB} between A and B for U_r, U_i is then

$g_{AB} = \exp \alpha'_{eff} R$

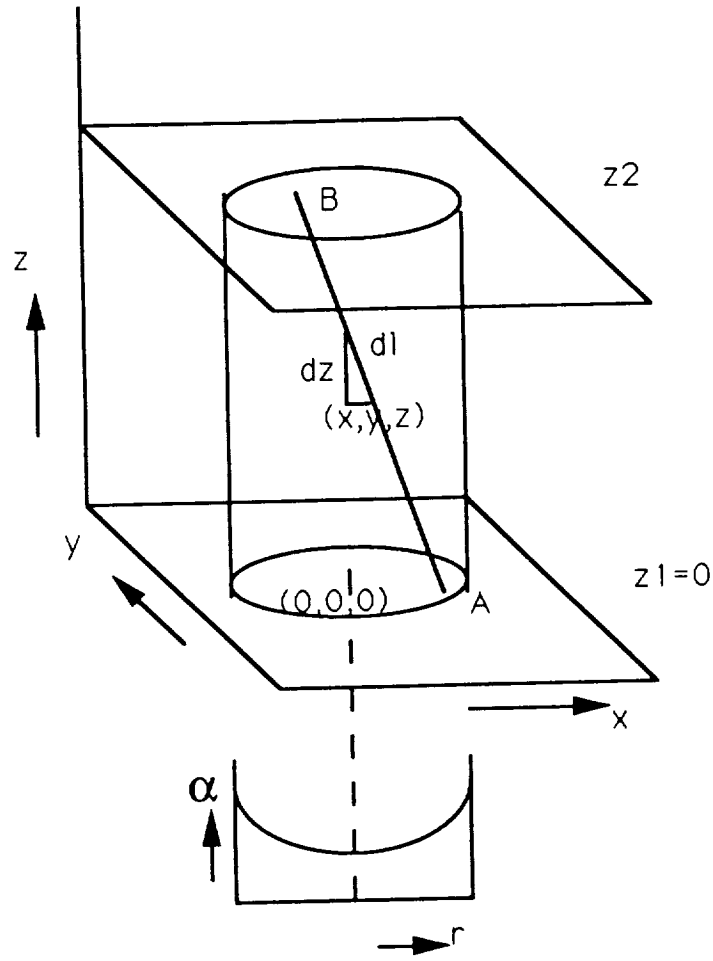

Figure 7. Gain α is a parabolic function of r. Ray AB travels through regions of varying $\alpha'(r)$.

where R is the distance between A and B. Thus when performing the integration of the Kirchoff integral over plane Z_1 for any point in plane Z_2, for each element at (x_1,y_1) at A, its contribution to U_{r2}, U_{i2} at point B is multiplied by g_{AB} which in turn depends on the coordinates of A and B.

The function in (Eq. 19) can be checked in the following ways: first, it holds for all Z_2, and if $Z_2 = 0$ or B is in plane A but not coincident with A, we still get gain, as the radiation still traverses a distance AB. Second, if $x_2 = x_1$, $y_2 = y_1$ on the beam is parallel to the axis the gain reduces to $\exp \alpha_o' (1 - \beta r^2) Z_2$ where r is constant. Third, if $\beta = 0$ and α' is independent of r, then the gain is $\exp \alpha_o' Z_2$. So the case $\alpha' =$ constant independent of r is included.

The intensity patterns for a laser where the gain α was 20 at the outside and center (Fig. 8-2) show considerably more intensity after amplification than the case for a gain of 20 at the outside and 2 at the center, as expected (Fig. 8-4). The question arises that for a parabolic variation of α which of the gains G_{max} or G_{min} decides the collection efficiency (Sec. 6.3). A series of runs were made where $G_{max} = 20$ and G_{min} varied from 20 to 2, and the collection efficiency plotted versus G_{min}/G_{max} (Fig. 9). Qualitatively, it can be seen that the power output is approximately proportional to G_{min}, although G_{max} was kept constant at 20.

The results so far have been for plane waves, of constant amplitude and phase over the initial wave front. Results were also obtained for waves with Gaussian amplitude profiles for similar Fresnel numbers. Gaussian profiles are more applicable to an actual case where previous laser/amplifiers would have already formed such a profile, with constant phase, and it was assumed $U_r = U_i$ over plane 1. The expression used was

$$U_r = \exp (- (r - r_o)^2 / \Delta r^2) \qquad (20)$$

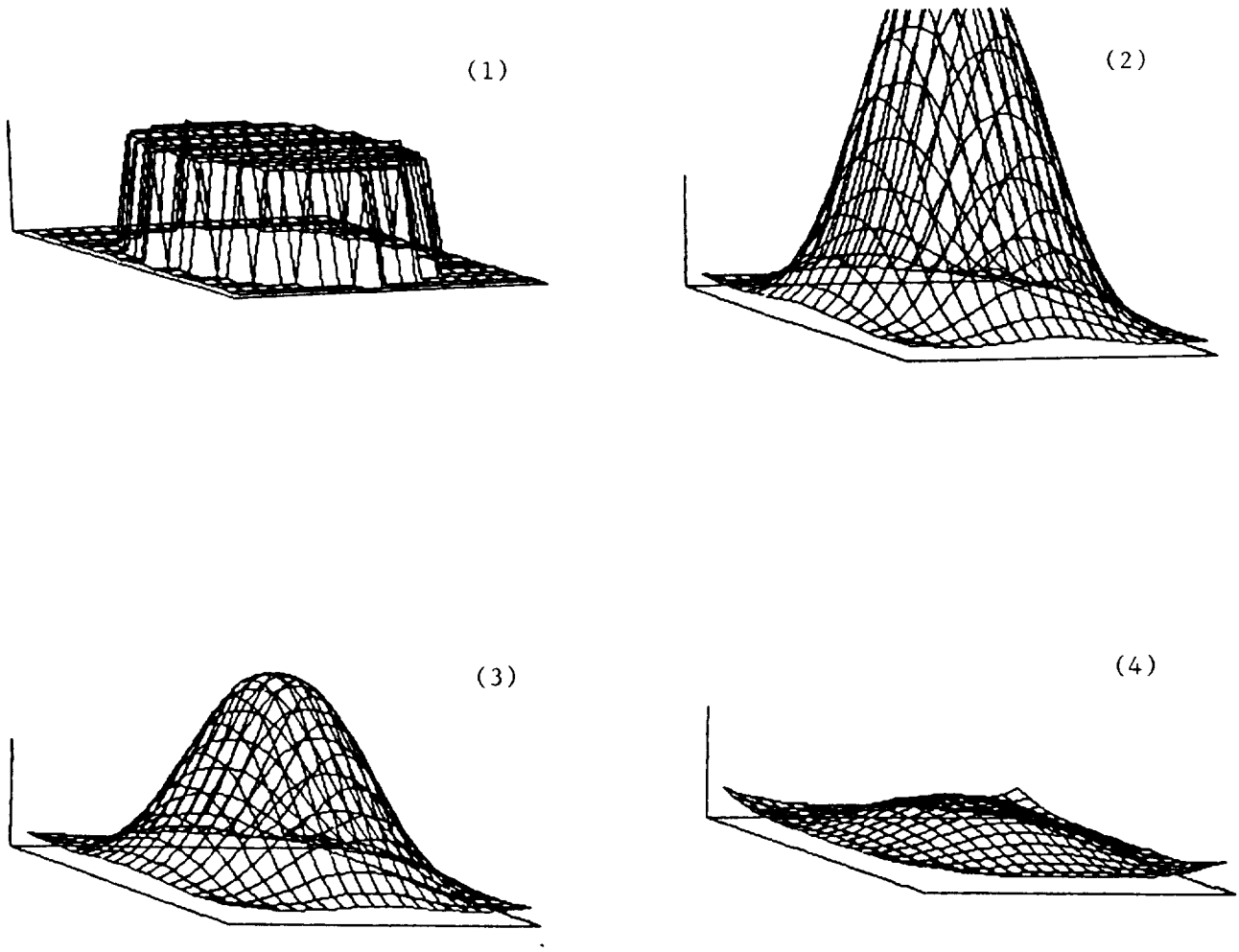

Figure 8. Results with α a parabolic function of radius with total gain G_{max} = 20 at edge of cylinder and total gain G_{min} on axis (1) Initial intensity (2) Intensity after one pass with $G_{min} = G_{max} = 20$ (3) With $G_{min} = 10$ (4) With $G_{min} = 2$. As G_{min} is reduced, intensity on axis falls, but at the edge stays almost constant. In (4), the intensity rises at the edges. $N_F = 0.465$.

where r_o was the coordinate of the axis, and Δr was the radius where U_r drops to e^{-1}. In our case, for plane Z_1 enclosing 20 x 20 linear units, Δr was chosen as 5 units, and the emitting and collection surface on planes 1 and 2, respectively were confined to circles of radii 8 units. Using circles rather than the square surfaces did little to alter the results for Gaussian profiles when Δr was much less than r.

The effect of varying G_{min}/G_{max} on the collecting efficiency was repeated and the results agreed well with Fig. 9, except that their values were about 10% lower due to the smaller collecting area on plane 2. Qualitatively, exactly the same dependence on G_{min}/G_{max} was obtained.

The variation in total intensity versus G_{min} can be explained by the spreading of the beam of radiation. In Fig. 8-2, the intensity at the edge of plane 2 is only a small fraction of that on axis; in Fig. 8-4, the intensity at the edge is as great as on axis, showing the beam was spreading and the mode structure modified. These results were for a laser with $N_F = 0.465$, and radius of 0.8 mm, length 1 m, with wavelength 1.37 μm.

VII. CONCLUSIONS

The emission of large power from a laser would best be accomplished by a master oscillator-power amplifier system where the amplifier has a large cross-section. For one pass in such an amplifier, the method of solving the Kirchoff integral gave results which worked successfully, but only so far for small Fresnel numbers - i.e. amplifiers with a diameter to length ratio much smaller than envisaged for high power. The preliminary results show that for a cylindrical amplifying medium pumped from the outside, difficulties would

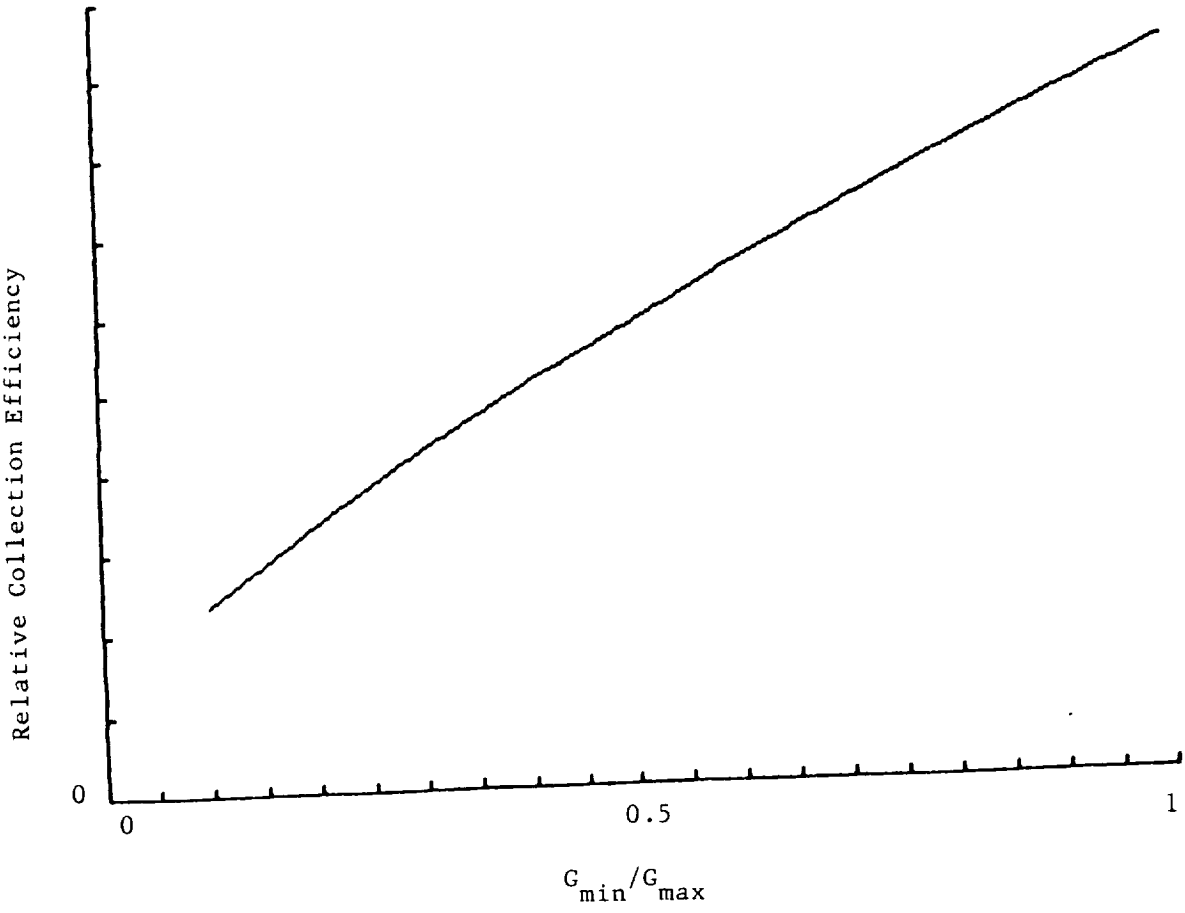

Figure 9. Plot of relative collecting efficiency vs G_{min}/G_{max}, where G_{min} is the overall intensity gain on axis, and G_{max} the gain at the outer surface of medium.

arise in attaining an efficient absorption efficiency and at the same time collecting all the power at the far end of the medium, due to deterioration of the mode pattern.

VIII. FUTURE WORK

Future work should include:

1. Extending the above treatment for one pass by increasing the cross-section of plane 2.
2. Extending the above treatment to include onward transmission of the radiation after leaving the laser to a plane many laser lengths away to find the far field pattern and collection efficiency.
3. Estimating the gain coefficient for a cylindrical medium pumped from the outside which includes the laser paramenters.
4. Including the effect of saturation of α.
5. Converting the programs to include higher numbers of steps, thus to treat higher Fresnel numbers, and lasers with larger diameter to length ratios.

REFERENCES

1. W.L. Harries, W.E. Meador, G.A. Minor, G.L. Schuster, G.H. Walker and M.D. Williams, "Laser-Powered Martian Rover," NASA Conference Publication 3034, Second Beamed Space-Power Workshop held at NASA Langley Research Center February 28 - March 2, 1989.

2. W.L. Harries, "Criteria for the Evaluation of Laser Solar Energy Converter System," AIAA Journal of Propulsion and Power Vol. 1, No. 5, p. 411, (1985).

3. J.H. Kwon, M.D. Williams and J.H. Lee, "A Survey of Beam-Combining Technologies for Laser Space Power Transmission," NASA Technical Memorandum 10, p. 1529, December 1988.

4. J.H. Kwon and J.H. Lee, "Far field pattern of one MW combined beam of Laser Diode array Amplifiers for Space Power Transmission." Presented at the 24th Intersociety Energy Conversion Conference, August 7 - 12, 1989.

5. A.G. Fox and T. Li, Bell System Tech J 40, p. 453, (1961).

6. W.L. Harries, W.E. Meador, "Kinetic Modeling of an IBr Solar Pumped Laser," Space Solar Power Review A, p. 189 (1983).

7. O. Svelto, "Principles of Lasers," Plenum Press, N.Y., p. 56 etc.

8. B. Lengeyl, "Lasers," Wiley Interscience, N.Y. 2nd Edition, 1971, p. 74 etc.

9. A. Siegman, "Lasers," University Science Books, Mill Hill, California, p. 282.

10. P.W. Milow and J.H. Eberly, "Lasers," 1988, John Wiley, p. 701 etc.

11. A.E. Siegman and E.A. Szikles, "Mode Calculations in Unstable Resonators with Flowing Saturable Gain," App. Optics 13 No. 12, p. 2775, 1974.

12. O. Svelto, ibid, p. 118.

APPENDIX C

Space Solar Power Review Vol. 2, pp. 367–381, 1981
Printed in the USA.

0191-9067/81/040367-15$02.00/0

SOLAR-PUMPED ELECTRONIC-TO-VIBRATIONAL ENERGY TRANSFER LASERS

W. L. HARRIES
Old Dominion University
Norfolk, Virginia 23508, USA

J. W. WILSON
NASA Langley Research Center
Hampton, Virginia 23665, USA

Abstract — The possibility of using solar-pumped lasers as solar energy converters is examined. The absorbing media considered are halogens or halogen compounds, which are dissociated to yield excited atoms, which then hand over energy to a molecular lasing medium. Estimates of the temperature effects for a Br_2–CO_2–He system with He as the cooling gas are given. High temperatures can cause the lower energy levels of the CO_2 laser transition to be filled. The inverted populations are calculated and lasing should be possible. However, the efficiency is less than 10^{-3}. Examination of other halogen-molecular lasant combinations (where the rate coefficients are known) indicate efficiencies in all cases of less than 5×10^{-3}.

I. INTRODUCTION

One concept for collecting solar energy is to use large solar collectors on orbiting space stations, which then transmit the energy as laser beams. If the solar energy could be converted directly into laser radiation, the inefficiencies in converting the energy through different transducers could be avoided. Gas lasers would be advantageous because they provide a uniform medium, structural problems are reduced, and the volume could be large. Here the concept of solar-pumped gas lasers used as energy converters is examined.

The difficulties lie in the fact that the major fraction of the solar radiation lies in the longwave (visible) region of the spectrum with a peak at about 2 eV. An efficient absorber [1] must be broadband, [2] must absorb near the peak of the solar spectrum, and [3] the excited state must be at an energy level sufficiently great to yield reasonable quantum efficiency. The halogens can be dissociated at these energies, resulting in one atom being in an electronically excited state due to an electron spin flip. The excited levels are at a few tenths of an eV, comparable with the levels of molecular lasants. Only the halogens and halogen compounds are considered here as absorbers, although of course other materials may be feasible.

Two possibilities are open once the energy has been absorbed: either the absorbing medium lases or it hands over the energy to a different medium. The case where the absorber and lasing medium are the same will be treated elsewhere. In view of the high efficiencies of CO_2 lasers, a BR_2–CO_2–He laser is considered as a first example with the helium acting as a cooling medium.

Recently Gordiets, Gudzenko and Panchenko (1) published a theoretical analysis

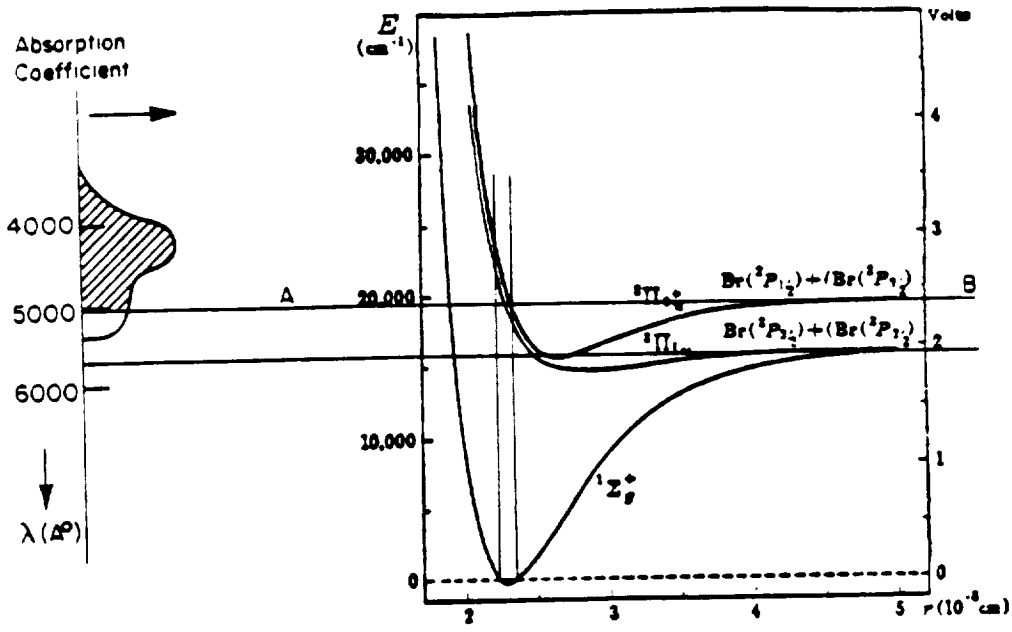

Fig. 1. Potential curves of the Br_2 molecule and the absorption coefficient. The photons corresponding to the shaded area cause dissociation. Those that cause the electron to be raised to the $^3\Pi_{0_u^+}$ level below *AB* create vibrational states and hence increase the temperature. The potential curves were taken from Ref. 3.

of such a solar-pumped gas laser. The physical mechanisms assumed here are largely the same, but our analysis differs in several respects. First, extra nonlinear terms are included to take account of the depletion of the particles, otherwise at low pressures the above theory predicts more excited states than there were neutral particles in the first place. Second, the energy flow is discussed more fully, and estimates are shown of the temperatures of the medium at high concentrations of solar radiance. The temperature decides the density of the lower laser level. Third, solutions are obtained for the inversion density in terms of a wide range of parameters, including the gas composition and pressures. Fourth, an estimate of the efficiency is given.

The physical mechanisms are discussed in Sec. 2, and estimates of densities of Br* and the upper laser level are obtained in Sec. 2.1. Section 2.2 considers the temperature rise of the laser medium and the population of the lower laser level. The inversion population is then displayed graphically as a function of gas composition. The efficiency estimates are presented in Sec. 3. Other combinations of halogen absorber-molecular lasants are then discussed in Sec. 4 and their overall efficiencies estimated.

II. PHYSICAL MECHANISMS OF A Br_2–CO_2–He LASER

The frequency of dissociations per bromine molecule is $D = \Phi\Delta\lambda\sigma$, where Φ is the solar flux (photons $cm^{-2}\,s^{-1}$ per Å), $\Delta\lambda$ the absorption bandwidth, and σ the cross section at the photodissociation peak. The cross section varies with wavelength λ and also with the gas temperature T. The absorptivity of Br_2 vs λ and T has been studied by Passchier, Christian, and Gregory (2), who showed good agreement between theory and experiment. The theory showed that increasing the temperature

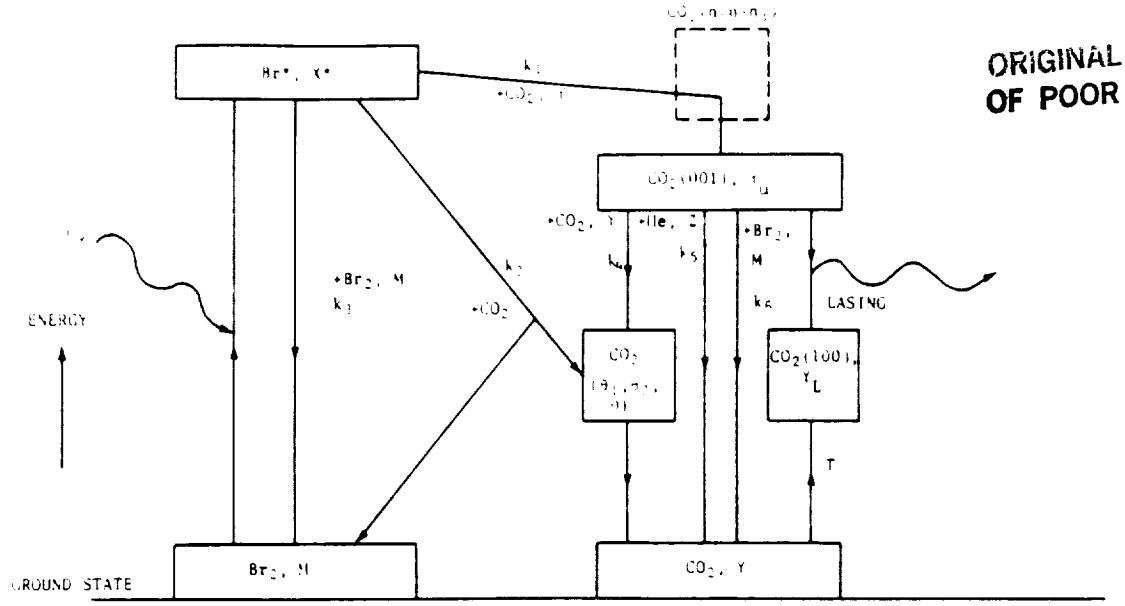

Fig. 2. Energy flow diagram of a Br_2–CO_2–He solar-pumped laser and for an absorber M, a lasing medium Y, and a cooling gas Z.

from 300 to 800 K reduced the peak value of σ at 4200 Å by 26%, but the $\Delta\lambda$ increased correspondingly and hence the temperature had little effect on D.

The absorbed photons cause an electronic transition to a higher upper energy level (3) (Fig. 1), and in Br_2 there are two potential curves associated with such transitions in the visible. The transitions obey the Franck–Condon principle, and only those electrons which arrive in the upper level above the line AB can cause dissociation, $Br_2 + h\nu \rightarrow Br^* + Br$, corresponding to only the shaded part of the absorptivity curve (3). Below AB, the molecule ends in an electronically excited vibrational state. The transitions into the $^3\Pi_{1_u}$ state all result in dissociation, but the cross section is probably lower. It will be assumed only a fraction F of the absorbed photons creates Br*, while the remainder causes heating of the gas, with F somewhere between 0.5 and 0.9.

It is convenient to summarize the reactions in an energy flow diagram (see Fig. 2). The Br* can hand over energy to CO_2 to raise it to an asymmetric oscillation mode (001) at about 0.3 eV: $CO_2 + Br^* \rightarrow CO_2(001) + Br + \Delta E_1$, with $\Delta E_1 \sim 0.2$ eV, and a rate coefficient $k_1 \approx 6 \times 10^{-12}$ cm^3 s^{-1} (4). The Br* can also be deactivated by collisions with CO_2 which end up in levels other than (001) [rate coefficient $k_2 \approx 10^{-11}$ cm^3 s^{-1} (5)], and by collisions with Br_2 [$k_3 \approx 4.7 \times 10^{-13}$ cm^3 s^{-1} (6)]. The rate coefficient for deactivation by He is negligible. The CO_2 (001) can be deactivated by collisions with CO_2 [$k_4 \approx 10^{-14}$ cm^2 s^{-1} (7)], He [$k_5 \approx 10^{-14}$ cm^3 s^{-1} (7), Br and Br_2 [$k_6 \approx 8 \times 10^{-15}$ cm^3 s^{-1} (8)]; however, it will be seen that Br << Br_2 under usual conditions. The CO_2 (001) can then lase into the lower level, CO_2 (100).

II. 1. Densities of Br and the Upper Laser Level*

The rate equation for Br* is

$$\frac{dBr^*}{dt} = CF\Phi\Delta\lambda\sigma(Br_2 - Br^*) - Br^*[(k_1 + k_2)\,CO_2 + k_3(Br_2 - Br^*)], \qquad (1)$$

where C is the number of times the solar radiation is concentrated. If a focusing mirror concentrates C' times and there are x multiple passes, then $C = C'x$. Equation (1) differs from Ref. 1 in that, instead of Br_2, the expression $Br_2 - Br^*$ is written to include the effect of depleting the Br_2. The effect of depletion of Br_2 is small for $C<100$ and pressures <1 Torr.

The rate equation for the CO_2 (001) = N_{001} is

$$\frac{dN_{001}}{dt} = k_1 Br^*(CO_2 - N_{001}) - N_{001}[k_4(CO_2) + k_5(He) + k_6(Br_2)] . \quad (2)$$

The first parentheses include the effect of depleting the CO_2, which causes large differences to the results when the CO_2 concentration is small. Deexcitation by Br_2 is included; the latter was mentioned in Ref. 1 but not included in the final expression. Its inclusion with $k_6 = 8 \times 10^{-15}\ cm^3\ s^{-1}$ reduces the results for the inversion population by about an order of magnitude.

Using the steady-state solution of Br* from Eq. 1:

$$N_{001} = \frac{Br^*}{(k_4 + k_5 b/a + k_6/a)/k_1 + Br^*/(3.5 \times 10^{16}\ pa)} . \quad (3)$$

where the gas composition is described by the ratios $a = CO_2/Br_2$ and $b = He/Br_2$, p is the pressure of Br_2 in Torr; the term $3.5 \times 10^{16}\ pa = (CO_2)$, and its inclusion ensures $N_{001}<CO_2$.

II.2. Temperature of the Medium

The lower lasing level is assumed to be the CO_2 (100) state, at $E_{100} = 0.17$ eV above ground level. If the temperature of the gases is T, then by Boltzmann statistics

$$N_{100} = N_{000}\exp(-E_{100}/kT) = (CO_2 - N_{001})\exp(-1972/T) , \quad (4)$$

with k = Boltzmann's constant, T in K. The depletion of CO_2 if N_{001} becomes appreciable at very high radiance is included. Clearly T must be kept as low as possible.

As a first consideration the container wall will increase in temperature. If the average wall transparency is τ, then a fraction $(1 - \tau)$ of the incident radiation will be absorbed. However, the largest heat contribution to the wall comes from the gases.

The collector of area A_c receives 1.4 kW m^{-2}. If the overall laser efficiency is η, and η_A is the absorption efficiency or fraction of the solar radiation absorbed, then $1.4A_c\eta_A(1-\eta)$ kW have to be dissipated by radiation into space. Assume the heat is perfectly conducted to a radiator of area A_r and emissivity ϵ, which is at approximately the same temperature (T_w) as the wall. Then by Stefan's law:

$$T_w \simeq 400\left[\frac{\eta_A(1-\eta)}{\epsilon}\frac{A_c}{A_r}\right]^{1/4} \text{ (in degrees Kelvin)} . \quad (5)$$

The quantity $\eta_A(1-\eta)/\epsilon \simeq \eta_A \simeq 0.2$ if η is small. The area A_r could be made equal to A_c by using the back of the collector to radiate, in which case T_w would be about 300 K; if $A_c/A_r = 40$, then, $T_w \simeq 700$ K. However, the heat has to be conducted efficiently to the radiator, and so the problem of weight arises.

The temperature of the gases can be roughly estimated by considering the energy

deposited and then assuming it is carried to the walls by gaseous conduction. The amount of absorbed energy that goes into heating is obtained from Fig. 2 by considering the branching ratios. The fraction of the absorbed quanta (of average energy $\bar{\epsilon}$) that ends up in producing CO_2 (001) is $Fk_1a/[(k_1 + k_2)a + k_3]$, and hence the fraction contributing to heating (F') is

$$F' = 1 - \frac{Fk_1a}{(k_1 + k_2)a + k_3} . \tag{6}$$

For example, if $F = 0.5$, then F' lies between 1 ($a \rightarrow 0$) and 0.81 ($a \rightarrow \infty$).

The heat absorbed per sec per cm^3 is dQ/dt:

$$\frac{dQ}{dt} = C\Phi\Delta\lambda\sigma F'\bar{\epsilon}\,[Br_2] = 10^{-3}CF'p\ (W\,cm^{-3}) \tag{7}$$

as $\Phi\Delta\lambda\sigma = 1.15 \times 10^{-2}\ (s^{-1})$ and $\bar{\epsilon} = 2.7$ eV for Br_2.

The coefficient of heat conduction of a single gas is given by $\kappa = \lambda\bar{c}nC_v/3$, where λ is the mean free path, $\bar{c}$ the particle velocity, n the gas density, and C_v the specific heat of the gas at constant volume. The conduction is independent of the pressure (λn = constant) and $\propto \sqrt{T}$. The conduction mechanism is a transport of the hot particles with a diffusion coefficient $\lambda c/3$; hence, for a mixture of gases 1, 2, 3, where 1 = He, 2 = CO_2, 3 = Br_2, the resultant coefficient κ is

$$\kappa = \kappa_1 \left[\frac{1 + a\sqrt{\frac{m_2}{m_1}}\frac{C_{v,2}}{C_{v,1}} + b\sqrt{\frac{m_3}{m_1}}\frac{C_{v,3}}{C_{v,1}}}{1 + a\frac{\sigma_2}{\sigma_1} + b\frac{\sigma_3}{\sigma_1}} \right] \sqrt{\frac{T}{273}} = \kappa_1 S\sqrt{\frac{T}{273}} , \tag{8}$$

where m_n = molecular weight, $C_{v,n}$ = specific heat at constant volume, σ_n = collision cross section, and S is defined as shown. The coefficient is in terms of κ_1 as He has the highest conductivity and is regarded as the cooling gas.

Assuming a one-dimensional heat flow out from the center of the gas to the enclosing side wall: $dQ/dt = \kappa A_1 (T - T_w/)l$, where A_1 = unit cross section, l = distance, then a rough estimate of T at the center is obtained:

$$T\,(K) = \left[5.85 \times 10^{-3} \left(\frac{C'xpl}{\kappa_1 A_1} \right)\left(\frac{F'}{S} \right) + T_w^{3/2} \right]^{2/3} \tag{9}$$

The numerical constant assumes $\kappa_1 = 3.27 \times 10^{-4}$ cal s^{-1} cm^{-1} K^{-1} (9). Apart from the one-dimensional approximation, Eq. 9 may also not be accurate if the radiation produces considerable dissociation. However, it can be seen that T is a function of (xpl/A_1), or a similarity law is obeyed (note that T_w contains C'). Increasing p is equivalent to increasing either x or l/A_1. The gas ratios are described by (F'/S).

Computer plots of T at pressures of 1 and 3.6 Torr on an $a-b$ plane are shown in Fig. 3 for $C = 100$, $F = 0.5$, $T_w = 300$ K. A flat laser is assumed of depth $d = 2$ cm, so $l \simeq d/2$ and $A/l \simeq 1$ for unit area. Then Fig. 3a corresponds to $p(Br_2) = 0.17$ Torr, and Fig. 3b corresponds to 3.7 Torr. The small increase in pressure causes a dramatic increase in T because more radiation is trapped, yet the conduction does not increase

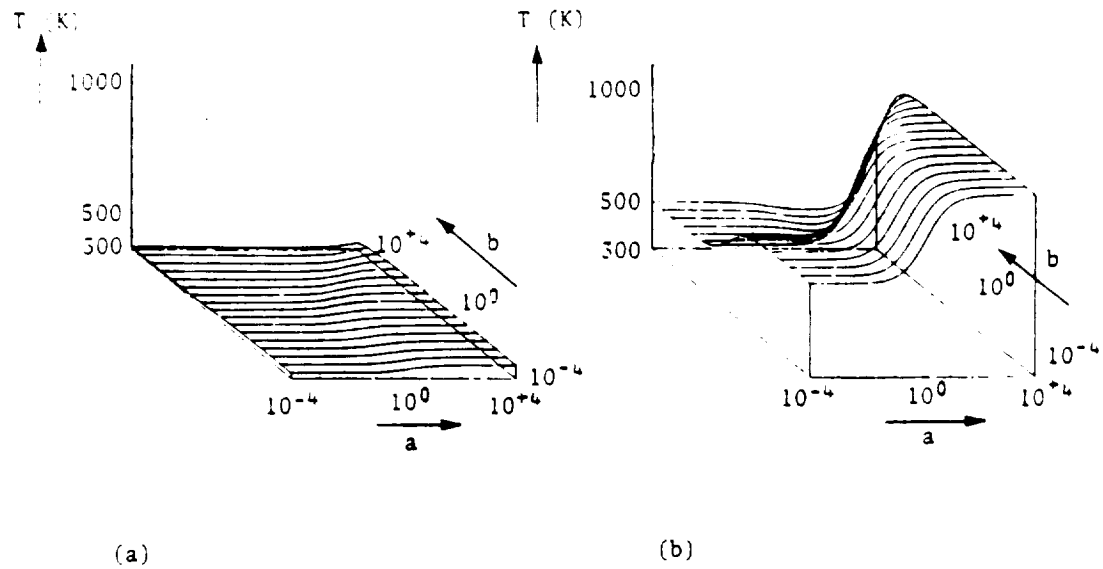

Fig. 3. Plots of gas temperature T(K) on an a–b plane: $a = CO_2/Br_2$, $b = He/Br_2$, $C = 100$, $F = 0.5$, $T_w = 300$ K; if $A/l = 6$, then (a) corresponds to $p = 1$ Torr, (b) to $p = 20$ Torr; if $A/l = 1$, then (a) corresponds to 0.17 Torr, (b) to $p = 3.3$ Torr.

accordingly. If $A/l = 6$ (for example, $A/l = 2\pi$ for a cylinder, if l = radius, but the one-dimensional argument is then inaccurate), then Fig. 3a would correspond to 1 Torr and Fig. 3b to $p = 20$ Torr.

For any given p, the variations of T with a and b are mostly due to the quantity $1/S$, or variations in the heat conductivity of the mixture, which can vary over a range of 6 to 1, whereas F' varies only from 0.81 to 1. Evidently overheating may curtail high-pressure operation of the laser system.

II.3. Inversion Population

Evaluation of T yields N_{100} by Eq. 4, and the inverted population $N = N_{001} - N_{100}$ can be estimated from Eqs. 3 and 4. Computer plots of N on $a-b$ planes for different pressures are shown in Fig. 4. The ratios a and b vary over the range 10^{-4} to 10^{4}, and N is on a linear scale. Where N is negative, the plots indicate zero. The values assumed are $C = 100$, $F = 0.5$, $A/l = 1$, $T_w = 300$ K.

When the effect of Br_2 deexcitating the CO_2 is omitted (the k_4Br_2 term), the values of N are an order of magnitude greater. Also, failure to include the depletion terms results in N's too high for low p, and low a: for example, if $p = 0.001$ Torr, and $a = 10^{-3}$, $b = 10^{-2}$, the estimated $N_{001} \simeq 10^{13}$, whereas there are only 3.5×10^{10} molecules of CO_2 present. The depletion terms result in the flattening of the graphs at low p and low a, so that $N_{001} < CO_2$.

The drop in N at high values of a is the effect of the lower level filling up because of temperature rise for increased CO_2 content (Fig. 3b). The temperature rise gets rapidly worse as p increases and results in the lower level exceeding the upper level at about 1 Torr for $A/l = 1$. On recalculating N with $A/l = 6$, the curves for $p = 10^{-3}$, 10^{-2}, and 10^{-1} Torr are indistinguishable from the above, consistent with the low temperature rise at lower p (Fig. 3). However, the values in the 1-Torr plot are about

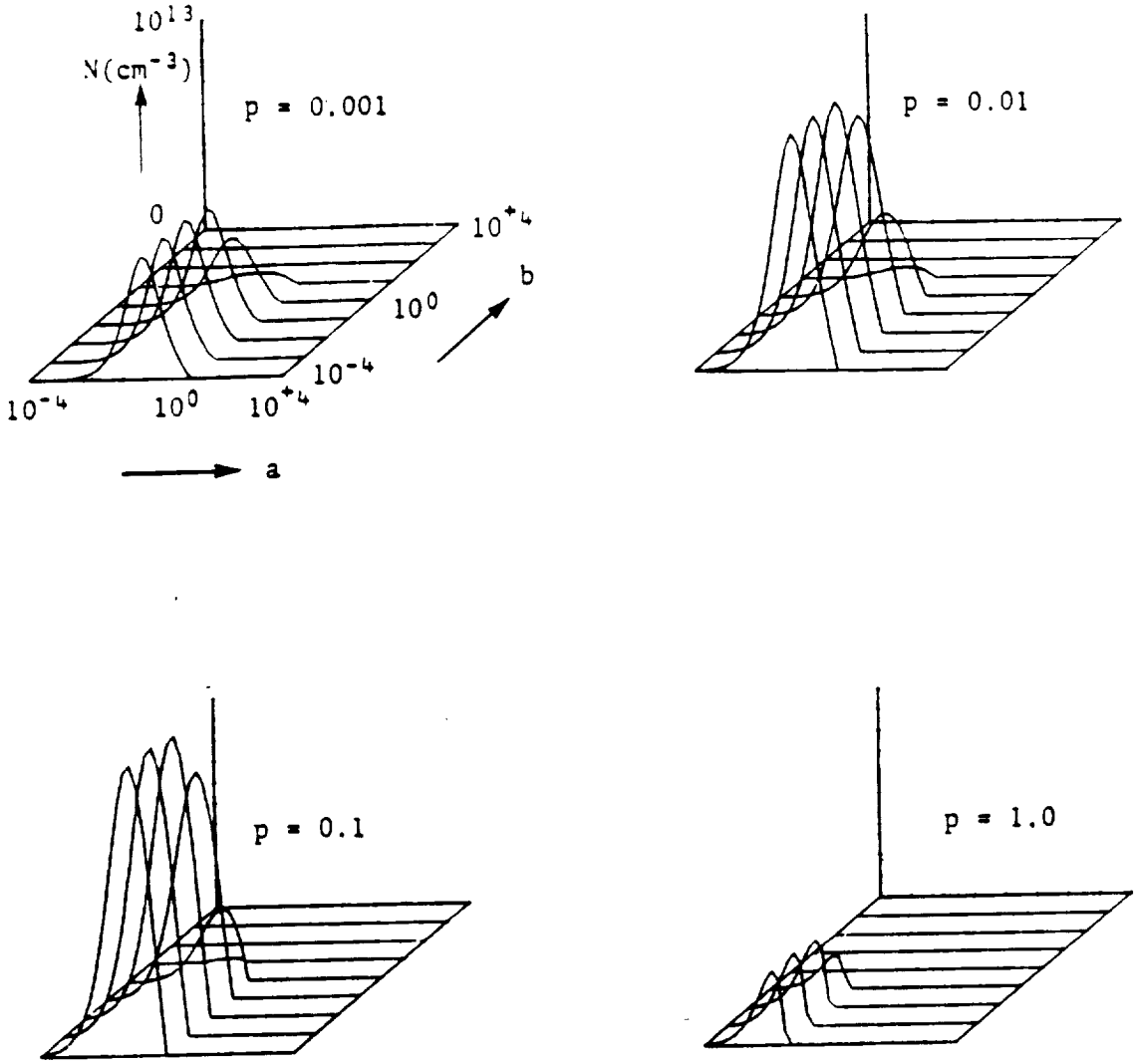

Fig. 4. Plots of N on an a–b plane at different Br_2 pressures (Torr): $C = 100$, $F = 0.5$, $A/l = 1$, one pass, $T_w = 300$ K.

five times higher, and at 3 Torr there is still an inverted population. All these results are obtained assuming the wall temperature T_w is 300 K.

At $T_w = 400$ K, the curves for 0.001, 0.01, and 0.1 Torr become identical to those in Fig. 4, but the 1-Torr curves show maximum N falling from 3.5×10^{12} to 3.5×10^{11} cm^{-3}. At $T_w = 700$ K, the 0.001 and 0.01 Torr curves are still unchanged, but the 0.1-Torr curve now drops to half the above values, and the 1-Torr curves show no inverted population. It seems that if the wall temperature is not kept low, then lower gas pressures will be required.

Reduction of N at high values of b for all p is due to the He deexciting the N_{001} level, yet the heat conduction does not increase with the pressure.

For both $A/l = 1$ and 6, the highest N values are obtained for $T_w = 300$ to 400 K, $C = 100$, at $p \simeq 0.1$ Torr with $a \simeq 10^{-2}$ and $10^{-4} < b < 10^{-2}$, and are about 10^{13} cm^{-3}. An inversion population of this value would result in very high gain, making practical solar-pumped systems superradiant. Hence, if necessary, p, a, and b could be changed from their values at optimum N to improve the efficiency.

There is a region of parameters where laser action is possible despite high gas and wall temperatures. Plots of N at $b = 1$ and 10^{-4} show that, at $b = 1$, N is drastically reduced as T_w is increased, but when $b = 10^{-4}$ there is still an inverted population even at $T_w = 1000$ K. (However, this result should be treated with caution as temperatures this high can introduce rotational effects which are not included.) The high temperature region occurs where the concentration of He and CO_2 is small. At high temperatures He as a coolant is unnecessary; Eq. 8 converts to the resultant conductivities of the other gases as $b \to 0$, and with $T^{1/2}$ dependence the conductivity is adequate. Again, as $b \to 0$ the deexcitation of CO_2 (001) by He becomes unimportant.

III. EFFICIENCY AND POWER OUTPUT OF THE LASER

III.1. Efficiency

The overall efficiency can be subdivided into the product of several efficiencies. First, if absorption occurs over a bandwidth λ_1 to λ_2, the fraction of the solar spectrum used or "solar utilization efficiency" is η_s:

$$\eta_s = \int_{\lambda_1}^{\lambda_2} \Phi(\lambda)\, d\lambda \Big/ \int_0^{\infty} \Phi(\lambda)\, d\lambda = 0.18 \tag{10}$$

for Br_2.

If the radiation passes through the gases x times by reflection and the absorption is small, the fraction absorbed or "absorption efficiency" $\eta_A = x\sigma(Br_2)d$ is independent of C' and obeys a similarity law, $\eta_A = \eta_A(xpd)$. However, p is limited by temperature rise considerations and x is limited by the reflectivity of the reflecting wall ($\approx 99\%$) to about 50. If p were 0.1 Torr, $\sigma = 3 \times 10^{-19}$ cm^2, $d = 2$ cm, then η_A would be 0.1. An increase in η_A could be achieved at higher pressure. If the gas were cooled more effectively by fins ($A/l = 6$), there would still be adequate population inversion at $p = 3$ Torr, and with $x = 15$ then $\eta_A \to 1$.

The fraction of absorbed quanta that ends up producing CO_2 (001) is obtained from the gas kinetics (Fig. 2) and is $Fk_1a/[(k_1 + k_2)a + k_3]$. This fraction we call the "kinetic efficiency," η_k. Assuming $F = 0.5$, $k_1 = 6 \times 10^{-12}$, $k_2 = 10^{-11}$, and $k_3 = 4.7 \times 10^{-13}$ cm^3 s^{-1}; then $\eta_k \to 0$ as $a \to 0$, $\eta_k = 0.18$ for $a = 1$, and $\to 0.19$ as $a \to \infty$.

The laser possesses a quantum efficiency $\eta_Q = (E_{001} - E_{100})/\bar{\epsilon}$ where $\bar{\epsilon}$ is the averaged energy absorbed, ≈ 2.7 eV, and $E_{001} - E_{100} \approx 0.1$ eV, so $\eta_Q = 0.039$.

The product $\eta_A\eta_Q\eta_K$ can be termed the "energy utilization efficiency" of the fraction of spectrum absorbed, and the "total solar efficiency" $\eta = \eta_s\eta_A\eta_Q\eta_K$. A plot of η vs a is shown in Fig. 5 for $p(Br_2) = 0.1$ Torr, $d = 2$ cm, and different values of x. If it is assumed that $\eta_A = 1$ or complete absorption occurs, then a value of 1.3×10^{-3} (or slightly more, depending on F) is possible. It is to be understood that these efficiencies are achieved only in those regions of Fig. 4 where the gain is sufficient for steady lasing.

III.2. Power Output of the Laser

The cooling requirements suggest the laser should be a flat plate of shallow depth of a few cm, and hence the exposed laser area A_1 should be large to handle high

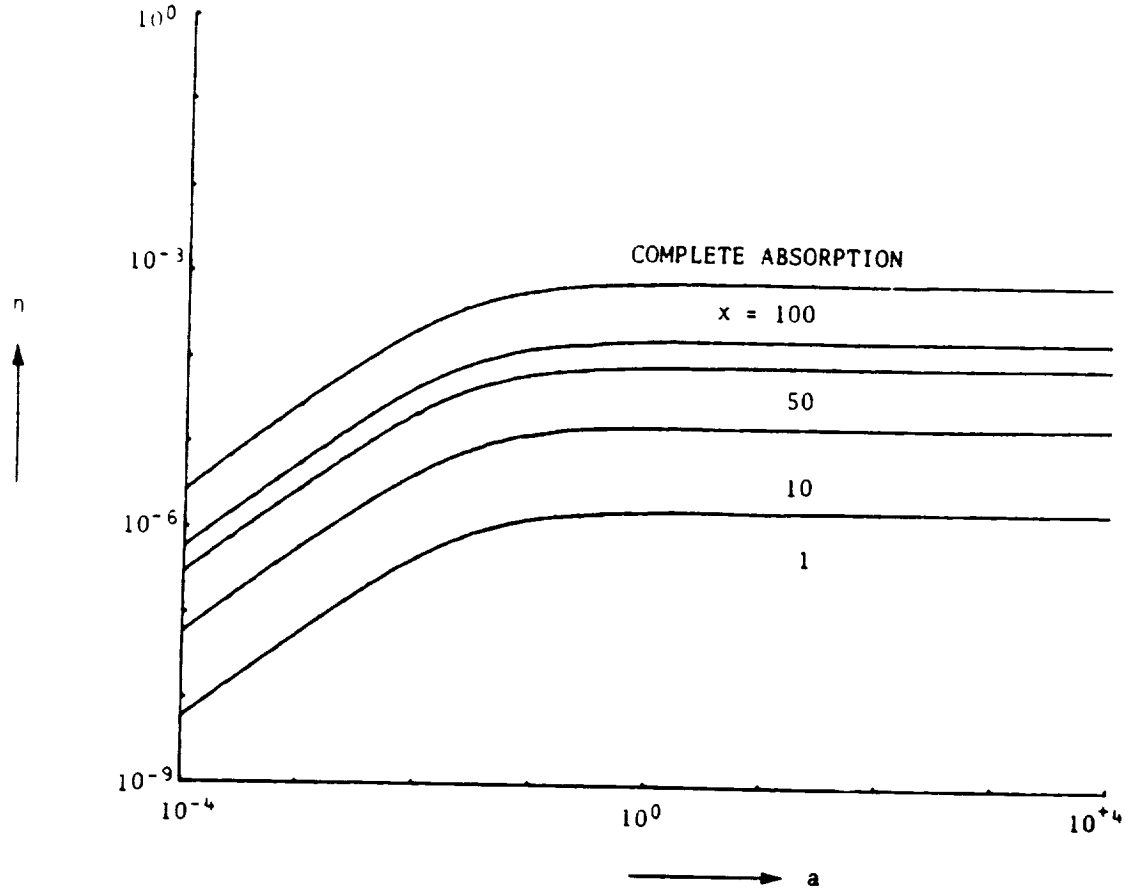

Fig. 5. Efficiency of a Br_2–CO_2–He laser at $p(Br_2) = 0.1$ Torr vs $a = CO_2/Br_2$ for different numbers of passes x.

power. Assume A_1 faces a collector of area A_c so $A_c/A_1 = C'$. If the solar flux is 0.14 W cm^{-2}, the power absorbed per cm^3 is $0.14C'\eta_s\eta_A$, and with $\eta_s = 0.18$, $\eta_A \rightarrow 1$, then the power absorbed $P_{ab} = 2.6 \times 10^{-2}C'$ (W cm^{-3}). The laser power emitted is $P_{ab}\eta_K\eta_Q$, and at $a \leq 0.1$, $\eta_k = 0.18$, $\eta_Q = 0.039$ the power emitted is $1.8 \times 10^{-4}C'$ (W cm^{-3}) = 18 kW m^{-3} for $C' = 100$. A laser 1 m^2 and 2-cm thick should emit up to 360 W and would require a collector of 200 m^2. A 10-kW laser would have a volume of 0.56 m^3 and would require a collector of 5.5×10^3 m^2. Such a system is at least comparable with other possible solar-pumped laser systems (12).

IV. OTHER SOLAR LASER MATERIALS

As the efficiency of a Br_2–CO_2–He laser seemed low, other combinations of materials were considered. The difficulty of obtaining rate coefficients especially for collisions between unlike components led to estimates of the laser performance based on a series of "figures of merit." The method assumes the partial pressures of the gases are equal — an oversimplification. Even so, it turns out that the results are useful for indicating poor performance, which usually is the case where one rate coefficient far exceeds the others, and the others can be neglected. The figures of merit can only be used in comparing one system with another.

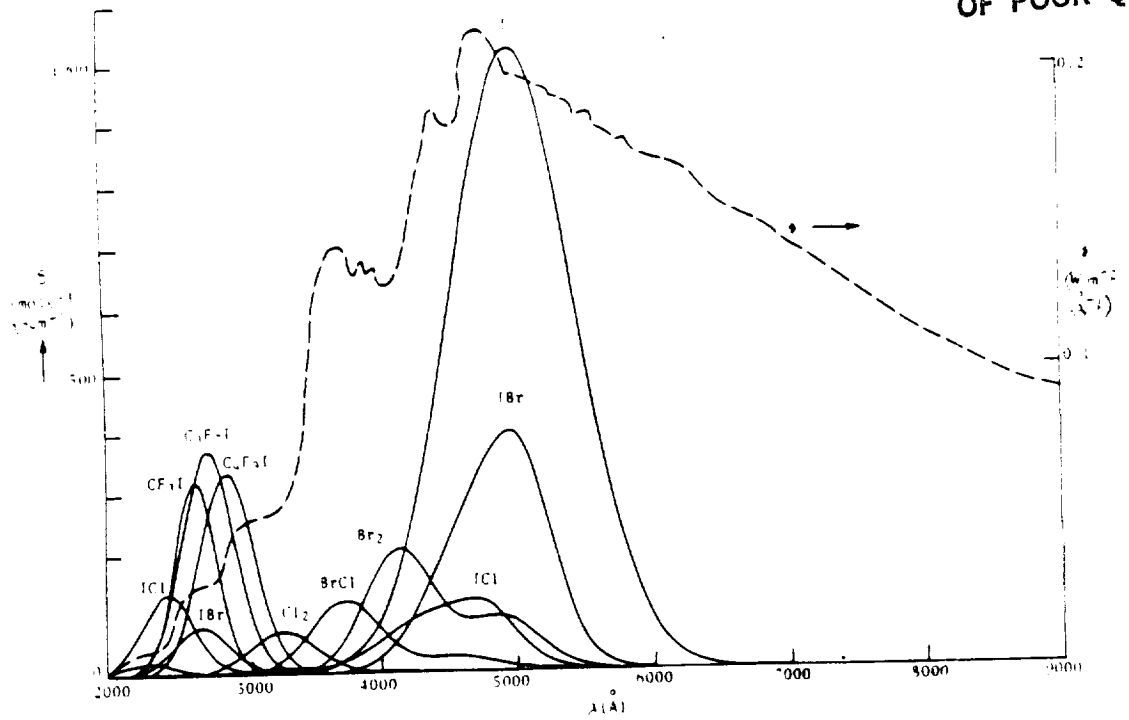

Fig. 6. The solar radiance R and the absorption coefficients of the halogens and halogen compounds.

The energy flow chart for a laser consisting of molecular absorber M, a molecular lasant Y, and a coolant Z is included in Fig. 2. Material M is a compound containing the halogen X, and dissociates to yield the excited specie X^*. The excitation energy of X^* is then handed over to the upper level Y_U of the lasing medium Y. The lower lasing level is Y_L. The rate coefficients are defined as shown.

The absorption coefficients ϵ (mole^{-1} l cm^{-1}) for the halogens and halogen compounds (10) are plotted vs wavelength and compared with the solar radiance Φ (W m^{-2} Å^{-1}) (11) in Fig. 6. It can be seen that the three compounds of the perfluoralkyl halide family have high absorption in the ultraviolet and that several materials can absorb up to 6000 Å. The absorbing power of a single gas $D = \Phi \Delta\lambda \sigma$, where σ (cm^2) $= 1.66 \times 10^{-21}$ ϵ and D is averaged over wavelength λ. The $\sigma(\lambda)$ can be expressed by a single or the sum of several Gaussian curves vs λ, and $\Delta\lambda$ is the full width of the curve at the rms value of σ. Values of D are given in the fifth column of Table 1. Only a fraction F of the absorbed photons will yield the excited state X^*, and F is between 0.5 and 1 for most halogens.

The "absorber storage" is a measure of the density of excited halogen atoms X^* present for a given amount of solar radiation. The rate of production of X^* is proportional to D, while the loss rate depends on the rate constants k_1, k_2, and k_3 (Fig. 2). If $k_3 >> k_1, k_2$, then X^* is essentially determined by D and k_3, and a figure of merit for absorber storage is defined:

$$F_s = D/k_3 \,. \tag{11}$$

A low value of F_s indicates that the absorbing material M is deexciting X^* by collisions, and a high value of D does not necessarily guarantee lasing.

TABLE 1

CHARACTERISTICS OF THE HALOGENS AND HALOGEN COMPOUNDS. λ_0 = WAVELENGTH FOR THE PEAK ABSORPTION, $\Delta\lambda$ = BANDWIDTH, σ_0 = ABSORPTION CROSS SECTION, $D = \phi\Delta\lambda\sigma$, WHERE ϕ = SOLAR RADIANCE, k_3 = DEEXCITATION RATE COEFFICIENT, AND THE FIGURE OF MERIT, $F_r = D/k_3$, SHOULD BE AS HIGH AS POSSIBLE

Gas	λ_0 (Å)	$\Delta\lambda$ (Å)	σ_0 (cm²)	D		k_3 (*for Br*)	D/k_3
I_2	5000	640	1.70×10^{-18}	8.4×10^{-2}		3.6×10^{-11}	2.33×10^{9}
Br_2	4889	378	1.50×10^{-19}	4.33×10^{-3}	1.15×10^{-2}	4.7×10^{-13}	2.45×10^{10}
	4141	360	3.9×10^{-19}	7.18×10^{-3}			
Cl_2	3283	332	1.19×10^{-19}	1.23×10^{-3}		—	—
ICl	4804	284	8.42×10^{-20}	1.80×10^{-3}	7.2×10^{-3}	—	—
	4425	549	1.66×10^{-19}	6.03×10^{-3}			
	3249	254	1.56×10^{-20}	1.18×10^{-4}			
	2440	258	2.29×10^{-19}	4.58×10^{-4}			
IBr	5072	291	2.82×10^{-19}	6.55×10^{-3}	2.5×10^{-2}	$*1.0\times10^{-12}$	2.5×10^{10}
	4773	508	4.78×10^{-19}	1.79×10^{-2}			
	2682	277	1.31×10^{-19}	4.74×10^{-4}			
BrCl	4555	404	4.17×10^{-20}	1.17×10^{-3}	4.5×10^{-3}	$*2.9\times10^{-14}$	1.55×10^{11}
	3736	354	2.01×10^{-19}	3.29×10^{-3}			
	2278	261	3.54×10^{-20}	4.71×10^{-5}			
CF_3I	2650	210	5.40×10^{-19}	1.37×10^{-3}		6×10^{-17}	2.28×10^{13}
C_2F_5I	2745	270	6.20×10^{-19}	2.45×10^{-3}		1×10^{-17}	2.45×10^{14}
C_3F_7I	2880	280	5.60×10^{-19}	2.88×10^{-3}		—	—

The "transfer efficiency" is a measure of the fraction of collisions between X^* and Y that result in the formation of the upper level Y_U. Actually the fraction should be $k_1Y(k_3M + k_2Y)$, but here it is simplified to the number F_T, defined by

$$F_T = k_1/(k_2 + k_3) \cong k_1/k_3 . \tag{12}$$

The expression is useful if $k_3M >> k_2Y$, and also assumes the densities Y and M are of the same order.

The "upper laser level storage" is a measure of the density in the upper laser level Y_U. The rate of production of Y_U is proportional to k_1X^*Y, and the rate of loss is proportional to $k_4M + k_5Y + k_6Z$. The density Y_U is large when the quantity F_u is large, defined by

$$F_u = k_1/(k_4 + k_5 + k_6) \simeq k_1/k_4 . \tag{13}$$

The value of the individual figures of merit lies in that they can pinpoint the quality of performance in one particular reaction or region of the energy flow chart.

Numerical values for D and the rate coefficients for the systems Br_2–CO_2–He, Br_2–H_2O–He, Br_2–HCN–He, and I_2–HF–He are shown in Table 2, which also gives the figures of merit and the quantum efficiencies.

TABLE 2

VALUES OF D, RATE COEFFICIENTS, FIGURES OF MERIT, AND VALUES OF QUANTUM EFFICIENCY FOR VARIOUS HALOGEN LASER COMBINATIONS

Type	D	k_1	k_2	k_3	k_4	$F_s = D/k_3$	$F_T = k_1/k_3$	$F_u = k_4/k_1$	$E_u - E_l$ (eV)	ϵ (eV)	η_q
Br_2–CO_2–He	1.15×10^{2}	6×10^{12}	10^{11}	4.7×10^{13}	3×10^{11}	2.45×10^{10}	12.8	200	0.12	3	3.8×10^{-2}
Br_2–H_2O–He	1.15×10^{2}	6.2×10^{-11}	6.2×10^{13}	4.7×10^{13}	3×10^{11}	2.45×10^{10}	132	2.07	0.174		5.8×10^{-2}
									0.160		5.3×10^{-2}
Br_2–HCN–He	1.15×10^{2}	1.8×10^{11}	2×10^{11}	4.7×10^{13}	1.7×10^{12}	2.45×10^{10}	38.3	10.59	0.32		1.1×10^{-1}
									0.15		5.2×10^{-2}
									0.14		4.7×10^{-2}
I_2–HF–HE	8.4×10^{2}	9.4×10^{-13} ($v=2$) 1.7×10^{-12} ($v=1$)	1.75×10^{-12}	3.6×10^{11}	3.9×10^{-11} ($v=2$)	2.33×10^{9}	2.6×10^{2} 4.7×10^{2}	2.4×10^{2}	0.47	2.47	1.9×10^{-2}

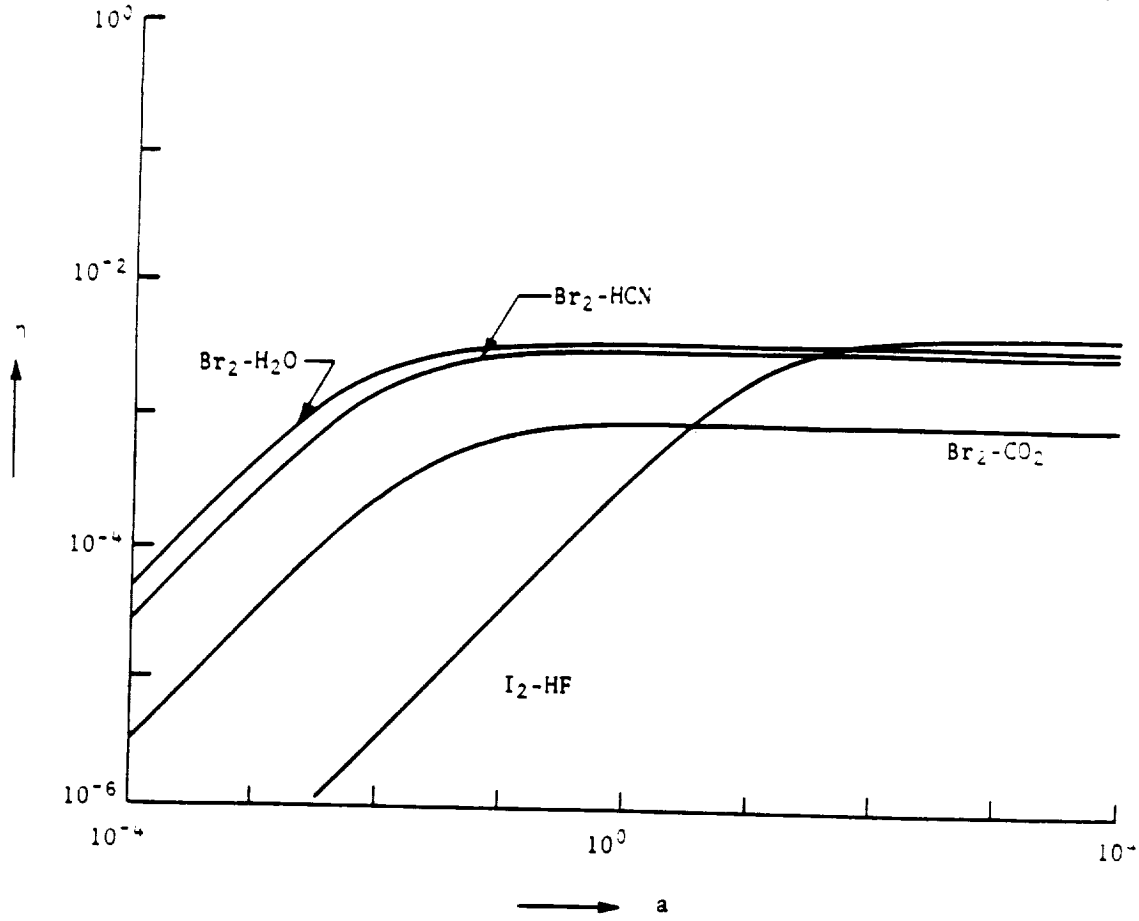

Fig. 7. Overall solar efficiency η of various laser combinations as a function of $a = M/Y$ (= lasant/absorber). Complete absorption is assumed.

Despite the very large cross section of I_2 for photoabsorption, the high rate of deexcitation of I* by I_2 (k_3) reduces the F_s value to one-tenth that for Br_2, implying that for equal conditions the value of I* is an order of magnitude less than Br*.

The coefficient k_1 is much less for I_2–HF than any of the Br_2 systems, implying poor transfer of energy to HF, (F_T), and also low retention in the upper level because of deexcitation (F_u). The highest value of k_1 is that of Br_2–H_2O, which also has the highest transfer efficiency F_T. Unfortunately, it has a very high deexcitation rate of the upper laser level (low F_u). The Br_2–HCN–He system has values of F_T and F_u which are intermediate between the combinations of CO_2 and H_2O.

The overall efficiency of the laser can be expressed as $\eta = \alpha\eta_k\eta_Q$, where it is assumed that complete absorption occurs. The constant $\alpha = 1.4 \times 10^{-18} D\bar{\epsilon}/\sigma$ and for Br_2 is 1.32×10^{-2} and for I_2 is 1.4×10^{-1} units. The value of F, the fraction of excited species formed, is taken as 0.5. Plots of η vs a, the ratio M/Y (Fig. 7), show $\eta \approx 5 \times 10^{-3}$ for Br_2–H_2O–He and Br_2–HCN–He, provided $a > 10^{-1}$ and for I_2–HF–He if $a > 10^{2}$. Unfortunately, in the latter case the high value of a will probably result in the gases becoming overheated, thus filling the lower laser level. The Br_2–CO_2–He laser has an efficiency of around 10^{-3} for $a > 0.1$.

V. CONCLUSIONS

A solar-pumped Br_2–CO_2–He laser should lase provided the radiation is concentrated sufficiently (> 100 times) and the pressure of the gases is low. High pressures cause overheating, which results in the lower laser level being filled. A suitable choice of gas pressures for optimum inverted population would be Br_2 = 0.1 Torr, CO_2 = 10^{-3} Torr, He = 10^{-3} Torr; but for greater efficiency a better combination would be Br_2 = 3 Torr; CO_2, 10^{-3} to 10^{-2} Torr; He, 10^{-4} to 10^{-2} Torr (Fig. 4).

As a power source, the laser is limited by low efficiency. The efficiency is the product of the fraction of the solar spectrum used, the fraction of radiation absorbed, a kinetic efficiency depending on the branching ratios, and a quantum efficiency. The absorption efficiency can be improved by increasing (*xpd*). The pressure can be increased to about 3 Torr if the cooling is enhanced by introducing fins into the gas for good heat conduction to the walls. Alternatively, a number of flat "box" lasers could be placed on top of each other to absorb different sections of the spectrum in sequence, with each producing its own output beam. With complete absorption, a 10-kW Br_2–CO_2–He laser would require a collector approximately 70 × 70 m, and would have a volume of about 0.5 m^3; such dimensions would be feasible for space applications. The radiator has to be large to reduce the temperature, ($A_c/A_r \rightarrow 1$). If the temperature is high, lasing still seems possible at low concentrations of He and CO_2, but at further reduced efficiency.

Other systems using halogen absorbers were also examined: namely, Br_2–CO_2–He, Br_2–H_2O–He, Br_2–HCN–He, and I_2–HF–He. Assuming complete absorption the efficiencies were all below 5×10^{-3}. A 10-kW laser with this efficiency would require a collector of several thousand m^2 and a radiator of comparable size.

Acknowledgments — The authors wish to thank Dr. Frank Hohl, head of the Space Technology Branch, NASA/Langley Research Center for his interest and support. The work was partially funded by NASA grant NSG 1568.

The Editor wishes to thank W. H. Christiansen and John Rather for assistance in reviewing the paper.

REFERENCES

1. B.F. Gordiets, L.I. Gudzenko, and V. Ya Pachenko, *Pis' ma Zh Eksp. Teor. Fiz.* **26**, 163, 1977.
2. A.A. Passchier, J.D. Christian, and N.W. Gregory, *J. Phys. Chem.* **71**, 937, 1967.
3. G. Herzberg, *Molecular Spectra and Molecular Structure. I: Spectra of Diatomic Molecules*, p. 456, Van Nostrand, New York, 1950.
4. A.B. Peterson and C. Wittig, *Appl. Phys. Lett.* **27**, 305, 1975.
5. R.J. Donovan and D. Husain, *Chem. Rev.* **70**, 489, 1970.
6. H. Hofmann and S.R. Leone, *Chem. Phys. Lett.* **54**, 314, 1978.
7. B.F. Gordiets, A.I. Osipov, E.V. Stupochenko, and L.A. Shelepin, *Usp. Fiz. Nank* **108**, 655, 1972.
8. A. Hariri and C. Wittig, *J. Chem. Phys.* **67**, 4454, 1977.
9. *Handbook of Chemistry and Physics*. 49th ed., p. E2, The Chemical Rubber Co., 1968.
10. J.R. Serry and D. Britton, *J. Phys. Chem.* **68**, 2263, 1964.
11. J.R. Carter and H.Y. Tada, *Solar Radiance Handbook*. Jet Propulsion Laboratory Report 21945-6001-RV-00, 1973.
12. J.W. Wilson and J.H. Lee, *Virginia J. Sci.* **31**, 34, 1980.

LIST OF SYMBOLS

The following represent the densities (cm^{-3}) of the respective materials: Br_2, Br, CO_2, $CO_2(001) = N_{001}$; (001) is the vibrational state;

Br*, X^*	excited atoms
M	molecular absorber containing the halogen atom X
Y	lasing medium; Y_U upper, Y_L lower level
Z	cooling medium
N	inverted population

Density ratios: $a = CO_2/Br_2$; $b = He/Br_2$

p	pressure of Br_2 (Torr)
C'	number of times focusing mirror concentrates
x	number of passes through lasing medium
C	$C'x$ — effective concentration of solar radiance
$\Phi(\lambda)$	solar radiance (watts per unit area per Angstrom)
$\Delta\lambda$	bandwidth of absorption
σ	cross section for absorption by molecule (cm^{-2})
h	Planck's constant
k	Boltzmann's constant
ν	frequency of photon (s^{-1})
$\bar{\epsilon}$	average energy of quanta
ΔE_1	excess kinetic energy released in absorption
E_{100}	energy of CO_2 in (100) state

Rate coefficients:

k_1	for Br* handing over energy to $CO_2(001)$ ($cm^3\,s^{-1}$)
k_2	deactivation of Br* by CO_2 which ends up in levels other than the upper laser level
k_3	deactivation of Br* to Br by Br_2
k_4, k_5, k_6	deactivation of $CO_2(001)$ by CO_2, He, and Br and Br_2, respectively
F	fraction of absorbed photons resulting in Br*
F'	fraction of absorbed photons contributing to heating
A_c, A_r, A_l	areas of collector, heat radiator, and subtended by laser
A_1	unit area of cross section of laser
l	depth of laser
η_s, η_A, η_K, η_Q, η	solar, absorption, kinetic, quantum, and overall efficiencies
τ	transparency of container wall
ϵ	emissivity of heat radiator
Q	quantity of heat deposited
κ	effective heat conductivity of mixture of gases
κ_n	heat conductivity of nth gas
λ	mean free path of gas molecule
$\bar{c}$	mean gas particle velocity
n	gas density (cm^{-3})
m_n	molecular weight of nth gas
$C_{v,n}$	specific heat at constant volume of nth gas
S	constant representing the effects of three gases on heat conductivity (Eq. 8)
T	gas temperature
T_w	wall temperature

APPENDIX D

Space Solar Power Review, Vol. 4, pp. 189–202, 1983
Printed in the USA.

0191-9067/83 $3.00 + .00

KINETIC MODELING OF AN IBr SOLAR PUMPED LASER

W. L. HARRIES

Old Dominion University
Norfolk, Virginia 23508, USA

W. E. MEADOR

NASA/Langley Research Center
Hampton, Virginia 23665, USA

Abstract — The possibility of using an IBr laser as a solar energy converter is examined theoretically, and reasons for its choice are given. Broadband absorption results in dissociation with the formation of excited Br* atoms, some of which then lase to the ground state Br. The ground state is depopulated by three-body recombination and, more importantly, by exchange reactions which more than compensate for the high quenching in heteronuclear halogen systems. Kinetic modeling indicates lasing is possible in the pulsed mode and possibly in the steady state with a cooled gas flow system. Temperature effects are discussed. The efficiency of the laser approaches 1.2% at optical thicknesses large enough for complete absorption of the photons.

I. INTRODUCTION

The concept of collecting solar radiation in large mirrors on orbiting space stations, and then transmitting the energy via laser beams has been considered previously (1–3). The efficiency of the system is expected to be highest if the laser could be directly pumped by the solar radiation.

The criteria for an efficient solar pumped laser are as follows:

- There must be broadband absorption;
- Peak absorption should occur near the peak of the solar spectrum;
- High quantum yield into a long-lived (metastable) state which serves as the upper laser level;
- In general, quenching of the excited state should be small, but, as will be pointed out later, this condition is alleviated if
- The lower level is rapidly depopulated to maintain inversion;
- The upper and lower levels must be sufficiently separated to yield a reasonable quantum efficiency;
- The process must be reversible; if not the components must be reconstituted by flow methods.

Gas lasers are advantageous because of uniformity of medium and because size is not a limitation. Two classes of laser can be considered: [1] where the absorbing medium is distinct from the lasant, and [2] where one material performs both functions.

The first solar pumped laser examined theoretically was type [1] above, namely a

Br_2–CO_2–He mixture (2–3). The Br_2 acted as a broadband absorber, the CO_2 was the lasing medium, and the He acted as a coolant. This laser was an electronic-to-vibrational energy transfer laser, and the low "transfer efficiency" as well as absorption efficiency resulted in an overall efficiency of less than 0.13%

Higher overall efficiency might be attained if the transfer efficiency could be eliminated, as in lasers of type [2] above. An example would be photodissociation of a molecule to yield an excited atom, which then lases to the ground state. The population of the lower level might be removed by chemical processes. High pressure working should be possible which would enable more efficient absorption.

The objectives of this paper are to study theoretically the IBr solar pumped laser as an example of class [2], to understand the essential lasing features by determining the dominating reactions, and to estimate the efficiency for power conversion. The criteria that have been listed for the selection of candidate lasants will also be assessed. In particular the question of whether steady-state lasing is possible will be discussed.

As the solar radiance must be concentrated many times, and since the IBr absorption is broadband near the peak of the solar spectrum, the laser will quickly heat up and lasing inhibited (by mechanisms to be discussed), unless cooling is provided. In the theoretical study it is therefore assumed that the lasant is maintained around room temperature, the purpose being to examine the potential for lasing under favorable operating conditions. Methods for accomplishing cooling are proposed in Sec. IX.

While this study was in progress, an experimental investigation of an IBr laser pumped by a xenon lamp was performed by L. Zapata (4). The objective of that experiment was to demonstrate lasing, and not necessarily to provide definitive quantitative data. Hence, only limited comparisons could be made, but the experimental results were useful in assessing the effects of excessive heating in the actual experimental environment.

II. CHOICE OF IBr

Broadband absorption is essential for high solar efficiency and there are many compounds which can be photodissociated to yield excited atoms X^*. Here only halogens are considered for X. They can be divided into three types: diatomic homonuclear molecules X_2, diatomic heteronuclear molecules YX, and complex molecules of the form RX, where R is a molecular radical.

Solar pumped lasing has already been demonstrated for type RX, using a xenon arc to radiate perfluoropropyliodide C_3F_7I (5–7). Absorption occurred in the ultraviolet (230–320 nm) so that the fraction of the solar radiation absorbed (solar efficiency) was small. (Chemical recycling was also necessary for continuous working.) Types X_2 and YX on the other hand can absorb near the peak of the solar spectrum when both X and Y are halogen atoms.

The excited atoms F*, Cl*, Br*, and I* have energies of about 0.1, 0.2, 0.44, and 1 eV, respectively, above ground; only Br* and I* have values high enough to give acceptable quantum efficiencies. Lasing characteristics depend on the competition between the rate of reduction of the excited species X^* by quenching and the depopulation of the lower level X by the exchange reaction $X + XY \rightarrow X_2 + Y$. Exchange reactions are possible only for heteronuclear molecules. Since the photodissociation of XY always seems to leave the lighter atom in the metastable excited state, and since the quantum efficiency increases with the atomic number of the lasing atom, it

appears that IBr should be the best laser candidate of type [2]. It absorbs near the solar peak with a high probability of dissociating into I + Br*.

III. PHYSICAL MECHANISMS

The processes occurring in IBr are assumed to be photodissociation with the formation of excited and ground state atoms, quenching of the excited atoms, recombination and exchange reactions. The species are assumed to be eight in all, namely, IBr, I, Br, I_2, Br_2, Br*, and I*, and photons created by spontaneous and stimulated emission. Vibrational excitations are neglected at room temperature because of very rapid relaxation. The reactions and rate constants are summarized in Table 1.

The absorption of photons results in reactions 1 through 6. The photodissociation rates S are equal to $C\Phi(\lambda)\Delta\lambda\sigma_a(\lambda)(N)$, where C is the number of times the solar radiation is concentrated, $\Phi(\lambda)\Delta\lambda$ is the number of photons arriving per unit area per second (8), $\sigma_a(\lambda)$ the absorption cross-section in question, and (N) the number density of absorbers. As the ratio Br*/Br initially produced by the photodissociation of IBr is critical to attaining an inverted population, care must be taken in evaluating S_1 and S_4 in Table 1. The potential curves for the $X(^1\Sigma^+)$, $A^3\Pi_1$, and $B^3\Pi_0^+$ levels for IBr were plotted by computer on the energy diagram (Fig. 1) using data from Huber and Herzberg (9). The $B'^3\Pi^+$ is included, and is drawn in approximately. The lowest vibrational level (v = 0) and the Franck–Condon transitions are shown. The horizontal dashed lines B and C are based on the transitions from the lower to the upper $A^3\Pi_1$ and $B^3\Pi_0$ levels and indicate the peaks and widths of the absorption curves. The absorption cross-section for IBr as a function of wavelength has been measured (10–11), and the function can be represented by three Gaussians whose peaks are at 268, 477, and 507 nm, respectively. These are plotted on the left. The peak of Gaussian F coincides almost exactly with the line C, but the peak of the Gaussian G is displaced from B. We believe the Gaussians to be accurate as well as the asymptotes A and D.

The integral

$$\int_{\lambda_1}^{\lambda_2} \phi(\lambda)\sigma_a(\lambda)\,d\lambda$$

is a measure of what fraction of absorption events are caused by transitions to the level in question and $\sigma_a(\lambda)$ is the respective Gaussian. Thus Gaussian H produces Br, but can be neglected as $\phi(\lambda)$ is small here (8). The part of Gaussian F above asymptote A produces Br*; the part below A does not produce dissociation. The $B'^3\Pi_0^-$ and $B^3\Pi_0^+$ curves cross and possibly absorption into the latter could result in Br. However, the translational energy at the crossing is sufficiently high and the nature of the crossing is such that the probability is near unity that all parts of the absorption curve above A in Fig. 1 correspond to dissociation into I + Br*, as confirmed experimentally (13). The Gaussian G, corresponding to absorption into the $A^3\Pi_1$ level produces I + Br. Performing the integration of $\phi(\lambda)\sigma_a(\lambda)\,d\lambda$ then yielded the fractions of absorption events resulting in the production of Br*, Br, and I (Table 1). The total absorption rate for IBr was found to be $C \times 1.25 \times 10^{15}$ (IBr),

TABLE I

LIST OF REACTIONS

Term		Reaction	Rate Constant	References for Rate Constants
Source	1	$h\nu + IBr \rightarrow I + Br^*$ $\rightarrow I + Br$	$S_{11} = C \times 1.25 \times 10^{15}(IBr)$ Br^*: $- S_1 = 0.704 S_{11}$ Br: $- S_4 = 0.259 S_{11}$ I: $- S_7 = 0.963 S_{11}$	9, 10, 11, 13 14, 15, 16 17, 18, 19
	2	$h\nu + I_2$	$S_{21} = C \times 2.5 \times 10^{15}(I_2)$	20, 21
	3	$\rightarrow I + I^*$ $\rightarrow I + I$	I^*: $- S_2 = 0.2 S_{21}$ I: $- S_5 = 0.48 S_{21}$	
	4	$h\nu + Br$	$S_{31} = C \times 1.25 \times 10^{15}(Br_2)$	
	5	$\rightarrow Br + Br^*$	Br^*: $- S_3 = 0.605 S_{31}$	
	6	$\rightarrow Br + Br$	Br: $- S_6 = 1.387 S_{31}$	
Quenching	7	$Br^* + IBr \rightarrow Br + IBr$	$Q_1 = 1 \times 10^{-12}$ (cm^3 s^{-1})	22, 23
	8	$+ I_2 \rightarrow Br + I_2$	$Q_2 = 1.86 \times 10^{-12}$	22
	9	$+ Br_2 \rightarrow Br + Br_2$	$Q_3 = 4.7 \times 10^{-13}$	22
	10	$+ I \rightarrow Br + I$	$Q_4 = 1.8 \times 10^{-11}$	14
	11	$+ Br \rightarrow 2Br$	$Q_5 = 1.8 \times 10^{-11}$ or 0	—
	12	$I^* + IBr \rightarrow I + IBr$	$Q_6 = 6 \times 10^{-11}$	24
	13	$+ I_2 \rightarrow I + I_2$	$Q_7 = 3.5 \times 10^{-11}$	24, 25
	14	$+ Br_2 \rightarrow I + Br_2$	$Q_8 = 5.6 \times 10^{-11}$	24, 26
Recombination (2 body)	15	$I_2 + Br_2 \rightleftharpoons 2IBr$	$K_7 \rightarrow 1 \times 10^{-13}$ $K_8 \leftarrow (1.6 \times 10^{-16})$	31
Recombination (3 body)	16	$Br^* + Br + IBr \rightarrow Br_2 + IBr$	$C_1 = 4 \times 10^{-32}$ (cm^6 s^{-1})	Assumed equal to C_3
	17	$Br + Br + IBr \rightarrow Br_2 + IBr$	$C_2 = 3 \times 10^{-30}$	Assumed equal to C_4
	18	$Br^* + Br + Br_2 \rightarrow 2Br_2$	$C_3 = 4 \times 10^{-32}$	27
	19	$Br + Br + Br_2 \rightarrow 2Br_2$	$C_4 = 3 \times 10^{-30}$	27
	20	$Br^* + I + IBr \rightarrow 2IBr$	$C_5 = 1 \times 10^{-32}$	28
	21	$Br + I + IBr \rightarrow 2IBr$	$C_6 = 1 \times 10^{-32}$	28
	22	$I^* + I + IBr \rightarrow I_2 + IBr$	$C_7 = 3 \times 10^{-32}$	28
	23	$I^* + Br + IBr \rightarrow 2IBr$	$C_8 = 3 \times 10^{-32}$	28
	24	$I + I + IBr \rightarrow I_2 + IBr$	$C_9 = 3 \times 10^{-30}$	28
Exchange (2 body)	25	$Br + IBr \rightarrow I + Br_2$	$E_1 = 3.5 \times 10^{-11}$ (cm^3 s^{-1})	29
	26	$Br + I_2 \rightarrow IBr + I$	$E_2 = E_1$ or 0	29

where C is the number of times the solar radiation is concentrated, of which a fraction 0.704 resulted in Br*, 0.259 in Br and 0.963 in I. Similar estimates for I_2 and Br_2 are also included.

For all the initial pressures of IBr considered, it was assumed that 4% by number density of I_2 and Br_2 were present at 300°K, according to the law of mass action. Thereafter, all the densities varied with time. The absorption rate is proportional to IBr pressure for low pressures (and absorption lengths of 1 cm), until at about 50 torr essentially all the photons are absorbed.

The degeneracy factor for the upper laser level Br* is 2, while that of the lower laser level Br($^2P_{3/2}$) is 4. The population inversion ΔN for lasing is then

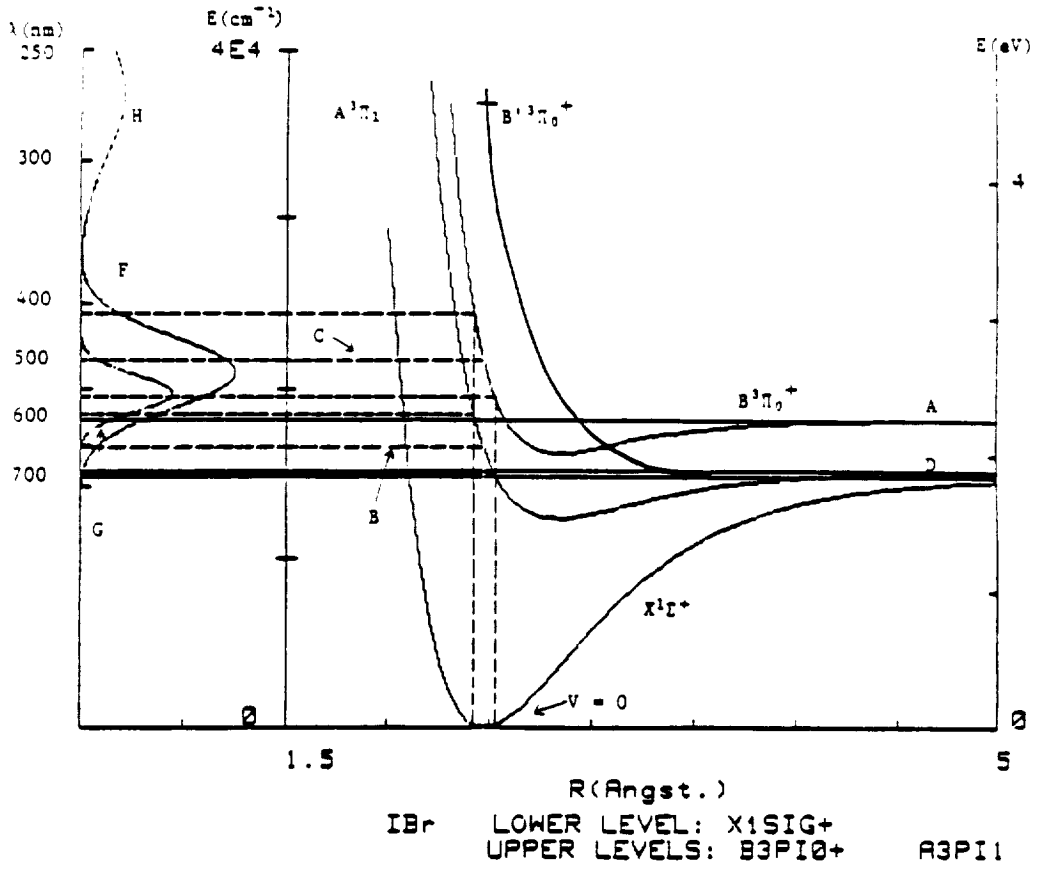

Fig. 1. Energy level diagram for IBr. The potential curves $X(^1\Sigma^+)$, $A^3\Pi_1$, $B^3\Pi_{0^+}$ are Morse functions generated from data of Huber and Herzberg. The repulsive curve $B'^3\Pi_{0^+}$ is approximate. The Gaussian absorption curves are plotted from data of Seery and Britton.

$$\Delta N = \mathrm{Br}^* - \mathrm{Br}/2 \,. \tag{1}$$

The degeneracy factors in this instance help to reduce the threshold for lasing.

The quenching of Br* and I* is given by reactions 7–14 in Table 1; the quenching of Br* and I* by Br* and I* was neglected as well as the quenching of Br* by Br and I* by I and Br. Computer runs in which these latter coefficients were arbitrarily assigned values equal to Q_4, instead of zero, showed no great difference in the results. The large rate coefficient for the quenching of Br* by I is due to the electronic to translational energy transfer resulting from the "crossing" of (IBr)* potential energy curves (see Fig. 1). The process has been called the inverse predissociation mechanism (14).

The two body recombination of I_2 and Br_2 (item 15) is the only reversible reaction included. At room temperature, by the law of mass action (assuming no photodissociation), the concentration of I_2 and Br_2 in IBr is 0.04. It then follows that if the forward reaction $2IBr \rightarrow I_2 + Br_2$ has a rate coefficient K_7, then the reverse coefficient K_8 is $(0.04)^2 \times K_7$.

Three-body recombinations are listed and it is seen that the reactions involving I* and Br* are less likely than those involving I and Br because of the difficulty of

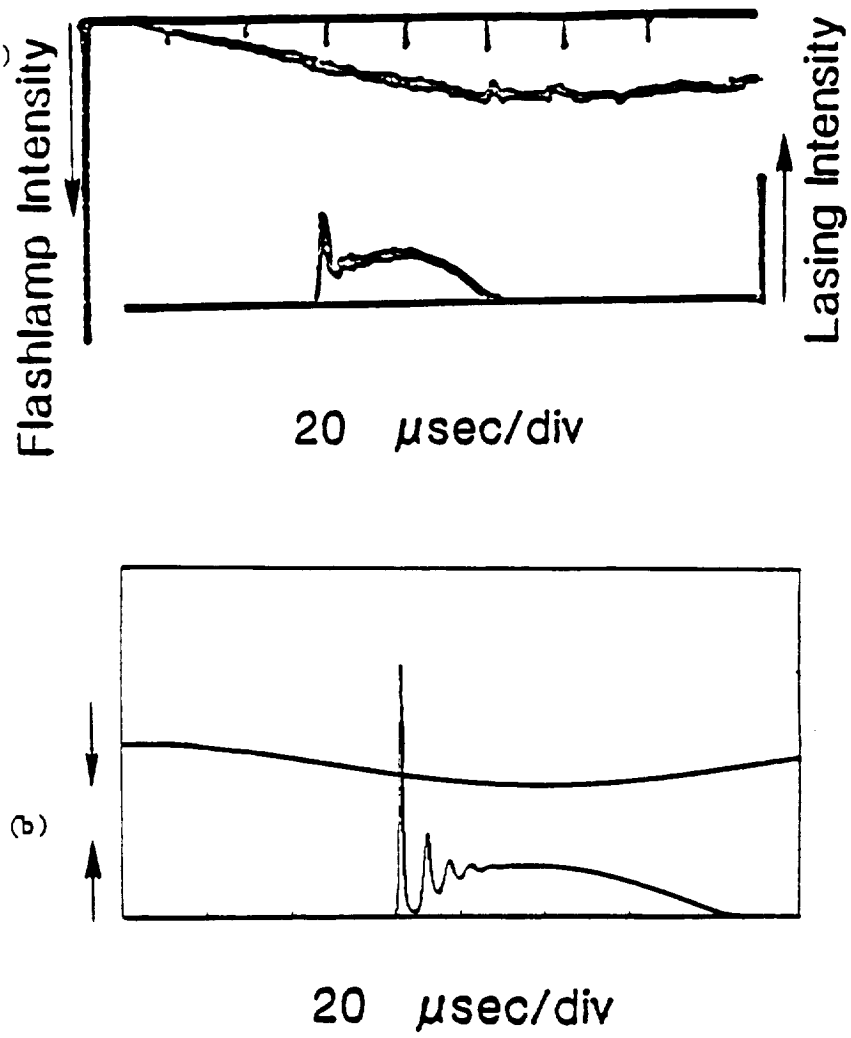

Fig. 2. Comparison of (a) measured laser light output vs time compared with (b) calculated values. The pressure of IBr was 3 torr, with 4% Br_2, I_2. In the calculations $C = 5000$. The pumping light intensity is inverted.

getting rid of the excitation energy. Some of the values are uncertain and are based on similar reactions in I_2.

The exchange reactions that depopulate the lower laser level and make lasing possible are listed as items 25 and 26. Experimental measurements of reaction 25 have been reported by Clyne and Cruze, (27) who deduce a high rate coefficient $E_1 = 3.5 \times 10^{-11}$ cm^3 s^{-1}. We have been unable to find a rate coefficient for reaction 26, but computer runs for $E_2 = 0$ and $E_2 = E_1$ did not differ greatly because the concentration of I_2 is much less than that of IBr.

IV. RATE EQUATIONS

In the following equations the terms in parenthesis represent the densities of atomic and molecular species; n is the density of photons. The quantity A is the

Einstein coefficient for spontaneous emission, while Γ is the rate of stimulated emission. The rate equations for the eight species present are

$$\frac{d(IBr)}{dt} = -S_{11}(IBr) + C_5(I)(Br^*)(IBr) + C_6(I)(Br)(IBr) + C_4(I^*)(Br)(IBr) - E_1(Br)(IBr) + E_2(Br)(I_2) + 2K_7(I_2)(Br_2) - 2K_8(IBr)^2 \quad (2)$$

$$\frac{d(I)}{dt} = S_7 + S_2 + 2S_5 - C_5(I)(Br^*)(IBr) - C_6(I)(Br)(IBr) - C_7(I^*)(I)(IBr) - 2C_9(I)(I)(IBr) + E_1(Br)(IBr) + E_2(Br)(I_2) \quad (3)$$

$$\frac{d(I_2)}{dt} = -S_{21}(I_2) + C_7(I^*)(I)(IBr) + C_9(I)(I)(IBr) - E_2(Br)(I_2) \quad (4)$$

$$\frac{d(Br_2)}{dt} = -S_{31}(Br_2) + C_1(Br^*)(Br)(IBr) + C_2(Br)(Br)(IBr) + C_3(Br^*)(Br)(Br_2) + C_4(Br)(Br)(Br_2) + E_1(Br)(IBr) - K_7(I_2)(Br_2) + K_8(IBr)^2 \quad (5)$$

$$\frac{d(Br^*)}{dt} = S_1 + S_3 - C_1(Br^*)(Br)(IBr) - C_3(Br^*)(Br)(Br_2) - C_5(Br^*)(I)(IBr) - Q_1(Br^*)(IBr) - Q_2(Br^*)(I_2) - Q_3(Br^*)(Br_2) - Q_4(Br^*)(I) - Q_5(Br^*)(Br) - A(Br^*) - \Gamma \quad (6)$$

$$\frac{d(Br)}{dt} = S_3 + S_4 + 2S_6 + Q_1(Br^*)(IBr) + Q_2(Br^*)(I_2) + Q_3(Br^*)(Br_2) + Q_4(Br^*)(I) + Q_5(Br^*)(Br) - C_1(Br^*)(Br)(IBr) - 2C_2(Br)(Br)(IBr) - C_3(Br^*(Br)(Br_2) - 2C_4(Br)(Br)(Br_2) - C_6(Br)(I)(IBr) - C_8(Br)(I^*)(IBr) - E_1(Br)(IBr) - E_4(Br)(I_2) + A(Br^*) + \Gamma \quad (7)$$

$$\frac{d(I^*)}{dt} = S_2 - Q_6(I^*)(I_2) - Q_7(I^*)(IBr) - Q_8(I^*)(Br_2) - C_7(I^*)(I)(IBr) - C_8(I^*)(Br)(IBr) \quad (8)$$

$$\frac{dn}{dt} = \Gamma + GA(Br^*) - \frac{n}{\tau_c} \quad (9)$$

The quantity G in Eq. 9 is the geometrical factor $2r_b^2/L^2$, where r_b is the radius of the laser beam and L the length of the laser; for isotropic spontaneous emission only this fraction of photons is confined within the laser cavity. The last term represents the loss through the end mirrors of reflectivites r_1 and r_2, and τ_c is the lifetime of an average stimulated emission photon travelling parallel to the axis;

$$\tau_c = -L/c \ln(r_1 r_2),$$

where c is the velocity of light. Here, $\tau_c = 5 \times 10^{-8}$ s. The quantity Γ, the stimulated emission rate, is equal to $n\sigma_e c\Delta N$ where σ_e is the stimulated emission cross-section. Then

$$\sigma_e = \lambda_e^4 A / 4\pi^2 \Delta\lambda_e ,$$

where λ_e is the emitted wavelength, A (≈ 1) is the Einstein coefficient for spontaneous emission from the upper laser level, and $\Delta\lambda_e$ is the emission bandwidth. With $\Delta\lambda_e$ taken as the bandwidth for Doppler broadening at 300°K, then $\sigma_e = 1.6 \times 10^{-17}$ cm^2.

Equations 2 through 9 were solved by computer, and are compared with the experimental results of Zapata in Figs. 2a and b. In the experiment, the light intensity from the xenon lamp was measured with a photodetector, and varied approximately as

$$\sin^2 \frac{2\pi t}{2 \times 10^{-4}} ,$$

where t is in seconds. The theoretical source terms included this function.

IV. COMPARISON WITH EXPERIMENT

The idealized model differed from the experiment in a number of ways. The theory assumed absorption occurred one-dimensionally in a thickness d. Experimentally the pumping source was a xenon lamp placed parallel to the laser tube. Its light was focussed onto the laser tube axis by a reflecting cylinder of elliptical cross-section. The illumination increased towards the axis, but as the source was distributed and the reflector was not perfectly elliptical, the maximum value of the pumping photon flux density was uncertain. The pumping density was equated to C times the solar radiance. The values of the equivalent C in the experiments were probably between 2000 and 40,000 for the various runs. There were also differences in the spectral distribution of the xenon lamp and the solar spectrum assumed.

Figure 2 compares the measured light output from a 1-m long IBr laser pumped by a xenon discharge lamp powered from a capacitor bank, with the computer solution of Eqs. 2 through 9. The IBr pressure was 3 torr and C was about 5000 in the experiment, which are the values assumed in the calculations.

The overall shape of the experimental and calculated laser output are similar. Both start about the same time, and consist of a sharp spike followed by a tail. The ratio of spike to tail is higher in the calculated version, and the oscillations in the theoretical wave shape are not evident in the experiment. Estimates of the time constant of the InAs photodetector circuit showed it was high enough to reduce the high frequency components of the signal.

The duration of the experimental pulse for this and all other runs was always shorter than the calculated values by a factor of about two. We believe this was due to the lasant being heated near the axis. Rough calculations of the IBr gas temperature, assuming $C = 5000$, indicated a temperature rise of several hundred °K in 50 μs. The temperature rise would cause dissociation of IBr and deplete the lasant. This view is consistent with an experimental measurement of IBr density on the laser axis during a pulse, which showed a drop of about 50%, a value too high to have been

caused by photodissociation (it would require $C \geq 10^5$). High temperatures could also increase the ratio of reverse to forward rates of the exchange reactions, thus tending to neutralize the mechanisms necessary to depopulate the lower laser level (30). Also, the quenching reaction $Br^* + I \rightarrow Br + I$ is enhanced in the heated gas because of the greater number of I atoms. The calculations assumed no heating.

On changing the pressure p both experiment and theory showed the output laser pulse duration was roughly independent of p for pumping pulses of 200 μs duration. Experimentally the output light signal amplitude increased with p up to about 20 torr, where it reached a maximum and then decreased: as p increased, absorption in the outer layers decreased the pump power on axis. The theory showed the amplitude proportional to p because constant pumping energy density was assumed throughout the gas.

Both experiment and theory showed that increasing C increased the laser amplitude proportionally.

There was also agreement between the measured and calculated output power of the laser. In an experiment with a tube length of 1 m and 2.22 cm radius, and an output mirror of 95% transmittance, the measured output was approximately 2 kW for an IBr pressure of 4 torr, with $C \approx 10^4$ (4).

The calculated peak output power P is

$$P = \frac{1}{2} cnh\nu\tau\pi r^2 . \tag{10}$$

Our results showed $n = 1.2 \times 10^{12}$ cm^{-13} for $C = 1 \times 10^4$, corresponding to 1.7 kW which is in reasonable agreement.

V. INTERPRETATION

By varying the parameters in the program one at a time, it was established that the dominant mechanisms were quenching of Br* by IBr and I and the exchange reaction $Br + IBr = I + Br_2$. In particular, the program indicated lasing would not occur if the exchange reaction was removed. Three-body recombinations made little difference to the shape of the light output for pumping pulses of 200 μs duration. Fortunately the rate coefficients most accurately known turned out to be dominant ones. However, for computer runs of longer duration pulses, it was found essential to include all the terms.

Evidently the exchange reactions can overcome quenching, and high quenching cross-sections per se may not be a valid selection criterion for rejecting otherwise promising gases.

VI. THRESHOLD CONDITION

The threshold condition is $r_1 r_2 \exp(2\alpha L) = 1$, where $r_1 r_2$ are the reflectivities of the laser mirrors, $\alpha = \sigma_e \Delta N$ is the gain per unit length, and L is the length of the laser (29). The threshold condition is contained in Eq. 9, and occurs when

$$\Gamma > \eta/\tau_c - GA(Br^*) \simeq n/\tau_c .$$

The two relations are equivalent as can be seen from the definition of τ_c and require

$$\Delta N \cdot L \geq \ln(1/r_1 r_2)/2\sigma_e = \text{constant} .$$

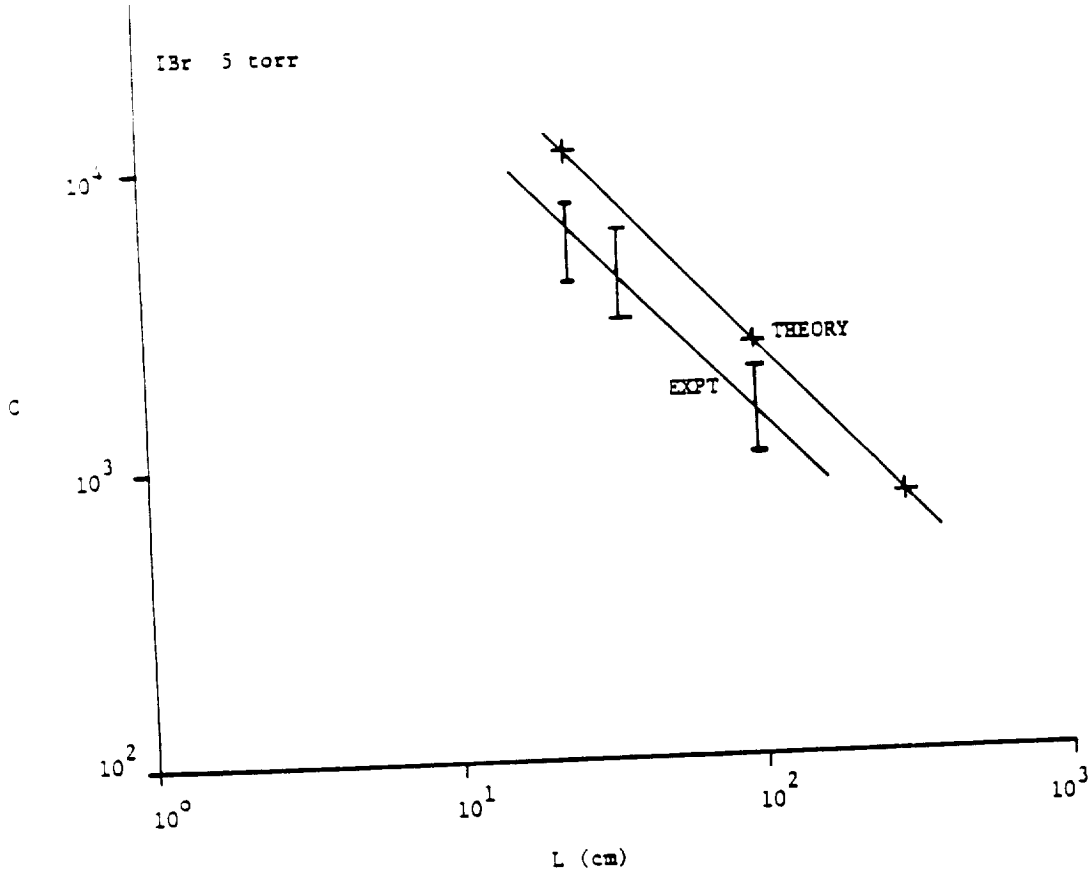

Fig. 3. Plot of lowest C for lasing vs laser length L.

As $\Delta N \propto C$ it follows that the threshold value for C is proportional to $1/L$. Computer runs were performed for successively lower values of C for L = 400,100, and 25 cm, and the threshold values of C estimated. The values are compared with experimental results in Fig. 3. The absolute values of the latter were difficult to estimate as the pumping light was focused on a cylinder, but both theory and experiment show $C \propto L^{-1}$. Thus C can be reduced by increasing L.

VII. EFFICIENCY OF THE LASER

Estimates of the efficiency can be obtained from solutions of the rate equations. For a laser of length L, collecting width w and of 1 cm absorption depth, the total solar power into the laser is $0.14CLw$ W. The power output is $0.5cnh\nu\tau w$. If the transmission factor τ is 0.05, the efficiency is $\eta = 3.93 \times 10^{-10} n/CL$, where n (the photon density) is in cm^{-3}, and L is in cm. Computer runs at various values of L, C, and gas pressures were made and the maximum n obtained to give η (Fig. 4). For $L > 5$ m, η is roughly independent of L and C, and at 5 torr, $\eta = 5 \times 10^{-4}$. At these low pressures $\eta \propto p$ and it can be seen that higher pressures increase η, provided overheating can be avoided.

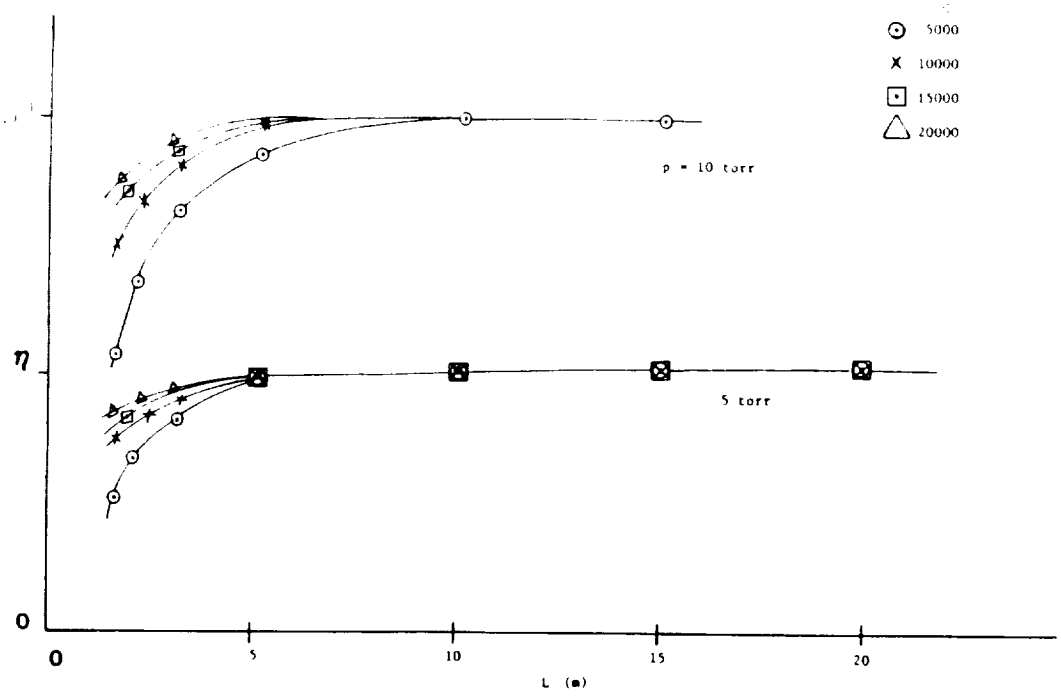

Fig. 4. Efficiency of IBr solar pumped laser plotted vs length L at different pressures, and concentration factors C. The reflectivities are $r_1 = 1$, $r_2 = 0.95$, respectively.

An understanding of why the efficiency is low can be obtained if the overall efficiency is considered to be the product of four efficiencies (3): $\eta = \eta_s \eta_a \eta_k \eta_Q$. Here η_s, the solar efficiency depends on the absorption bandwidth of the total solar radiance, and its value for IBr is 0.12. The absorption efficiency η_a depends on the IBr gas pressure and depth of absorption d; for low pressures $\eta_a = \sigma_a(\text{IBr})d = 10^{-2}pd$, where p is the pressure in torr, d the depth in cm. The expression is valid up to $pd \approx 50$; for higher pd most of the photons are absorbed and $\eta_a \rightarrow 1$. The kinetic efficiency η_k depends on the number of absorption events producing Br* and also on the competition between stimulated emission and quenching. Approximately 0.7 Br* atoms are produced for every absorbed photon (Table 1). The fraction of Br* atoms which yield a stimulated photon can be obtained by examining Eq. 6, and comparing the value of Γ with the rest of the loss processes, as all eight variables vs time were known. The ratio Γ/(all loss processes) was 0.82, when η was a maximum, the major competitors with Γ being quenching by IBr and I. The quantum efficiency is $\eta_a = 0.44\ \text{eV}/2.5\ \text{eV} = 0.18$. Hence for $pd < 50$ torr-cm, $\eta = 6 \times 10^{-4}$ at 5 torr, $d = 1$ cm, agreeing with 5×10^{-4} in Fig. 4. With $pd > 50$ torr-cm, $\eta_a \rightarrow 1$ and the maximum efficiency would be about $1{\cdot}2 \times 10^{-2}$.

Pulsed working would further reduce the efficiency because of the duty cycle, unless there was adequate storage of energy when the laser was not emitting.

VIII. POSSIBILITY OF CONTINUOUS LASING

The computer runs showed that IBr was depleted, while the quenchers I_2, Br_2, and

I grew with time. For 200 μs pumping pulses, the photon density n had a maximum value just prior to the peak input.

The input light pulse was then assumed to be proportional to $\sin^2(2\pi t/10^{-4})$ up to 50 μs and thereafter to be constant. For $p = 3$ torr the calculations indicated a pulse of 350 μs, and for $p = 13$ torr the duration was of order 10 ms with $C = 5000$. Plots of the other variables indicated a gradual depletion of IBr and a growth of I. The long time scale suggests that a gas flow system would be feasible for steady-state working provided the gas temperature was kept within limits.

IX. TEMPERATURE EFFECTS

As the absorbed photons have an average energy of several eV, and as the heat conduction of IBr is low, very high temperatures can occur. If the pressure p of IBr is greater than 50 torr in a vessel 1 cm deep, then the temperature of the lasing gas can be roughly estimated assuming all the photon energy is deposited in the gas; if $p \ll 50$ torr, then roughly a fraction $10^{-2}p$ is deposited. The heat produced travels an average distance x to the walls of the containing vessel by gaseous conduction. The walls are assumed at a temperature T_w and are thermally connected to a radiator into space. Above about 1000 °K, the gas would also act as a blackbody radiator. Estimates show that if $x = 0.5$ cm, then for $C = 2000$ and $p = 5$ torr the gas temperature would be of order 1000 °K.

If the pressure is increased (a requirement for high absorption efficiency) still higher temperatures are possible, as heat conduction in gases is independent of pressure. Cooling can be enhanced by reducing x by inserting fingers in the gas, or by admitting a noble gas with a high heat conductivity and a low quenching cross section. Assuming perfect conduction from the walls to a radiator the same size as the collector, then the radiator temperature would be somewhat less than 300 °K.

High temperatures can have large effects on quenching, recombination and dissociation rates, and on exchange reactions.

To our knowledge experimental data on the effect of temperature on the quenching of Br* by IBr or I_2 are not available. The possible analogous case of quenching of I* by I_2 was reported by Kartazaef *et al.* (31), whose measurements showed the quenching rates at 1000 °K were 20 times lower than at 300 °K. If a similar dependence occurred for the quenching coefficient of Br* by IBr or I_2, the high temperatures would prove advantageous in this respect.

Turner and Rapagnani (26) have reported measurements of the recombination rates for $I + I + I_2 \rightarrow 2I_2$, where $k = 1.1 \times 10^{-10}T^{-5.884}$. The coefficient is 1000 times smaller at 1000 °K than at 300 °K and is analogous to C_6 used above where I recombined with Br and the third body was IBr.

High temperatures cause thermal dissociation of IBr with the formation of I, Br, and Br_2, which have large cross sections for the quenching of Br*. The depletion of the lower level by exchange reactions would also be reduced as the increase in I would enhance the reverse exchange reaction. On balance then, heating would seem to be very detrimental to IBr solar laser operation.

X. CONCLUSIONS

The time varying solutions of the species rate Eqs. 2 through 9 show that inversion

is possible near the start of a pumping pulse, but continuous lasing may not occur. The reason is that early in the pulse the Br created from Br* by quenching and stimulated emission is sufficiently removed by exchange reactions to maintain inversion. Eventually, however, the IBr decreases and the Br density increases to cut off the lasing.

The dominating mechanisms are the source terms, quenching by IBr and I, two body exchange reactions and stimulated emission. With 200 μs pumping pulses the behavior of the light output can be represented using only these reactions. However, if long pulses are to be simulated, then all the reactions must be included. Our computer results showed that for 3 torr of IBr, steady depletion occurred and the pulse lasted for about 350 μs with $C = 5000$, $L = 1$ m. At 13 torr the pulses were many tens of ms for the same conditions.

The exchange reactions can overcome the effect of high quenching cross sections, and high quenching need not necessarily indicate that a material is unsuitable for solar pumped lasing.

Heating will reduce quenching. It will also cause dissociation and depletion of IBr with the formation of I, I_2, Br and Br_2 all of which quench Br*. The exchange reaction rates will be reduced causing the population inversion to disappear, thus killing the laser.

If the path length L is small, requiring the solar concentration C to be high for threshold to be reached, then the pressure has to be kept low to prevent heating ($\ll$50 torr). The overall efficiency η is then $10^{-4}p$ (torr) or 0.1% at 10 torr. Such a 10 kW laser would require a collector of 85 × 85 m^2. If L is large, so that overheating does not occur, and p is high enough to absorb all the photons, then η could reach 1.2% — a 10 kW laser collector would be 30 × 30 m^2. The above efficiencies can be compared to the calculated efficiencies of a Br_2–CO_2–He laser and a C_3F_7I laser, each of which was around 0.1%.

The effective length L can be increased by multiple passes in a flat "box type" laser. If $L = 10$ m, then lasing should be possible with $C \simeq 300$. The temperature rise would then be 700°K even if $p = 50$ torr, with a depth of 0.5 cm, $T_w = 300$ and no admixture of a cooling gas. The receiving area of the laser would be 400/300 = 1.4 m^2 and an effective length L of 10 m could be achieved in about 8 passes.

The possibility of steady-state working seems feasible if a continuous flow system is used.

Acknowledgements — The authors acknowledge useful discussions with Drs. J.W. Wilson, S. Raju, and L. Zapata. The work was partially supported by grant NSG 1568 from the National Aeronautics and Space Administration/Langley Research Center, Hampton, Virginia.

REFERENCES

1. J.F. Coneybear, The Use of Lasers for the Transmission of Power. Radiation Energy Conversion in Space, K.H. Billman, ed., *Program Astronaut. Aeronaut.* **61**, 279, 1979.
2. B.F. Gyordiets, L.I. Gudzenko, and V. Ya Pachenko, *Pis' ma Zh Eksp Teor. Fiz.* **26**, 163, 1977.
3. W.L. Harries and J.W. Wilson, *Space Solar Power Rev.* **2**, 367, 1981.
4. L. Zapata, Private communication.
5. J.H. Lee and W.R. Weaver, *Appl. Phys. Lett.* **39**, 137, 1981.
6. W.R. Weaver and J.H. Lee, Proceedings of the 16th Intersociety Energy Conversion Engineering Conference, Atlanta, Georgia, p. 84, 1981.
7. J.W. Wilson and J.H. Lee, *Proc. Virginia Acad. Sci.* **31**, 34, 1980.
8. J.R. Carter and H.Y. Tada, Solar Cell Radiation Handbook. Jet Propulsion Laboratory, California Institute of Technology, Report No. 21945-6001, RV OU 1973, Table 2.1, p. 2-2.

9. K.P. Huber and G. Herzberg, *Molecular Spectra and Molecular Structure-Constants of Diatomic Molecules*, Van Nostrand, NY, 1978.
10. D.J. Seery and D. Britton, *J. Phys. Chem.* **68**, 2263, 1964.
11. A.A. Passchier, J.D. Christian, and N.W. Gregory, *J. Phys. Chem.* **71**, 1937, 1967.
12. M.S. DeVries, N.J.A. Van Teen, T. Baller, and A.E. De Vries, *Chem. Phys. Lett.* **75**, 27, 1980.
13. A.B. Petersen and W.M. Smith, *Chem. Phys.* **30**, 407, 1978.
14. M.B. Faist and R.B. Bernstein, *J. Chem. Phys.* **64**, 2971, 1976.
15. K. Hohla and K.L. Kompa, *Handbook of Chemical Lasers*, R.W.F. Lyon and J.F. Bolt, eds., ch. 12, John Wiley, NY, 1976.
16. D.H. Burde, R.A. McFarlane, and J.R. Wiesenfeld, *Phys. Rev. A*, 1917, 1974.
17. J. Tellinghuisen, *J. Chem. Phys.* **58**, 2821, 1973.
18. B. Wellegehausen, K.H. Stephan, D. Friede, and H. Welling, *Optics Commun.* **23**, 157, 1977.
19. R.E. Beverly and M.C. Wong, *Optics Commun.* **20**, 23, 1977.
20. A.B. Petersen and W.M. Smith, *Chem. Phys.* **30**, 407, 1978.
21. H. Hofmann and S.R. Leone, *Chem. Phys.* **54**, 314, 1978.
22. E.B. Gordon, A.I. Nadkhin, S.A. Sothichenko, and I.A. Boriev, *Chem. Phys. Lett.* **86**, 2, 1982.
23. H. Hofmann and S.R. Leone, *J. Chem. Phys.* **69**, 641, 1978.
24. D.H. Burde and R.A. McFarlane, *J. Chem. Phys.* **64**, 1850, 1976.
25. E.H. Appleman and M.A.A. Clyne, *J. Chem. Soc. Farad Trans. 2* **72**, 191, 1976.
26. These numbers are based on similar reactions in I_2: C. Turner and N.L. Rapagnani, Laser Fusion Program Semi-Annual Report UCRL-50021-13-1, Lawrence Livermore Laboratory UCID-16935, 1973.
27. The values of $C_5 - C_9$ are based on similar reactions, $I + I + I_2$ and $I^* + I + I_2$: K. Hohla and K.L. Kompa, The Photochemical Iodine Laser, *Handbook of Chemical Lasers*, R.W.F. Lyons and J.F. Bolt, eds., ch. 12, John Wiley, NY, 1976.
28. M.A.A. Clyne and H.W. Cruze, *J. Chem. Soc. Farad Trans. 2* **68**, 1377, 1972.
29. B.A. Lengyel, *Lasers*, 2nd Ed., p. 61, John Wiley, NY, 1971.
30. This suggestion was made by L. Zapata.
31. V.A. Kartazaef, N.P. Penkin, and Yu. A. Tolmachev, *Sov. J. Quantum Electron.* **7**, 608, 1977.

APPENDIX E

ELECTRONIC ENERGY TRANSFER IN MOLECULAR SODIUM

(by N.W. Jalufka and W.L. Harries,
submitted to J. of Molecular Spectroscopy)

ABSTRACT

Emission from the $A^1\Sigma_u^+ - X^1\Sigma_g^+$ band of Na_2 has been observed following excitation of the $B^1\Pi_u$ state by the 488 nm line of an Argon ion laser. The populating mechanism of the $A^1\Sigma_u^+$ state appears to be a transfer from $B^1\Pi_u$ to the $2^1\Sigma_g^+$ state followed by radiative transition to the $A^1\Sigma_u^+$. The experiment was performed with no buffer gas in the sodium cell and at a pressure where the time between collisions of $Na(^3S)$ and Na_2 $B^1\Pi_u$ was long compared to the radiative lifetime of $B^1\Pi_u$. Since collisions can not be responsible for the $B^1\Pi_u \rightarrow 2^1\Sigma_g^+$ transfer the results suggest a different mechanism. We suggest that the mechanism is stimulated emission from $B^1\Pi_u$ to the lower vibrational levels of $2^1\Sigma_g^+$ with the stimulating radiation field provided by the black-body emission of the cell walls.

I. INTRODUCTION

Electronic energy transfer is known to occur in alkali metal dimers from the observation of A-X band fluorescence in both Li_2 and Na_2 following laser excitation to the B state (1-3). The recently discovered $2^1\Sigma_g^+$ electronic energy level of Na_2 (4) has been identified as playing a role in the transfer (3). The transfer of energy from $B^1\Pi_u$ to $2^1\Sigma_g^+$ is generally explained in terms of collisionally induced transitions (2, 5, 6, 7). While there is no doubt that the transfer of energy from $B^1\Pi_u$ to $2^1\Sigma_g^+$ and subsequent radiative decay to $A^1\Sigma_u^+$ is responsible for the observed $A^1\Sigma_u^+$ - $X^1\Sigma_g^+$ fluorescence (3) it is not clear that collisions are always responsible for the transfer. We have observed $A^1\Sigma_u^+ \rightarrow X^1\Sigma_g^+$ fluorescence following excitation of $B^1\Pi_u$ by the 488.0 nm line of an Argon ion laser under conditions of no buffer gas and densities such that the time between collisions for $Na(^3S)$ - $Na_2(B^1\Pi_u)$ were long compared to the radiative lifetime of $B^1\Pi_u$. The radiative lifetime of $B^1\Pi_u$ is known to be $\approx$ 8 ns (8) so that whatever mechanism transfers energy from $B^1\Pi_u$ to $2^1\Sigma_g^+$ must have a rate comparable to the rate of radiative decay of the $B^1\Pi_u$ state. In our experiment this can not be collisional processes. Direct radiative transfer by spontaneous emission can also be ruled out due to the small energy separation and the ν^3 dependence which makes the spontaneous transition probability small. However, this transition probability is not zero and we suggest that radiative transition from $B^1\Pi u$ to $2^1\Sigma_g^+$ by stimulated emission with the blackbody radiation of the cell walls providing the radiation field is possible. We report in this paper a detailed study of the $B^1\Pi_u$ - $2^1\Sigma_g^+$ transfer based on this possibility.

II. EXPERIMENTAL DETAILS

The experimental arrangement consisted of a stainless steel cell containing the sodium vapor. The cell was fitted with four viewing ports arranged in the shape of a cross. The viewing ports were sealed with sapphire windows and a stainless steel cylinder was welded perpendicular to the plane of the cross and served as a reservoir. The reservoir and the cross were encased in separate stainless steel blocks. Each block could be heated by four commercial cartridge heating elements (300 watts each). The temperature of each block was controlled separately and temperatures were measured with chromel/alumel thermocouples. This cell design allows the reservoir to be maintained at a fixed temperature which controls the total vapor pressure in the cell while the cell itself may be maintained at a different temperature which controls the Na/Na_2 ratio.

Fluorescence from the excited Na_2 molecules was collected at right angles to the laser beam and focused on the entrance slit of a 0.3 meter monochromator. The monochromator was equipped with a 1200 line/mm grating and had a first order resolution of 0.10 nm. A photomultiplier tube (S-20 response) was placed at the exit slit of the monochromator. The output of the photomultiplier tube was recorded on a strip chart recorder. Calibration of the wavelength drive was accomplished by use of a low pressure mercury lamp.

The laser had a power output of 10 mWatts at 488.0 nm which excited the $B^1\Pi_u$ (v = 6, J = 43) level. Spectral scans of the $B^1\Pi_u \rightarrow X^1\Sigma_g^+$ fluorescence provided verification of the excitation of $B^1\Pi_u$ (v = 6, J = 43) as the spectrum was dominated by transitions from this level.

III. EXPERIMENTAL RESULTS

The system was operated with no buffer gas and at a reservoir and cell temperature of 723 K. At this temperature the Na atom density is 4.4 x $10^{16} cm^{-3}$ and the Na_2 molecular density is 2.6 x 10^{15} cm^{-3}. The 488.0 nm line of the argon ion laser corresponds to the $X^1\Sigma_g^+$ (v = 3, J = 43) → $B^1\Pi_u$ (v = 6, J = 43) transition (9). The observed fluorescence consisted of the B → X band as well as transitions in the region 600 nm-750 nm. While our resolution was inadequate to allow identification of the individual transitions the overall characteristics were in agreement with the observation of Astill et al. (2) who identified the feature as $A^1\Sigma_u^+$ - $X^1\Sigma_g^+$ emission. It appears, therefore, that $B^1\Pi u \rightarrow 2^1\Sigma_g^+$ transfer occurs even with no buffer gas present and at densities where the time between Na-Na_2 collisions is long compared to the radiative lifetime of the $B^1\Pi_u$ state.

IV. CALCULATION OF COLLISION TIME

The time between collisions is taken as the reciprocal of the collision frequency $Z = \sigma n \bar{v}$ where σ = collision cross-section, n = number density of collision particles and $\bar{v}$ = R.M.S. speed between the particles. The collision cross section was taken to be $\sigma = \pi(r)^2$ where r = 1.5 x 10^{-8} cm, i.e. 1/2 the inter-nuclear spacing. For sodium vapor at 723 K the frequency of collisions of an Na_2 molecule with Na atoms is $\tau = 1/Z = 3 \times 10^{-7}$ sec. This is two orders of magnitude longer than the radiative lifetime of 8 nsec for $B^1\Pi_u$ and therefore collisional rates are not competitive with the radiative rates.

V. CALCULATIONS OF THE BLACKBODY RADIATION INTENSITY

We treat the cell as a blackbody cavity. The energy density of radiation in the wavelength range λ to $\lambda + d\lambda$ is given by Planck's radiation formula $\rho(\lambda,T)\, d\lambda = 8\pi hc\lambda^{-5} (\exp(hc/\lambda kT-1)^{-1} d\lambda$ ergs$\cdot$cm^{-3} where the symbols have their usual meaning. The peak of the blackbody radiation field is given by Wien's law, $T\lambda_{max} = 0.28978$ cm deg and for T = 723 K, $\lambda_{max} = 4.008$ μm. The energy difference between $B^1\Pi_u$ (v=6) and $2^1\Sigma_g^+$(v=0) is 2492 cm^{-1} from the energy level values of Kusch and Hessel (9) for $B^1\Pi_u$ and Effantin et al. (4) for $2^1\Sigma_g^+$. This energy difference corresponds to a radiation wavelength $\lambda \approx$ 4.013 μ. The Doppler width at λ = 4 μm and T = 723K is $\Delta\lambda$ = 0.835 nm and the blackbody radiation intensity in this range $\Delta\lambda$ is $\rho = 3.99 \times 10^{-7}$ ergs$\cdot$cm^{-3}.

VI. ESTIMATES OF TRANSITION RATES

1. Possible Transitions

The experimental results indicated that absorption of the 488 nm Argon ion laser light in sodium occurred from the transition X(v=3) $\rightarrow$ B(v=6) (path #1, Fig. 1). Fluorescence occurred at wavelengths of 730 nm or greater, and the emission apparently came from the transition A $\rightarrow$ X (path #4, Fig. 1). The dotted path #5 from $B^1\Pi_u$ to $A^1\Sigma_u^+$ is forbidden (u$\rightarrow$u). However, the pathways $B^1\Pi_u \rightarrow 2^1\Sigma_g^+$, and subsequent path $2^1\Sigma_g^+ \rightarrow A^1\Sigma_u^+$ are allowed. We consider the rate of transfer for these last two transitions, especially the transition for "curve-crossing," $B^1\Pi_u \rightarrow 2^1\Sigma_g^+$.

The transition $B^1\Pi_u$ - $2^1\Sigma_g^+$ would be competitive only if the stimulated emission rates were as great as the spontaneous emission rates $B^1\Pi_u \rightarrow X^1\Sigma_g^+$. We first estimate the ratio R of the stimulated emission rate W ($B^1\Pi_u \rightarrow 2^1\Sigma_g^+$) with the spontaneous emission rate ($B^1\Pi_u \rightarrow X^1\Sigma_g^+$).

2. Preliminary Estimate of Ratio of Stimulated to Spontaneous Rates

As is well known, the rate of stimulated emission is given by $W = \rho B$, where ρ is the energy density of the black body radiation and B is the Einstein coefficient. The value of ρ was obtained from Planck's radiation formula and depended on the wavelength λ_{v_1,v_2} determined by the transition from level v_1 to level v_2 and the absorption bandwidth. The latter was obtained by assuming absorption occurred over a width of order 100 rotational lines, so $\Delta\lambda$ was 100 times the Doppler bandwidth of one line. Pressure broadening was negligible under the conditions here.

The Einstein coefficient B is (10):

$$B = \pi |\mu_{1,v_1,v_2}|^2 \Big/ 3\ \varepsilon_o\ \hbar^2 \qquad (1)$$

where $|\mu_{1,v_1,v_2}|$ is the matrix element for the electron dipole moment of the transition $B^1\Pi_u \rightarrow 2^1\Sigma_g^+$ from level v_1 to level v_2, ε_o is the dielectric constant for free space, and $\hbar$ is Planck's constant/2π.

The matrix elements are of the form $|\mu| = e \int \psi_1\ r\ \psi_2^*\ dr$ where ψ_1, ψ_2 are the wavefunctions of the two respective states, e is electronic charge, and r the length of the dipole. According to the Franck-Condon principle r varies only slightly during the transition and we may treat r as a constant and take it outside the integral. Then $|\mu|$ can be expressed as

$$|\mu_{1,v_1,v_2}| = e\ r\ F_{1,v_1,v_2} \qquad (2)$$

where F_{1,v_1,v_2} is the Franck-Condon factor for the transition v_1,v_2. The rate of transitions from the $v_1 = 6$ to a level v_2 in the $2^1\Sigma_g^+$ state is then

$$W_{v_1 v_2} = \pi(er)^2 \rho(\lambda_{v_1,v_2}, T) F^2_{1,v_1,v_2}/3\epsilon_o \hbar^2 \quad ; v_1 = 6 \qquad (3)$$

The total rate of all transitions from $v_1 = 6$ to all the levels in the $2^1\Sigma_g^+$ state below v_1 in energy (corresponding to an upper value of $v_2 = v_n$) is

$$W = \sum_{v_2=0}^{v_n} W_{v_1,v_2} \quad ; \quad v_1 = 6 \qquad (4)$$

The level corresponding to v_n in the $2^1\Sigma_g^+$ state must lie below the $v = 6$ level for the B state for stimulated emission, and its value is $v_n = 24$.

Next, we consider spontaneous emission, $B^1\Pi_u \rightarrow X^1\Sigma_g^+$ with a rate coefficient A given by (10):

$$A = \frac{8\pi^2}{3\, h\, \epsilon_o} \left| \frac{\mu_{2,v_1,v_2}}{\lambda_a^3} \right|^2 \quad ; \quad v_1 = 6 \qquad (5)$$

with the same nomenclature as Eq. (1); $|\mu_2|$ is for the transition $B^1\Pi_u \rightarrow X^1\Sigma_g^+$ and λ_a the wavelength corresponding to the transition between the vibrational quantum state, $B(v_1)$ to $X(v_3)$. However, the energy difference is about 2.6 eV for $v_1 = 6$ and $\lambda_a \simeq 0.5\ \mu m$, a value 10 times smaller than the peak wavelength for black body radiation.

Again, in the electronic transition, r is assumed constant, and is the same value as in Eq. (3). The total rate of spontaneous emission is then (10)

$$A = \frac{8\pi^2 (er)^2}{3\hbar\,\varepsilon_o \cdot \lambda_a^3} \sum_{v_3}^{\infty} \left(F_{2,v_1,v_3}\right)^2; \quad v_1 = 6 \tag{6}$$

where F_{2,v_1,v_3} is the Franck-Condon factor for the transition v_1, v_3. Experimentally, the spontaneous lifetime of the $B^1\Pi_u$ state is known to be 8 ns, so $A = 1.25 \times 10^8\ s^{-1}$.

Equations (5) and (6) can be evaluated if r and the Franck-Condon factors are known, but first it is instructive to take the ratio $R = W/A = \rho B/A$:

$$R = \frac{\lambda_a^3}{4\hbar} \frac{\sum \rho\,(\lambda_{v_1,v_2},\ T) \cdot \left(F_{1,v_1,v_2}\right)^2}{\sum \left(F_{2,v_1,v_3}\right)^2} \tag{7}$$

Here, as both transitions started from the $B^1\Pi_u$ state, r cancels. The Franck-Condon factors are finite for only specific values of λ_{v_1,v_2}. To get a rough order of magnitude value for R, we assume the contributions from the Franck-Condon factors in the numerator and denominator are about equal and cancel, and define a quantity $R' = \rho\,(\lambda_{v_1,v_2},\ T)\ \lambda_a^3/4\hbar$. The quantity R' essentially reflects the contribution from the radiation density. Assuming $\lambda_a = 0.5\ \mu m$ and constant, R' is plotted as a continuous function of λ_{v_1,v_2}, for different temperatures (Fig. 2). It can be seen that for $\lambda_{v_1,v_2} > 4\ \mu m$ that $R' \approx 10^6$, but if $\lambda_{v_1,v_2} \approx 0.5\mu$ then $R' \ll 1$, indicating that here R would be much less than 1. Hence, stimulated emission should predominate at around $4\mu m$, but not around 0.5 μm.

3. Calculation of Transfer Rates

We confirmed this conclusion by calculating the stimulated and spontaneous rates based on estimates of the Franck-Condon factors. The Franck-Condon factors were calculated in two ways: first Morse functions (13) were fitted to the potential curves of Jeung (11); second the same curves were digitized using a computer interpolation technique. Values of ω_e were obtained from Huber and Herzberg (12) and Effatin, et al. (4). Values of $\omega_e x_e$ were obtained from $\omega_e x_e = \omega_e^2/4 D_e$ where D_e was read from the curves. Values of $\omega_e y_e$ were taken as zero. For the second method, the value of ω_e from reference (4) gave poor results and ω_e was obtained by fitting a parabola to the curve near the equilibrium displacement to give a spring constant K and estimating ω_e assuming the known effective mass of the atom.

The wave functions were calculated by first obtaining asymptotic solutions for large r_i, the internuclear distance, and then reducing r_i in small increments and obtaining iterative solutions. They were well behaved for at least 20 levels and satisfied the critera of orthogonality, the vibrational sum rule, and displayed a Condon parabola on a v_1, v_2 plane. The Franck-Condon factors varied between 0 and 0.2 and agreed with Kusch and Hessel (9) in order for the $B^1\Pi_u \rightarrow X^1\Sigma_g^+$ transition.

The Franck-Condon factors obtained from the two methods differed by factors of up to 5 when comparing the transitions from $v_1 = 6$ in the upper level to individual levels in the lower state. For some values of v_2 the Morse curve results were larger, for others it was the reverse. The two sets of Franck-Condon factors were then used to calculate the stimulated emission rates, where again the answers were different for individual levels. However, when the rates were added for 21 lower levels, the differences

averaged out and gave total transition rates in good agreement as shown below.

4. Stimulated Emission Rates

The value of W was obtained using the value of B from Eq. (1) where μ_1 was taken as (er) F_{1,v_1,v_2} with F_1 the value for the transition $B^1\Pi_u \rightarrow 2^1\Sigma_g^+$:

$$W_{v_1 v_2} = \rho \frac{\pi e^2 r^2 \left(F_{1,v_1,v_2}\right)^2}{3 \varepsilon_o h^2}. \qquad (8)$$

The value of r was obtained from the known value of A, Eq. (5), where $|\mu_2|$ = er F_2, and $\lambda_a = 0.5\mu$; then $r \simeq 1.5A$, a reasonable value, half the equilibrium internuclear distance.

A plot of W vs λ_{v_1,v_2}, the wavelength of the oven black-body radiation is shown (Fig. 3), for values of $v_1 = 5, 6, 7$, using the Morse curve numbers and shows a series of "lines" occurring near $\lambda = 5$ μm with values $\approx 10^{12}$ s^{-1}. The addition of all the lines between 0 and 20 μ gave a total rate of several times 10^{12} for the stimulated emission rate $B^1\Pi_u \rightarrow {}_1\Sigma_g^+$. The interpolation method gave individual values of W, ($v_1 = 6$) for different v_2 in quantitative agreement with Fig. 3, but, with individual values which showed differences of up to 5. However, when the rates for all the lines were added the net rates calculated by the two methods agreed within 20 percent. The spontaneous emission rate from $B^1\Pi_u \rightarrow X^1\Sigma_g^+$ is of order 10^8, so the ratio R again approaches 10^5.

Stimulated emission does not occur from $B^1\Pi_u \rightarrow X^1\Sigma_g^+$. The 2 eV difference in the electronic levels calls for wavelengths of 0.5 μm where the value of ρ is about six orders of magnitude smaller at T = 450°C.

In a similar manner the stimulated and spontaneous emission rates were calculated for the various pathways shown (Fig. 1) and are shown in Table 1. It is evident that the stimulated emission rate $B^1\Pi_u \rightarrow 2^1\Sigma_g^+$ far exceeds any stimulated or spontaneous rate B → X. For the A → X transition the stimulated and spontaneous rates are comparable.

VII. CONCLUSIONS

The model we have assumed in the calculations is approximate only. It may have inaccuracies in the value of r and also in the estimates of the energy levels and hence the actual values of the wavefunctions and Franck-Condon factors. Nevertheless, the insensitivity of our estimated total rates to variations in parameters such as D_e, and the differences of 5 orders of magnitude between the estimated stimulated and spontaneous emission rates (Table 1) suggest the pathways in Fig. 1 are valid. Moreover the suggested mechanism of stimulated emission due to the oven black body radiation seems valid for transfer from electronic energy states which overlap, and for transfer in "curve crossing" in sodium.

ACKNOWLEDGEMENTS

This work was supported by grants NSG 1568 and NCC1-137 from NASA/Langley Research Center, Hampton, Virginia.

REFERENCES

1. G. Ennen and Ch. Ottinger, J. Chem. Phys. 76, 5812 (1982).
2. A. G. Astill, A. J. McCaffery, and B. J. Whitaker, Chem. Phys. Lett. 125, 33-37 (1986).
3. C. Effantin, O. Babaky, K. Hussein, J. D'Incan, and R. F. Barrow, J. Phys. B 18, 4077-4087 (1985).
4. C. Effantin, J. D'Incan, A. J. Ross, R. F. Barrow, and J. Verges, J. Phys. B 17, 1515-1523 (1984).
5. K. Hussein, M. Aubert-Frecon, O. Babaky, J. D'Incan, C. Effantin, and J. Verges, J. Mol. Spectry. 114, 105-125 (1985).
6. A. G. Astill, A. J. McCaffery, S. C. Taylor, B. J. Whitaker, and M. J. Wynn, J. Chem. Phys. 89, 184-191 (1988).
7. A. Sharma, G. L. Bhale, M.A.N. Razvi, and M. N. Dixit, Pramana, J. Phys. 30, 309-317 (1988).
8. W. Demtroder, W. Stetzenbach, M. Stock, and J. Witt, J. Mol. Spectry. 61, 382-394 (1976).
9. P. Kusch and M. M. Hessel, J. Chem. Phys. 68, 2591-2606 (1978).
10. O. Svelto, Principles of Lasers, p. 43, 2nd Ed., Plenum Press, New York, 1986.
11. C. J. Jeung, J. Phys. B 16, 4289 (1983).
12. K. P. Huber, and G. Herzberg, Constants of Diatomic Molecules, p. 432, Van Nostrand, New York, 1979.
13. G. Herzberg, Molecular Spectra and Molecular Structure I: Spectra of Diatomic Molecules, p. 101, Van Nostrand Reinhold, New York, 1950.

LIST OF SYMBOLS

Molecular Electronic Energy Levels

$X^1\Sigma_g^+$, $A^1\Sigma_u^+$, $2^1\Sigma_g^+$, $B^1\Pi_u$

Z	Collision frequency
σ	Collision cross section of molecule
n	Density of molecular sodium vapor
$\bar{v}$	R.M.S. speed of molecules
r	Internuclear space, or length of dipole
λ, $d\lambda$, $\Delta\lambda$	Wavelength; increments
ρ	Radiation density per unit wavelength
T	Absolute temperature in K
Π	Pi
h	Planck's constant
$\hbar$	Planck's constant/2Π
c	Velocity of light
v_1, v_2, v_n	Vibrational levels in molecule
μ_1, v_1, v_2	Matrix element for transition from vibrational level v_1 to v_2 for $B \rightarrow 2^1\Sigma_g^+$
μ_2, v_1, v_2	Matrix element for transition from vibrational level v_1 to v_2 for $B \rightarrow X$
ε_o	Dielectric constant for free space
ψ_1, ψ_2, ψ_2^*	Wave functions
F_{1,v_1,v_2}	Franck-Condon factor for transition from vibrational level v_1 to v_2

F_{2,v_1,v_3}	Franck Condon factor for transition from vibrational level v_1 to v_3
B	Einstein coefficient for stimulated emission
W_{v_1,v_2}	Stimulated emission rate from vibrational level v_1 to level v_2
W	Sum of stimulated emission rates for all levels
A	Einstein coefficient for spontaneous emission
λ_a	Wavelength for transition $B(v_1)$ to X (v_3)
R	Rate of stimulated to spontaneous emission = $W/A = \rho B/A$
e	Electronic charge

Table 1. Transitions rates in Na_2 with initial and final vibrational levels, average energy difference Δ(eV) and average wavelength of transitions $\bar{\lambda}$.

Initial State	Transition	Upper vb level v_1	Final vb level v_2	Δ(eV) Max	$\bar{\lambda}$ (μm)	Max $W(s^{-1})$	Spont. $A(s)^{-1}$
$B^1\Pi_u$	$B^1\Pi_u \rightarrow 2^1\Sigma_g^+$	6	0-20	0.3	4	8×10^{12}	2×10^{5}
	$B^1\Pi_u \rightarrow X^1\Sigma_g^+$	6	0-35	2.5	0.5	$\approx 7\times10^{2}$	1.4×10^{8}
$2^1\Sigma_g^+$	$2^1\Sigma_g^+ \rightarrow A^1\Sigma_u^+$	0-20	0-35	0.6	2	2×10^{13}	1.6×10^{6}
$A^1\Sigma_u^+$	$A^1\Sigma_u^+ \rightarrow X^1\Sigma_g^+$	0-35	0-35	1.7	0.7	$\approx 4\times10^{7}$	3.7×10^{7}

LIST OF FIGURE CAPTIONS

Fig. 1 Energy level diagram for Na_2 according to Jeung (3), with the transition pathways shown. The dotted curves are best fitted Morse functions.

Fig. 2 Plots of $R' = \rho\lambda_a^3/4h$ vs λ_{v_1,v_2} for different oven temperatures T(°C). The experiment was carried out at 450°C (723K).

Fig. 3 Plot of transition rates W from vibrational energy levels v_1 (5,6,7) in $B^1\Pi_u$ state of Na_2 to vibrational level v_2 in the $2^1\Sigma_g$ state vs λ_{v_1,v_2}. The bandwidths ($\approx$ 1.4x10-3 μm) are too narrow to be evident. Oven temperature 723K.

Journal of Molecular Spectroscopy, W. L. Harris, Figure 1

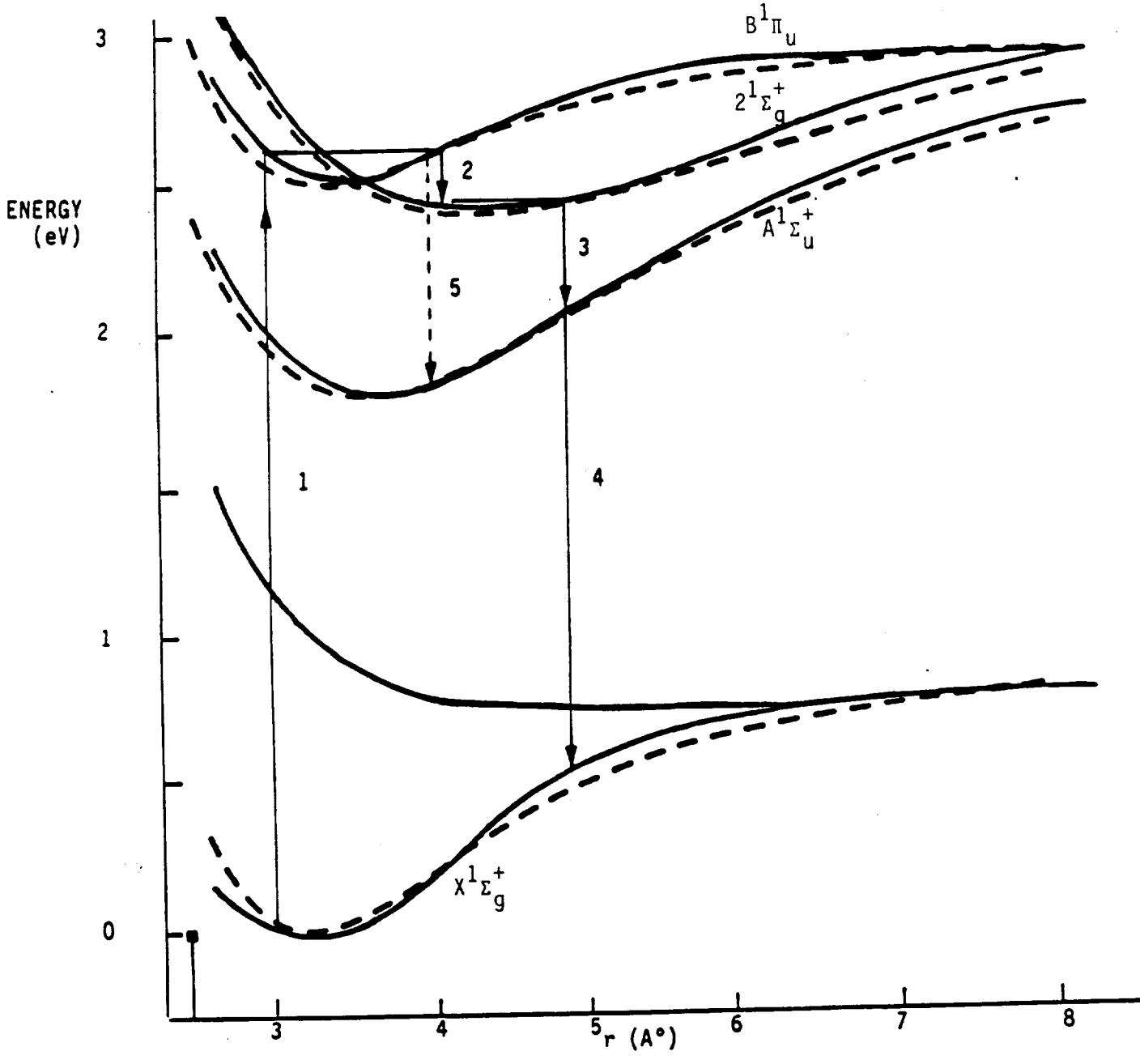

Journal of Molecular Spectroscopy, W.L. Harries,
Figure 2

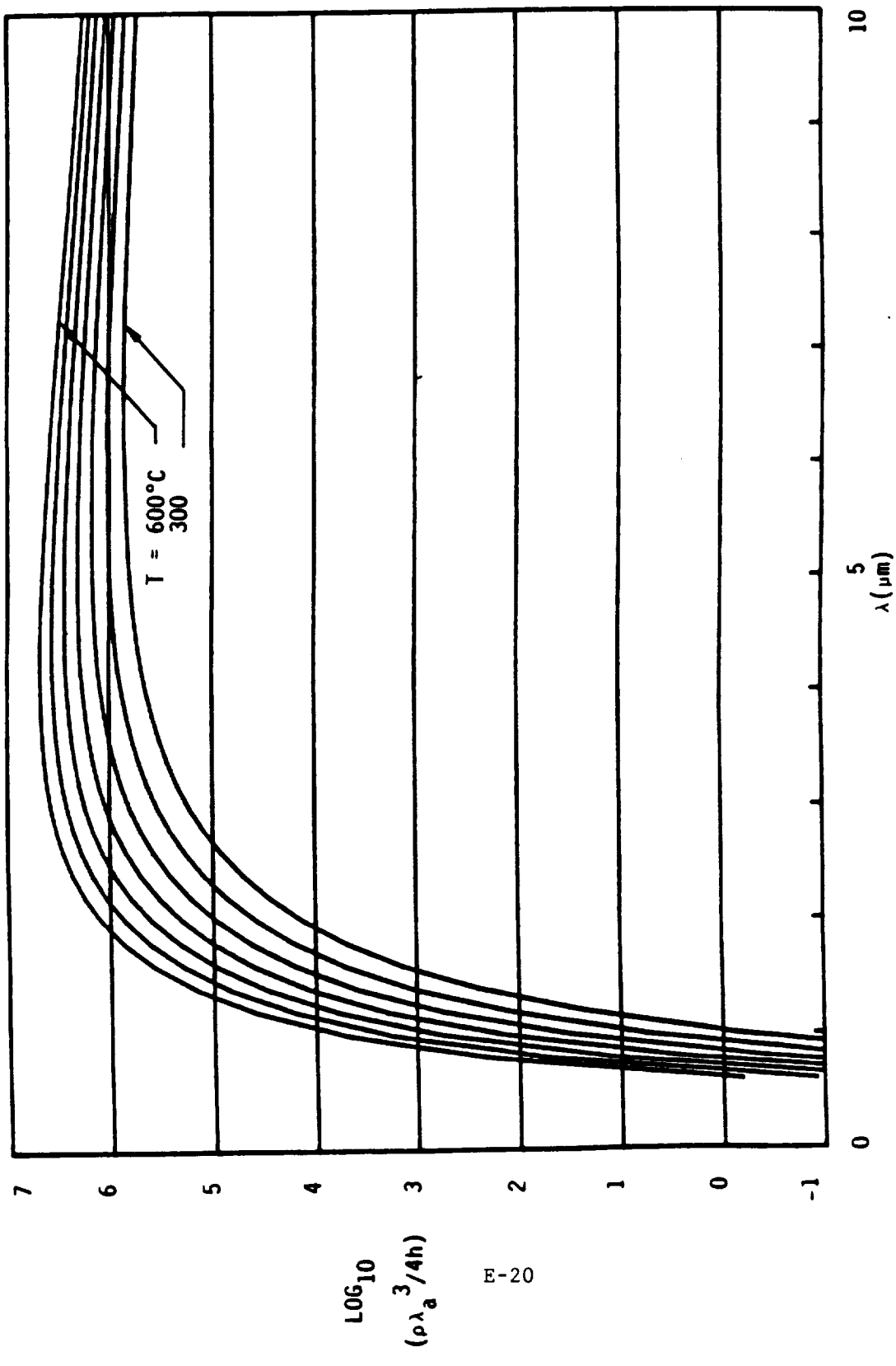

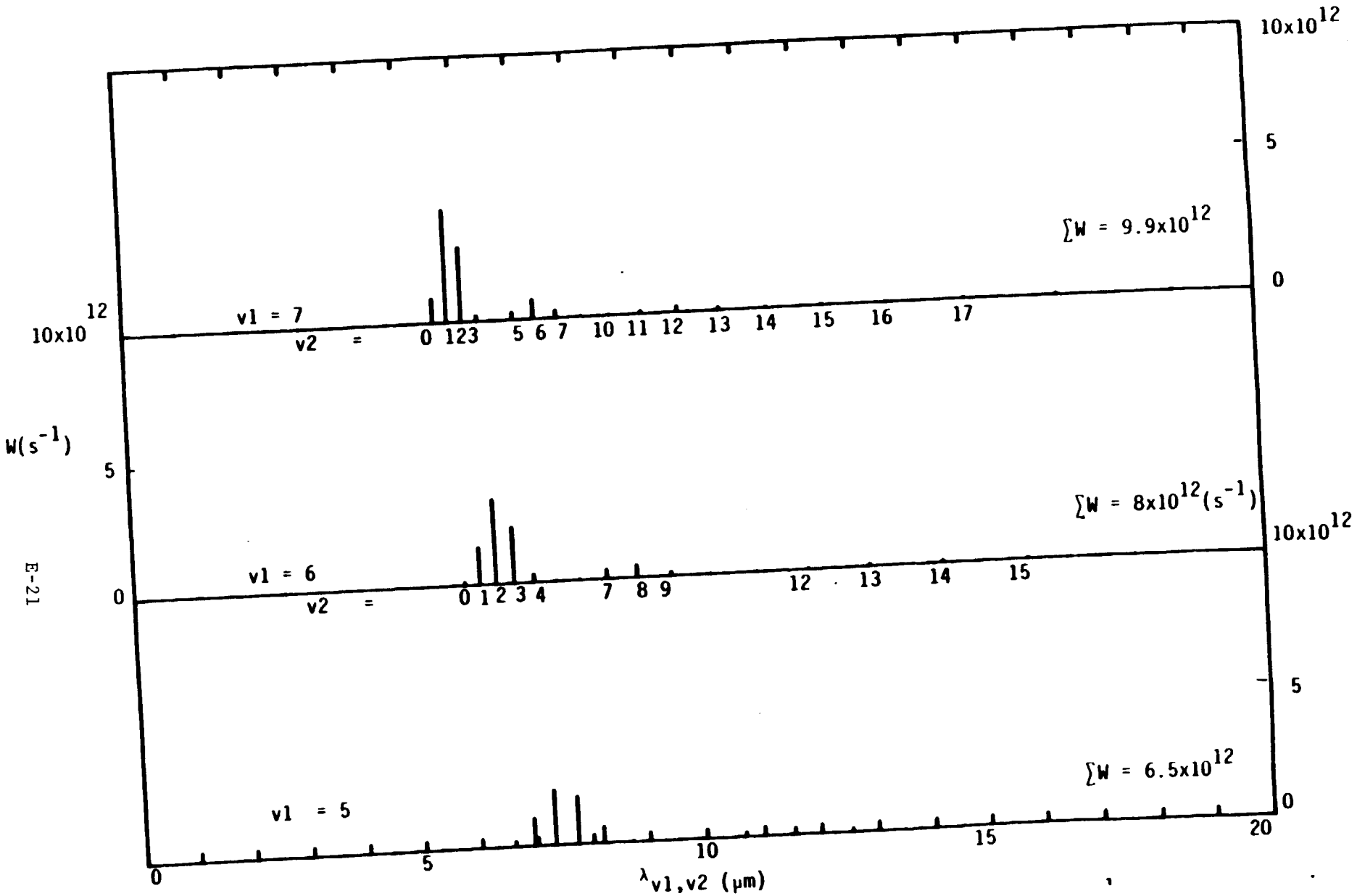

Journal of Molecular Spectroscopy, W.L. Harris, Figure 3

APPENDIX F

ABSORPTION OF ISOTROPIC RADIATION

Wynford L. HARRIES
Department of Physics, Old Dominion University, Norfolk, VA 23508, USA

Received 4 May 1987

Estimates of the absorption of isotropic radiation are given for an absorbing medium whose geometrical shape is either a plane-parallel sided slab or a cylinder. By including the directional variation of absorption path length, the results show appreciable differences to the "unidirectional radiation" formulae.

The absorption of isotropic radiation such as blackbody radiation, is of interest for estimates of rates of energy deposition into a medium either as heat or molecular vibrational energy. We assume the medium is uniform and isotropic and has a characteristic absorption length λ. For narrow band absorption of the radiation into molecular vibrational energy, as in laser pumping [1], $\lambda = (n\sigma)^{-1}$, where n is the density of absorbing centers and σ the absorption cross-section which is single valued. The fraction of radiation absorbed along a path length l in crossing through the medium is then $F = 1 - \exp(-l/\lambda)$, and for unidirectional radiation, l can be related easily to the medium geometry. However, for isotropic radiation, l varies with direction. Here the total fractional absorption for two medium geometries, a flat lab and a cylinder, is estimated and comparisons made with the "unidirectional formula".

The radiation energy enters the medium from the black body cavity walls according to Planck's radiation formula and the emission and absorption coefficients of the wall are assumed unity. If the medium is contained within a transparent vessel inside the cavity, reflections from the vessel surface may occur, which are not considered.

For a plane parallel infinite slab of thickness d (fig. 1) let the energy enter from a small surface dS at PQ. A spherical coordinate sytem (ρ, α, β) has origin at O. It is convenient to work in terms of angle $\chi = \pi/2 - \alpha$. For isotropic emission the amount of

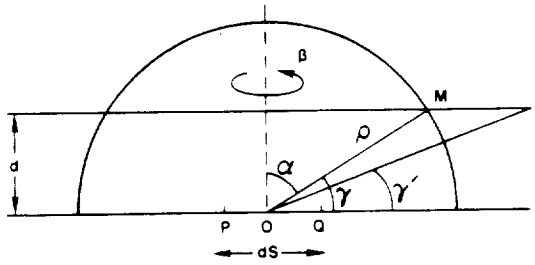

Fig. 1. Infinite slab geometry with energy entering through a small area dS at PQ. Spherical coordinates (ρ, α, β) have origin at O. Isotropic radiation entering at angles less than γ' is assumed completely absorbed within an error ϵ.

radiation in direction γ is proportional to the opening, namely, $dS\cos\alpha$ (Lambert's law) $= dS\sin\gamma$ and the fraction of solid angle between γ and $\gamma + d\gamma$ is $\cos\gamma\, d\gamma$. The path length in the slab is $OM = d/\sin\gamma$ and thus the fraction absorbed is

$$f_\gamma\, d\gamma = k_1 \sin\gamma\cos\gamma \times [1 - \exp(-d/\lambda\sin\gamma)]\, d\gamma\,, \qquad (1)$$

where k_1 is a constant. To integrate numerically we assume for $\gamma < \gamma'$, all the energy is absorbed within an error ϵ, because of the long path lengths, i.e., $\exp(-d/\lambda\sin\gamma) = \epsilon$, where ϵ is a small quantity, chosen as 10^{-99}. Then

$$\gamma' = \sin^{-1}\frac{d}{\lambda\ln(1/\epsilon)}\,, \qquad (2)$$

and the fraction of radiation absorbed for $0 \leq \gamma \leq \gamma'$ is f_1:

$$f_1 = k_1 \int_0^{\gamma'} \sin\gamma \cos\gamma \, d\gamma$$

$$= \tfrac{1}{2} k_1 [d/\lambda \ln(1/\epsilon)]^2 . \quad (3)$$

The fraction absorbed for $\gamma' \leqslant \gamma \leqslant \pi/2$ is f_2:

$$f_2 = k_1 \int_{\gamma'}^{\pi/2} \sin\gamma \cos\gamma \times [1 - \exp(-d/\lambda \sin\gamma)] \, d\gamma . \quad (4)$$

Integration was performed using Simpson's Rule, with 11 values of γ between γ' and $\pi/2$. The total fraction absorbed is $f_3 = f_1 + f_2$ and f_3 is a function of the ratio λ/d, so universal curves can be plotted. The normalization constant k_1 can be evaluated by realizing that $\int_0^{\pi/2} k_1 \sin\gamma \cos\gamma \, d\gamma$ is the total power through dS, or $0.5\, k_1$. The results were insensitive to ϵ provided it was small, except where $\lambda/d \to 0$. For $\lambda/d \leqslant 0.3$ it is seen $f_3 > 1$ due to numerical errors. Table 1 gives f_3 versus λ/d and also shown is the function $F_1 = 1 - \exp(-d/\lambda)$, for comparison. The ratio f_3/F_1 indicates the error introduced by using the "unidirectional formula".

A more common geometry for black-body cavity experiments is a cylinder of radius r with energy entering from the sides (fig. 2). Let the cylinder and the small area dS at L be tangential to plane AFGD at AD. The amount of radiation at angles θ and ϕ to plane AFGD is proportional to $dS \sin\theta \sin\phi$. For section ABCD at angle θ, path length LM is $2r \sin\theta/\sin\phi$. As before, we require $\exp(-\mathrm{LM}/\lambda) = \epsilon$ at ϕ', or $\phi'(\theta) = \sin^{-1}[2r \sin\theta/\lambda \ln(1/\epsilon)]$, and between θ and $\theta + d\theta$ all the radiation for $0 \leqslant \phi < \phi'$ is absorbed, consisting of a fraction $f_4(\theta)$:

$$f_4(\theta) = k_2 \int_0^{\phi'} \sin\theta \sin\phi \, d\phi$$

$$= k_2 \sin\theta (1 - \cos\phi') . \quad (5)$$

Between ϕ' and $\pi/2$ the fraction absorbed is $f_5(\theta)$:

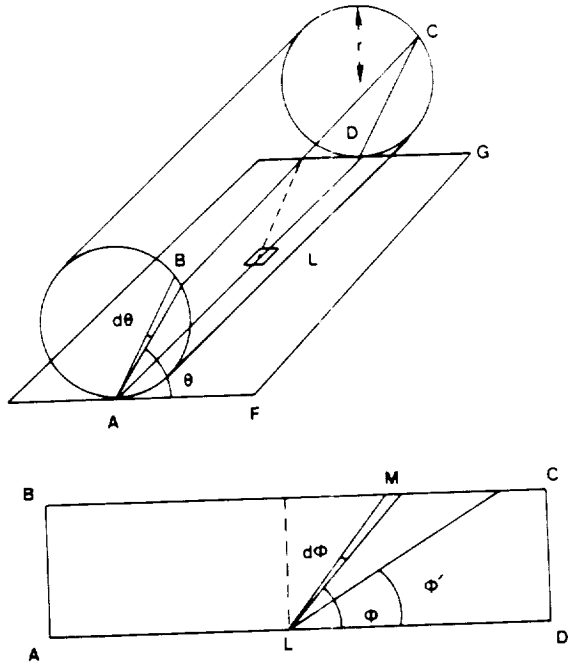

Fig. 2. Energy enters through a small area dS at L. Plane AFGDL is tangential to cylinder. Section ABCD is at angle θ to AF, and absorption paths LM are at angle ϕ to LD. Isotropic radiation entering this section at $\phi < \phi'$ is assumed completely absorbed, within an error ϵ.

$$f_5(\theta) = k_2 \int_{\phi'}^{\pi/2} \sin\theta \sin\phi \times [1 - \exp(-2r \sin\theta/\lambda \sin\phi)] \, d\phi , \quad (6)$$

and $f_6(\theta) = f_4 + f_5$ is the fraction absorbed between θ and $\theta + d\theta$. For $0 \leqslant \theta \leqslant \pi/2$ the fraction absorbed is f_7.

$$f_7 = \int_0^{\pi/2} f_6(\theta) \, d\theta . \quad (7)$$

The value of k_2 is obtained by observing that the total power in through dS for θ, ϕ between 0 and $\pi/2$ is $K_2 \int_0^{\pi/2} \int_0^{\pi/2} \sin\theta \sin\phi \, d\theta \, d\phi$ and $K_2 = 1$. A double integration of f_7 over ϕ and θ was performed numerically using 11 values of ϕ between $\phi'(\theta)$ and $\pi/2$ for each of 11 values of θ. Again f_7 is a function of λ/r (table 1). Comparison with a "unidirectional" calculation for path length $2r$, $F_2 = [1 - \exp(-2r/\lambda)]$,

Table 1
Estimates of the fraction of isotropic radiation absorbed versus λ/d for a slab, and versus λ/r for a cylinder; λ is the absorption length, d the thickness of the slab and r the radius of the cylinder. The functions f_1, f_2 are the fractions alculated here. F_1 and F_2 are the results of the "unidirectional radiation formulae". The ratios f_1/F_1 and f_2/F_2 are a measure of the errors in using the latter. The values of f_1 for $\lambda/d \leq 0.3$ should be ≤ 1.

Slab geometry				Cylinder			
λ/d	f_1	F_1	F_1/F_1	λ/r	f_2	F_2	f_2/F_2
0.10	1.042	1.000	1.04	0.10	1.000	1.000	1.00
0.20	1.020	0.993	1.03	0.20	0.999	1.000	1.00
0.30	1.002	0.964	1.04	0.30	0.997	0.999	1.00
0.40	0.978	0.918	1.07	0.40	0.994	0.993	1.00
0.50	0.948	0.865	1.10	0.50	0.990	0.982	1.01
0.60	0.916	0.811	1.13	0.60	0.984	0.964	1.02
0.70	0.882	0.760	1.16	0.70	0.978	0.943	1.04
0.80	0.848	0.713	1.19	0.80	0.970	0.918	1.06
0.90	0.816	0.671	1.22	0.90	0.962	0.892	1.08
1.00	0.785	0.532	1.24	1.00	0.952	0.865	1.10
1.10	0.756	0.597	1.27	1.10	0.942	0.838	1.12
1.20	0.728	0.565	1.29	1.20	0.931	0.811	1.15
1.30	0.702	0.537	1.31	1.30	0.919	0.785	1.17
1.40	0.678	0.510	1.33	1.40	0.908	0.760	1.19
1.50	0.655	0.487	1.35	1.50	0.895	0.736	1.22
1.60	0.633	0.465	1.36	1.60	0.883	0.714	1.24
1.70	0.613	0.445	1.38	1.70	0.871	0.692	1.26
1.80	0.594	0.426	1.39	1.80	0.851	0.671	1.28
1.90	0.576	0.409	1.41	1.90	0.846	0.651	1.30
2.00	0.559	0.393	1.42	2.00	0.833	0.632	1.32
3.00	0.432	0.283	1.52	3.00	0.720	0.487	1.45
4.00	0.352	0.221	1.59	4.00	0.628	0.394	1.60
5.00	0.297	0.181	1.64	5.00	0.556	0.330	1.69
6.00	0.257	0.154	1.68	6.00	0.498	0.284	1.76
7.00	0.227	0.133	1.70	7.00	0.450	0.249	1.81
8.00	0.203	0.118	1.73	8.00	0.411	0.221	1.86
9.00	0.184	0.105	1.75	9.00	0.378	0.199	1.90
10.00	0.168	0.095	1.76	10.00	0.350	0.181	1.93
11.00	0.154	0.087	1.78	11.00	0.326	0.166	1.96
12.00	0.143	0.080	1.79	12.00	0.305	0.154	1.99
13.00	0.133	0.074	1.80	13.00	0.287	1.143	2.01
14.00	0.124	0.069	1.81	14.00	0.270	0.133	2.03
15.00	0.117	0.064	1.81	15.00	0.256	0.125	2.05
16.00	0.110	0.061	1.82	16.00	0.243	0.118	2.07
17.00	0.104	0.057	1.83	17.00	0.231	0.111	2.08
18.00	0.099	0.054	1.83	18.00	0.220	0.105	2.09
19.00	0.094	0.051	1.84	19.00	0.211	0.010	2.11
20.00	0.090	0.049	1.84	20.00	0.202	0.095	2.12

shows f_7 can be considerably greater than F_2.

In conclusion, estimates of the absorption of isotropic radiation should take account of the contribution of rays proceeding at angles which result in very long path lengths. The above procedure can be extended for broad band absorption if σ is a known function of wavelength by reiterating over small wavelength ranges.

The work was supported by Grant NSG-1568 from the National Aeronautis and Space Administration Langley Research Center, Hampton, Virginia. Useful discussions with M.D. Williams of NASA are acknowledged.

References

[1] R.J. Insuik and W.H. Christiansen, IEEE J. Quantum Electron. QE-20 (1984) 622.

[2] J.K. Roberts, Heat and thermodynamics (Blackie & Son Ltr., 1928) p. 387.

APPENDIX G

THEORETICAL STUDIES OF A SOLAR-PUMPED BLACK-BODY CO_2 LASER

By

Wynford L. Harries and Zeng-Shevan Fong

SUMMARY

A method of pumping a CO_2 laser by a hot cavity has been demonstrated (ref. 1). The cavity, heated by solar radiation, should increase the efficiency of solar pumped lasers used for energy conversion. Kinetic modeling is used to examine the behavior of such a CO_2 laser. The kinetic equations are solved numerically vs. time and, in addition, steady state solutions are obtained analytically. The effect of gas heating filling the lower laser level is included. The output power and laser efficiency are obtained as functions of black body temperature and gas ratios (CO_2-He-Ar) and pressures. The values are compared with experimental results.

1. INTRODUCTION

The possibility of using solar collectors on orbiting space vehicles and transmitting the energy to earth via laser beams has been discussed already (refs. 2, 3, 4). A critical factor for energy conversion is the laser efficiency. One suggestion for increasing the efficiency is to heat a black body cavity by solar radiation and then let the cavity pump the laser, according to the Planck radiation law. If the laser medium absorbed a narrow bandwidth from the spectrum then the black body cavity would immediately refill any "hole" in the distribution. The pumping radiation is thus

replenished and the potential efficiency should be much higher than if the laser is pumped directly.

It is the purpose of this paper to examine the kinetics of a black body pumped laser. In addition to directly pumped CO_2 lasers, there are schemes whereby N_2 is pumped and the energy transferred to CO_2, but these are not considered here. The direct CO_2 lasers usually have He and Ar as additives which perform the functions of deexcitation of the lower level and heat conduction; these are included.

The physical mechanisms of the laser are discussed in Section 2. For the first time to our knowledge the effect of gas heating, which serves to fill the lower laser level and inhibit lasing, is included. The temperature rise is calculated, and an estimate of the effect of filling the lower laser level from Boltzmann statistics is made.

In Section 3, time varying solutions of the kinetic equations show the behavior of the upper and lower laser level densities, and also the photon density and output power vs. time. The solutions show that steady state conditions can be achieved.

Analytical solutions are obtained for the steady state in Section 4. The steady state output power is shown as a function of black body temperature and gas constituent pressures. Estimates of the laser efficiency as a function of the variables are also given.

Throughout the discussion it is assumed that the laser tube of 0.4 cm radius has a length of 50 cm heated in an oven at 1000-1500 K and contains CO_2+He+Ar at total pressures of 1 to 12 torr in varying ratios. The radiation from the oven is passed through nitrogen which is transparent to it and enters the laser tube. The purpose of the nitrogen, which is flowed, is to cool the laser medium. The measured exit temperature of the nitrogen was 340 K (ref. 1), and this was assumed to be the wall temperature. The gas

temperature is slightly higher than this and is discussed in Section 2.2. The above numbers correspond to experimental conditions in reference 1.

2. PHYSICAL MECHANISMS IN THE LASER

A flow diagram of the processes occurring during lasing is shown in figure 1.

2.1 Absorption of Radiation

The black body radiation is absorbed at 4.256μ over a bandwidth of 0.1 μ. The radiation flux per unit length entering the laser tube of radius r is $E(\lambda)\, d\lambda\, 2\pi r$ when $E(\lambda)$ is determined by Planck's radiation formula and $d\lambda$ is 0.1 μ. The fraction absorbed depends on σ_a, the absorption cross section. The latter can be calculated: $\sigma_a = \lambda^2 A/4\pi^2\Delta\nu$, where A = 424.6 is the Einstein coefficient for the transition (000)→(001), λ = 10.6μ, $\Delta\lambda$ = 0.1μ and $\sigma_a = 1.2\times10^{-18}\text{cm}^2$. However, a measured value of the absorption length is 1.56×10^{-3}cm at 1 atmosphere (ref. 5), which yields $\sigma_a = 2.41\times10^{-17}$cm. Both values were tried.

Two possibilities exist for the calculation of the fraction absorbed. If the absorption is small, then the fraction absorbed per unit volume can be expressed approximately as

$$F_1 = 2\,(1 - \exp\,(-(CO_2)\,\sigma_a 2r)/r \qquad (1)$$

where the radiation is assumed to cross a distance 2r and the amount per unit length is proportional to $2\pi r$ and per unit volume, $2\pi r/\pi r^2$. If the pressure increases, however, the absorption will take place at the outer edges of the tube. The excited species can, however, diffuse to the center in a time t where $t \approx r^2/D$ and D is the diffusion coefficient. Assuming a mean free path of 2.9×10^{-3}cm at 1 torr, a total gas pressure of 1 torr

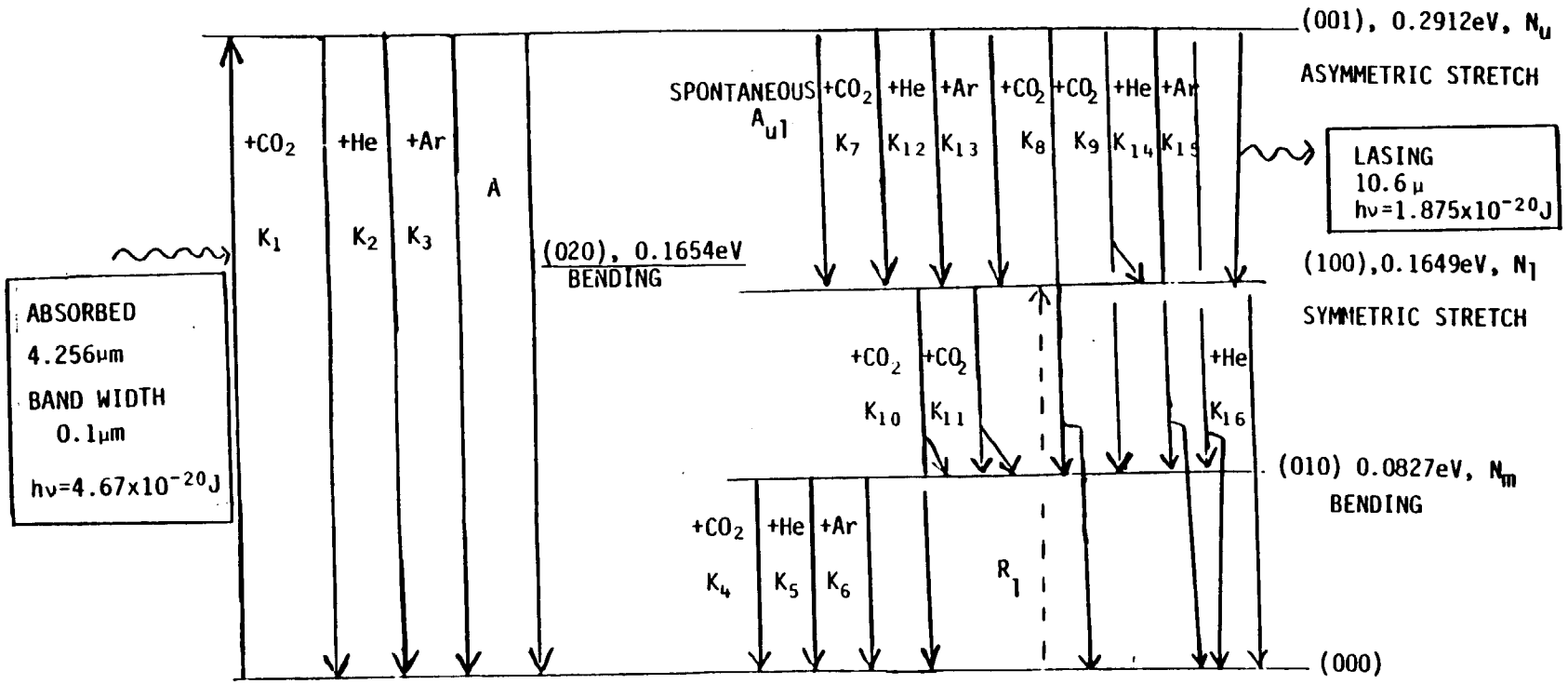

Figure 1. Flow Diagram for CO_2 Black Body Laser

(ref. 6) and a temperature of 340°, then t ≈ 3 ms, a time comparable with other rates. Neglecting diffusion, a second estimate is obtained by assuming the radiation is absorbed at the center of the tube between a depth x_1 and x_2. Then the fraction F absorbed per unit volume is

$$F_2 = (\exp(-(CO_2)\sigma_a x_1) - \exp(-(CO_2)\sigma_a x_2))/(x_2 - x_1) \qquad (2)$$

where here $x_1 = 0.35$, $x_2 = 0.45$ cm. The effect of the outer layer of gas shielding the center of the tube at high pressures is now included, but a one dimensional, not cylindrical, geometry is assumed.

A number of computer runs were made using F_2, however, the results did not agree with the experiment (ref. 1). The computer results showed a sharp cutoff of power at a few torr and, accordingly, the coefficient F_1 was used for the following calculations.

The number of absorption events per unit volume is then

$$S = \frac{E(\lambda)d\lambda}{h\nu} F_1 = 5.76 \times 10^{19} F_1/(\exp(3381/T_b)-1) \qquad (3)$$

where T_b is the black body temperature, which gives the number of $CO_2(000)$ molecules raised to the upper laser level $CO_2(001)$ per cc per second.

2.2 Heating of the Medium

Experimentally it was realized that unless a nitrogen coolant was flowed past the laser tube, that lasing ceased (ref. 1). The implication was that the medium became heated causing the lower level to be filled. A rough estimate of the increase in temperature, and its effect on the density of the lower level follows.

As the efficiency of the laser would probably not be greater than a few percent, it is assumed that all the radiation absorbed goes into heating the gases. The rate at which heat energy enters a unit volume, dQ/dt, increases with the pressure of CO_2 which is included in $F_{1,2}$.

$$dQ/dt = E(\lambda)\, d\lambda \cdot F_1/4.2 \text{ Cals cm}^{-3}\text{s}^{-1} \qquad (4)$$

The heat conduction K of a mixture of gases CO_2, He, Ar depends on the gas ratios and the absolute temperature (ref. 3). It is independent of gas pressure.

$$K = 3.27 \times 10^{-4}\ S\ \sqrt{T/273} \qquad (5)$$

where

$$S = \left(\frac{1 + 0.71\ CO_2/He + 0.32\ Ar/He}{1 + 4.55\ CO_2/He + 2.67\ Ar/He}\right) \qquad (6)$$

It is assumed that the heat is conducted over an effective area A through an effective distance d to the wall at a temperature T_w. As the conduction is proportional to $\sqrt{T}$, the conduction equation yields that the temperature in the center of the gas T_g is:

$$T_g = \left(Tw + 1.8 \times 10^4 \cdot (dQ/dt)/(S \cdot A/d)\right)^{2/3} \qquad (7)$$

The expression is approximate as a one dimensional geometry is assumed. For example, with T_w = 340 K,[1] a black body temperature of 1500 K, a total pressure of 10 torr (CO_2 20%, He 20%, Ar 60%), tube radius 0.4 cm, then T_g approaches 360 K.

2.3 Filling of the Lower Laser Level

The lower laser level which has a density N_1 of $CO_2(100)$ atoms, will be filled according to Boltzmann statistics which depend on T_g. However competing against this will be the depletion processes due to collisions. To include the temperature effects they must be expressed as a rate of production of N_1 vs. time. It is assumed that CO_2 molecules in the tail of the energy distribution, which have energies greater than E_1 = 0.1649eV, the energy of the lower laser level, can collide with the rest of the CO_2 population with a finite probability of producing CO_2 (100). The density of molecules with sufficient energy is (CO_2) exp $(-E_1/kT)$ and the rate of production R_1 from this process is:

$$R_1 = (CO_2)\ (CO_2 \cdot \exp\ (-E_1/kT_g)\ \overline{\sigma v} \qquad (8)$$

Here k is Boltzmann's constant, σ is the cross section for the reaction, v the particle velocity. R_1 increases as T_g increases.

2.4 Diffusion Losses

At low pressures losses of particles by diffusion to the tube walls may be important. We assume that the diffusion loss time of CO_2 molecules, τ_D obeys (ref. 7):

$$\tau_D = (r/2.405)^2/D\gamma \qquad (9)$$

where D is the diffusion coefficient for CO_2 in a mixture of CO_2, He and Ar, (Appendix I) and the 2.405 corresponds to losses in an infinitely long cyl-

inder. The quantity γ is the probability of deexcitation at the wall and is somewhere between 0.2 and 1. The diffusion losses apply equally to all excited levels of CO_2.

2.5 The Kinetic Equations

The CO_2 laser (Fig. 1) is a four level system. The absorbed photon raises the $CO_2(000)$ level to the upper laser level $CO_2(001)$ the asymmetric stretching mode at 0.2912 eV above ground. Lasing at 10.6u occurs by a transition between the (001) and (100) levels, the latter a symmetric stretching mode at 0.1649 eV above ground.

The upper laser level of density N_u is depopulated by collisions with CO_2, He, Ar (rate constants K_1, K_2, K_3) to the ground level, and by spontaneous emission (Einstein coefficient A). Transitions can also occur to the lower laser level (100) (K_7, K_9, K_{12}, K_{13}, and the spontaneous coefficient A_{ul}) and the (010) level (K_8, K_9, K_{14}, K_{15}).

The (100) level (density N_l) has a (020) bending mode which is, 0.0005 eV higher in energy. The conversion $(020) \rightleftarrows (100)$ is very rapid, and the two are lumped together here.

The lower laser level is filled by collisions from the upper level (K_7, K_9, K_{12}, K_{13}) and by the spontaneous emission A_{ul}. It is also filled during lasing by stimulated transitions of rate constant Γ. The lower level is depleted by collisions with CO_2 (K_{10}, K_{11}) and with He (K_{16}), (no data on Ar was available), and the transitions end either on the (010) level or the (000). However, at high gas temperatures, the lower laser level will be filled at a rate R_l.

The (010) level of density N_m is in turn depleted by collision with CO_2, He, Ar (K_4, K_5 K_6). The reactions are given in more detail in Table 1,

Table 1. Rate Coefficients for CO_2 at 360°K

Reaction	Coeff.	Ref. 8 EXPT.	Ref. 9 CALCULATED	Ref. 10 EXPT.	Ref. 11 EXPT.	Ref. 12	Value Assumed
$CO_2(001)+CO_2 \rightarrow CO_2(000)+CO_2(000)$	K_1		$+N_2$ 4.2×10^{-13} $+CO$ 2.35×10^{-13}	1.33×10^{-14}			1.33×10^{-14}
$+He \rightarrow$ $+He$	K_2						? 3.6×10^{-15}
$+Ar \rightarrow$ $+Ar$	K_3						? 2.5×10^{-15}
$CO_2(001)+CO_2 \rightarrow CO_2(100)+CO_2(000)$	K_7		4.73×10^{-16}	4.2×10^{-15}			4.2×10^{-15}
$+He$ $+He$	K_{12}						? 2.48×10^{-15}
$+Ar$ $+Ar$	K_{13}						? 1.87×10^{-15}
$CO_2(001)+CO_2 \rightarrow (010)+CO_2(000)$	K_8	5.5×10^{-15}	7.13×10^{-19}	6.3×10^{-18}	6×10^{-15}		6.10^{-15}, 6.3×10^{-18}
$+He$ $+He$	K_{14}	2×10^{-15}			1.08×10^{-15}		1.08×10^{-15}
$+Ar$ $+Ar$	K_{15}				1.03×10^{-15}		1.03×10^{-15}
$CO_2(001)+CO_2 \rightarrow CO_2(100)+CO_2(010)$	K9		9.72×10^{-15}				9.72×10^{-15}
$CO_2(100)+CO_2 \rightarrow CO_2(010)+CO_2(000)$	K10		4.64×10^{-18}				4.6×10^{-18}
$CO_2(100)+CO_2 \rightarrow CO_2(010)+CO_2(010)$	K11		2.53×10^{-14}				2.53×10^{-14}
$CO_2(010)+CO_2 \rightarrow CO_2(000)+CO_2(000)$	K_4	8×10^{-15}	8.29×10^{-15}	6.67×10^{-15}	1×10^{-14}		8×10^{-15}
$+He$ $+He$	K_5	1.5×10^{-13}			2×10^{-13}		1.39×10^{-13}
$+Ar$ $+Ar$	K_6				2×10^{-15}		2×10^{-15}
$CO_2(100)+He \rightarrow CO_2(010,000)+He$	—						
$+Ar \rightarrow CO_2(010,000)$	—						
Spontaneous A $(001) \rightarrow 000$	A			424.6			424.6
A $(001) \rightarrow (100)$	A_{ul}					0.186	0.186
$CO_2(100)+He \rightarrow CO_2(000)+He$	K_{16}	1.025×10^{-13}					1.025×10^{-13}
$+Ar \rightarrow CO_2(000)+Ar$	—						

with values from four different sources. In the column under reference 9, the values are calculated from the expression

$$\ln K = A + BT^{-1/3} + CT^{-2/3} \tag{10}$$

where the constants A, B, C, are given for the different reactions. The values may not be accurate when extrapolated to 360K. References 8, 10 and 11 give experimental values.

The unknown quantities are then assumed to be N_u, N_1, N_m and N the 10.6μ photon density. In the following equations, the quantities in parenthesis (CO_2) etc. are the densities of the species. The rate equations for the four species are:

$$\frac{dN_u}{dt} = S - N_u \left[(K_1 + K_7 + K_8 + K_9)(CO_2) + (K_2 + K_{12} + K_{14})(He) + (K_3 + K_{13} + K_{15})Ar\right] - N_u(A + A_{u1}) - \Gamma - {}^{N_u}/_{\tau_D} \tag{11}$$

$$\frac{dN_1}{dt} = \Gamma + N_u A_{u1} + N_u \left[(K_7 + K_9)(CO_2) + K_{12}(He) + K_{13}(Ar)\right] - N_1 \left[(K_{10} + K_{11})(CO_2) + K_{16}(He)\right] - {}^{N_e}/_{\tau_D} + R_1 \tag{12}$$

$$\frac{dN_m}{dt} = N_1 (K_{10} + 2K_{11})(CO_2) + N_u \left[(K_8+K_9)(CO_2) + K_{14}(He)+K_{15}(Ar)\right] - N_m \left[K_4(CO_2) + K_5(He) + K_6(Ar)\right] - {}^{N_m}/_{\tau_D} \tag{13}$$

$$\frac{dN}{dt} = \Gamma + G A_{ul} N_u - {}^{N}/_{\tau_c} \qquad (14)$$

The stimulated emission rate Γ is given by:

$$\Gamma = N \sigma_e c \ [N_u - N_l] \qquad (15)$$

and is proportional to the stimulated emission cross section σ_e whose value was calculated: $\sigma_e = \lambda_e^4 A_{ul} / 4\pi^2 c \, \Delta\lambda_e$, where $\lambda_e = 10.6\mu$, $A_{ul} = 0.186$ and $\Delta\lambda_e$ was taken as the bandwidth from Doppler Broadening. Here c is the velocity of light. Assuming a gas temperature of 360°, then $\Delta\lambda_e = 0.217\text{Å}$ and $\sigma_e = 9.14 \times 10^{-17} cm^2$.

In equation 15 the quantity G is a geometrical factor which takes into account that the spontaneous emission is isotropic; $G = 2r^2/L^2$ where r and L are the radius and length of the laser. The quantity τ_c is the containment time for photons, $\tau_c = -2L/c \ln (r_1 r_2)$ where $r_1 = 0.99$, $r_2 = 0.95$ are the reflectivities of the laser mirrors.

The equations can be simplified by noting that N_u, N_l, $N_m << (CO_2)$, and that (CO_2) can be regarded as constant. Then the following constants can be defined:

$$a_1 = [(K_1 + K_7 + K_8 + K_9)(CO_2) + (K_2 + K_{12} + K_{14})(He) + (K_3 + K_{13} + K_{15})(Ar)$$

$$+ A + A_{ul} + {}^{1}/_{\tau_D} \ ]$$

$$a_2 = [(K_{10}+K_{11})(CO_2) + K_{16}(He) + \frac{1}{\tau_D})]$$

$$A' = [(K_7+K_9)(CO_2) + K_{12}(He) + K_{13}(Ar) + A_{u1}]$$

$$a_3 = [K_4(CO_2) + K_5(He) + K_6(Ar)]$$

$$a_4 = [(K_{10}+ 2\ K_{11})(CO_2)]$$

$$a_5 = [(K_8+K_9)(CO_2) + K_{14}(He) + K_{15}(Ar)]$$

Then equations 11 through 14 can be reduced to

$$\frac{dN_u}{dt} = S - a_1 N_u - \Gamma \qquad (16)$$

$$\frac{dN_1}{dt} = \Gamma + A' N_u - a_2 N_1 + R_1 \qquad (17)$$

$$\frac{dN_m}{dt} = a_5 N_u + a_4 N_1 - a_3 N_m \qquad (18)$$

$$\frac{dN}{dt} = \Gamma + G\ A_{u1}\ N_u - N/\tau_c \qquad (19)$$

3. TIME VARYING SOLUTIONS

Computer graphic solutions of equations 15 through 19 are shown in Figure 2. It was assumed for convenience that the pumping signal from the black body rose from zero to full value in a time of 100 μs, and that the signal was proportional to $\sin^2 2\pi\ (t/10^{-4})$ (where t is the time in seconds) up to 100 μs; thereafter it was constant. The pumping signal is shown in the upper curve.

In the second plot, N_u, N_1 and $(N_u-N_1)x10$ are plotted. The densities of the upper and lower laser levels increase with time, but at first, when the signal is small, $N_1 > N_u$. (This can be seen on amplified plots). However, N_u overtakes N_1 at 28μs, and the signal (N_u-N_1) starts to grow. It increases with time until threshold at $t = 53$ μs. Then N_u falls and N_1 rises, and the inversion (N_u-N_1) falls. At the same time the photon density N increases sharply and then falls to zero as the inversion falls. The upper level is then increased again until a second light pulse appears and so on. This behavior is characteristic of kinetic equations similar to these, where σ_e is small; if σ_e is much larger these violet oscillations are smoothed out.

The inversion quickly assumes a constant value, and at 135 μs the value of the photon density N also becomes constant. This implies that continuous lasing is possible.

4. STEADY STATE SOLUTIONS

As they stand, equations 16 through 19 are nonlinear. In the steady state, however, the stimulated emission rate far exceeds the spontaneous rate, and in equation 19, $\Gamma >> GA_{ul}N_u$ or:

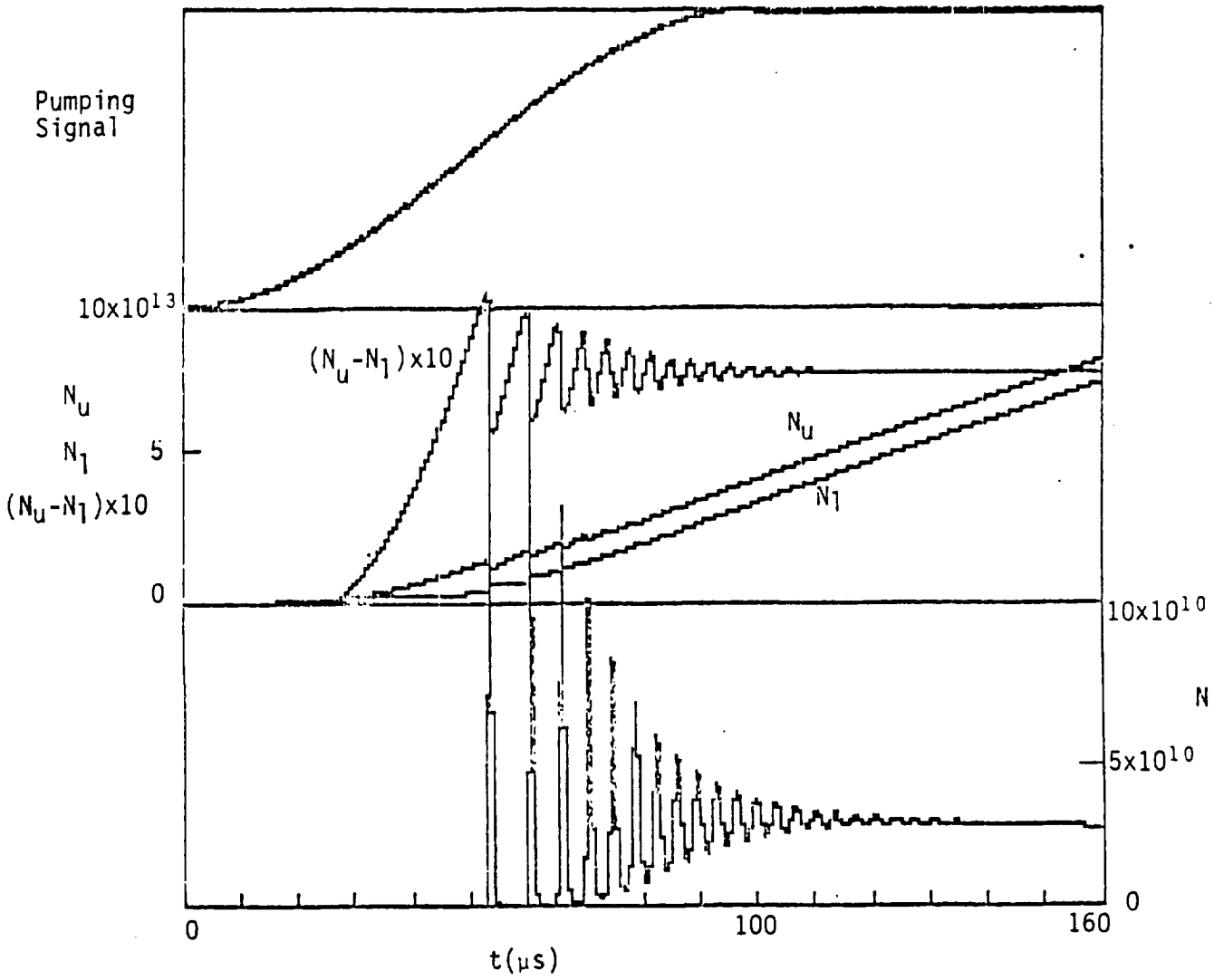

Figure 2. Time behavior of black body pumped laser. The pumping signal was assumed proportional to $\sin^2(\pi t/2\times10^{-4})$ up to 100μs, then became constant. The middle diagram shows N_u, N_l and $(N_u-N_l)\times10$. The lower diagram shows the 10.6μ photon.

$$\Gamma \simeq N/\tau_c \tag{20}$$

and from 15 and 19

$$N_u - N_1 \simeq \frac{1}{\sigma_e c \tau_c} = \text{const} \tag{21}$$

The constancy of the inversion N_u-N_1 is evident in Figure 2, and the value is given by equation 21. Replacing Γ in equations 16 through 19 by N/τ_c the solutions are

$$N_u = \frac{S + R_1 + a_2/\tau_c \sigma_e c}{a_1 + a_2 - A'} \tag{22}$$

$$N_1 = N_u - \frac{1}{\tau_c \sigma_e c} \tag{23}$$

$$N_m = \frac{a_5 N_u + a_4 N_1}{a_3} \tag{24}$$

$$N = \tau_e S \left[1 - \frac{a_1}{a_1+a_2-A'}\right] - \left[\frac{a_1 a_2}{\sigma_e c(a_1+a_2-A')}\right] - \left[\frac{\tau_c R_1 a_1}{a_1+a_2-A'}\right] \tag{25}$$

The effect of gas temperature is included in R_1 and as R_1 increases the value of N falls.

The value of N from equation 25 agrees with the value, late in time, from the time varying computer solutions.

4.1 Steady State Power Output

The evaluation of N enables the power output of the laser to be evaluated:

$$P = \frac{1}{2} Nc\, h\nu\, T_r\, \pi r^2 \qquad (26)$$

The factor 1/2 takes into account that half the photons are travelling away from the output mirror of transmission $T_r = (1-r_2)$, c is the velocity of light, $h\nu$ the energy of the lasing photons of 1.868×10^{-20} J. Experimentally it was found that the output beam had a radius of 0.3 cm corresponding to a Gaussian profile in a 4 cm radius tube, (ref. 13) and for $T_r = 0.05$,

$$P = 3.97 \times 10^{-12} N \text{ (W)} \qquad (27)$$

Plots of power output vs. total pressure p (torr) for different black body temperatures are given in Figure 3. The gases were in the ratio CO_2 16%, He 4%, Ar 80°. The output power rises with black body temperature, but as p increases, the power falls. The effect is due to the R_1 term in the equations; on making $R_1 = 0$ the output power rose with increasing pressure.

The variation of output power with black body temperature at a fixed total pressure of 7 torr, but with the same gas ratios, is shown in Figure 4. A linear rise is observed.

The gas temperature of T_g can be altered by assuming different wall temperatures T_w. Assuming a gas mixture as before of 7 torr (16% CO_2, 4% He, 80° Ar) and a black body temperature of 1450K, then the power output vs. T_g is plotted in Figure 5. It shows that an increase in gas

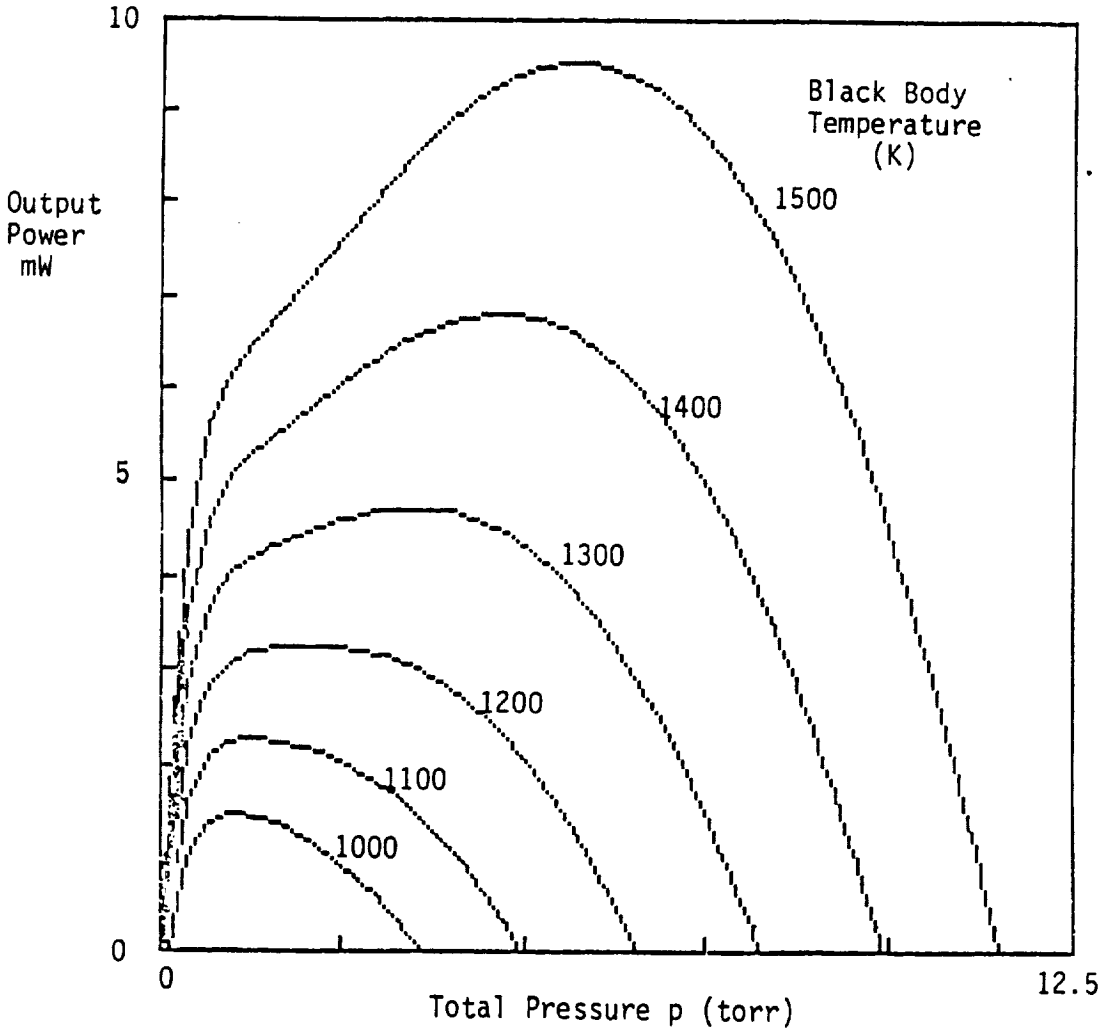

Figure 3. Power output of black body pumped laser vs total pressure for various black body temperatures. The gases were CO_2-16%, He-4%, Ar-80%. The wall temperature was 340K.

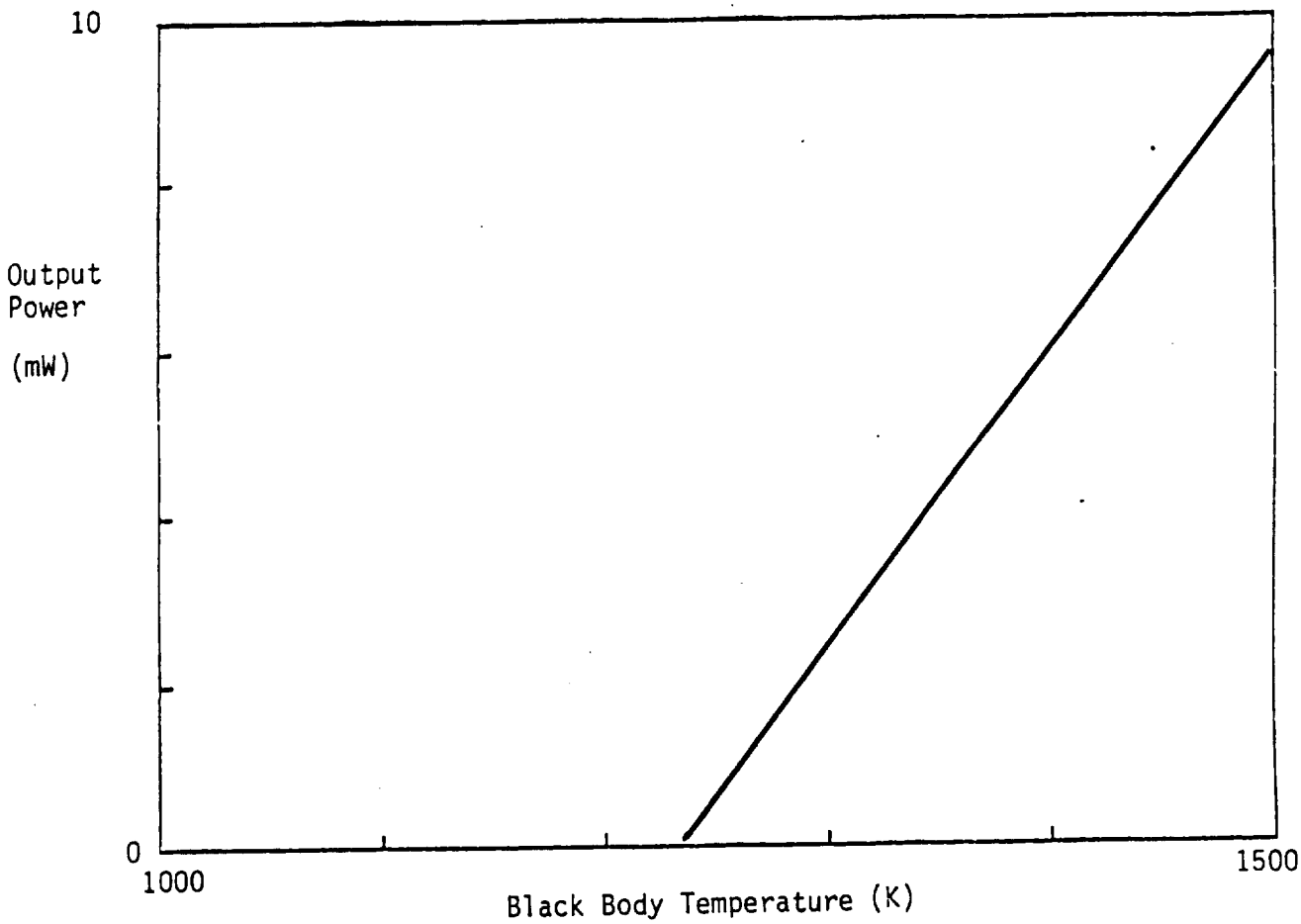

Figure 4: Power output vs black body temperature. Total pressure = 7 torr, 16% CO_2, 4% He, 80% Ar, wall temperature 340K.

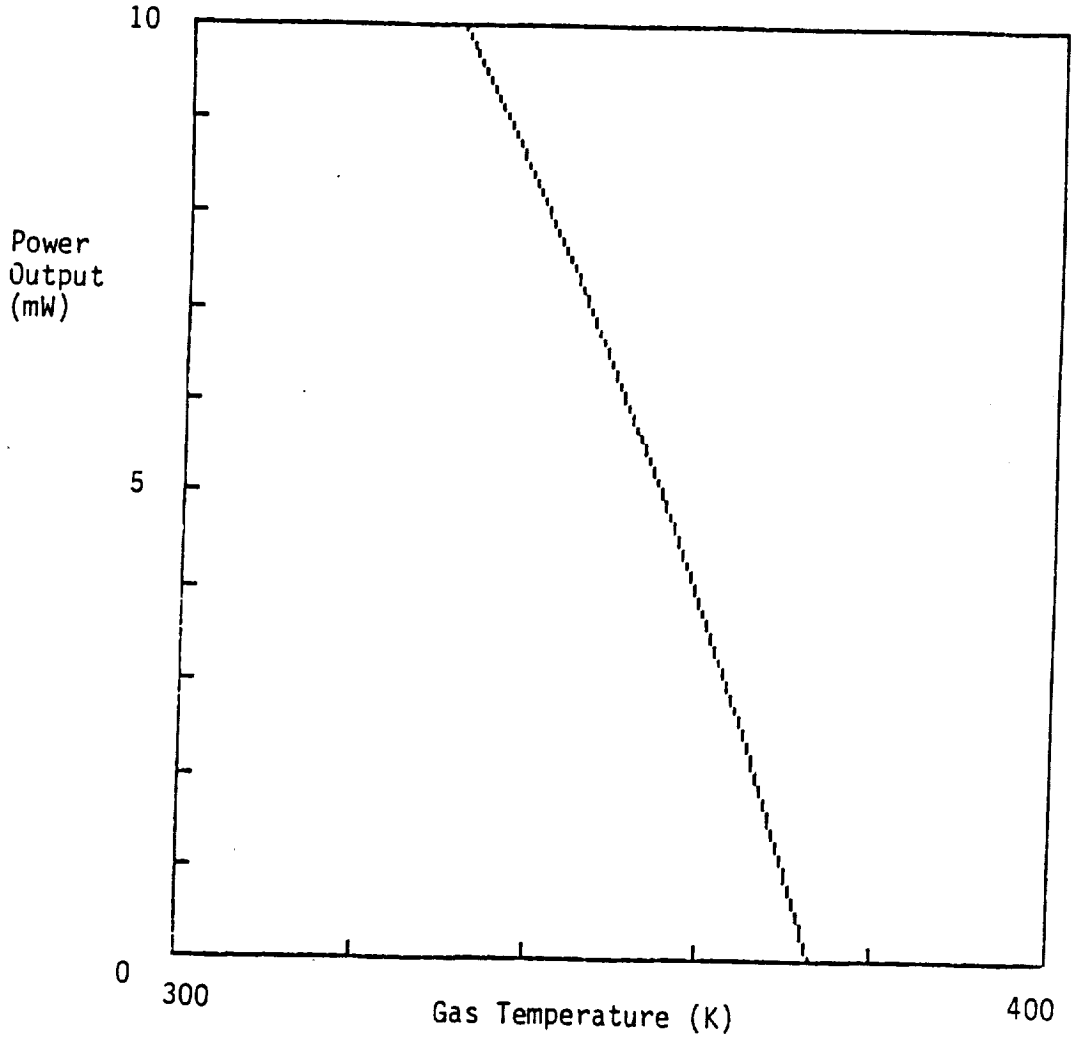

Figure 5. Plot of power output vs gas temperature, 7 torr 16% CO_2, 4% He, 80% Ar, black body temperature 1450K.

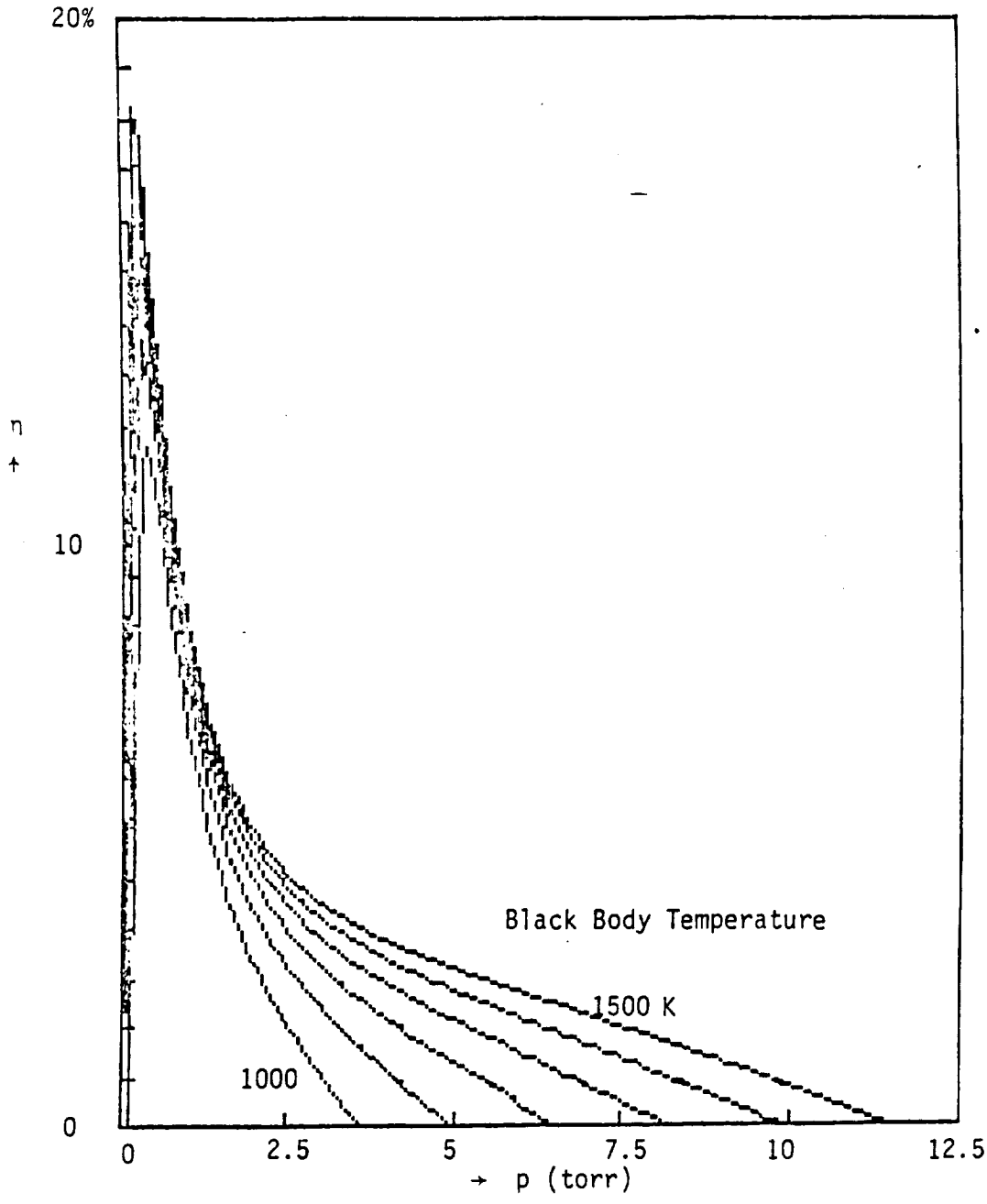

Figure 6. Efficiency (as defined in equation 29) of the black body pumped laser vs total pressure p for various black body temperatures. The gases are CO_2 16%, He 4% and Ar 80°.

temperature greatly reduces the output power indicating that cooling of the medium is essential.

4.2 Efficiency

The input power P_{in} is the power absorbed by the laser:

$$P_{in} \approx E(\lambda)\, d\lambda\, 2\pi r\ L\ (1-\exp(-(CO_2)\sigma_a 2r) \qquad (28)$$

and the efficiency η is defined here as output power/the power absorbed from the black body radiation:

$$\eta = P/P_{in} \qquad (29)$$

(It should be noted that the black body pumped laser has other "efficiencies" besides η, however, these are not considered here.)

Using equation 29 to define the efficiency, Figure 6 shows plots of η vs. p for different black body temperatures. There seem to be high efficiencies at very low pressures where the output power is small. In the regime around 7 torr where experimentally the highest output powers were observed, the efficiency is only a few percent.

CONCLUSIONS

The results here depend critically on the values of the rate coefficients in Table 1. They are insensitive to K_4, K_5, K_6, but are very dependent on K_9, K_{11} and K_{13}. The most sensitive parameter seems to be K_{11} where a change of a few percent altered the output power by several times. Also τ_D was a sensitive parameter.

Unfortunately, the rate coefficient for R_1 was not known. The values

chosen indicate that about one collision in 10^5 of two ground state atoms resulted in the creation of one $CO_2(100)$ which does not seem unreasonable.

Figures 3, 4, and 5 show reasonable qualitative agreement with experimental measurements (ref. 1). However, it did not seem possible to get agreement with experimental measurements of power output vs. total pressure (ref. 12), at a black body temperature of 1450K where the ratios CO_2:He:Ar were varied. In view of this, these results must be treated with caution, and must be regarded as preliminary.

REFERENCES

1. R.J. Insuik and W.H. Christiansen, IEEE J. Quantum Electronics QE-20, 622, (1984).

2. J.F.Coneybear, "The Use of Lasers for the Transmission of Power. Radiation Energy Conversion in Space," K.H. Billman, ed., Program astronaut Aeronaut 61, 279, 1979.

3. W.L. Harries and J.W. Wilson, Space Solar Power Review 2, 367, 1981.

4. W.L. Harries and W.E. Meador, Space Solar Power Review 4, No. 3, 189, 1983.

5. A. Javan and M. Guerra, NASA Contractor Report H3428 under contract NAS1-14688, p. 13, 1981.

6. A.von Engel, "Electric Plasmas and their Uses," Taylor & Francis Ltd., p. 37, 1983.

7. A.von Engel, "Ionized Gases," Oxford University Press, p. 140, 1964.

8. R.L. Taylor and S. Bitterman, Rev. Mod. Phys. 41, 26, 1969.

9. J.A. Blauer and G.R. Nickerson, AIAA 4th Fluid and Plasma Dynamics Conference, Palo Alto, CA, June 17-19, 1974, Paper 74-536.

10. J.A. Blauer and G.R. Nickerson, Technical Report AFRPL-TR-73-57 for Nov. 72-May 1983.

11. P.A. Lewis and D.W. Trainor "Survey of Relaxational Data for O_2, N_2, NO H_2, CO, HF, HCl, CO_2 and H_2O, Avco Everett Research Lab Inc., Contract No. F04701-73-C-0284. Nov. 1974.

12. S.A. Munji and W.H. Christiansen, App. Optics 12, 993, (1973).

13. R. J. Insuik, Private communication.

APPENDIX

Diffusion of CO_2 When Mixed with He and Ar

The mean free paths of molecules in their own gas at 1 torr for CO_2, He and Ar are 2.7×10^{-3}cm, 13.1×10^{-3}cm and 4.6×10^{-3}cm, respectively (ref. 7). These values give the cross sectional diameters, and it is then assumed that for a collision between unlike molecules that the cross section diameter is the arithmetic mean of the individual diameters. Adding the collision frequencies of CO_2-CO_2, CO_2-He, CO_2-Ar, the total collison frequency ν for CO_2 is:

$$\nu = 2.37 \times 10^{-11}(CO_2)\left(1 + 1.79 \frac{He}{CO_2} + 2.54 \frac{Ar}{CO_2} \right)\sqrt{T} \qquad (A1)$$

The diffusion coefficient D is then

$$D = \frac{1}{3} \frac{v_r^2}{\nu} = 1.928 \times 10^6 T/\nu$$

where $v_r = 2405 \sqrt{T}$ is the random velocity of CO_2.